

HYDRODYNAMICS AND PROFILE RESPONSE DUE TO CROSS-SHORE
PROCESSES IN THE SURF ZONE

By

RAJESH SRINIVAS

A DISSERTATION PRESENTED TO THE GRADUATE SCHOOL
OF THE UNIVERSITY OF FLORIDA IN
PARTIAL FULFILLMENT OF THE REQUIREMENTS
FOR THE DEGREE OF DOCTOR OF PHILOSOPHY

UNIVERSITY OF FLORIDA

1993

UNIVERSITY OF FLORIDA



3 1262 08552 4568

ACKNOWLEDGEMENTS

I would like to express my sincere gratitude and appreciation to my committee chairman, Dr. Robert G. Dean, for providing me with inspiration for my work through his zeal and love for coastal engineering. His unflagging spirits, constant accessibility and valuable ideas went a long way in making my work easy and enjoyable. Even after knowing him for so many years, he still never ceases to amaze me by the depth of his knowledge. Similarly, Dr. Ashish Mehta's help in innumerable aspects is really appreciated. My discussions with Dr. Robert J. Thieke went a long way in clearing many nebulous facets of hydrodynamics. My thanks also go to Dr. D.M. Sheppard and Dr. B.A. Christensen for serving on my committee. I am especially appreciative of Dr. B.A. Christensen for consenting to serve on such short notice. I am also grateful to Sidney Schofield for his invaluable overall help, Subarna Malakar for his help with computing facilities, and Jim Joiner at the laboratory. Special thanks are due to all staff, especially Helen Twedell and Cynthia Wey. Finally, I would like to thank my friends and, most of all, my parents for their unqualified support and faith in me.

This work was supported with funding provided by the Florida Department of Natural Resources.

TABLE OF CONTENTS

ACKNOWLEDGEMENTS	ii
LIST OF FIGURES	v
LIST OF TABLES	x
ABSTRACT	xi
CHAPTERS	
1 INTRODUCTION	1
1.1 Surf Zone Hydrodynamics	1
1.2 Sediment Transport Modeling	2
1.3 Overwash Process and Relevance to Barrier Islands	4
1.4 Objectives	8
1.5 Plan of Study	9
2 PHYSICAL MODELING OF CROSS-SHORE SEDIMENT TRANSPORT	11
2.1 Similitude Considerations	11
2.2 Laboratory Facility and Apparatus	17
2.3 Investigation of Overwash	20
2.3.1 A Brief Literature Review	20
2.3.2 Scope of the Overwash Experiments	24
2.3.3 Procedure, Measurements and Test Conditions	26
2.3.4 Results	33
2.3.5 Discussion of Results	55
2.4 Bar Formation Mechanisms	57
2.4.1 Background	57
2.4.2 A Brief Literature Review	60
2.4.3 General Characteristics of Present Laboratory Experiments	67
2.4.4 Correlation of Bar Characteristics and Infragravity Waves	71
2.4.5 Effects of Wave Spectra and Height Distributions	90
2.4.6 Discussion of Results	98
3 CROSS-SHORE TRANSPORT HYDRODYNAMICS	103
3.1 Background	103
3.2 Convergence of Sediment Transport	105
3.3 A Note on Breaking Waves	107

3.4	Characteristics of Breaker Evolution	108
3.5	Cross-Shore Hydrodynamics Contributing to Suspended Transport . .	119
3.5.1	First-Order Contribution	122
3.5.2	Return Flow Model	122
4	CONCENTRATION MODEL	132
5	CROSS-SHORE SEDIMENT TRANSPORT MODEL	138
5.1	Suspended Sediment Transport	138
5.1.1	Contribution due to Intermittent Suspension	138
5.1.2	Contribution due to Mean Cross-Shore Currents	139
5.2	Bedload Transport	141
5.2.1	Transport due to Effects of the Bottom Boundary Layer . . .	141
5.2.2	Transport due to Wave Asymmetry	144
5.3	Parameterization of Constants	147
5.4	Model Verification	147
5.5	Assessment of Model Limitations	174
5.6	Discussion of Results	178
6	SUMMARY, CONCLUSIONS AND RECOMMENDATIONS	184
6.1	Summary	184
6.2	Conclusions	185
6.3	Recommendations for Further Work	188
	APPENDIX <u>BREAKING WAVE MODEL</u>	190
	BIBLIOGRAPHY	192
	BIOGRAPHICAL SKETCH	202

LIST OF FIGURES

1.1	The barrier beach as a complete system (from Godfrey, 1976).	6
2.1	Size distribution of sand used in the present study.	16
2.2	Schematic layout and cross-section of wave tank facility.	18
2.3	Field measurements of beach erosion and overwash, Leatherman 1979.	22
2.4	Initial beach profile in the wave tank for each experiment.	25
2.5	Illustration of estimated rising and falling storm surges.	31
2.6	Storm surge simulation used in Experiment E5.	32
2.7	A regular wave train (Experiment E4) (a) seaward of the toe of the beach (340 m), and (b) landward of the toe of the beach (240 m).	34
2.8	A regular wave train (Experiment E4) (a) seaward of the breakpoint (176 m), and (b) just landward of the breakpoint (136 m).	35
2.9	A regular wave train (Experiment E4) (a) over the crest of the barrier island (98 m), and (b) over the crest of the barrier island (49 m).	36
2.10	An irregular wave train at the toe of the beach (Experiment E8).	37
2.11	Spectrum of an irregular wave train at the toe of the beach (Experiment E8).	38
2.12	Experiments (a)E1 and (b)E2, Mean profiles at 00 and 18 hours.	40
2.13	Experiment E3, Profile B1, 00-06 hours.	43
2.14	Experiment E3, Profile B1, 06-12 hours.	44
2.15	Experiment E3, Profile B1, 12-18 hours.	45
2.16	Experiments (a)E3 and (b)E4, Mean profiles at 00 and 18 hours.	46
2.17	Experiment E3, profile variance at 18 hours.	47

2.18	Experiment E5, (a)Mean profiles at 00 and 06 hours, (b)Mean profiles at 06 and 16 hours, (a)Mean profiles at 16 and 24 hours.	49
2.19	Experiment E5, Mean profiles at 06 and 24 hours.	50
2.20	Experiments (a)E6 and (b)E7, Mean profiles at 00 and 18 hours.	52
2.21	Experiments (a)E8 and (b)E9, Mean profiles at 00 and 18 hours.	54
2.22	Definition sketch of a longshore bar in a beach profile.	59
2.23	Formation and movement of a longshore bar during the 10/82 storm at FRF, DUCK, NC (from Sallenger and Howd 1989). . .	66
2.24	Formation and movement of the longshore bar during 9/85 storm at FRF, DUCK, NC (from Sallenger and Howd 1989).	67
2.25	Positioning of general morphological features in the air-sea tank.	69
2.26	Case 1. $x = 18\text{m}$ (toe of beach). (a)Measured total wave system (b)Measured long wave (c)Energy spectrum of the total wave system (d)Energy spectrum of long waves.	73
2.27	Case 1. $x = 15.5\text{ m}$ (just seaward of the surf zone). (a)Measured total wave system(b)Measured long wave (c)Energy spectrum of the total wave system (d)Energy spectrum of long waves.	75
2.28	Case 1. $x = 15\text{ m}$. (just inside the surf zone) (a)Measured total wave system(b)Measured long wave (c)Energy spectrum of the total wave system (d)Energy spectrum of long waves.	76
2.29	Case 1. $x = 14\text{ m}$ (well inside the surf zone).(a)Measured total wave system(b)Measured long wave (c)Energy spectrum of the total wave system (d)Energy spectrum of long waves.	77
2.30	Case 1. $x = 11.6\text{ m}$ (nearshore). (a)Measured total wave system (b)Measured long wave (c)Energy spectrum of the total wave system (d)Energy spectrum of long waves.	78
2.31	Case 1 Evolution of the bed profile 0-4.5 hours.	79
2.32	Case 1: Sediment transport rates at different times for Case 1. .	80
2.33	Numerical (line) and analytical (symbols) solutions for a long wave with a frequency of 0.10 Hz on a planar (1:19) beach.	83
2.34	Case 1 (a) Measured and predicted IG wave envelope, (b) Initial and Final (4.5 hours) bed profiles.	85
2.35	Case 2 (a) Measured and predicted IG wave envelope, (b) Initial and Final (4.5 hours) bed profiles.	86

2.36	Case 3 (a) Measured and predicted IG wave envelope, (b) Initial and Final (4.5 hours) bed profiles.	87
2.37	Case 4 (a) Measured and predicted IG wave envelope, (b) Initial and Final (4.5 hours) bed profiles.	88
2.38	Change in bar position with changes in position of nodes and antinodes.	89
2.39	Case 5, Multifrequency waves. Total and long waves and associated energy spectra at $x = 18$ m (toe of beach).	91
2.40	Case 5, Multifrequency waves. Total and long waves and associated energy spectra at $x = 12$ m (nearshore).	92
2.41	Case 5 WHPD, Initial and Final bed profiles.	93
2.42	Case 6 WHPD, Initial and Final bed profiles.	94
2.43	Case 7 WHPD, Initial and Final bed profiles.	95
2.44	Case 8 WHPD, Initial and Final bed profiles.	96
2.45	Case 9 WHPD, Initial and Final bed profiles.	97
2.46	Wave Height Probability Distribution Function for Cases 1 and 2.	99
2.47	Wave Height Probability Distribution Function for Cases 3 and 4.	100
3.1	Comparison of mass flux predictions and measurements (from Nadaoka 1986).	113
3.2	Turbulent intensities immediately below the trough level (from Nadaoka 1986).	114
3.3	Irrotational and rotational velocity components in a breaking wave (from Nadaoka 1986).	115
3.4	Suspended transport regions.	121
3.5	Mass flux distribution in cases without overtopping.	126
3.6	Mass flux distribution in cases with overtopping.	126
3.7	Measurements of radiation stress and the mean water line gradients (from Stive and Wind 1982).	129
4.1	Measured levels of τ_{ke} (from Svendsen 1987).	135
4.2	Predictions of production, dissipation and flux of τ_{ke} , Experiment E1.	137

5.1	Experiment E1: Actual suspended sediment transport and redistributed suspended sediment transport due to the weighting function.	150
5.2	An example cumulative probability function for random waves at the toe of the beach ($x=18$ m): Experiment E8.	151
5.3	Experiment E1: initial profile and model prediction compared with the measured final profile.	154
5.4	Experiment E1: initial profile and model prediction (without bedload) compared with the measured final profile.	156
5.5	Experiment E1: initial profile and model prediction after 14 hours of wave action compared to the measured final profile (after 4.5 hours).	157
5.6	Experiment E2: initial profile and model prediction compared with the measured final profile.	158
5.7	Experiment E3: initial profile and model prediction compared with the measured final profile.	160
5.8	Experiment E4: initial profile and model prediction compared with the measured final profile.	162
5.9	Experiment E4: initial profile and model prediction (no bedload) compared with the measured final profile.	163
5.10	Experiment E5: initial profile and model prediction compared with the measured final profile.	165
5.11	Experiment E5: measured profile before the advent of the storm (1.5 hours) and the model prediction after 4 hours (peak storm tide) compared with the measured profile after 4 hours.	166
5.12	Experiment E6: initial profile and model prediction compared with the measured final profile.	167
5.13	Experiment E6: initial profile and model prediction (no bedload) compared with the measured final profile.	169
5.14	Experiment E7: initial profile and model prediction compared with the measured final profile.	170
5.15	Experiment E8: initial profile and model prediction compared with the measured final profile.	172
5.16	Experiment E9: initial profile and model prediction compared with the measured final profile.	173
5.17	Model prediction for Experiment E1 with the friction factor increased by a factor of 10.	176

5.18 Experiment E1, measured profiles and model prediction with bed-load mechanisms only. 177

5.19 (a)Measured local changes in elevation after 1.5 hours, and measured profiles for Experiments (b)E5 and (c)E1. 179

LIST OF TABLES

1.1	Storm surge prediction for a Category 5 hurricane at 20 locations in Florida	7
2.1	Comparison of various approaches for determination of basic scale ratios of coastal movable bed models (from Coastal Hydraulic Models, CERC, 1979).	12
2.2	Experimental conditions of tests (E1-E9) of overwash study (prototype units).	29
2.3	Variation in the magnitude of storm surge parameters.	30
2.4	Bar formation criteria	61
2.5	General features of bar formation investigation experiments. . . .	68
2.6	Characteristics of experiments with biharmonic waves	72
2.7	Characteristics of experiments with non biharmonic waves. . . .	90
5.1	Parameters required in the numerical model.	147
5.2	Test conditions of Experiments E1-E9 (model units).	153

Abstract of Dissertation Presented to the Graduate School
of the University of Florida in Partial Fulfillment of the
Requirements for the Degree of Doctor of Philosophy

HYDRODYNAMICS AND PROFILE RESPONSE DUE TO CROSS-SHORE PROCESSES IN THE SURF ZONE

By

RAJESH SRINIVAS

December 1993

Chairman: R.G. Dean

Major Department: Coastal and Oceanographic Engineering

Experiments were conducted to simulate cross-shore effects of storms, including overtopping conditions, on barrier islands and characterizing their response. The barrier island was represented by a horizontal crest and an initially planar beach. The experiments included regular and irregular wave types. Conditions of overtopping with concomitant overwash were incorporated by considering elevated water levels. Regular waves without overtopping caused berm deposition, a prominent longshore bar and surf zone erosion. Increasing levels of overtopping caused loss of sediment from the beach system and overwash. Simulation of a storm-tide hydrograph indicated that the bar occurs only during periods of steady or slowly changing water levels. Cases with irregular waves had similar but subtler responses. The major difference was in the bar characteristics. In comparison to cases with regular waves, the bar was less distinct without and with marginal overtopping and absent in cases with substantial overtopping.

Additional experiments were formulated to investigate causes of bar generation with emphasis on infragravity (IG) wave and break-point hypotheses. Various wave spectral characteristics with concomitantly varying IG wave structures did not significantly affect the bar. The position of the bar was not correlated to the position

of the nodes or antinodes of the IG wave envelope. Presence of primary or secondary peaks of the wave height probability distribution function near the maximum wave height is essential for bar formation. These experiments reinforce the conclusion that the undertow or break-point hypothesis is responsible for bar formation.

The issue of hydrodynamics causing cross-shore sediment transport was examined analytically. Undertow was represented based on recent experimental evidence. A relatively “complete” physics-based cross-shore sediment transport model, including mechanisms for suspended and bedload transport, was developed that has the capacity for onshore and offshore transport. Effects of turbulence, momentum transfer and augmented mass flux in the surf zone, intermittent suspension, wave asymmetry, bottom boundary layer and gravity were included. Caution must be exercised in extending model results to the prototype because of lack of complete Reynolds number similarity. The model was tested with data from the overwash experiments and was fairly successful in predicting prominent features. The model does not have long-term stability.

CHAPTER 1 INTRODUCTION

A challenging aspect of many coastal and estuarine problems is the elucidation of nearshore sediment transport as beaches are constantly evolving in response to time-varying waves, tides, winds and nearshore currents. The increasing use of the coastal zone has made the quantitative understanding of the causative mechanisms of beach change and the nature of beach response essential for coastal engineers to predict the evolution of beaches. Thus, the aspects to understanding beach behavior involve both the prediction of nearshore hydrodynamics and the coupled prediction of sediment transport causing beach response.

The most dynamic region in the ocean floors is the surf and runup zone. This is the region where incoming waves break and run up the beach foreshore. Typical widths vary from tens of meters to about a thousand meters depending on the sea state and the bottom morphology. The bottom is characterized by sediments and rocks of all sizes, shapes and constituents. It is not surprising that under these circumstances there is no universal model to explain sediment transport mechanisms and related bedforms in the cross- shore direction. In the present work, an attempt is made towards quantitatively accounting for some of the mechanisms causing beach change in order to develop a simple physics-based cross-shore sediment transport model inculcating recent developments in modeling surf zone hydrodynamics and bottom boundary layer approximations.

1.1 Surf Zone Hydrodynamics

Waves and related phenomena in shallow water are of particular interest to coastal engineers as they act as external forcings that shape the beach. The steepening and deformation of waves in the nearshore region due to non-linearity, dispersivity, bottom topography, etc., are generally well understood. However, their eventual breaking in

shallow water results in a number of problems in water wave mechanics which have not been resolved rigorously and unambiguously. Specifically, in terms of sediment transport modeling, the correct representation of surf zone hydrodynamics is most essential as greatest morphological changes occur here. The surf zone is characterized by motions of different types and scales including turbulence, large-scale coherent vortical motions, infragravity waves, horizontal (rip currents) and vertical (undertow) circulation patterns. There have been considerable advances in identification and modeling of the majority of these surf zone flows, but the interactions are not well understood and no single unified model exists capable of predicting all possible flows; for example, the rate of spreading of turbulence from the free surface (due to wave breaking), the rate of decay and the interaction of this turbulence with the bottom are still poorly understood. Another poorly understood region is the zone immediately shoreward of the breakpoint (transition zone) where loss of wave momentum does not translate instantly into a pressure gradient. Turbulence produced by wave breaking is often modeled as a wake or a mixing layer, but it is quite possible that breaking induced turbulence is another unique type of free shear flow. Thus, some of the related modeling is quite heuristic due to the intrinsic complex nature of turbulence.

1.2 Sediment Transport Modeling

It is generally convenient to divide sediment transport in the nearshore into two components: longshore (shore-parallel) sediment transport and cross-shore (shore-normal) sediment transport. Gradients in sediment transport cause changes in the beach planform and profile. Although precise sediment transport modeling requires accounting for both components of sediment transport, it is possible to judge the relative importance of one with respect to the other from a rough knowledge of the site. Longshore sediment transport determines beach planform evolution and is especially important in the vicinity of sediment sinks (inlets), littoral barriers (including jetties and groins) and beach nourishment fills and at sites with strong variations in wave direction and longshore variations of wave height. Cross-shore sediment transport determines beach profile change primarily for beaches located away from structures

and inlets. The time scales of beach change are also quite different, with major planform evolution being on the scale of years while strong cross-shore transport and substantial profile change can occur during a storm with associated time scales of hours to a few days. A storm with energetic wind (short period) waves accompanied by augmented tide levels often results in substantial cross-shore reconfiguration of the beach profile. Broadly speaking, augmented water levels and high waves result in dune and beachface erosion, with the eroded sediment being transported and deposited offshore with the formation of a longshore bar. The advent of milder waves after the storm results in post-storm recovery as the eroded sand slowly moves onshore. Recent cases emphasizing the vulnerability of coastal communities to storm damage were extensive beach erosion along the central Caribbean and eastern Mexico during Hurricane Gilbert and along the northeast Caribbean and South Carolina during Hurricane Hugo. The present work solely addresses the facet of cross-shore sediment transport.

In contrast to numerical modeling of beach planform evolution, which has been actively studied for about five decades, cross-shore sediment transport (numerical) modeling is relatively recent (~ 20 years). Cross-shore sediment transport models are, for example, essential for identifying especially susceptible areas in times of storms and have safety implications for humans and property and the establishment of coastal “setback lines.” Cross-shore sediment transport models can be broadly classified into two groups: closed loop and open loop models. Closed loop sediment transport models have either an explicit or implicit assumption of a target (“equilibrium”) profile and consider transport to be the result of and proportional to variation from this equilibrium (e.g., Moore 1982, Kriebel and Dean 1985, Larson and Kraus 1989). The assumption of an equilibrium beach profile implies that changes in a beach profile will diminish and eventually die out if the beach is exposed to constant forcings for an infinite time. Equilibrium beach profiles are generally based on assumptions of equal energy dissipation per unit volume or per unit area. Equilibrium beach concepts are very useful and comparatively simpler to use as they mask the details of specific wave-sediment interactions; however, most models in use predict only mono-

tonic beach profiles. In contrast to closed loop models, open loop models do not have a target profile. They generally consider detailed mechanics of the flow and sediment concentration profiles and variations of related quantities to compute sediment transport and resultant changes in the profile. A standard drawback of such an approach is the lack of model stability due to the lack of any explicit stabilizing mechanisms. In the present study, a rational, physics-based open loop cross-shore sediment transport model is developed. The model accounts for both suspended and bedload sediment transport. Effects of intermittent suspension, turbulence and momentum transfer due to wave breaking, augmented mass flux in the surf zone, the bottom boundary layer, wave asymmetry and gravity have been accommodated. Unlike most of the previous cross-shore sediment transport models, the present model was formulated requiring the fewest possible conditions as input: for a given beach, only the wave conditions at the toe of the beach are required. The model computes the wave field, the required hydrodynamics, the sediment transport and depth changes across the beach. No local information is required as the profile response unfolds. It is mentioned that the extensive modeling required for a comprehensive model can easily lead to an unwieldy set of components that obfuscate the essential physics of the total sediment transport process. With this in mind, each of the processes was modeled as simply as possible.

1.3 Overwash Process and Relevance to Barrier Islands

A variety of cross-shore sediment transport models is available for predicting dune erosion due to storms; however, the facet of overtopping and resultant overwash of sediment has been almost completely ignored. Prediction of overwashed sand, one of the focal points of the current study, is especially relevant for barrier islands. Overwash is one of the principal processes by which sediment is transported across the barrier island. Overwash occurs when storm surges allow waves to overtop the beach and push sand across the beach and dune zones. This results in the deposition of sand above the normal high tide mark and the creation of barrier flats. The frequency of occurrence of overwash depends on the frequency and magnitudes of storms and the barrier island profile. The magnitude of overwash depends on the exposure and

orientation of the barrier island, wave energy, tidal range and the ecological response of barrier island vegetation to the overwash process. The magnitude of overwash is particularly high when storms coincide with times of high astronomical tides. Overwash is the process by which barrier islands maintain their relative elevations to keep pace with rising sea levels.

Barrier islands are long, narrow, low-level offshore islands generally parallel to the coastline. These islands are generally characterized by a beach and dunes on the ocean side and salt marshes and estuaries on the mainland side and are bounded by tidal inlets (natural or man-made). Figure 1.1 displays most of the geomorphological features commonly present in barrier beaches. Most of the U.S. Atlantic coast south of Long Island and the coast along the Gulf of Mexico is composed of barrier islands. Gierloff-Emden reported in King (1972) that barrier islands compose over 13% of the world's coastline. In Florida, barrier islands represent about 50% of the shoreline. It is crucial to recognize that of all coastal island types, barrier islands are one of the most unique, dynamic, fragile and vulnerable landforms. Long-term forcings affecting their equilibrium include sea level rise, land subsidence and longshore drift, while short-term forcings include storm effects. During storms, barrier islands act as a physical barrier, protecting the mainland and bays behind them by absorbing the brunt of the attack of waves and storm surges. However, many of the barrier islands themselves are highly developed human habitats and protection of their beaches is a major concern at many locations.

The National Hurricane Center, Coral Gables, Florida, has estimated the magnitude of the storm surge for Category 5 hurricanes making landfall normal to the shoreline at 20 locations in Florida. Hydrographs were predicted with the use of SLOSH model. The locations, estimated peak surge elevation and rates of rise and fall of the storm surge are presented in Table 1.1. The peak storm surge ranges from 3.2 m and 8 m. As the maximum crest elevation of most barrier islands typically varies between 1.5 m and 4.5 m above mean sea level, low-level segments of the islands may frequently be totally inundated under storm surges whereas islands with higher crest elevations may experience substantial overtopping only under extreme

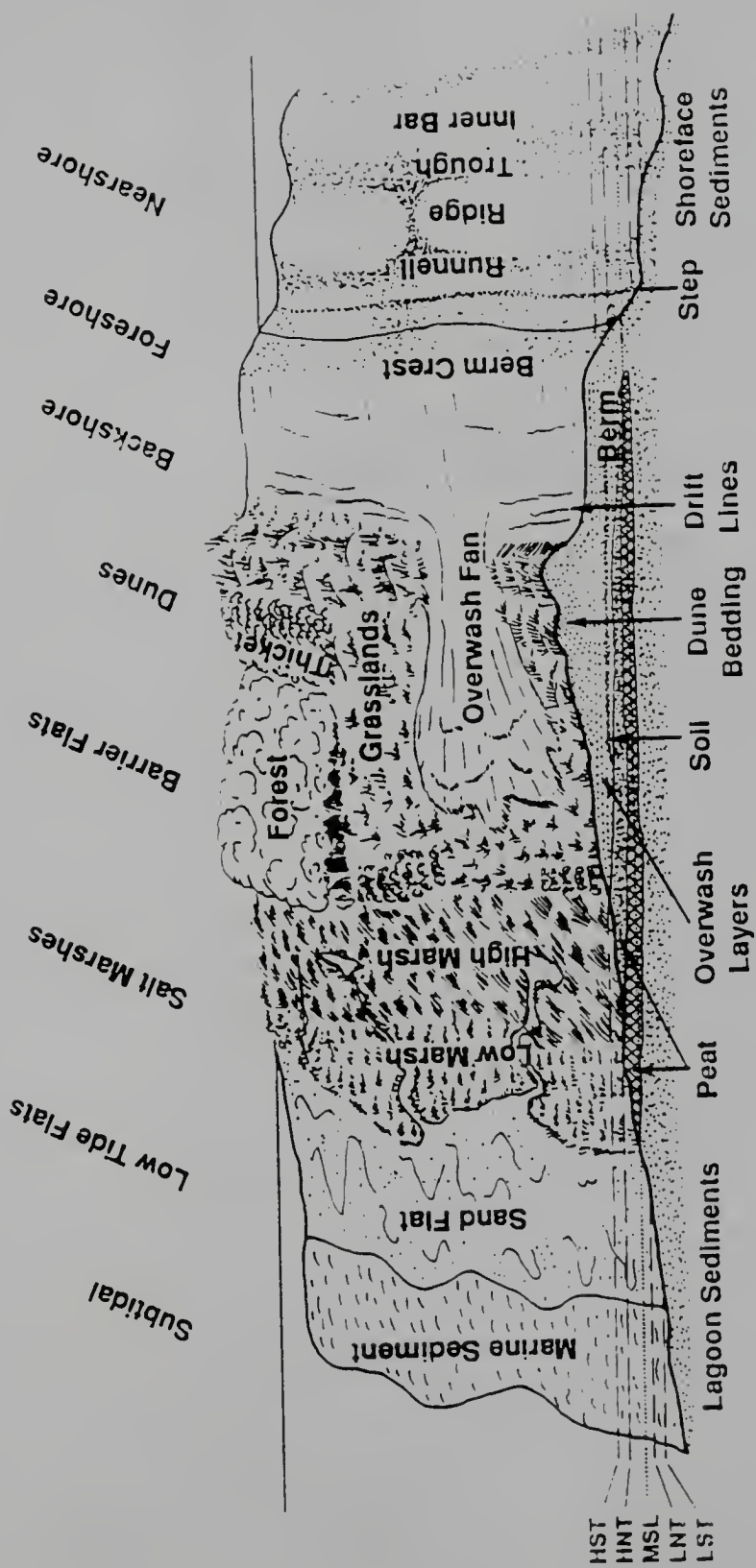


Figure 1.1: The barrier beach as a complete system (from Godfrey, 1976).

Table 1.1: Storm surge prediction for a Category 5 hurricane at 20 locations in Florida

Location	Peak Surge Elevation (m above MSL)	Rising Rate (m/hr)	Receding Rate (m/hr)
Pensacola Beach	3.8	1.8	5.8
Ft. Walton Beach	3.4	1.2	1.1
Panama City Beach	4.0	1.1	1.0
St. George Island	4.3	0.7	0.8
Wakulla Beach	8.0	2.8	1.3
Cedar Key	6.5	1.5	1.7
Clearwater Beach	6.1	1.8	4.4
Tampa Bay	7.8	2.3	1.4
Sarasota	5.7	1.9	2.2
Ft. Myers	6.9	1.7	2.1
Naples	6.6	1.4	2.3
Key West	3.2	0.6	0.6
Key Largo	3.4	0.9	0.7
Miami Beach	3.2	0.9	0.6
Palm Beach	3.7	1.0	0.9
Ft. Pierce	4.1	1.0	1.6
Cocoa Beach	4.4	1.0	1.1
Daytona Beach	4.0	0.6	1.2
St. Augustine	5.1	0.9	1.2

storm conditions.

Barrier islands often form a continuous beach extending, say, 3 km to 80 km between adjoining tidal inlets. Typical inlet widths are between 100 m and 1 km. The bay area (i.e., the waterway between the mainland and the barrier island) is connected to the sea only through these relatively narrow inlets. Hence, there is a substantial phase lag between the bay water level and the rapidly rising sea water level during storms. The differential hydrostatic head could be on the order of meters depending on the intensity and duration of the storm. If the island is already inundated, this gradient alone creates strong currents over the crest of the barrier island from the sea side to the bay side resulting in considerable erosion. Waves, in combination with these currents, further increase the erosion rate. It is interesting to note that the erosion of barrier islands can also take place with currents from the bay side to the sea during falling storm tides as torrential rains accompanying storms pile up large quantities of storm water within the bay area that cannot be quickly drained to the

sea through the narrow tidal inlets. A study of Hurricanes Carla (1961) and Cindy (1963) by Hayes (1967) showed that channels were cut in the barrier islands in Texas to a level below mean sea level. Significant amounts of sediment were lost from the barrier islands to the offshore by the flow of bay waters to the sea across the barrier island.

If barrier islands can be considered to be in long-term equilibrium, then storms can be considered to be episodic perturbations that result in considerable cross-shore reconfiguration.

1.4 Objectives

With the preceding discussion in mind and after a literature review revealed the lack of predictive tools to estimate overwashed sand volumes under overtopping conditions, it was decided to conduct experiments to simulate the effects of overtopping and overwash at barrier islands in the “air-sea” wavetank facility at the Coastal and Oceanographic Engineering Laboratory of the University of Florida. A laboratory provides a tightly controlled environment where important parameters and their effects may be isolated and studied, which is not readily possible in the field.

A physical model of the barrier island was developed with an initially horizontal crest and planar beach slope. The objectives of the present investigation involved monitoring the changes in the bed profile and identifying the resulting principal morphological features produced as a result of a variety of wave and tidal conditions. Longshore transport was minimized by using only unidirectional waves traveling normal to the shoreline. A common feature noted in all tests was surf zone erosion. As longshore bars were commonly generated, the next key objective was the elucidation of causative mechanisms, at least for the present conditions, for the pervasive longshore bars. Additional experiments were conducted for this purpose. Once the fundamental forcings were properly identified, the next objective was the modeling of hydrodynamics associated with cross-shore sediment transport and modeling concentration profiles associated with suspended load in the surf zone incorporating the additional effects of turbulence in stirring sediment. Equations for mean cross-shore flow were formulated

using recent experimental evidence. Bedload mechanisms causing onshore transport were also included as tests with overtopping conditions exhibited washover deposits over the crest of the barrier island. Finally, the ultimate objective was the formulation of a fairly comprehensive, physics-based sediment transport model including the above features and having the capabilities of predicting overwash and surf zone erosion and developing longshore bars.

1.5 Plan of Study

The following chapters document the investigation of the issues of overwash at barrier islands, longshore bar formation mechanisms, modeling of surf zone hydrodynamics and concentration profiles and the formulation of an “open loop” cross-shore sediment transport model having the capacity for both onshore and offshore transport. The sediment transport model was finally tested against data obtained from present laboratory experiments conducted to examine overwash. The format of the present investigation is slightly different from that prevalent: instead of having an all-encompassing literature review for all the above aspects right in the beginning, it was considered more logical to have literature reviews at the beginning of each of the above aspects as they were considered sequentially.

The investigation starts with Chapter 2, which documents the present physical modeling of the cross-shore sediment transport processes. Similitude considerations for the construction of the physical model of a barrier island and the experimental methodology of the present investigation including apparatus and procedure of experimentation are addressed. The laboratory investigations of overwash and longshore bar formation mechanisms are chronicled, and primary forcings and morphological signatures are identified and discussed.

Chapter 3 is devoted to modeling the relevant hydrodynamics that are associated with cross-shore sediment transport. Contributions to suspended transport arise from both first and second order (in wave steepness) wave effects. The formulation of undertow is examined and the choice of boundary conditions in different regions, as incoming waves shoal and break, are elucidated and inculcated.

The issue of representation of suspended sediments is discussed in Chapter 4 and the shear velocity due to breaking waves is evaluated taking into account the additional stirring effects of turbulence.

In Chapter 5, the equations for the numerical model of cross-shore transport process are formulated. Simple expressions for suspended and bedload transports are developed. The predictive capabilities of the model are tested using data from the overwash experiments. A discussion of model results, including limitations of the model, follows.

Finally, Chapter 6 presents a summary and documents the main conclusions of the present study.

CHAPTER 2 PHYSICAL MODELING OF CROSS-SHORE SEDIMENT TRANSPORT

2.1 Similitude Considerations

In order to achieve similarity between the model and the prototype in beach profile studies, several criteria have been recommended depending upon the principal phenomenon to be studied and the predominant active forces. Often, practical considerations such as the type and size distribution of bed material available for laboratory tests, size and capabilities of the available test facilities, funds and time available for study and the degree of accuracy desired are the governing constraints in laboratory investigations.

Some of the important similitude criteria recommended for scale model studies are based on the following:

- Froude Number
- Densimetric Froude Number
- Reynolds Number
- Bed Shear Velocity
- Friction Factor
- Kinematic Condition (ratio of horizontal to vertical displacement of sediment particles)
- Fall Velocity

The Coastal Engineering Research Center, U.S. Army Corps of Engineers (1979), conducted a comprehensive review of literature on similitude criteria for beach erosion investigations. A summary is presented in Table 2.1. The main conclusions were

Table 2.1: Comparison of various approaches for determination of basic scale ratios of coastal movable bed models (from Coastal Hydraulic Models, CERC, 1979).

Source	Basic relations	Method of derivation
Goddet and Jaffry (1960)	$n_D = \mu^{17/20} \Omega^{8/5}$ $n_{\gamma'} = \mu^{3/20} \Omega^{-3/5}$	Sediment motion due to combined action of waves and currents
Valembois (1960)	$\Omega = n_{\gamma'}^{-1}$ $n_{\gamma'} n_D^3 = 1$ $\mu = n_{\gamma'}^3 n_D \left(\frac{n_H}{\mu} \right)^4$	<p>Kinematic of motion of suspended sediments Similitude of D_s.</p> <p>Modified relation of initiation of sediment motion: $D_s = K R_*^{8/9}$</p>
Yalin (1963)	$n_D = \mu^{3/4} \lambda^{1/2}$ $n_{\gamma'} n_D^3 = 1$	Dimensional analysis
Bijker (1967)	$n_{\gamma'} n_D \Omega^{-1} = \mu n_{\mu r}$ <p>$\Omega \leftarrow$ equilibrium beach profiles</p>	<p>Similitude of F.</p> <p>Note: This relation was noted to be an error.</p>
Fan and Le Mehaute (1969)	$n_{\gamma'} n_D^3 = 1$ $n_{\gamma'} = \mu^3 \lambda^{-3/2} \text{ or } n_D = \lambda^{1/2} \mu^{-1}$ <p>$\Omega \leftarrow$ equilibrium beach profiles</p>	Similitude of sediment transport characteristics, i.e., F_s and R_s
Noda (1971)	$n_D n_{\gamma'}^{1.84} = \mu^{0.55}$ $\lambda = \mu^{1.32} n_{\gamma'}^{-0.386}$ <p>$\Omega \leftarrow$ equilibrium beach profiles</p>	Similitude of sediment transport characteristics, i.e., F_s and R_s

as follows. Complete similitude of all dynamic processes involved in the movement of coastal sediment is impractical. Similitude of certain dynamic processes fixes the relation between model and prototype linear dimensions, material characteristics and other factors. Therefore, no particular set of scale model laws for coastal sediment models was recommended. Each of the scale model laws given in Table 2.1 was believed to have its own special area of application, and the selection of the appropriate set of equations for a particular problem largely depends on the experience and expertise gained by the particular group of laboratory personnel performing mobile bed scale model tests.

Kemp and Plinston (1968) suggested a distortion relation for beach profile erosion study:

$$\frac{\lambda}{\mu} = (\mu)^\alpha \quad (2.1)$$

where

$$\begin{aligned} \lambda &= \frac{\text{model length}}{\text{prototype length}} \\ \mu &= \frac{\text{model depth}}{\text{prototype depth}} \\ 0.45 &< \alpha < 0.65. \end{aligned}$$

Noda (1972) has given a detailed account of scale model relationships for movable bed models. Data from experiments utilizing a number of materials and grain sizes suggested that the following relations need to be satisfied for reasonable similitude

$$\lambda = (\mu)^{1.32} (n_\gamma)^{-0.386} \quad (2.2)$$

$$n_D (n_\gamma)^{1.85} = \mu^{0.55} \quad (2.3)$$

where

n_D = ratio of sediment diameter in model to that in prototype

n_γ = ratio of relative specific weight of sediment in model to that in prototype

whereas data from experiments using sand suggested

$$n_D = \mu^{0.55} \quad (2.4)$$

$$\lambda = \mu^{1.32} \quad (2.5)$$

when $n_\gamma = 1$.

Dean (1973) and Kohler and Galvin (1973) have identified the importance of the dimensionless fall velocity parameter ($H/w_s T$) (now called the Dean number) as a criterion for berm-bar formation where H and T are the wave height and period, respectively, while w_s is the sediment fall velocity. Dean (1973) also noted the relevance of this parameter in modeling beach systems. Dalrymple and Thompson (1976) conducted a series of beach profile experiments in the laboratory and confirmed that

$$n\left(\frac{H}{w_s T}\right) = 1 \quad (2.6)$$

where n stands for the ratio of model to prototype, is the most promising scale relationship for modeling of beach processes. From earlier tests on dune erosion with two types of sand, van de Graaff (1977) found that the results of experiments with different sands compared very well using the Dean number concept. The movable bed model tests on dune erosion conducted by Vellinga (1978a,b) at the Delft Hydraulics Laboratory have found that equal Dean number values in model and prototype lead to geometrically similar beach profile development in the model.

It would be apparent from the above review of various similitude criteria that for the scale model study of beach profiles, dimensionless fall velocity criterion (Dean number) is the most appropriate and hence has been adopted for the present study. It is noted that disregarding exact Reynolds number similarity can potentially cause different flow conditions to exist in the model and the prototype. Since gravity is the predominant force for free-surface water waves in the ocean and in the laboratory, Froude similarity also needs to be achieved simultaneously, i.e.,

$$\frac{V_m}{\sqrt{g d_m}} = \frac{V_p}{\sqrt{g d_p}} \quad (2.7)$$

where V = velocity and d = depth; m and p denote model and prototype respectively. This directly leads to the time relationship for geometrically similar scale models as

$$\frac{T_m}{T_p} = \sqrt{\frac{l_m}{l_p}} \quad (2.8)$$

where l denotes the length scale.

According to Stokes' law, fall velocity, w_s , of a sediment particle is given by

$$w_s = \frac{1}{18} \frac{D^2 g (\gamma_s - \gamma_f)}{\nu} \quad (2.9)$$

where

D = diameter of sediment particle

g = gravitational acceleration

ν = kinematic viscosity of fluid

γ_s = specific weight of sediment

γ_f = specific weight of fluid

For the present study the prototype sediment diameter (D_p) was considered to be 0.5 mm. This corresponds to medium-sized sand which occurs on several barrier islands. Size gradation analysis of sand available for the model study showed that the median diameter (D_m) was 0.2 mm (Figure 2.1). Based on the standard relationship (e.g., Vanoni 1975) for fall velocity, $w_{s,p} \sim 0.09$ m/sec and $w_{s,m} \sim 0.023$ m/sec.

The dimensionless fall velocity criterion (Equation 2.6) specifies that

$$\left(\frac{H}{w_s T}\right)_m = \left(\frac{H}{w_s T}\right)_p \quad (2.10)$$

whereby

$$\frac{H_m}{H_p} \frac{T_p}{T_m} = \frac{w_{s,m}}{w_{s,p}} \quad (2.11)$$

Therefore, using Equation (2.8) and substituting for the fall velocities,

$$\frac{l_m}{l_p} \sqrt{\frac{l_p}{l_m}} \sim \frac{1}{4} \quad (2.12)$$

whence

$$\frac{l_m}{l_p} = \frac{1}{16} \quad (2.13)$$

Hence, a geometrically similar scale of 1:16 was adopted for the present study. Thus, all length and time scales in the prototype were 16 and 4 times those in the model, respectively.

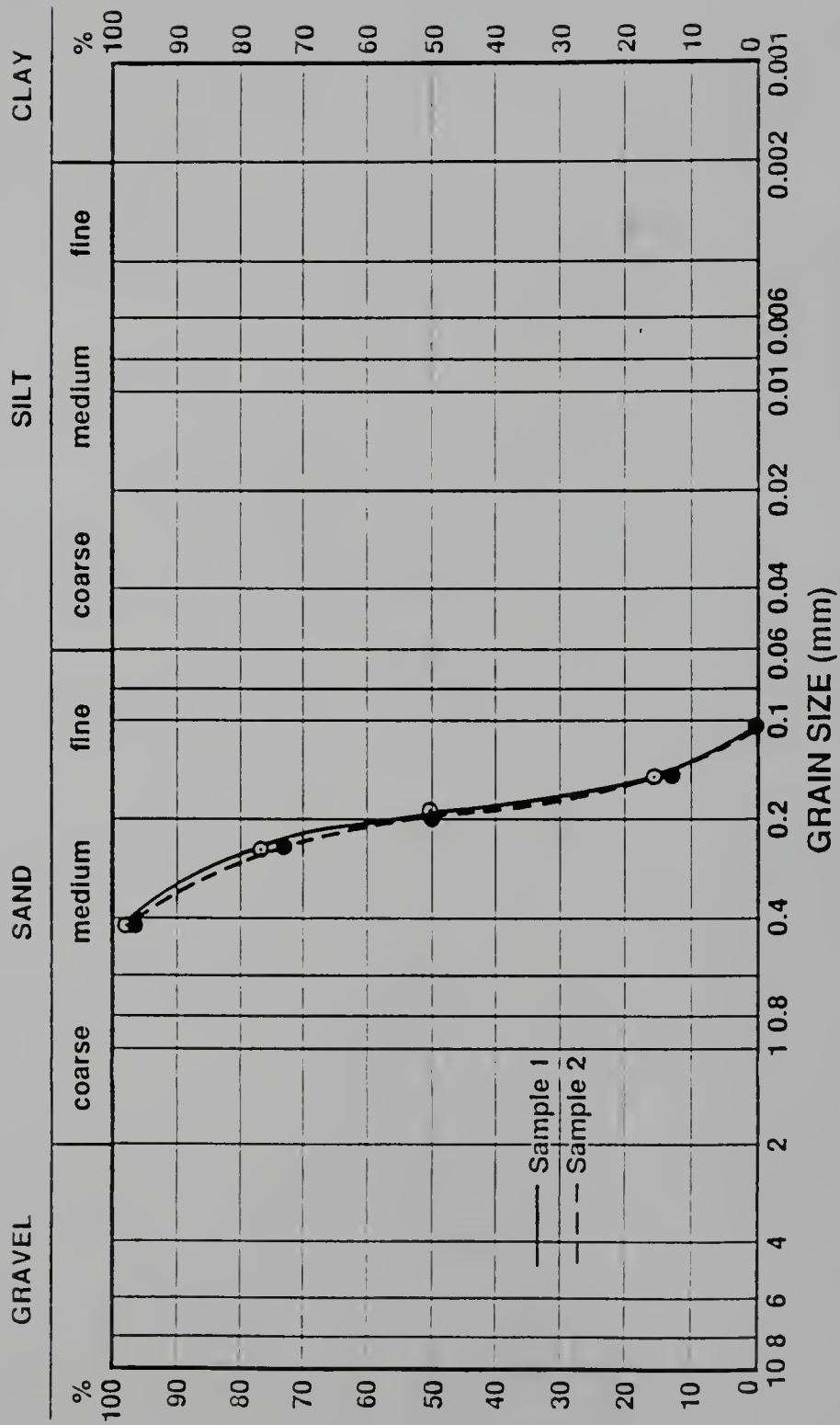


Figure 2.1: Size distribution of sand used in the present study.

2.2 Laboratory Facility and Apparatus

All experiments were conducted in the air-sea tank facility at the Coastal and Oceanographic Engineering Laboratory of the University of Florida. The tank was approximately 37 m long, 2 m wide and 1.9 m deep (Figure 2.2). A concrete block wall (splitter wall) had been placed along the tank centerline dividing it into two tanks each approximately 0.9 m wide. One outer wall was constructed of glass panels and all experiments were conducted in this side of the tank thereby facilitating direct observation. A wave generator was located at one end of the wave tank with hydraulic drive pistons at two elevations allowing piston, flap or a combination of motions to be generated. The paddle of the wavemaker was made of wood and was driven by a two-level rod and bearing system connected to a hydraulic power unit. The wavemaker was capable of generating regular or irregular waves. Wave signals for operating the wavemaker were generated using a SeaSim Function Generator and a Pegasus Servo Controller/Amplifier or an IBM-compatible PC. The wavemaker was fronted by wave screens to prevent cross-tank variation. The splitter wall along the tank centerline was separated from the wave maker by approximately 2 m; at the downwave end of the tank (beyond the beach), the splitter wall was composed of concrete blocks with horizontal openings, thereby allowing circulation around the splitter wall in cases of overtopping. A sloping frame with artificial "horse hair" and permeable nylon bags filled with pebbles was located at the downwave end of the tank side which was not used for the experiments. The toe of the beach of the barrier island was about 21 m from the wavemaker. The barrier island and beach were 18 m in extent.

Rails were located along the top of the tank and an electrically operated trolley was mounted on the rails for transporting a carriage containing a measuring equipment package along and across the wave tank. A resistance wave gage was used for measuring wave height and period. The gage was mounted on the carriage and it could be moved to any location within the tank for wave measurements. The wave gage was calibrated each time before data acquisition in order to eliminate errors caused by changes in water temperature or other factors.

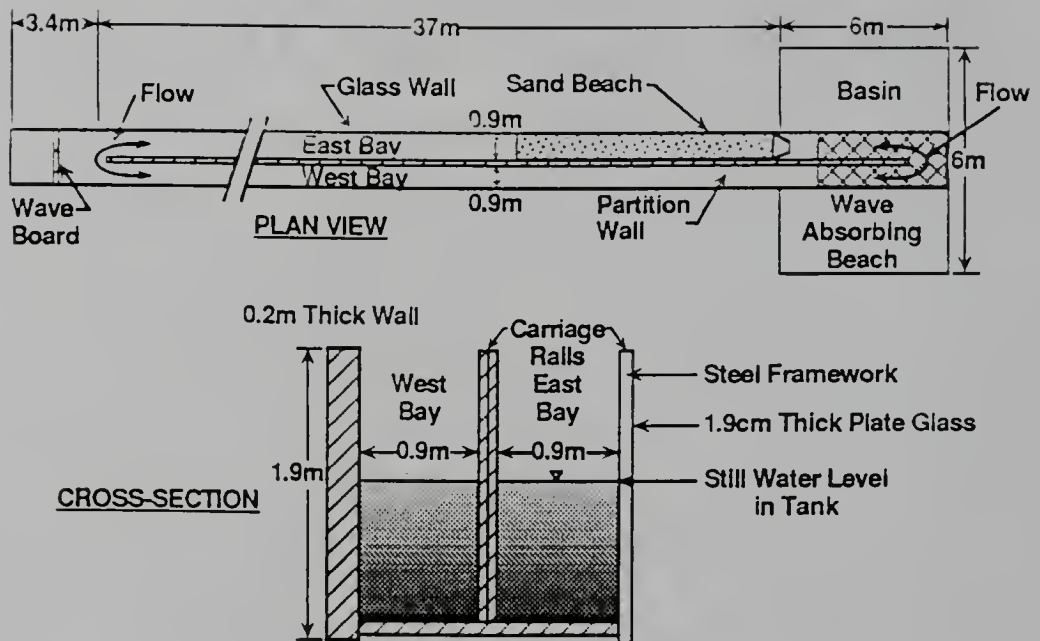


Figure 2.2: Schematic layout and cross-section of wave tank facility.

An additional apparatus was required for later experiments (Section 2.4) investigating the role of long waves in causing/affecting bar formation. This was a mechanical filter in the form of a manometer and stilling well arrangement which recorded long waves ("surf beat" or infragravity waves) while damping the short, primary waves. This approach was first used by Dally (1987b) and consisted of three 5 m sections of plastic tubing of increasing cross-sectional diameter joined together and connected to a fourth section which acted as a stilling well. The open end of the tube with smallest diameter served as a wave pressure sensor when placed along the bed and a resistance wave gage was mounted inside the stilling well. This gage recorded the long waves of the total wave system.

An automatic bed profiler mounted on the carriage was used for measuring the beach profiles at various time intervals during the course of an experiment. An electric motor drove the carriage at a constant speed along the length of the wave tank and, simultaneously, the bed sensor automatically moved up or down, closely following the bed profile by maintaining a fixed gap, adjustable from 0.5-3 mm, between the tip of the sensor and the bed. The direction of travel of the carriage could be reversed and the carriage speed varied to suit the requirements of data acquisition.

Bed elevation data, as a function of distance measured with respect to a pre-defined coordinate system, were stored on computer hard disks and magnetic diskettes. A DEC PDP/11 (LSI 1103) computer was used in the overwash experiments to acquire data, while later, more refined experiments to investigate bar formation mechanisms used an IBM-compatible 386 PC with the GLOBLAB program for data acquisition, display and analysis. A Data Translation 16 channel A/D converter was connected to all the data sources and the computer. The wave data were also stored on magnetic diskettes and were subsequently processed using either a VAX 8350 computer or an IBM-compatible PC and plotted using a laser plotter.

Since the effects of storm waves with overtopping conditions were to be examined, it was expected that sand from the island would be transported to the lee of the barrier island. Hence, a spout was provided on the leeside and arrangements were made for collection and weighing of the sand washed over the crest of the barrier island.

2.3 Investigation of Overwash

2.3.1 A Brief Literature Review

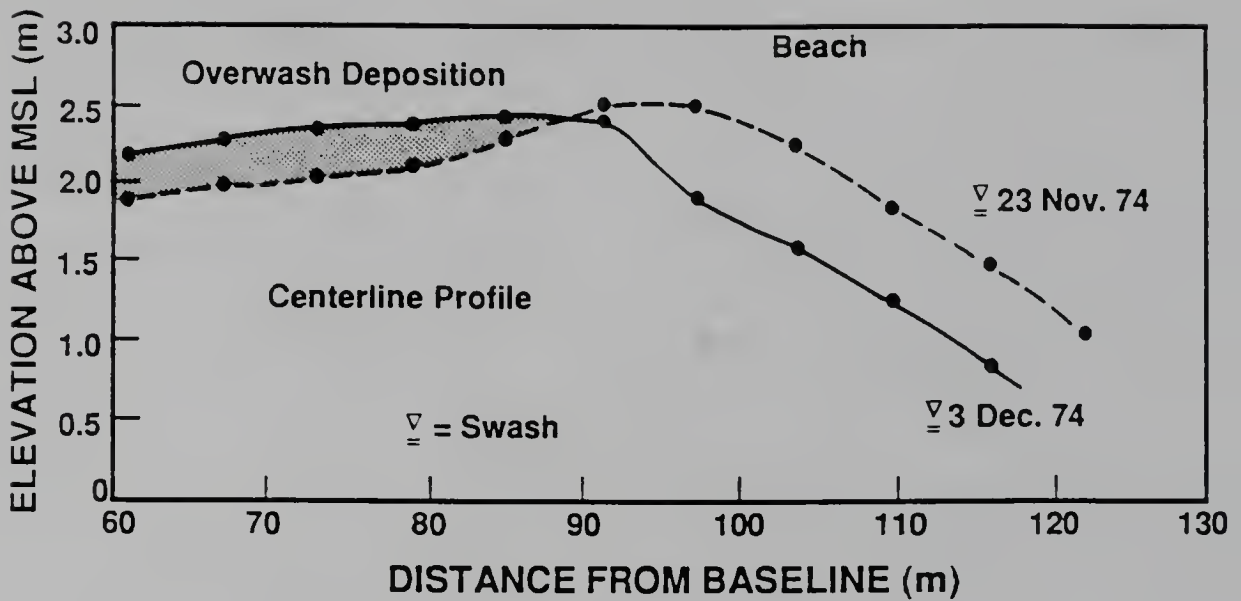
Several field studies have been conducted regarding geological processes, ecological aspects and management plans for barrier islands (including Fisher 1968, Swift 1975, Godfrey 1976 and 1978, Godfrey and Godfrey 1976, Leatherman 1977; Davis et al. 1979 and Stauble 1989).

Studies of the overwash process have been conducted almost exclusively by geologists. Early qualitative descriptions of the overwash process in the field were reported in Johnson (1919) and Lobeck (1939). Price (1947) noted the importance of storm surge for and defined specific terms associated with the overwash process. Hayes (1967) discussed the effects of Hurricanes Carla (1961) and Cindy (1963) on barrier islands in Texas. Godfrey (1970) studied the effects of the overwash process at the Outer Banks, North Carolina (NC) and concluded that overwash was a major cause of shoreline recession between Beaufort and Ocracoke Inlets. He also noted the fact that overwash allowed the barrier island to maintain its dynamic equilibrium with a rising sea level. Dolan (1972) examined barrier islands in NC where foredunes had been constructed to lend stability. He concluded that this stabilization, which prevented the overwash process from occurring, resulted in a decrease of beach width. Dolan and Godfrey (1973) examined the effects of Hurricane Ginger (1971) on stabilized and unaltered barrier islands of the Outer Banks, NC. There was severe erosion seaward of the crest of the foredune at Cape Hatteras (stabilized) and severe erosion of the dune at Core Banks (unaltered). Core Banks gained sand on the bayside of the foredune line while the stabilized barrier islands did not. From pre- and post-storm survey data, they concluded that unaltered barrier islands were better suited to withstand severe hurricanes. Surveys conducted about ten months after the hurricane showed the profile at Core Banks actually gained sand due to post-storm recovery. Leatherman (1977) reported that Assateague Island, Maryland, experienced an overwash deposit of the order of 2.8 m^3 per m width of dune during the storm of March 1975.

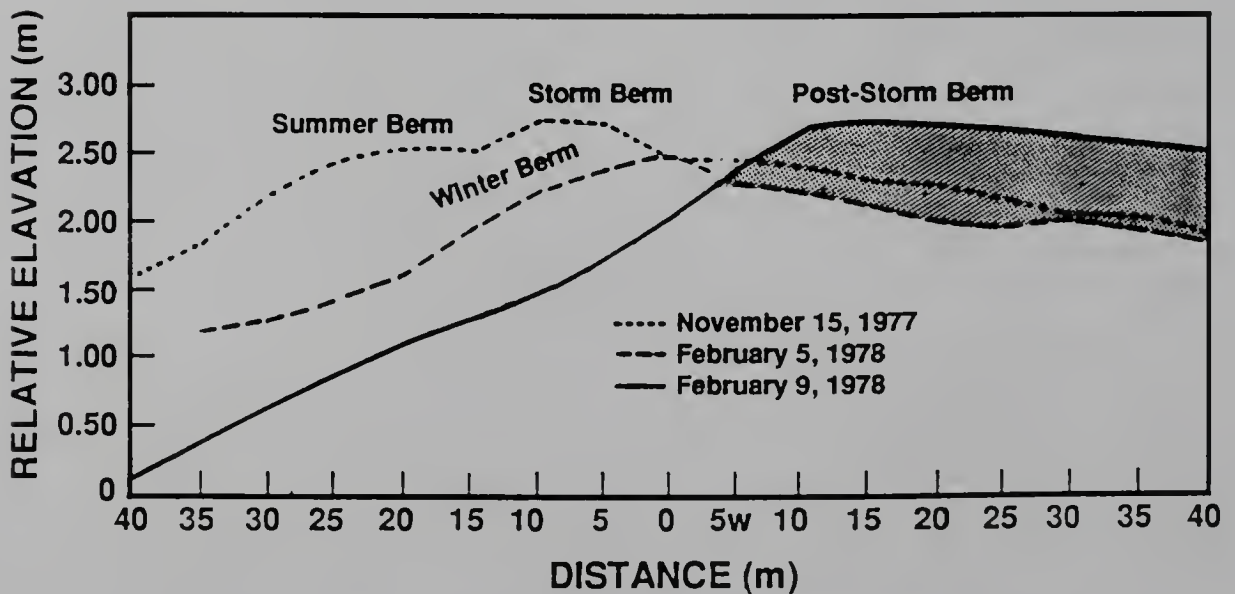
Leatherman (1979b) documented field observations at two sites: (i) Assateague Island, Maryland, along the mid-Atlantic coast for the December 1974 storm and (ii) Coast Guard Beach, Nauset Spit, Cape Cod, Massachusetts, for the February 1978 storm. Figure 2.3 shows the storm-induced changes along the centerline profile. At Assateague Island, the beach was characterized by medium-sized sand (0.3 mm) and a beach foreshore slope of 5 degrees. The mean tidal range was 1.1 m. During the storm of December 1, 1974, breaking waves of about 2.7 m were observed from the shore. The calculated significant wave height was 5 m in deep water, and the storm surge was 0.8 m. The beach experienced erosion of 10.2 m^3 per m length of beach. The dune lost 7.1 m^3 per m of beach sand and the dune crest was displaced 4.6 m landward. Dune erosion averaged from several profiles was calculated to be 5 m^3 per m of beach. An important conclusion drawn from the analysis of sand samples was that there was no evidence of beach sediment coarsening nor steepening of the beach profile as a result of the severe storm.

The sediments at Nauset Spit were medium-sized sand (0.4 mm), and the beach slope was rather steep (11 degrees). The mean tidal range was 2 m. During the storm of 6-7 February 1978, the significant deep-water wave height was about 5 m. The nearshore breaker heights exceeded 3 m, and the maximum storm surge was about 1.2 m. Comparisons are made here with respect to the winter (2/5/78) profile (Figure 2.3). As a result of this storm, the berm crest receded about 20 m with a loss of about 30 m^3 per m of beach. Large quantities of sediment were pushed across the berm by overwash surges and deposited as an overwash fan. The volume of overwashed sand was about 102 m^3 per m of beach. The overwash deposition thickness was up to 1.7 m above the living marsh and penetration distances extended up to 140 m landward of the dune line.

Williams (1978) conducted the only previous laboratory investigation of overwash. The experiments were conducted in a wave tank which was 30 m long, 2.5 m wide and 1.5 m deep. Only monochromatic waves were generated. The beach was composed of reasonably uniformly sorted sand with a median grain size of 0.21 mm. The barrier island was simulated with an initial profile slope of 1:15 on the seaward side and 1:40



Beach erosion and overwash deposition following the 1 December 1974 northeasterly storm at Assateague Island, Md.



6-7 February 1978 northeasterly storm resulted in severe beach erosion and overwash deposition at Coast Guard Beach, Nauset Spit, Ma.

Figure 2.3: Field measurements of beach erosion and overwash, Leatherman 1979.

slope landward of the beach crest. Each test comprised three phases. The first phase was the formation of an equilibrium profile. This generally required a period of six to ten hours. After the formation of the equilibrium profile, the water level in the tank was increased gradually in the second phase to a level at which overwashing of the beach crest commenced due to wave runup. In the third phase, the storm surge level was increased further by about 10 to 25% of the vertical difference between the dune crest-elevation and the water level at which overwash commenced. The tests were then carried out until overwash had occurred to the point that the resulting deposits prevented further overwash. The washover deposits exhibited some three-dimensionality in the relatively wide (2.5 m) tank. In all, 22 tests were conducted and the results from the best 10 tests were utilized to evaluate two proposed relationships for predicting the washover volumes. It was found that the predictive relationship was better for larger washover volumes. The best fit line agreed with the laboratory data to within approximately $\pm 50\%$.

The first model considered the overwash transport rate, q_s , to be proportional to the excess runup raised to an exponent α , i.e.,

$$q_s = \frac{K_1}{T}(A(t) - A_*)^\alpha \quad (2.14)$$

where q_s is the volumetric sediment discharge rate per unit width and K_1 is a dimensional coefficient. $A(t)$ is the excess runup in the elapsed time defined as the difference in elevation between the potential runup and the crest of the dune or structure, A_* is the critical excess runup defined as the minimum height which the potential runup must exceed the crest of the dune for sand to be transported and T was the wave period. The second model expressed the overwash sediment transport rate as a rapidly increasing function for small values of excess runup and asymptotically approaches zero for larger values of runup:

$$q_s = \frac{K_2}{T}(A(t) - A_*)e^{-K_3(A(t) - A_*)} \quad (2.15)$$

where K_2 and K_3 were dimensional coefficients.

A non-linear least-squares fit was used to determine the coefficients for both the

relationships. No attempt was made to apply the predictive relationship to prototype events because the method required data on the time-varying storm surge and assumed that the dune height was constant during the event.

The values of the coefficients were quantified as follows:

$$\begin{array}{lll} \text{Model I:} & K_1 = 0.09 & \alpha = 0.04 \quad A_* = 0.4 \\ \text{Model II:} & K_2 = 0.24 & K_3 = 0.66 \quad A_* = 0.32 \end{array}$$

Other laboratory studies with particular emphasis on overwash are not available.

The results of field investigations and model studies are often used to calibrate and supplement the analytical expressions developed for achieving predictive capabilities. Theoretical developments relative to overwash and beach erosion may be classified in two areas, namely, hydrodynamics of breaking waves and sediment-wave interaction. Hydrodynamics associated with wave breaking inside the surf zone have been studied by several researchers including Dally (1980), Dally and Dean (1984), Svendsen (1984a, b), Dally et al. (1985), Stive and Battjes (1985), Stive and Wind (1986) and Stive (1988). Models of sediment-wave interaction have been given by Kemp (1960), Inman and Bagnold (1963), Meyer (1972), Dean (1973), Swart (1976), Bowen (1980), Bailard (1981), Bailard and Inman (1981) and Trowbridge and Young (1989) among others. Pertinent models for wave-induced hydrodynamics and sediment transport are reviewed later as required, in Chapters 3, 4 and 5.

2.3.2 Scope of the Overwash Experiments

The objective of this stage of the present laboratory study was to measure changes in the profile of a barrier island due to storm waves with various sea levels including those which cause overtopping and inundation and concomitant overwash.

The topography of barrier islands prone to overwash can vary substantially, though low-relief barrier islands will be more prone to substantial overtopping during storm surges. The present laboratory study was not intended to be site-specific. Instead, a hypothetical barrier island with an arbitrary crest width of 122 m and a beach slope of 1:19 was considered for simulation. All dimensions in the overwash

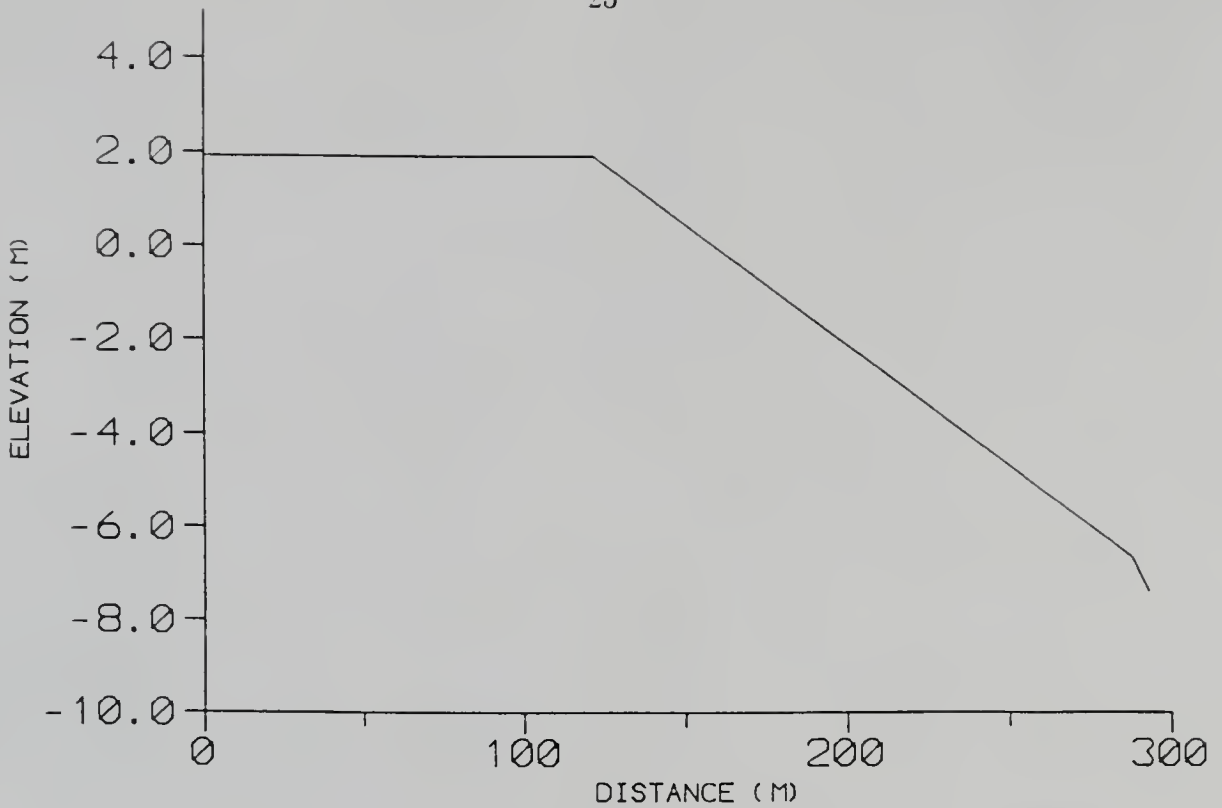


Figure 2.4: Initial beach profile in the wave tank for each experiment.

study (only) are in prototype units unless otherwise mentioned. As discussed in Section 2.1, a geometrically similar scale of 1:16 was adopted for the present study. The laboratory studies were conducted in a wave tank facility which was described in Section 2.2. The wave direction was always normal to the beach. Experiments were conducted for different sea water levels and both regular as well as irregular waves were simulated. For each experiment, the initial beach profile was linear from the crest of the barrier island to the toe (as shown in Figure 2.4). This provided a common reference profile for comparison of profiles obtained under different experimental conditions.

Vegetation on the barrier island could have a significant effect on the magnitude of erosion and overwash at some of the field sites, however, this factor was not taken into account in the present study and all the experiments reported here were carried out to represent barrier islands with no significant effects of vegetation. Also, the ecological aspects related to erosion and deposition have not been considered in the present study. The bay water level was the same as the sea water level in the present

study.

The nominal characteristics of the prototype for the nine experiments conducted in this stage were as described below:

- Initial crest elevation of barrier island – The entire island had an elevation of 1.9 m above the still water level for all the experiments.
- Initial beach profile – Linear with 1:19 slope, constant for all tests.
- Water depth at toe of beach – 7.3 m below mean sea level.
- Sediment – Fine sand with a median diameter of 0.2 mm (see Figure 2.1). No shells or protective armor layer were included.
- Still water level – The following water levels were used to simulate storm conditions:
 1. Mean Sea Level (MSL), referred to as zero.
 2. 1.9 m above MSL (same as the island crest): “marginal” overtopping.
 3. 3 m above MSL (causing complete inundation): “moderate” overtopping.
 4. 3.5 m above MSL (causing complete inundation): “severe” overtopping.
 5. Time-varying water level with peak surge of 3.4 m.
- Incident waves (storm conditions):
 1. Regular waves with a height of 2.6 m and a period of 8 seconds.
 2. Irregular waves with a mean period of 8 seconds and a range of 7.6-8.4 seconds (narrow-banded spectrum) with a maximum height of 2.6 m.
- Time of wave action – 18 hours.

2.3.3 Procedure, Measurements and Test Conditions

As previously mentioned, in the following description of the overwash experiments, unless noted otherwise, all quantities are presented in prototype units. Thus, all the

model data have been converted to equivalent prototype values in all beach profile plots for convenience of interpretation. Experiments were conducted in the wave tank for examining the reconfiguration of an initially horizontal crested barrier island with a planar beach subjected to regular and irregular waves and different water levels.

The initial profile of the barrier island was first laid out on the glass walls of the side of the wave tank. This outline helped in the construction of the profile. A vertical scale was affixed on the glass side wall at the position of the toe of the beach for monitoring the water level and for rough measurements of wave heights.

The barrier island was molded to conform to the initial profile, as specified in Figure 2.4, with the help of trowels, shovels and the human hand. Compaction of sand was achieved by spraying water on the sand and stepping on the sand repeatedly until the profile was smooth. The next step was filling the wave tank to the desired level with water using the city water supply.

The wave gage was calibrated before the start of each experiment by immersing known depths of the resistance wire on the gage in water and recording the corresponding voltages on the computer. A least-squares procedure was utilized to fit a straight line through the calibration points and establish the voltage to depth of immersion (linear) relationship.

The laboratory measurements included the following:

- Each experiment was started with a remolded linear profile from the crest of the island to the toe of beach as shown in Figure 2.4. The crest of the barrier island was horizontal and the entire profile was measured at the beginning of each experiment.
- Under wave action, the initial linear profile was changing with time during the course of an experiment. The resulting beach profiles were measured in the wave tank at intervals of 30 minutes (model units) using a bed profiler which provided data on bed elevation as a function of distance. The number of measured bed profiles for each experiment ranged from at least 2 to a maximum of 9, depending upon the reach and the variability of bed forms. Two profiles, designated as B1

and B2, were measured covering the entire length of the barrier island and the beach. Profile B1 was 0.25 m from the glass side wall while profile B2 was 0.25 m from the splitter side wall. In addition, for some of the experiments, where a three-dimensional bed pattern was noticed visually, an additional seven profiles were measured over a smaller area of the tank where the three-dimensional feature was evident.

- Wave heights were measured at various locations along the flume.
- Wave induced surface currents over the barrier island were measured using weighted floats in those cases where the barrier island was submerged.
- The weight of sand transported over the crest of the island was measured every 30 minutes (model units) by collecting it in a bucket and weighing it on a platform balance. These measurements were made only in those tests when the crest of the island was totally submerged with accompanying overwash. However, the maximum amount of sand collected over the extent of any experiment was only ~ 18 kg as most of the transported sand was in suspension which caused it to be transported over and across the sand trap. The measured weights were thus discounted and are not mentioned hereafter.

In all, nine experiments were conducted during the course of the study. The experimental conditions of these tests are summarized in Table 2.2. These experiments were divided into the following three groups.

Group 1 – Experiments E1 to E4

Under this group, the effect of raising the sea water level from MSL to complete inundation of the barrier island (as can often occur under high storm surges) was studied. These experiments were conducted with the water level at MSL, 1.9 m above MSL which corresponded to the crest level of the barrier island, 3.0 m above MSL (1.1 m inundation of island) and 3.5 m above MSL (1.6 m inundation of island), respectively. Regular waves with nominal dimensions of 2.6 m height and 8 seconds period were allowed to impinge upon the beach and each experiment was conducted

Table 2.2: Experimental conditions of tests (E1-E9) of overwash study (prototype units).

Expt. No.	Water Level		Wave Characteristics		
	Duration (hrs)	Level (ft)	Type	Height (ft)	Period (sec)
1	0--18	MSL	Regular	7.0	8.0
2	0--18	+6.3	Regular	8.5	8.0
3	0--18	+10.0	Regular	8.5	8.0
4	0-22	+11.5	Regular	8.5	8.0
5	0--6	MSL	Regular	8.5	8.0
	6--8	+0.5			
	8--10	+2.90			
	10--12	+6.82			
	12--14	+10.24			
	14--16	+11.30			
	16--18	+10.24			
	18--20	+6.82			
	20--22	+2.90			
	22--24	+0.50			
6	0--22	MSL	Random	7.0	7.6
7	0--18	6.3	Random	7.0	8.0
8	0--18	+10.0	Random	7.0	8.0
9	0--18	+11.5	Random	7.0	8.0

Table 2.3: Variation in the magnitude of storm surge parameters.

Condition	Minimum	Maximum
Peak storm surge	3.2 m	7.8 m
Rising rate	0.6 m/hr	2.3 m/hr
Receding rate	0.6 m/hr	5.8 m/hr

over a duration of 18 hours of prototype time which is equivalent to 4.5 hours model time. The duration of test was based on two criteria: 18 hours represent a fairly long duration for a severe storm, and the model beach profiles were seen to attain quasi-equilibrium and not significantly change beyond this test duration.

Group 2 – Experiment E5

Experiments under Group 1 and Group 3 were conducted under conditions of a steady storm surge level for 18 hours. In nature, the maximum storm surge level may not last longer than one or two hours. Three examples of storm surge estimates made by the National Hurricane Center are shown in Figure 2.5 where zero hours denotes the instant of landfall. At Tampa Bay, the rate of rise of water level is 2.3 m/hour and the rate of fall is 1.4 m/hour. At Pensacola, the rate of rise (1.8 m/hour) is slower than the rate of fall (5.8 m/hour) whereas the rates are equal for Key West (0.6 m/hour). The range of variation in the magnitudes as seen from Figure 2.5 is presented in Table 2.3. For purposes of preliminary study, equal rising and receding rates of 0.39 m/hour and a peak storm surge of 3.5 m above MSL were considered for simulation. Only one experiment was conducted which consisted of simulation of a storm surge hydrograph instead of a steady storm surge level. The effect was simulated by a series of stepped increases and decreases of the water level with each time step lasting two hours. The beach was first allowed to reach near-equilibrium by subjecting it to waves at MSL conditions for 6 hours before the onset of the storm. The storm surge simulation (after the aforementioned 6 hours) used in Experiment E5 is shown in Figure 2.6.

Group 3 - Experiments E6 to E9

Under this group, irregular waves were used with nominal dimensions of significant wave height and mean zero crossing period equivalent to 2.1 m and about 8 seconds,

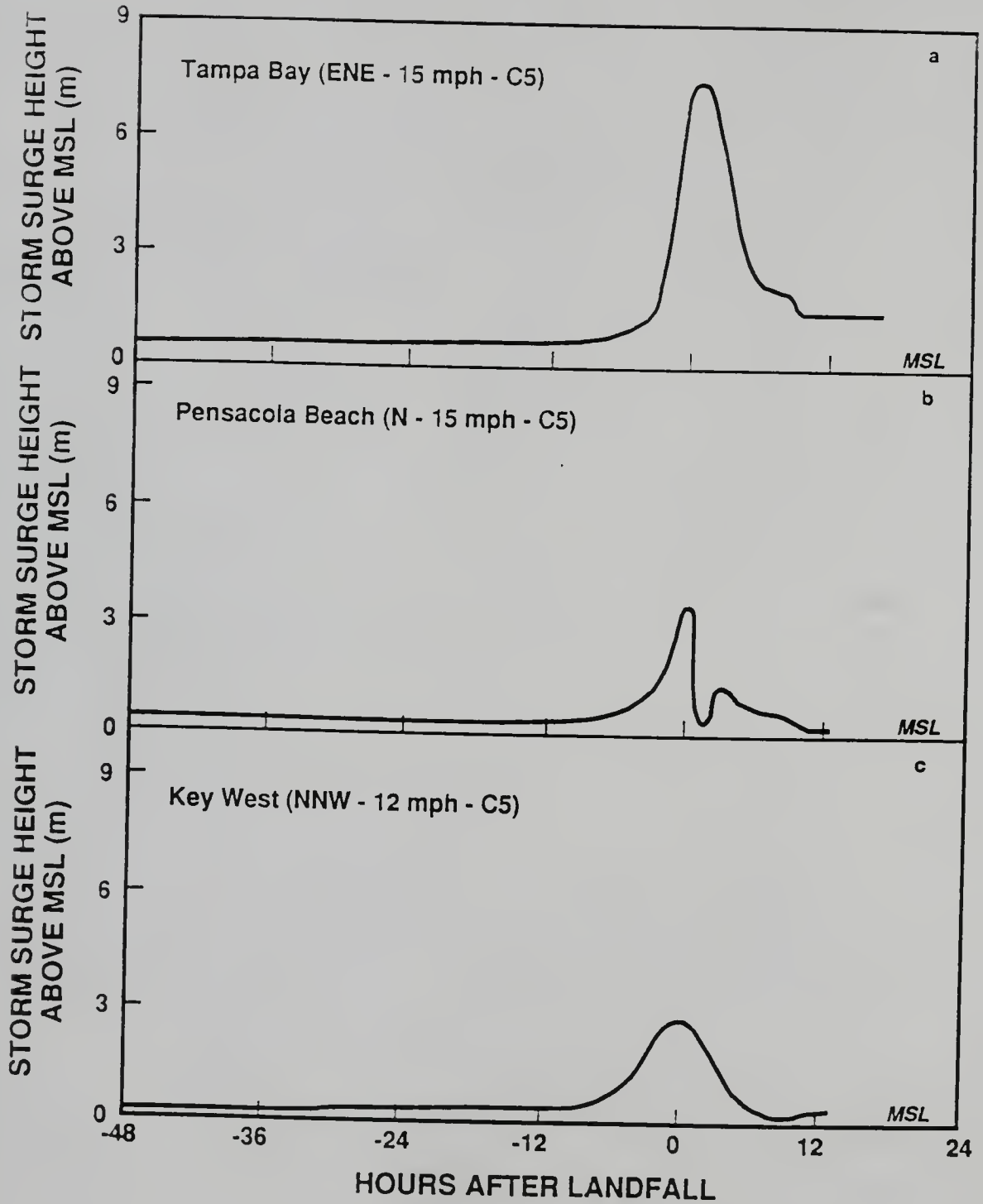


Figure 2.5: Illustration of estimated rising and falling storm surges.

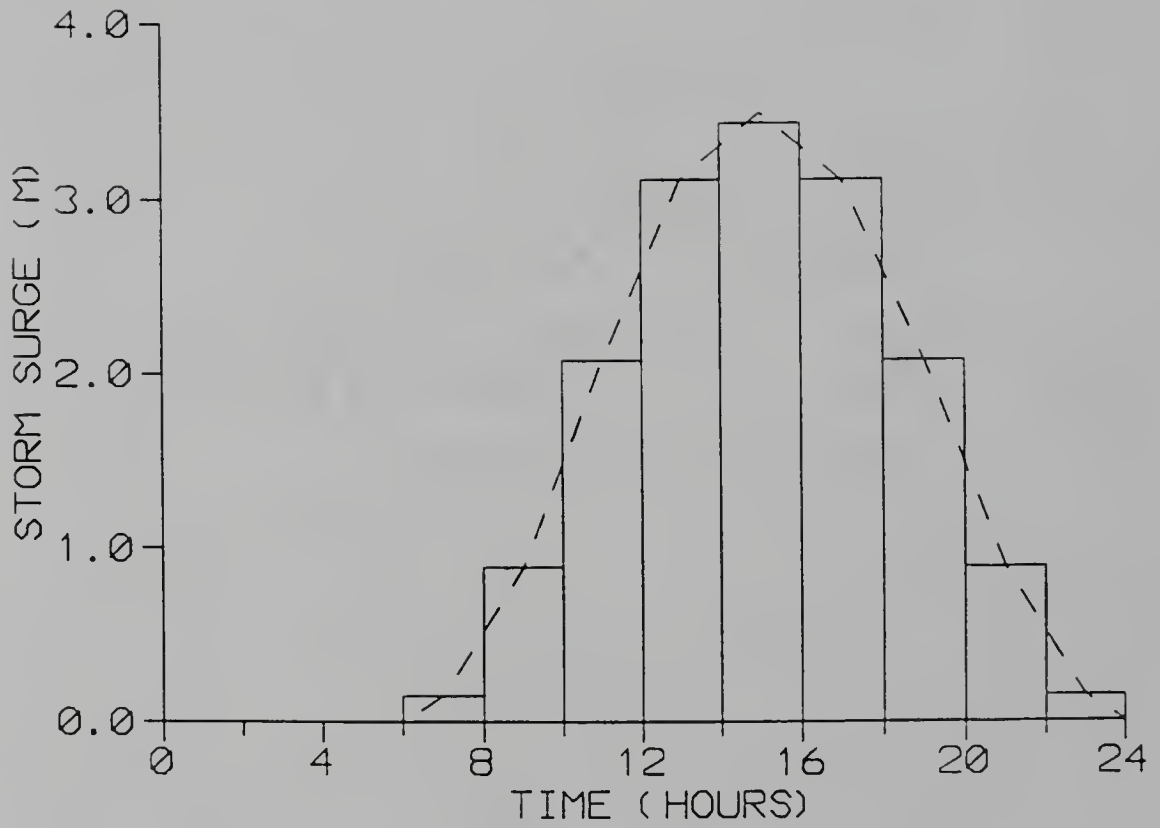


Figure 2.6: Storm surge simulation used in Experiment E5.

respectively, i.e., the wave heights and periods were maintained to be as close as possible to those of Experiments E1-E4 for comparison of results. The same storm surge levels were simulated for the irregular wave experiments as described previously for experiments involving regular waves, namely - MSL, 1.9 m above MSL which corresponds to the crest elevation of the barrier island, 3.0 m above MSL and 3.5 m above MSL.

2.3.4 Results

Wave data

An example of the evolution of a typical wave train in the wave tank is presented in Figures 2.7, 2.8 and 2.9. The data are for Experiment E4. Waves are symmetric towards the toe of the beach and develop vertical asymmetry as they approach breaking. After breaking, the waves are markedly asymmetric and resemble the classic “saw-tooth” shape over the crest over the barrier island.

Typical examples of an irregular wave train and the associated energy spectrum at the toe of the beach for Experiment E7 are presented in Figures 2.10 and 2.11.

Bed profile data

As mentioned before, 2-9 profiles were measured every 30 minutes. The mean profile was calculated using all measured profiles. The following discussion references the mean profile unless otherwise mentioned. The landward end of the barrier island was taken as the zero reference for measurements of distance. The seaward crest of the barrier island was then at 122 m and the toe of the beach at 288 m.

Sources of error in beach profiling. The automatic bed profiler needed calibration for each profile and this involved the voltage output corresponding to two “known” elevations which were chosen as those of the water surface and the bed far offshore (at 122 m) which was considered to be unaffected by the wave action. However, due to leakage, etc., the water level could not be monitored as effectively as desired and, also, the bed level at 122 m was noticed to change slightly with time. These are two possible sources of error in the bed profiles in terms of elevation. A combination of magnets embedded in the wheels of the trolley and a “Hall-effect” sensor established

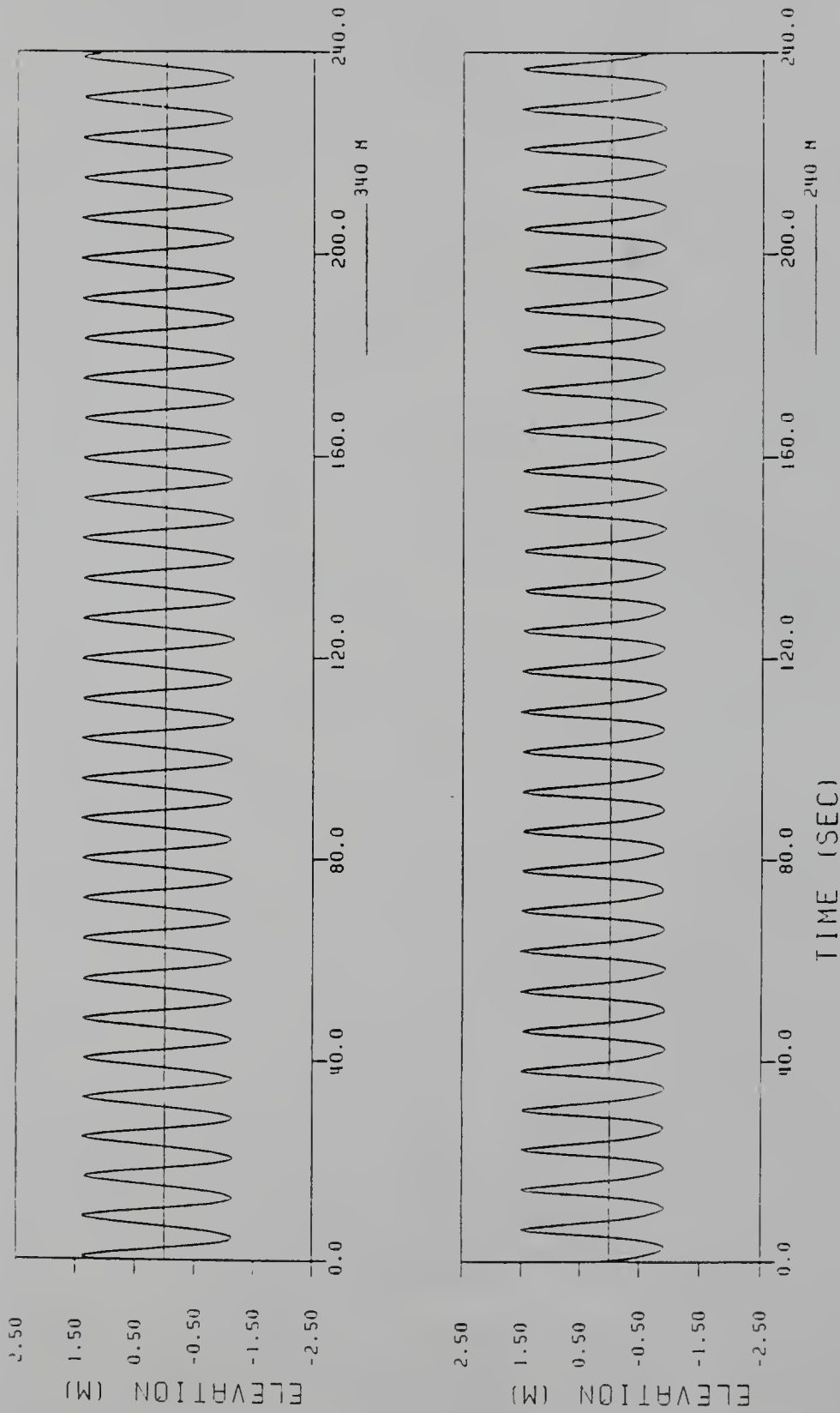


Figure 2.7: A regular wave train (Experiment E4) (a) seaward of the toe of the beach (340 m), and (b) landward of the toe of the beach (240 m).

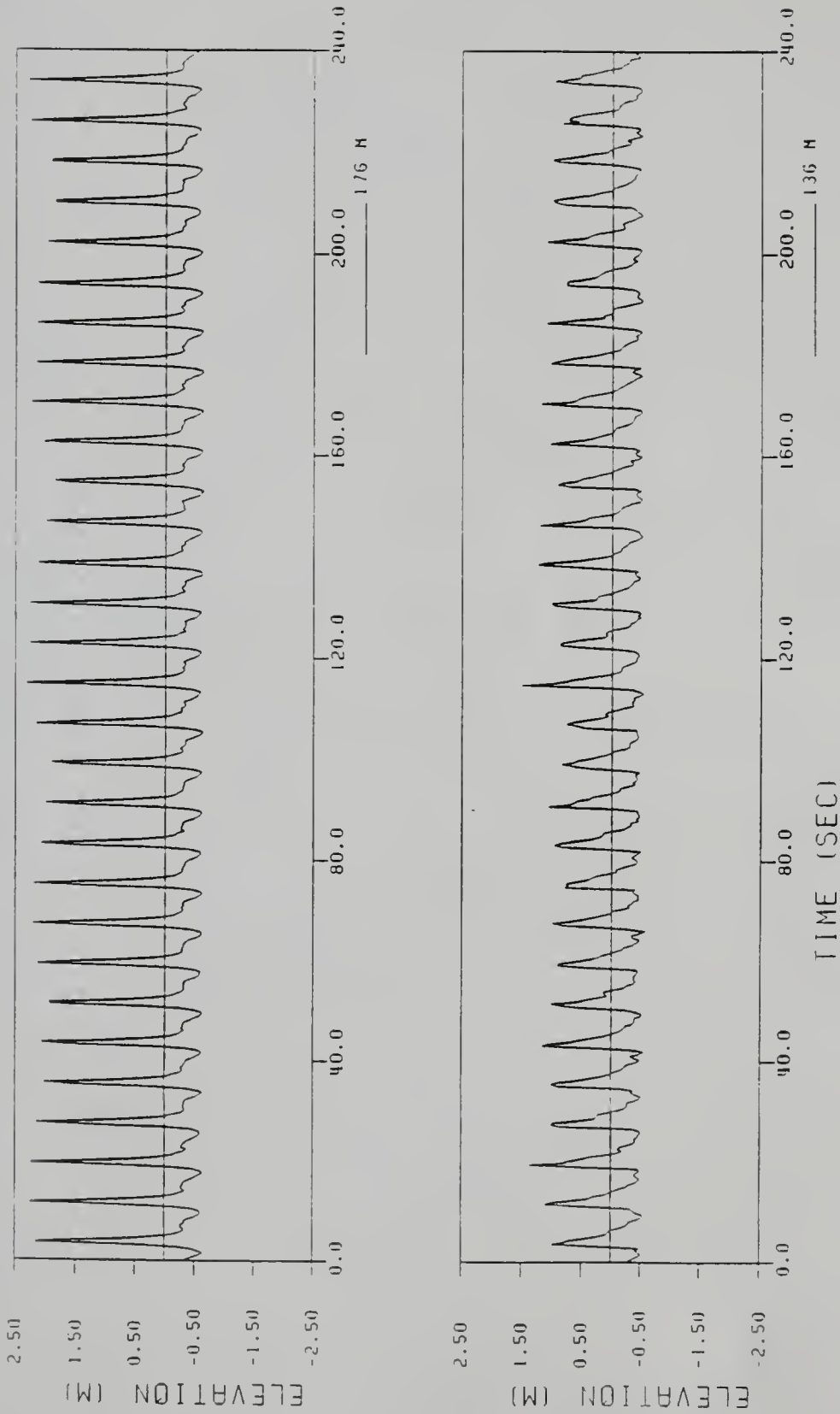


Figure 2.8: A regular wave train (Experiment E4) (a) seaward of the breakpoint (176 m), and (b) just landward of the breakpoint (136 m).

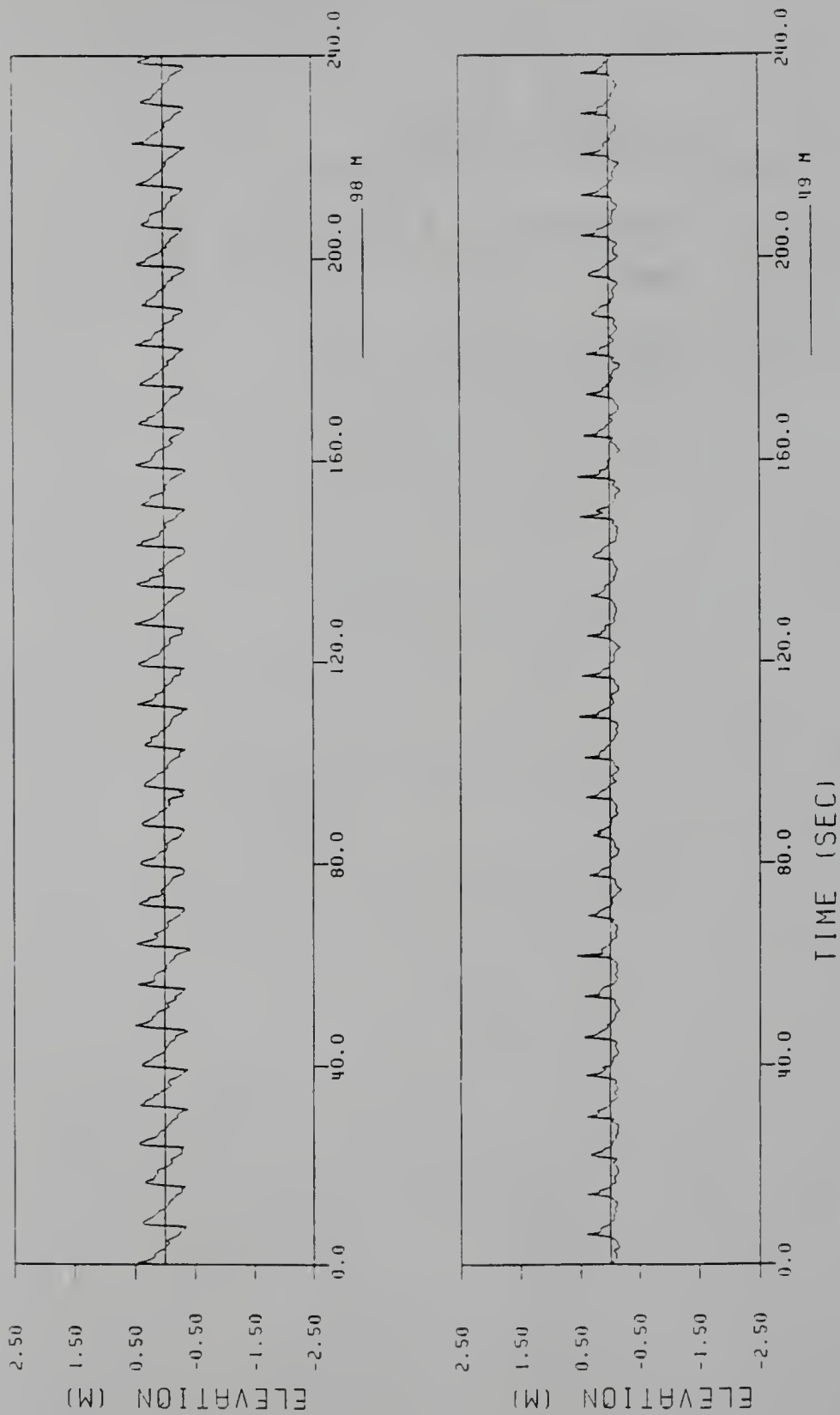


Figure 2.9: A regular wave train (Experiment E4) (a) over the crest of the barrier island (98 m), and (b) over the crest of the barrier island (49 m).

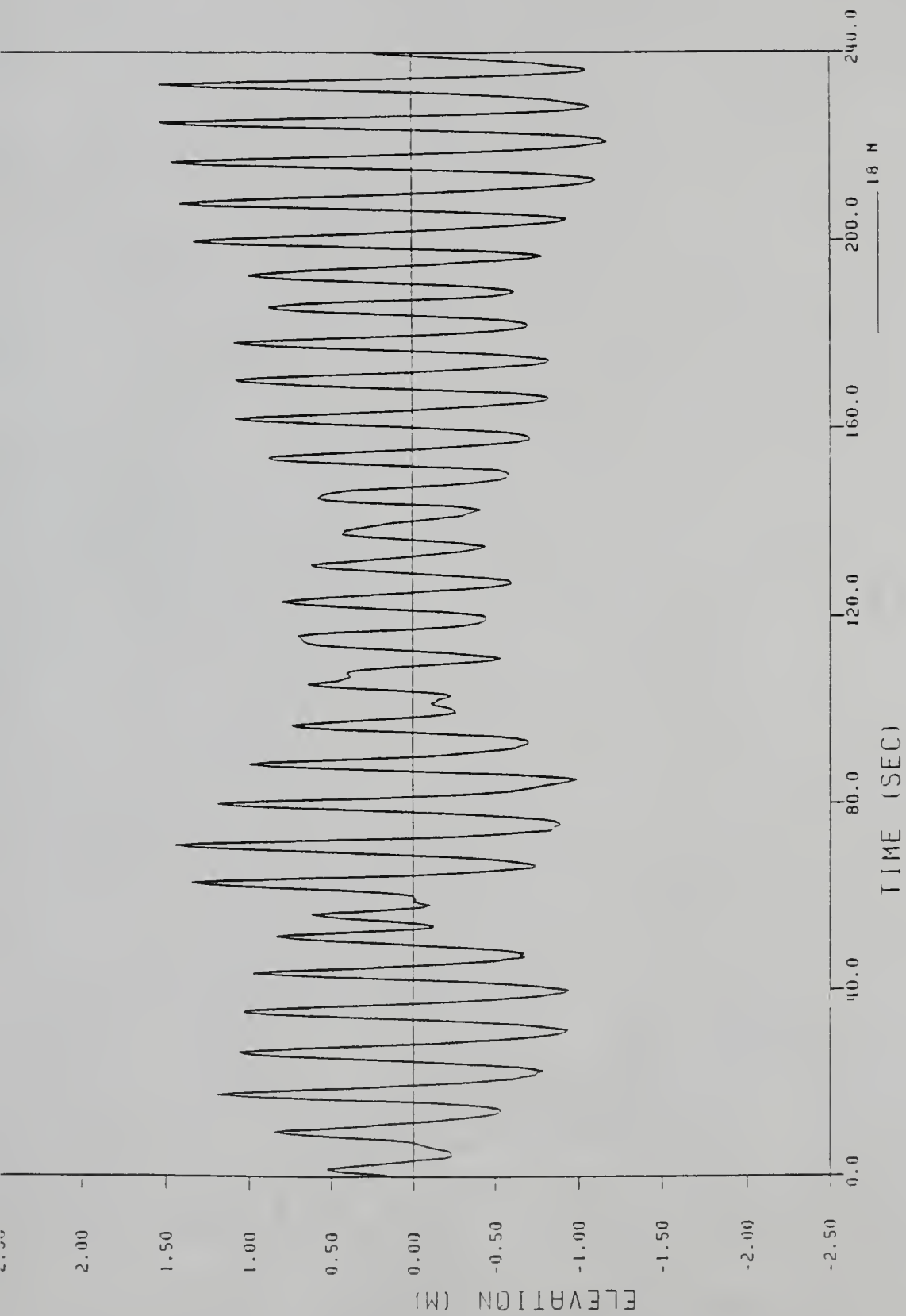


Figure 2.10: An irregular wave train at the toe of the beach (Experiment E8).

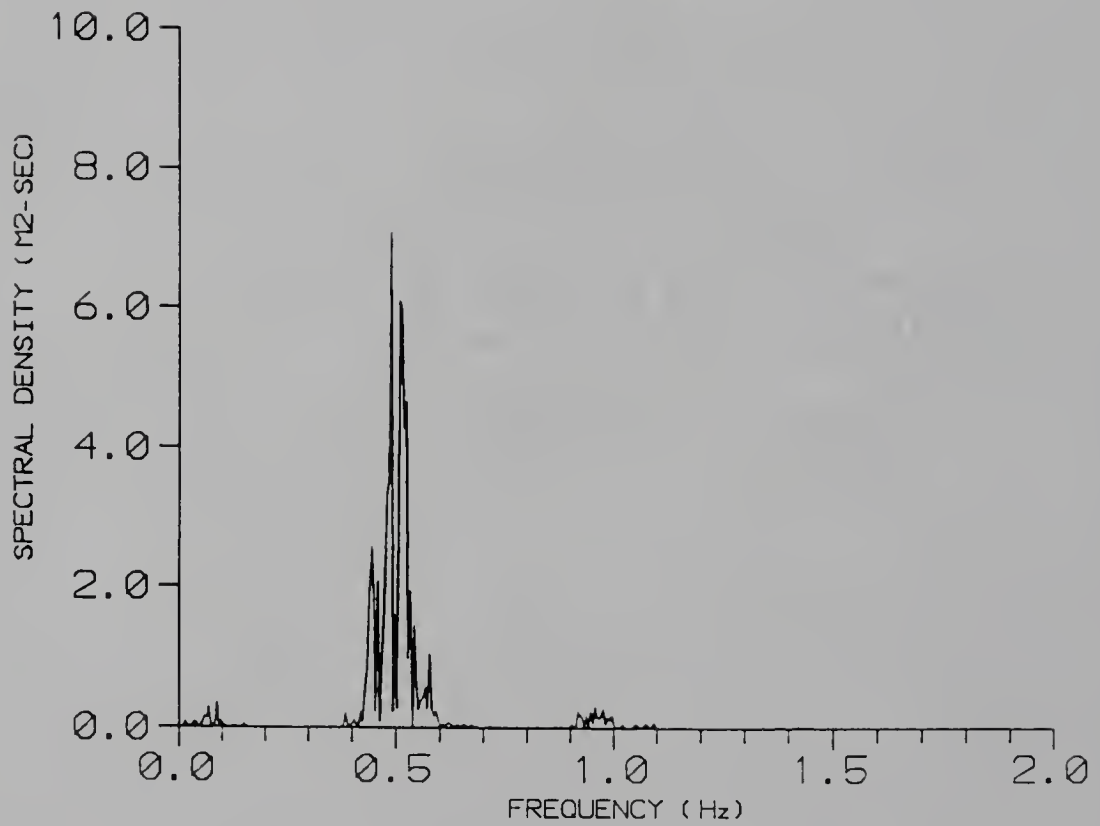


Figure 2.11: Spectrum of an irregular wave train at the toe of the beach (Experiment ES).

the horizontal position of the bed sensor. Slippage of the trolley wheels on the rails can cause errors in the prediction of the horizontal position.

Computations of net volume change. In the following, net volume changes in the profile are documented. The procedure of computation was as follows. All the measured profiles at the beginning and end of each experiment were separately averaged to obtain representative mean profiles. The net volume change, V , was then computed as

$$V = \int_{-\infty}^{\infty} (z_{t=18} - z_{t=0}) dx \quad (2.16)$$

where $z_{t=18}$ and $z_{t=0}$ were the mean local measured elevations at times $t = 18$ (final) and $t = 0$ (initial) hours. Of course, only portions of the profile affected by wave action show any change. The corresponding averaged change, V_{ave} was then computed as

$$V_{ave} = V/L_w \quad (2.17)$$

where L_w was the affected length of the profile.

Experiment E1

The initially linear-sloped beach was subjected to 2.1 m high monochromatic waves of 8 seconds period for 18 hours with the water level at MSL (no overtopping). This allowed ascertaining the response of the 1:19 planar beach to characteristic storm waves but without any storm surge and helps in interpreting the results of cases with overtopping. Swash excursions caused some deposition in the range 150-160 m and prominent deposition (~ 0.7 m) up to 170 m, see Figure 2.12. The region in the range 175-220 m experienced erosion (the maximum being ~ 0.8 m at $x = 220$ m). There was accretion up to a maximum of about 0.8 m in the range 220-235 m followed by very mild changes in the offshore.

Swash mechanisms deposited a prominent, narrow, triangular berm with the sand being supplied from the region seaward of the MSL shoreline. The mean profile exhibited a 1.5 m high steep-sided longshore bar with its crest at 223 m and trough at 219 m. The crest of the bar was just seaward of the breakpoint (confirmed visually) and the height of the bar was defined as the difference in the elevations of the crest and the landward-side trough. The longshore bar formed within the first 2 hours

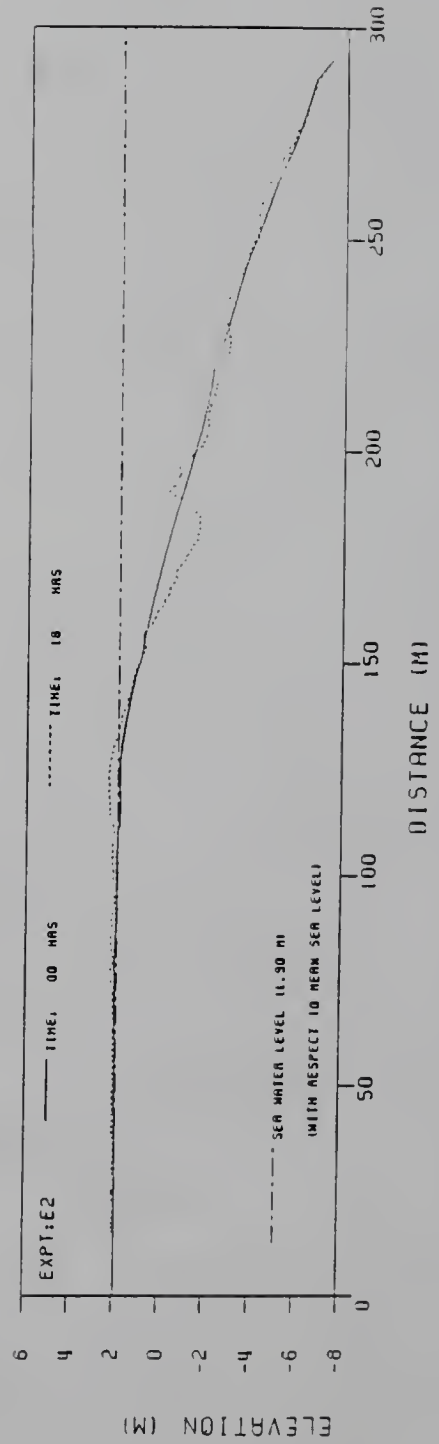
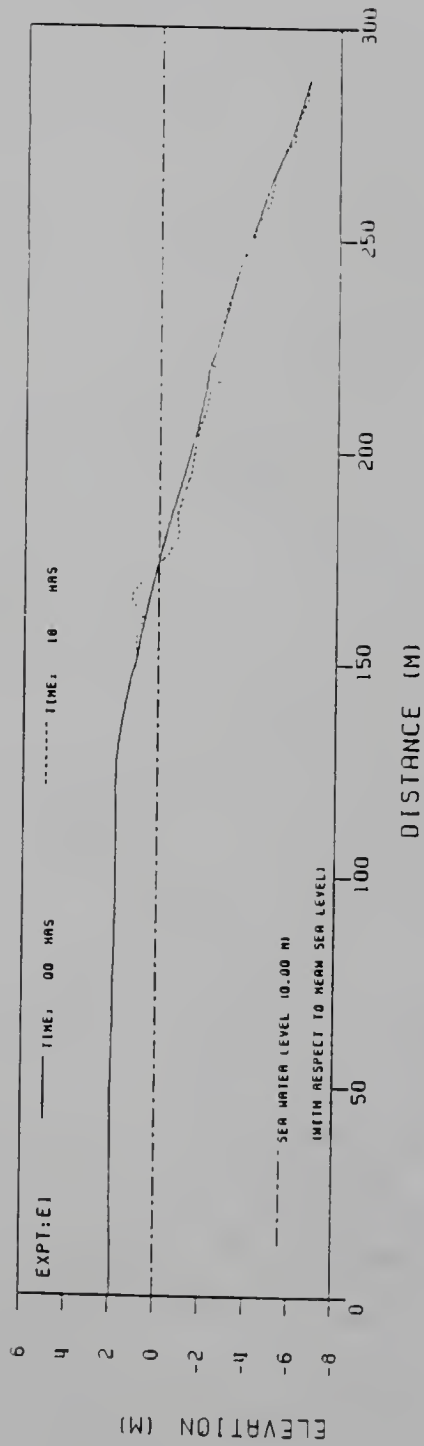


Figure 2.12: Experiments (a)E1 and (b)E2, Mean profiles at 00 and 18 hours.

and its position oscillated slightly before the profile attained equilibrium in about 12 hours. The MSL shoreline was unchanged (i.e., no horizontal or vertical retreat or advancement). The net change in the measured profile was $-4.1 \text{ m}^3/\text{m}$ (which corresponds to 0.09 cm in model units).

Experiment E2

The initially linear-sloped beach was subjected to 2.6 m high monochromatic (8 seconds period) waves for 18 hours with the water level at +1.9 m with respect to MSL which corresponded to the crest elevation of the barrier island. Thus, the onset of wave action caused a setup of the water level and mild overtopping over the crest of the barrier island (nominal overtopping of 0 m).

In the mean profile, there was mild washover of sand over the crest of the barrier island in the range 0-90 m, see Figure 2.12. The amount of deposition increased (reaching up to $\sim 0.6 \text{ m}$) in the range 90-135 m. The region 150-190 m experienced substantial erosion (up to about 1.4 m). The crest of the longshore bar extended from 190-200 m and this region exhibited accretion. This was followed by some erosion till 230 m and accretion offshore till 275 m. The MSL shoreline retreated $\sim 9 \text{ m}$. The net change in the measured profile was $+7.4 \text{ m}^3/\text{m}$ (which corresponds to 0.15 cm in model units).

Again, a prominent longshore bar developed within the first 2 hours. The position of the bar fluctuated by about 9 m in the next 2 hours. After 6 hours, the position of the bar appeared to approach quasi-equilibrium; however, even after 18 hours the position was still varying slightly, although there was only minimal change in the size and shape of the bar. In the final mean profile, the height of the longshore bar was about 1.5 m. Except for a wider crest and washover of sand over the crest of the barrier island, the patterns of deposition and erosion were similar to those in Experiment E1. Sediment transport was both onshore and offshore.

Experiment E3

The initially linear-sloped beach was subjected to 2.6 m high monochromatic (8 second period) waves for 18 hours with the water level at +3 m with respect to MSL. This resulted in a 1.1 m nominal overtopping depth over the crest of the barrier island.

Figures 2.13, 2.14 and 2.15 are samples of typical data analysis carried out during the experimental program and they document changes in profile B1 over the course of the experiment. Profiles taken every 2 hours are superposed. The longshore bar developed within the first two hours. The size of the bar grew with time and its position oscillated slightly while the crest of the bar seemed to flatten. In the final mean profile, the crest of the bar was at about 170 m while the trough was at 160 m.

In the mean profile, there was erosion (up to more than 0.3 m) in the range 0-60 m followed by accretion (up to 0.5 m) till 105 m (see Figure 2.16). The entire sloping profile was eroding extensively (up to 1.2 m) except in the region of the prominent, 1.3 m high longshore bar. Figure 2.17 presents the variance calculated using 9 measured profiles at 18 hours. The variance, σ^2 , is defined as

$$\sigma^2 = \overline{z^2} - \bar{z}^2 \quad (2.18)$$

where z is the elevation and the overbars denote spatial averaging. It can be observed that the profiles exhibited substantial variations around the position of the longshore bar. Significant erosion extended up to about 210 m. The MSL shoreline retreated about 18 m and it was noted that the elevation of the crest of the bar was above that of the MSL. The net change in the measured profile was $-57.3 \text{ m}^3/\text{m}$ (which corresponds to 1.2 cm in model units). In contrast to Experiment E2, there was both erosion as well as accretion over the crest of the barrier island, extensive erosion of the sloping beach and no accretion far offshore. In fact, the transport was completely onshore now.

Experiment E4

The experimental conditions were the same as for Experiment E3 except that the storm surge level was raised to 3.5 m, i.e., the nominal overtopping level was increased to 1.6 m.

A mild longshore bar developed within 2 hours. The position of the bar oscillated till about 10 hours before flattening out to a more gradual shape.

The final mean profile indicated that there was deposition (up to 0.5 m) till 100 m, see Figure 2.16. The crest of the barrier island eroded in the range 100-120 m (with

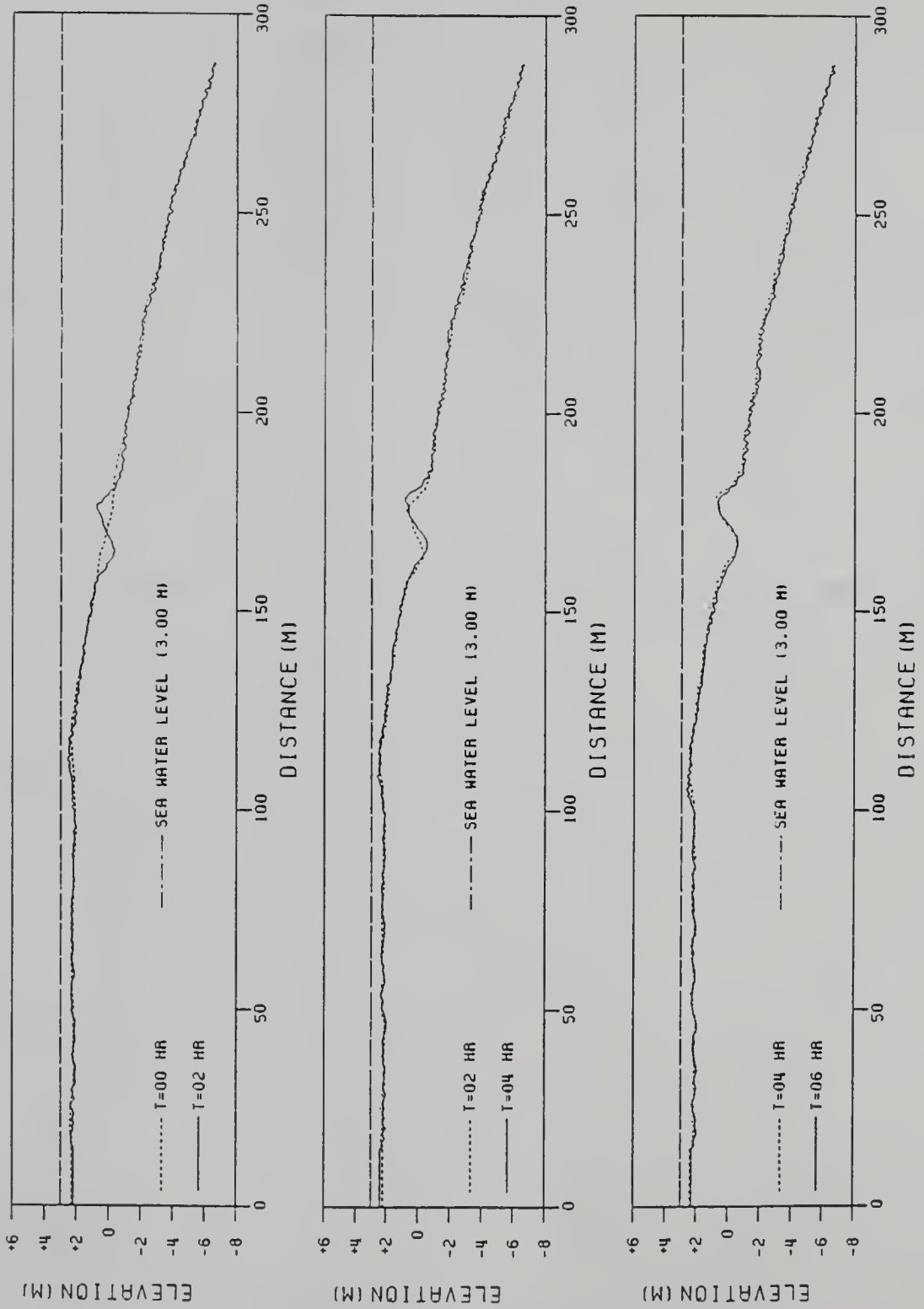


Figure 2.13: Experiment E3, Profile B1, 00-06 hours.

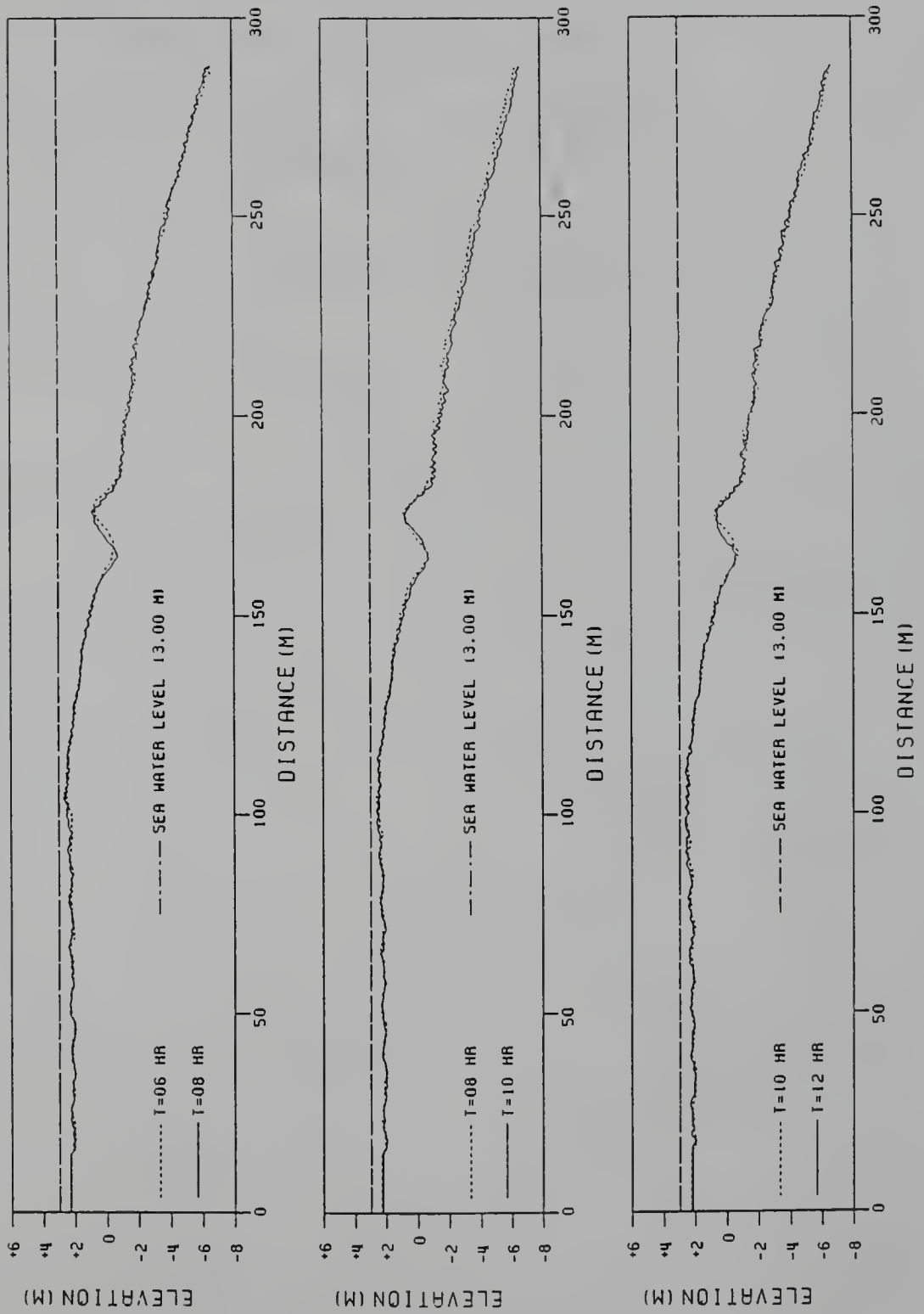


Figure 2.14: Experiment E3, Profile B1, 06-12 hours.

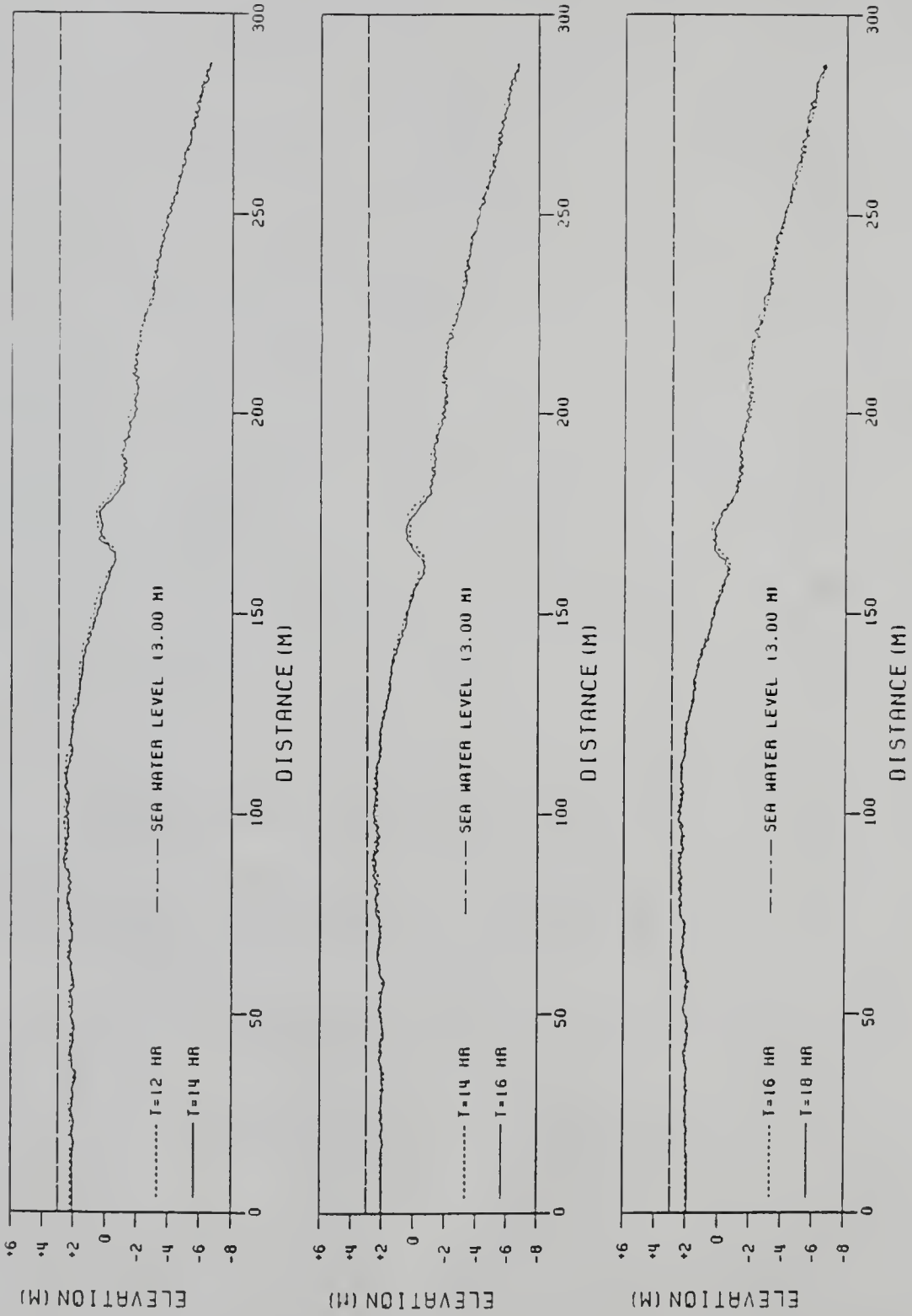


Figure 2.15: Experiment E3, Profile B1, 12-18 hours.

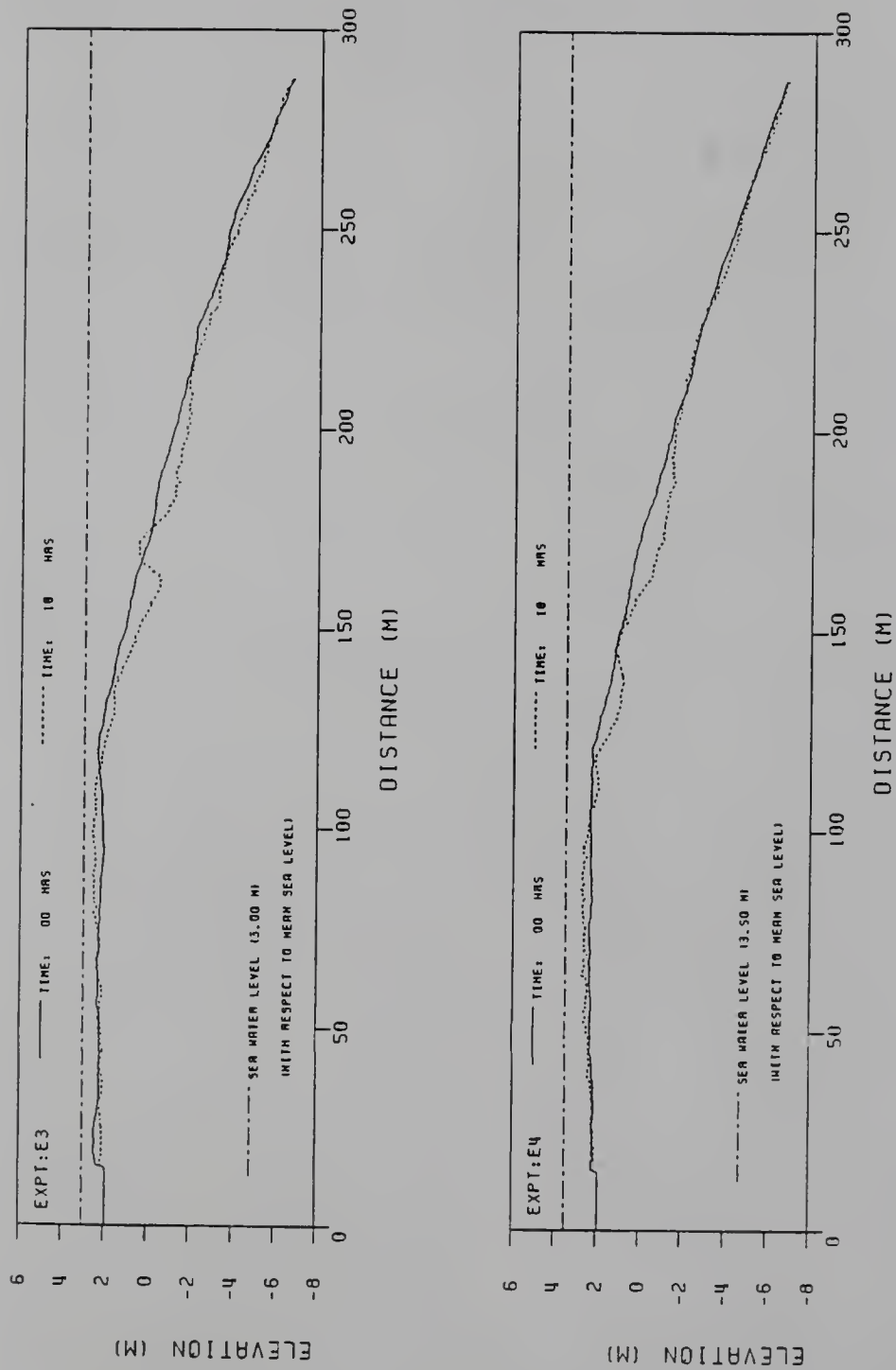


Figure 2.16: Experiments (a)E3 and (b)E4, Mean profiles at 00 and 18 hours.

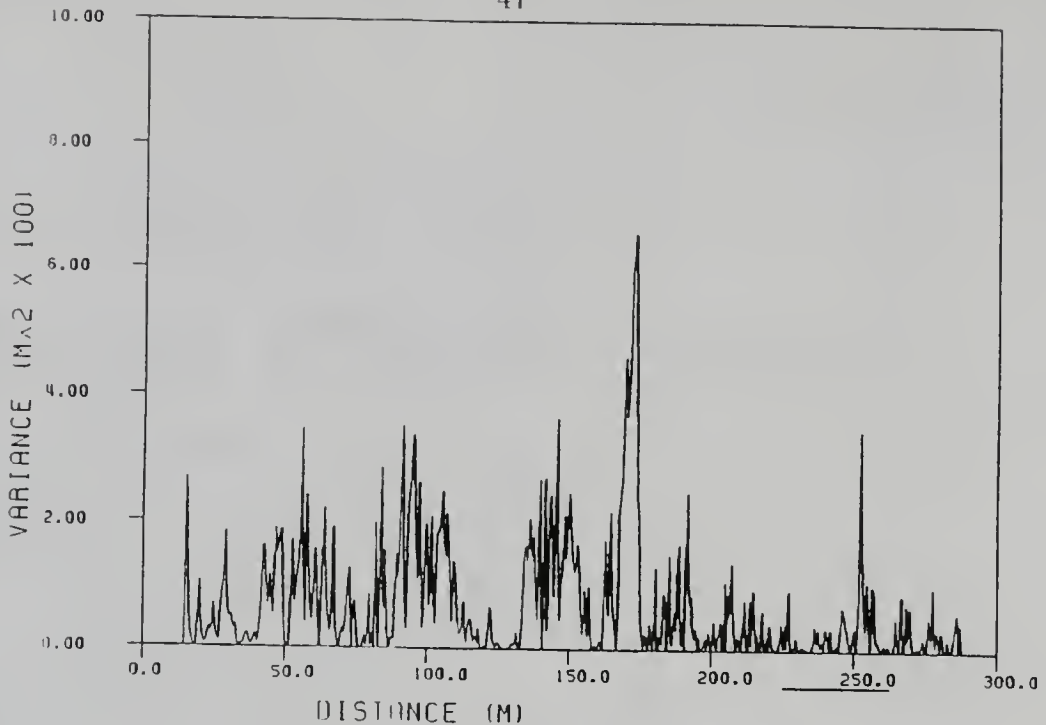


Figure 2.17: Experiment E3, profile variance at 18 hours.

erosion levels reaching up to 0.3 m). Beyond this, the entire profile was eroding except in the region 210-230 m which exhibited slight deposition. Extensive erosion (up to 1.1 m) occurred in the range 150-200 m. The entire sloping beach became undulatory. The elevation of the crest of the primary bar coincided with that of the initial beach at that position. The final position of the crest of the primary bar was 150 m (which was landward of the MSL shoreline) and the final height was about 0.6 m. A secondary bar was discernible landward of the slope break of the initial profile with its trough at ~ 115 m and its crest at ~ 120 m. The MSL shoreline retreated about 15 m. The net change in the measured profile was $-39.6 \text{ m}^3/\text{m}$ (which corresponds to 0.9 cm in model units).

The patterns of erosion and deposition were very similar to those of Experiment E3 except that the longshore bar was smaller, subdued and diffuse.

Experiment E5

This experiment simulated a storm of 18 hours duration with a peak surge of 3.45 m. Waves were allowed to mold the initially linear-sloped beach to near-equilibrium by impinging upon the beach for 6 hours at MSL conditions prior to the advent of

the storm. The rates of rise and fall of the surge were the same. The hydrograph used in this simulation was presented in Figure 2.6

The near-equilibrium profile (at 6 hours) prior to the storm exhibited a prominent longshore bar which persisted when the water level was raised to 0.15 m (6-8 hours). However, the bar disappeared when the water level was raised further (to 0.89 m) in the next stage of the storm (8-10 hours). No prominent longshore bar was evident as the water level was raised to 3.45 m above MSL and then lowered back to 0.89 m over the next 12 hours. A prominent longshore bar again developed when the storm surge subsided to 0.15 m and back to MSL conditions. Figure 2.18 shows the evolution of the bed in terms of the mean profile at different times.

Comparison is made here of the mean profiles at 06 hours (just prior to the storm) and at 24 hours (just after the surge had subsided). There was washover of sand over the crest of the barrier island with the amount of deposition increasing up to ~ 0.6 m towards the ocean-side of the barrier island, see Figure 2.19. The region 120-140 m exhibited slight erosion which was followed by mild deposition till 152 m feet. There was substantial erosion (up to 0.6 m) in the range 160-205 m and accretion (up to 0.3 m) further offshore except for mild erosion in the range 220-235 m. A prominent, 1.2 m high longshore bar was evident with its crest at about 223 m. Another small, very mild-sloped, broad-crested bar formed in the region 140-152 m. The MSL shoreline retreated about 6 m. During the process of rising water levels with accompanying overtopping of the crest of the barrier island, the entire sloping portion of the beach eroded and transport was entirely onshore. The longshore bar flattened out. Sand was deposited on the crest of the barrier island with the amount of deposition decreasing away from the slope break. Some sand was also lost in the bay. As the water level subsided, some of the sand was returned back to the longshore bar which had reformed with the cessation of overtopping. The longshore bar was in the same position as before the advent of the storm surge but was of milder relief. The profile landward of the bar experienced erosion, and overwash processes resulted in loss of sediment to the budget of the near-offshore region. The net change in the measured profile was $+5.5 \text{ m}^3/\text{m}$ (which corresponds to 0.12 cm in model units).

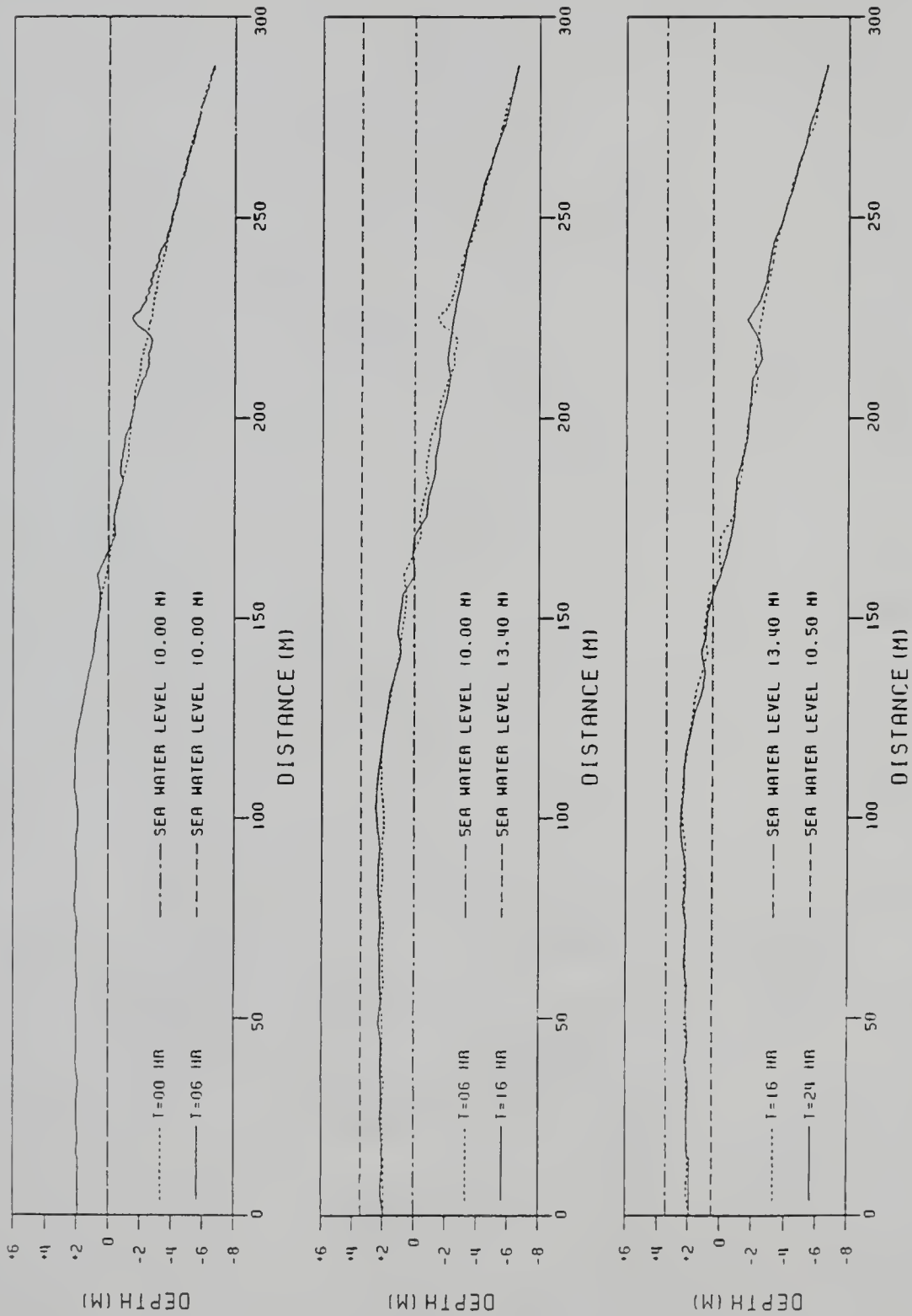


Figure 2.18: Experiment E5, (a) Mean profiles at 00 and 06 hours, (b) Mean profiles at 06 and 16 hours, (a) Mean profiles at 16 and 24 hours.

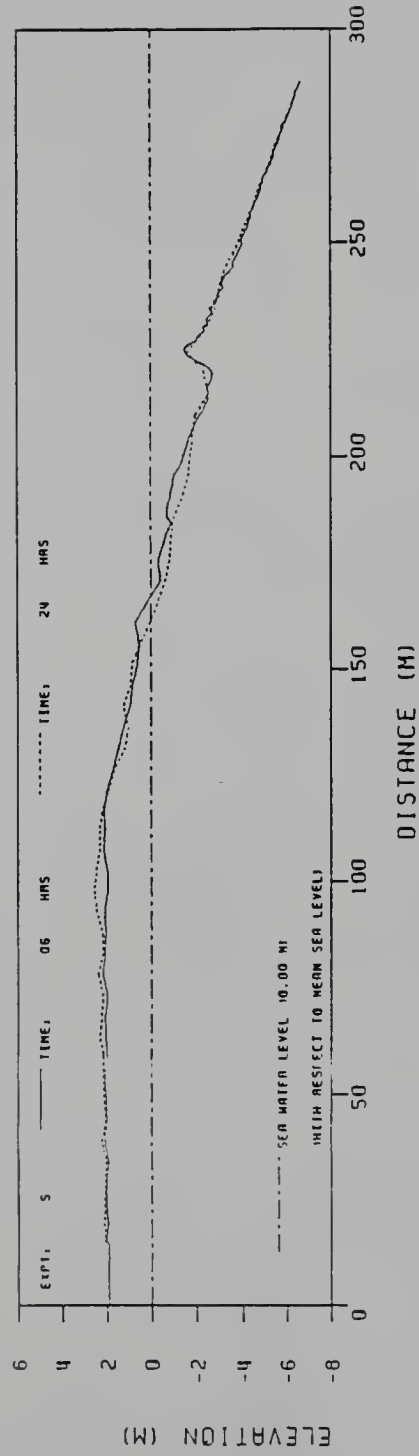


Figure 2.19: Experiment E5, Mean profiles at 06 and 24 hours.

Thus, the profile subsequent to the storm was quite similar to that prior to the storm especially in terms of the longshore bar position, size and shape. The storm caused washover of sand over the crest of the barrier island.

Experiment E6

The experimental conditions were the same as E1 (water level at MSL, no storm surge, no overtopping) except that a narrow-banded spectrum of irregular waves of 2.1 m significant wave height and carrier period of 7.6 seconds was allowed to impinge upon the barrier island.

Swash excursions caused deposition landward of the shoreline in the range 125-165 m with maximum deposition reaching up to ~ 0.6 m, see Figure 2.20. Seaward of the shoreline, the region 165-210 m exhibited erosion and this was followed by deposition still offshore. The crest of the 0.6 m high longshore bar was at about 230 m. The formation of the bar was not immediate (as was the case in Experiment E1), it took about 12 hours to develop. There was no change of the MSL shoreline.

The patterns of deposition and erosion were similar to Experiment E1 except that the changes were smaller, the longshore bar was much less prominent (and the inflexion of the bed profile was only on the landward side of the bar) and a greater portion of the beach face was affected by swash mechanisms. There was onshore transport seaward of the longshore bar. The net change in the measured profile was $+10.7 \text{ m}^3/\text{m}$ (which corresponds to 0.24 cm in model units).

Experiment E7

The experimental conditions were the same as E2 (1.9 m surge, water level equal to the crest of the barrier island) except that irregular waves were used with a carrier period of 8 seconds. Thus, the onset of wave action caused mild overtopping over the crest of the barrier island (nominal overtopping depth of 0 m over the crest of the barrier island).

Washover occurred over the crest of the barrier island, with the deposition increasing from the bay-side towards the ocean-side (see Figure 2.20). Accretion was more than 0.3 m in the region 60-105 m. Substantial erosion (up to 1 m) occurred from the MSL shoreline (which was nominally at 122 m) till about 210 m. There

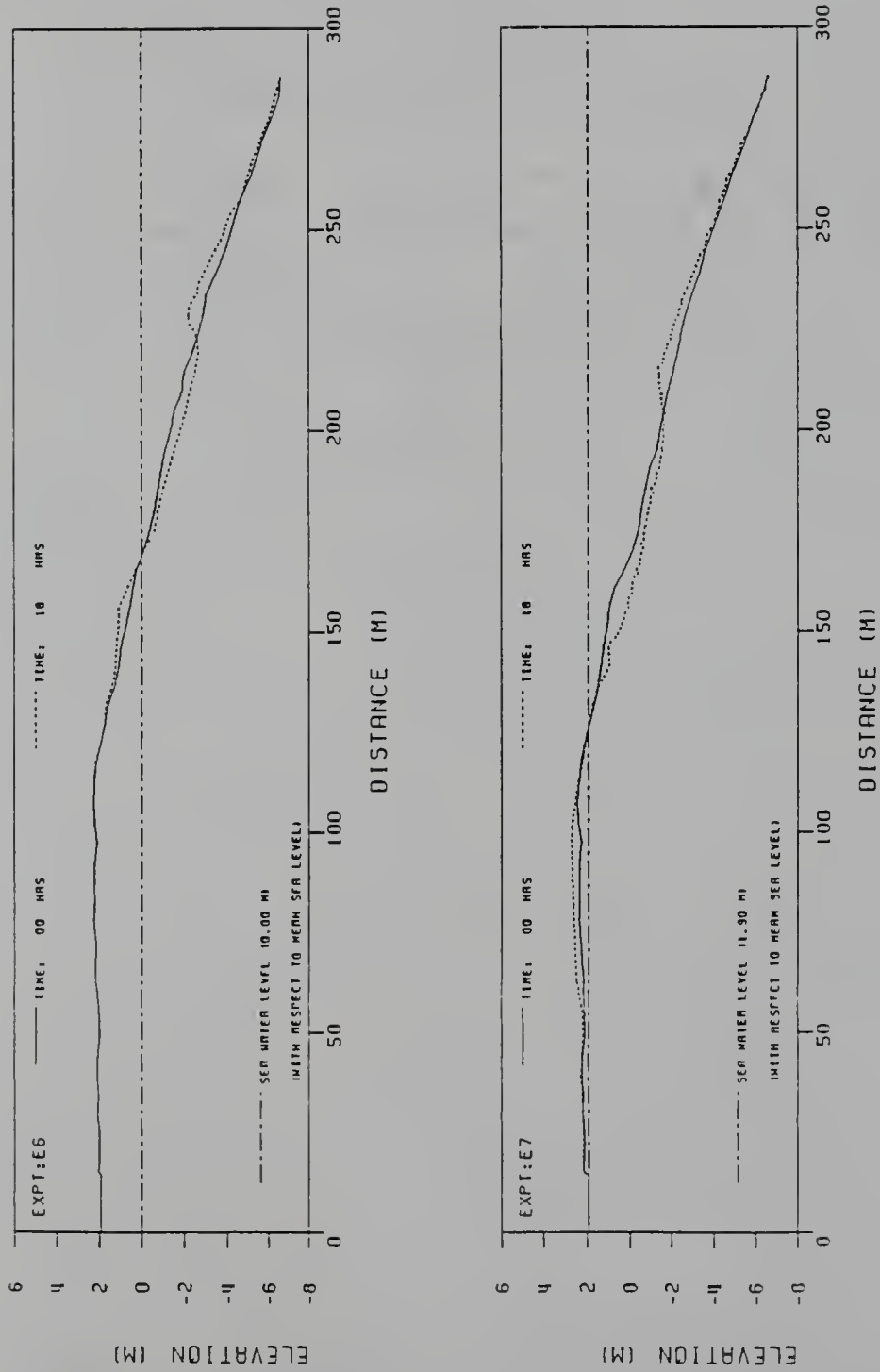


Figure 2.20: Experiments (a)E6 and (b)E7, Mean profiles at 00 and 18 hours.

was deposition of about 0.6 m at around 210 m and this was followed by decreasing amounts of accretion still further offshore. A small, low-relief bar was discernible with its crest at about 220 m. The formation of the bar was not immediate and took about 16 hours to develop. The MSL retreated about 9 m. The net change in the measured profile was $+7.32 \text{ m}^3/\text{m}$ (which corresponds to 0.1 cm in model units).

Again, the patterns of erosion and deposition were similar to those of Experiment E2 except that the changes were more subdued and the longshore bar was low and much less prominent (with the inflexion in the bed profile occurring on the landward side of the bar only).

Experiment E8

The experimental conditions were the same as E3 except that a narrow- banded spectrum of irregular waves was used with a carrier period of 8 seconds. Thus, the surge level was 3.0 m resulting in a 1.1 m nominal overtopping depth over the crest of the barrier island.

The crest of the barrier island exhibited mild uniform accretion (about 0.15 m) all over, see Figure 2.21. There was substantial erosion (up to 0.8 m) from 120 m to about 190 m, followed by decreasing amounts of deposition in the offshore. No longshore bar was evident. The MSL shoreline retreated about 8 m. The net change in the measured profile was $+8.9 \text{ m}^3/\text{m}$ (which corresponds to 0.18 cm in model units).

Patterns of deposition over the crest of the barrier island were similar to Experiment E3. However, unlike Experiment E3 where the entire sloping part of the profile was eroding, there was deposition offshore of about 180 m in this experiment. Also, Experiment E3 had a prominent longshore bar while no longshore bar formed here and changes in the beach profile were much subdued as compared to those in Experiment E3.

Experiment E9

The experimental conditions were the same as E4 except that a narrow- banded spectrum of irregular waves was generated with a carrier period of 8 seconds. The surge level was 3.5 m above MSL resulting in a 1.6 m nominal overtopping depth over the crest of the barrier island.

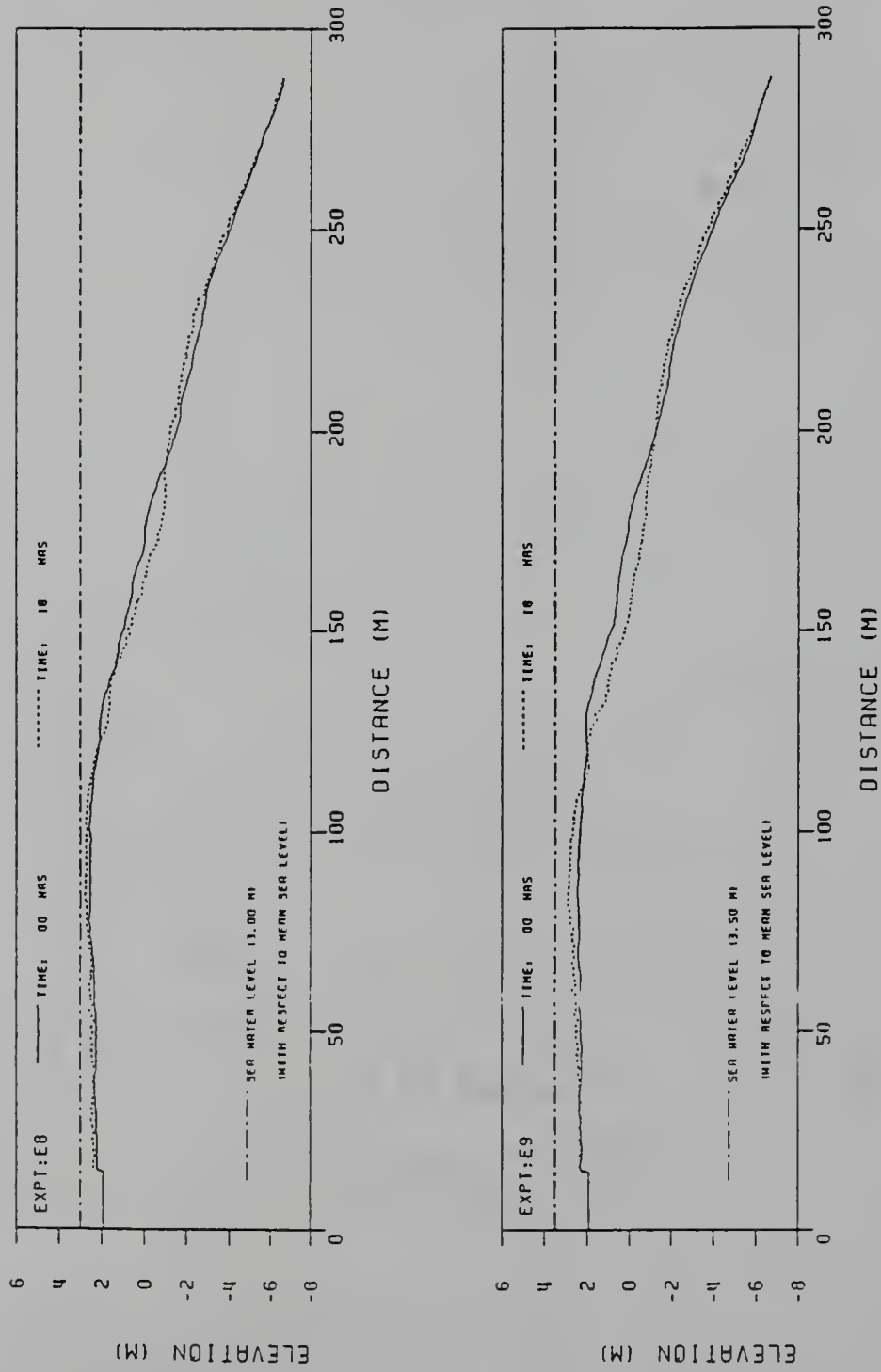


Figure 2.21: Experiments (a)E8 and (b)E9, Mean profiles at 00 and 18 hours.

Overtopping caused washover of sand up to ~ 0.5 m over the crest of the barrier island till 115 m, with the deposition again increasing from the bay-side to the ocean-side, see Figure 2.21. This was followed by substantial erosion (up to 0.8 m) in the range 120-200 m and mild, decreasing amounts of deposition still further offshore. No longshore bar was evident. The MSL shoreline retreat was ~ 21 m. The net change in the measured profile was $-4.4 \text{ m}^3/\text{m}$ (which corresponds to 0.09 cm in model units).

Patterns of deposition over the crest of the barrier island were similar to those of Experiment E4. However, the bed profile of Experiment E9 was devoid of the presence of a longshore bar and the profile exhibited mild accretion beyond about 200 m unlike Experiment E4. Changes in Experiment E4 were much more prominent when compared to those in Experiment E9.

2.3.5 Discussion of Results

The results of a series of nine wave tank tests to investigate the evolution of beach and barrier island profiles under the action of various wave and tide conditions are described. The range of tests included steady and time-varying normal and storm water levels and regular and irregular waves. Overtopping of the barrier island occurred for the elevated water levels. Sand with a mean size of approximately 0.2 millimeters was used in all tests. The crest of the model barrier island was 7.5 m wide and a nominal model to prototype scale of 1:16 was considered. The beach for all tests was initially planar with a slope of 1:19. For each test, documentation included the incident waves and beach profiles at intervals of 0.5 hours. More details of the data are provided in Srinivas, Dean and Parchure (1992).

The first series of four experiments maintained the wave characteristics reasonably constant while increasing the water level from test to test. Water levels tested were, in prototype units, 0 m, 1.9 m (the same as the barrier island crest), 3 m, and 3.4 m. For Experiment 1 with the normal water level (0 m), a prominent bar formed and a fairly substantial triangular berm was established immediately landward of the waterline. The profile evolution for the remaining tests may be interpreted in light of the forces which caused profile evolution in the first test (Experiment E1). For the second test

(E2) with the water level at the barrier island crest, a bar of approximately the same height but of much greater width formed. Since overtopping of the barrier island could occur, the sediment that had formed a triangular berm in the first experiment was deposited over the seaward portions of the barrier island. In Experiment E3 with a water level of 3 m, the bar was similar to that in Experiment E2; however, sand was transported over the barrier island resulting in substantial losses of sediment to the beach system. Experiment E4, the final test with a steady water level and regular waves, extended the trend established in the preceding two tests with the exception that the offshore bar was considerably more subtle. In all cases, the longshore bars were break-point bars (confirmed visually).

Experiment E5 was conducted with regular waves and a time-varying water level which simulated the rising and falling hydrograph associated with a storm. There were similarities and differences between this and previous experiments which contribute to understanding the causes of bar formation. During periods of slow changes in water level, a prominent bar formed on both rising and falling water levels. However, during those portions of the hydrograph when the water level was either rising or falling fairly rapidly, the bar became much more subdued to nonexistent, apparently because the processes of bar formation were not able to keep pace with the changing water level. There was substantial loss of sediment over the barrier island but of course less than for the case of an elevated water level over the entire testing period.

Experiments E6 through E9 replicated approximately the conditions of Experiments E1 through E4 with the exception that the waves were irregular. The following discussion focuses on the similarities and differences between the tests with regular and irregular waves. The processes at the landward end and over the barrier island were substantially the same for regular and irregular waves. Without overtopping (Experiment E6), the berm formed was less distinct than with regular waves. For the remaining experiments in which overtopping occurred, sand was carried over the barrier island where some was deposited and a portion transported beyond the island. The major difference occurred in the characteristics and degree of bar formation. With irregular waves, the bar was less prominent and less distinct for the case of

no overtopping as compared to the regular wave case. In those cases in which overtopping occurred, the bar feature was more subtle with the mean water level at the barrier island crest elevation and was not present at all during Experiments E8 and E9 with water elevations of 3 m and 3.4 m, respectively.

The experiments with overtopping show accretion over the crest region. This sand is lost to the subaqueous sediment budget with the return of normal conditions after the storm and if equilibrium beach concepts are assumed, this loss has to be made up with additional erosion occurring elsewhere. The situation then becomes complicated as a result of this interaction and longshore processes need to be taken into account.

Dissipation of wave energy acts as an effective sediment- mobilizing agent and in conjunction with other (non wave-driven) currents, which are apt to be present in nature, has a greater transport potential. Under these conditions, overtopping can result in a serious erosive impact to the barrier island system. This hypothesis was tested and validated by conducting additional tests (unpublished data and Pirrello 1992) combining the actions of waves and currents. The data presented here provide a basis for the development and calibration of a numerical model to simulate overwash of barrier islands during storms. In addition to these data, the principal results from these experiments include further evidence of the mechanisms of bar formation. It appears that contrary to other proposed causes, offshore bars are simply break-point bars and that the return flow of mass transport, sometimes termed “undertow” and the relative constancy of wave breaking location play important roles in bar formation, at least for the conditions tested here in the laboratory. The aspect of identification of causes of bar formation/generation is investigated next.

2.4 Bar Formation Mechanisms

2.4.1 Background

The initial step in the formulation of a rational, physics-based cross-shore sediment transport model is the correct identification and quantification of the dominant forcing functions. In terms of sediment transport, the most active region of any bed profile is the surf zone where wave breaking results in dissipation of organized wave

energy and the transfer of wave momentum to the water column. As mentioned earlier (Section 2.3), the final bed profiles of the conducted experiments with barrier islands were characterized by a distinctive, single longshore bar, as is the case with many natural coastlines. A good sediment transport model should have the capability of generating bars wherefore the proper physical mechanism(s) for bar formation needs to be identified. A bar is characterized as a local region of a bed profile (excluding the swash zone) exhibiting a surplus of sediment; that is, it is a subaqueous accretionary feature where sediment has deposited. However, the need to establish bar cross-shore parameters (extent, position, volume of sand stored) requires the definition of a reference profile to define “surplus sediment” such that, for example, the volume of sand stored in a bar may be quantitatively evaluated and compared with other investigations consistently. An unambiguous definition of a reference profile is difficult and not really necessary for the present purposes, as long as a more pragmatic definition is consistent and essential characteristics of the system can be quantified. For example, this reference can be a “fitted” equilibrium beach profile following Dean (1977) or it can be the initial profile of an experiment.

The concept of an equilibrium beach profile is inherent in studies of beach profile evolution where it is assumed that the beach will remain unchanged after being exposed to constant forcings for a long time. The concept of an equilibrium beach profile is a useful idealization which is difficult to achieve in practice because of variations in water temperature, wave heights and periods, tides, etc. It is also noted that the definitions of Bruun (1954) and Dean (1977) predict only monotonic profiles for equilibrium beaches. An equilibrium beach profile can be fit (using, for example, least-squares technique) to form the reference profile by assuming uniform wave energy dissipation per unit volume, that is, a $\text{depth} \propto (\text{distance})^{2/3}$ relationship (Dean 1977).

For the present series of experiments, the most practical definition for the reference profile was the initial bed profile in all experiments as it was readily available. Figure 2.22 illustrates the definition of a longshore bar and some of its parameters including the cross shore location in terms of distance to the bar center of mass,

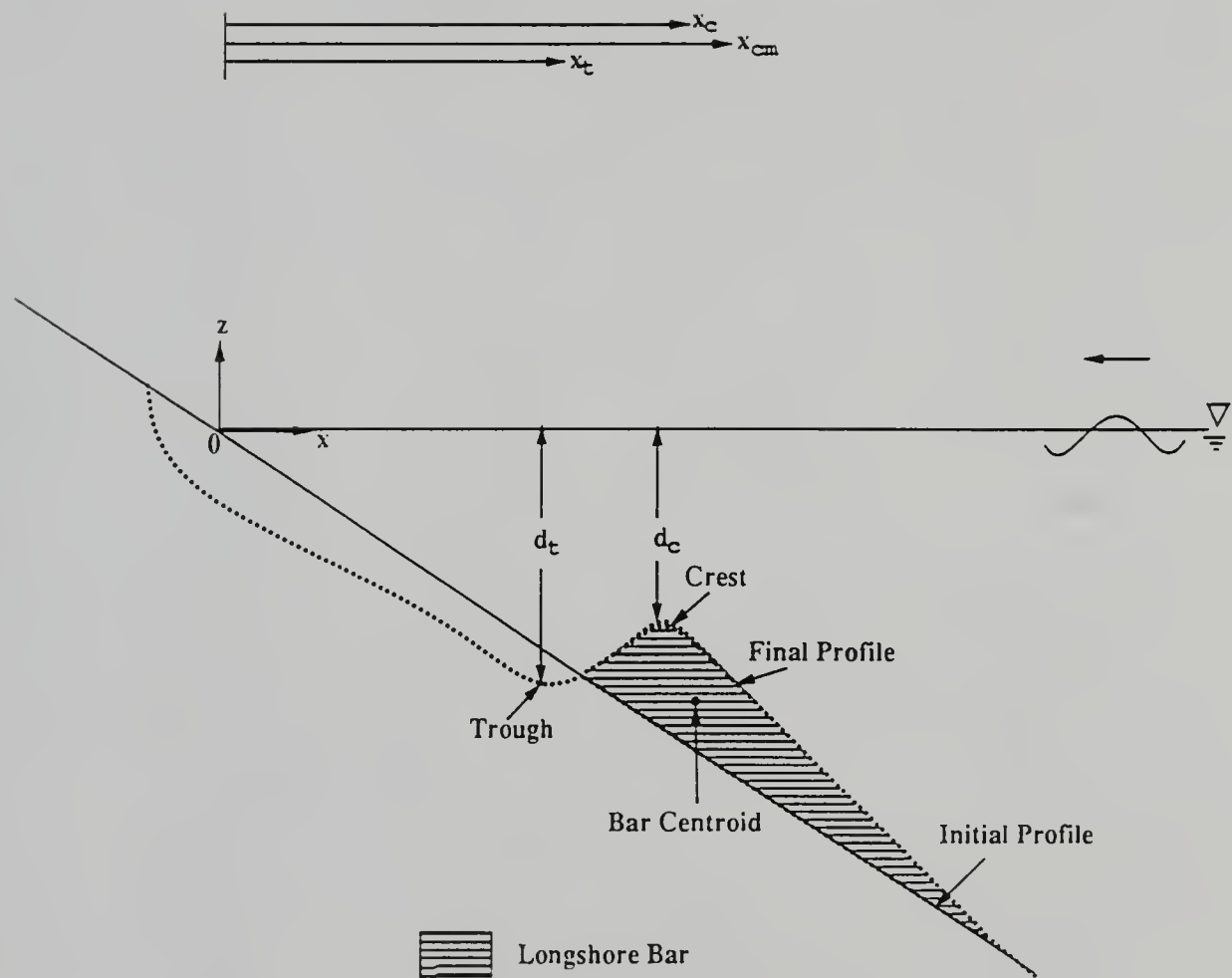


Figure 2.22: Definition sketch of a longshore bar in a beach profile.

x_{cm} , distance to the bar crest, x_c and depth at the bar crest, d_c . For the present experiments, the initial still water shoreline has been chosen as the local origin for describing the position of the longshore bar. In many cases, a trough exists on the seaward side of the bar crest. In nature, subaqueous beaches can be quite complicated with multiple bars, and rhythmic and complicated three-dimensional topography.

There is a noticeable lack of consensus in the literature about definitive bar generating mechanism(s). The existence of bars is due to the convergence of sediment transport. The shear stress near/at the bottom for the case of progressive waves (to second order) is in the direction of wave propagation (onshore transport considering normally incident waves). The presence of a single longshore bar then indicates an area of convergence of sediment transport with seaward directed (offshore) transport being required landward of the bar crest. Based on a volumetric conservation requirement, for a 2-D situation,

$$\frac{\partial h}{\partial t} = \frac{\partial q}{\partial x}, \quad (2.19)$$

where h is the local depth and q is the sediment transport in direction x , whereby a negative gradient of sediment transport is necessary for sand accumulation.

2.4.2 A Brief Literature Review

The ubiquity and importance of longshore bars has long been recognized and they have been studied for about a century. The earliest investigators include Lehmann (1884), Otto (1911) and Hartnack (1924). Hartnack (1924) noted the importance of breaking waves in bar formation in the Baltic Sea and that the spacing between longshore bars increased with increasing water depth. Other early investigators include Evans (1940) and Keulegan (1945).

Bar formation criteria

A number of generally heuristic relationships for offshore transport and bar formation are available in the literature in terms of various non-dimensional parameters including combinations of the deep water wave height (H_0) and wavelength (L_0), sediment fall velocity (w_s), wave period (T), initial beach slope ($\tan \beta$), median sand diameter d_{med} , etc. Earlier criteria involved wave steepness only (Waters 1939, Scott

Table 2.4: Bar formation criteria

Researcher(s)	Formation criteria
Waters (1939)	$H_0/L_0 > 0.025$
Sunamura and Horikawa (1975)	$H_0/L_0 > C(\tan \beta)^{-0.27}(d_{med}D/L_0)^{0.67}$
Wright and Short (1984)	$H_b/w_s T > 1 - 6$
Kriebel et al. (1987)	$H_0/L_0 > A \pi w_s/gT$
Larson and Kraus, SBEACH (1989)	$H_0/L_0 < 0.0007(H_0/w_s T)^3$
Dalrymple (1992)	$\frac{gH_0^2}{w_s^3 T} > 9000 - 10400$

1954), but later criteria have generally inculcated sediment characteristics (fall velocity or sand diameter). Some of these criteria are listed in Table 2.4.

Considering primarily suspended transport, one of the most rational criteria was suggested by Dean (1973). If a sediment particle is entrained to an elevation (z_i) proportional to the wave height (H) during the passage of the wave crest (when the magnitude of velocity is a maximum), the fall time is

$$t_F = \frac{\beta H}{w_s} \quad (2.20)$$

where w_s is the sediment fall velocity and β is a proportionality factor (free parameter). Thus, with instantaneous suspension at the wave crest phase position, we have the condition

$$\begin{aligned} t_F &< T/2, \text{ onshore transport} \\ &> T/2, \text{ offshore transport} \end{aligned} \quad (2.21)$$

As explained earlier, offshore transport is necessary for a bar to develop, whence

$$\frac{\beta H}{w_s} > \frac{T}{2} \quad (2.22)$$

and dividing both sides by L_0 , we have

$$H_0/L_0 > \frac{1}{\beta} \frac{\pi w_s}{gT} \quad (2.23)$$

where the wave height and wavelength are in terms of deep water conditions. Comparing various data sets, Dean (1973) found good agreement for this functional dependence with a value of $1/\beta$ of approximately 1.7 (for a lab scale). Kriebel et al. (1987)

extended this to include prototype scales and the new value of $1/\beta$ was between 4 to 5. It is noted that this criterion is applicable for first and higher order wave effects and the effects of bottom slope are not included.

Kraus and Larson (1988) and Larson and Kraus (1989) examined in detail data from large-scale wave tank tests (for monochromatic waves breaking on sandy beaches) of Saville (1957) and Kajima et al. (1982) and formulated two criteria, depending on the variables used as

$$\frac{H_0}{L_0} = 115\left(\frac{\pi w_s}{gT}\right)^{1.5} \quad (2.24)$$

$$\frac{H_0}{L_0} = 0.0007 D_0^3. \quad (2.25)$$

where $D_0 = \frac{H_0}{w_s T}$ is the Dean number in deep water, for separating storm (barred) and normal profiles. Dalrymple (1992) re-evaluated these criteria and developed a single new criterion in terms of a profile parameter, P , given as

$$P = \frac{g H_0^2}{w_s^3 T} \sim 9,000 - 10,400 \quad (2.26)$$

Bar formation mechanisms

In general, bar formation has been attributed to the convergence of sediment transport due to either wave breaking induced mechanism(s) or long (infragravity IG) waves (including leaky and trapped modes). The dissipation of wave energy due to wave breaking is the source of turbulent kinetic energy (tke). This promotes sediment entrainment into the water column, and cross-shore mechanisms due to the transfer of wave momentum and resultant torque on the water column can result in a bar. The energy of short waves is depth-limited in the surf zone (due to breaking); however, due to their low steepness, the energy of IG waves is not necessarily depth dependent in the inner surf zone. Energy spectra in the inner surf zone exhibit pronounced levels at infragravity scales which are at least of the same magnitude as that of the primary incident frequencies. This is the reason why IG waves are often called “surf beat”. These low steepness, incident IG waves can be efficiently reflected from the beach. Now, a standing long wave has mass transport towards the antinodes in the upper part and towards the nodes in the lower part of the

bottom boundary layer (Longuet-Higgins 1953) whence, depending upon the elevation of sediment entrainment, there can be accumulation under the nodes or the antinodes of the wave envelope. If bedload is dominant, bars can form under the nodes, while bars can form under the antinodes of a standing wave envelope if suspended transport dominates. Trapped long waves or edge waves can be another source of IG energy and different modes may produce complex topographies.

Bars have been related to the reflection of the incident short wave field (Carter, Liu and Mei 1973). Lau and Travis (1973) extended the idea by including a planar slope, however the spacing was still in terms of the short- wave envelope which is physically unrealistic for bars in nature. Short (1975) and Bowen (1980) related bars to free, reflecting long waves and the resultant spacing was qualitatively more accurate.

Symonds, Huntley and Bowen (1982) demonstrated how an oscillating break point due to a non-monochromatic incident wave field can generate free long waves in both directions (onshore and offshore). The resulting standing wave envelope in the surf zone can result in sediment convergence. The oscillating break-point mechanism has also been analyzed by Schaffer and Svendsen (1988).

Edge wave (trapped IG waves) modes have been investigated by Bowen and Inman (1971) and Guza and Inman (1975) and can cause barred topography. Holman and Bowen (1982) used the edge wave hypothesis to show that rhythmic and complicated three-dimensional topography can develop due to the interactions of different modes.

Hansen and Svendsen (1974) showed that the presence of free and forced harmonics of a dominant fundamental primary wave results in the alternate reinforcement and cancellation of the wave envelope as the celerities of the harmonics are different. This effect is possible in wavemaker-type laboratory experiments. Contrary to field evidence, this mechanism predicts decreasing bar spacing with increasing water depths.

Mei (1985) described the short wave interaction with a periodic bar field while Boczar-Karakiewicz and Davidson-Arnott (1987) describe the interaction between the first and second harmonics of a wave train and its effect on bar formation.

The presence of a surf zone is not necessary for the above mechanisms (except for Symonds et al. 1982 and Schaffer and Svendsen 1988). Models for bar formation including surf zone processes take into account some/all of the following effects

- Undertow (due to momentum flux transfer)
- Asymmetric flow (due to wave non-linearities)
- Turbulence (due to wave breaking)
- Infragravity waves (forced waves due to wave groups can be free after breaking of the primary waves)

Dyhr-Nielson and Sorensen (1970) first associated surf zone return flow, generally termed “undertow”, with bar formation. As a result of wave breaking, there is a transfer of wave momentum to the water column and an augmented mass flux in the region above the wave trough. Continuity requires a strong return flow in the lower part of the water column (below the wave trough). Dally (1980) was the first to develop a quantitative description for undertow with monochromatic waves and also pointed out the necessity for including wave-breaking induced turbulence to account for the increase in suspended load. Stive and Battjes (1984) and Stive (1986) extended the undertow formulation to include random waves. Stive (1986) indicated the importance of including wave asymmetry. Roelvink and Stive (1989) developed a numerical model inculcating undertow, wave asymmetry, turbulence and long wave effects and concluded that including all effects gave the best results. Even though there have been impressive advances in understanding and analytically/numerically modeling the essential physics of cross shore flows in terms of integral (time and sometimes depth integrated) wave properties (e.g., the radiation stress), the solution of the governing second-order equation for undertow requires two boundary conditions whose proper choice is not very obvious (Svendsen and Hansen 1988). This facet is elaborated later during the discussion of cross-shore flows (Chapter 3).

It is realized that any, some or all of these causative processes may be dominant depending upon the specific physical model (including field situations) parameters.

Field observations

In terms of field observations, precise positioning of the nodes and antinodes of an IG wave envelope has never been actually documented. Munk (1949) and Tucker (1950) first documented augmented IG energy levels in the nearshore. Dolan (1983) analyzed bar spacings in Chesapeake Bay, Lake Michigan, Cape Cod Bay and the Alaskan coast. He found little support for the IG wave hypothesis and concluded that wave breaking was the more successful hypothesis (using Dally's (1980) breaking wave model).

Extensive beach profile surveys and long term remote sensing by Howd and Birke-meier (1987a, 1987b) and Lippman and Holman (1990) at Field Research Facility (FRF), DUCK, North Carolina revealed that normal rhythmic topography becomes barred and two dimensional during storms. It is instructive to compare the findings of Sallenger and Howd (1989) and Trowbridge and Young (1989) regarding the long-shore bar during different times. Sallenger and Howd (1989) documented results for two storms (October 1982 and September 1985) at FRF, DUCK, NC. During the October 1982 storm, significant wave heights were ~ 1.8 m and storm periods were 6-8 seconds. The winds shifted and energetic swell of 16-18 seconds existed the last day (10/12/82). A mild longshore bar became more developed and moved seaward with time (see Figure 2.23) during the course of the storm.

For analysis, they defined the surf zone energy saturation in terms of a parameter

$$\gamma_{rms} = H_{rms}/h \quad (2.27)$$

where H_{rms} is the RMS wave height, h is the water depth and γ_{rms} is a function of the beach slope ($\tan \beta$). Two points can be raised against this method of analysis. By their definition of γ_{rms} , H/h is constant in the inner surf zone regardless of offshore wave characteristics, which is open to question. Furthermore, beach slope is an ambiguous parameter for non-planar beaches and is difficult to specify precisely and consistently. Also, their measurement packages were seaward of the bar crest and in water depths greater than 3 m whereas the depth at the crest of the bar was ~ 1 m. By this method, the bar position was definitely landward of the outer

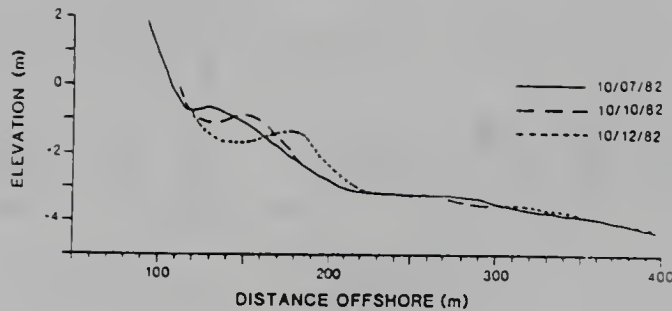


Figure 2.23: Formation and movement of a longshore bar during the 10/82 storm at FRF, DUCK, NC (from Sallenger and Howd 1989).

limit of the inner surf zone. The second (September 1985) storm resulted in deep-water significant wave heights over 1.5 m. Wave periods were always less than 10 seconds due to strong winds. A prominent bar quickly developed and moved seaward (Figure 2.24). They did not discount the break-point hypothesis as a bar- generating mechanism during this storm. In the field with a random wave climate it is very important, albeit quite difficult, to precisely quantify energy saturation and specify profile equilibrium. It is felt that a wave model like Dally (1980, 1987a) with energy flux considerations is more rational for defining energy saturation. For this reason, the wave height computations in the cross-shore model presented later use the Dally (1980) model which is discussed in the Appendix.

Trowbridge and Young (1989) presented an attractive model for onshore sediment transport under random, weakly non-linear and relatively long waves for sheet flow conditions and turbulent bottom boundary layers. The model was tested and successfully reproduced the onshore movement of a longshore bar, and the motion of depth contours near the bar crest, reported in field data sets at FRF, DUCK, NC (Howd and Birkemeier 1986) during the period February 1982 - October 1982 when wave conditions were comparatively mild.

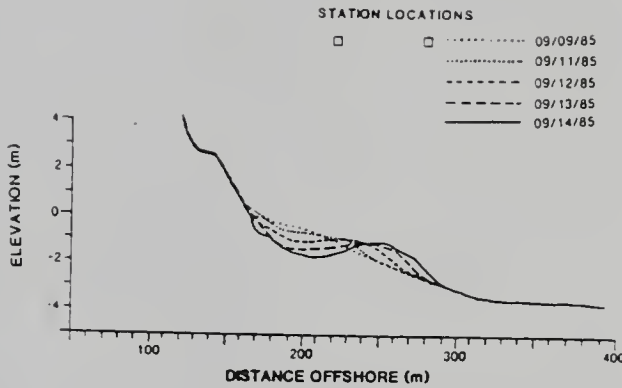


Figure 2.24: Formation and movement of the longshore bar during 9/85 storm at FRF, DUCK, NC (from Sallenger and Howd 1989).

For the October 82 storm, it is possible that a storm of greater duration might have moved the longshore bar farther offshore and more proximate to the exterior edge of the surf zone. Thus, the position of the longshore bars in the field can be considered to be responding to changes in wave height. Higher waves during storms result in seaward movement of the exterior edge of the surf zone and the longshore bar, when compared to normal/summer conditions. When this is followed by milder wave activity during summer, the exterior edge of the surf zone is shifted landward and so is the position of the longshore bar.

2.4.3 General Characteristics of Present Laboratory Experiments

A series of nine experiments was formulated to investigate bar formation mechanisms with emphasis on infragravity (IG) wave and break-point hypotheses. The experiments, which were conducted in the air-sea tank at COEL, tested the effects of wave action only, effects of tides were not represented. IG waves were generated as a result of the interaction of the primary wave field whose spectral characteristics were monochromatic (single discrete frequency), bichromatic (two discrete frequencies) or multifrequency (discrete and continuous frequencies over a narrow band). Of course, there were no IG waves for cases with monochromatic primary waves. The primary

Table 2.5: General features of bar formation investigation experiments.

Condition	Characteristic
Initial bottom slope	1:19.5
Mean sand diameter	0.2 mm
Offshore depth, h_0	0.46 m
Carrier Period, $T_{ave.}$	2 sec
Breaking wave height, H_b	0.14, 0.20 cm
Breakpoint steepness, $\frac{H_b}{L_0}$	0.057
Deepwater steepness, $\frac{H_0}{L_0}$	0.043
Deepwater fall velocity parameter, $\frac{H_0}{w_s T}$	2.7
Breakpoint fall velocity parameter, $\frac{H_b}{w_s T}$	3.4

waves were fully documented. The spectral characteristics of IG waves were either monochromatic or multifrequency, and the IG waves were also fully documented. Eight experiments commenced from an initially planar slope ($\sim 1 : 19.4$) while one experiment had an initially barred profile. Table 2.5 details the general features and nominal values of some non-dimensional parameters of the experiments, while Figure 2.25 illustrates the general morphological configuration of the experiments and the typical positioning of beach features in the air-sea tank.

Similitude considerations and model characteristics were discussed in Sections 2.1 and 2.2. The essential aspects of the same are reiterated here briefly. The (mean) diameter of sand in the air-sea tank was 0.2 mm. The prototype sand diameter was chosen as 0.4 mm. Using Froude number and fall velocity parameter scaling, the model to prototype geometric scale ratio was 1:16, while the time scale was 1:4. Using storm-like prototype conditions (Chapter 2), the offshore maximum wave height was fixed at 2.3 m with mean period around 8 seconds for all experiments, which, in model units, correspond to a wave height of 0.16 m and a time period of 2 seconds. Hereafter, all dimensions in the text are in model units unless otherwise noted.

The displacement of the free surface was measured along the wave tank using standard resistance-type wave gages. Infragravity wave characteristics were measured at various points along the profile using a manometer and stilling well arrangement

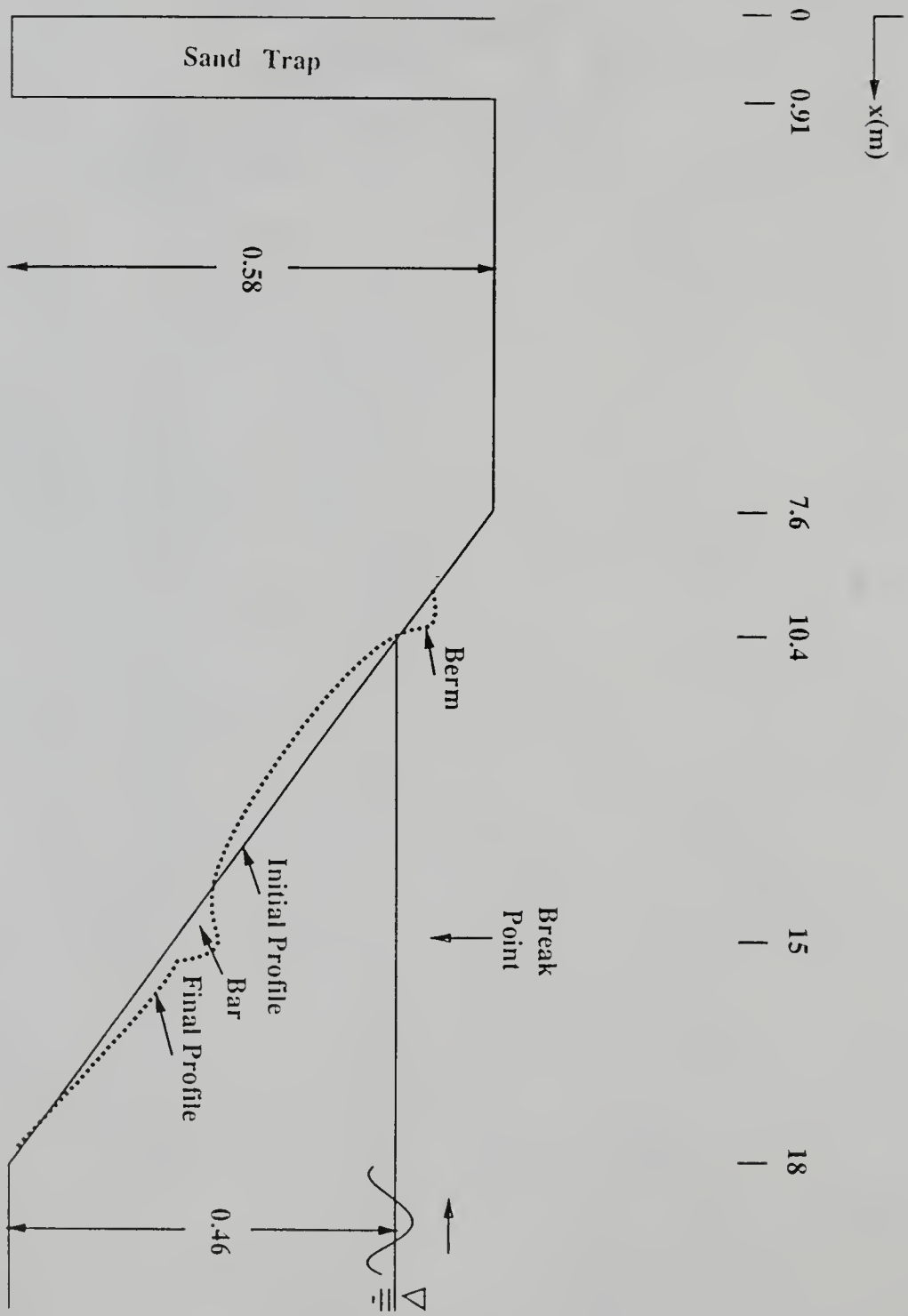


Figure 2.25: Positioning of general morphological features in the air-sea tank.

that acted as an analog low-pass filter.

All wave gages were connected to an IBM-compatible 386 PC using the software GLOBLAB for signal acquisition, display and analysis. Signal acquisition was via the GLOBLAB A/D module (Data Translation 2801 board) and analysis was in both time and frequency domains, as necessary. The primary and IG waves were sampled at 10 Hz and the sampling duration was at least 102.3 seconds. This results in a spectral resolution of 0.0098 Hz and a Nyquist frequency of 5 Hz.

All experiments were carried out for at least 4.5 hours by which time a state of quasi-equilibrium existed for the bed profiles. Three parallel, cross-shore profiles (B1, B2 and B3) were measured at one hour intervals and the measuring interval between successive points was 0.15-0.30 m. B3 was the tank centerline profile while B1 and B2 were 0.21 m on either side. The standard deviation of the three profiles was calculated and indicated generally strong two-dimensionality. Thus, the mean bed profile was used in all calculations (unless otherwise noted).

The carrier/average frequency was maintained at 0.5 Hz and the maximum wave height was approximately 0.16 m at the toe of the beach for all cases. In cases with bichromatic waves, the input signal to the wavemaker consisted of equal energies at the two primary frequencies only. However, energy spectra of measured total waves along the air-sea tank showed energies at interaction frequencies which is a result of non-linear wave-wave interaction. Analysis of wave data from various stations along the flume indicated generally moderate harmonic generation seaward of the surf zone. However, levels of energy at infragravity frequencies well inside the surf zone was comparable to or more than that at the primary frequencies. In the field, two obvious mechanisms for long waves are present. One is wave non-linearities causing the (second-order) "beat" (IG) envelope associated with a narrow-banded spectrum, and the other is the oscillating break-point associated with the narrow-banded spectrum primary waves. Desired long wave generation using wavemakers is quite complicated. A bichromatic signal to the wavemaker results in a second-order forced progressive, long wave at the difference frequency. As shown by Madsen (1971), if the second-order boundary condition for the paddle motion is not specified,

a spurious free long wave, also of second-order (Flick and Guza 1980), is generated which is initially 180° out of phase with the forced long wave. Ottensen Hansen et al. (1980) showed how to account for this boundary condition in the signal to the wavemaker. After several wave periods, continuous reflection along the shoaling beach and at the shoreline generates a quasi-steady standing wave pattern. It is also quite possible to have substantial to complete reflection of IG waves at the wavemaker paddle. Neither of these spurious effects was eliminated from the tests. Instead, the long wave envelope was always measured (at 1 hour intervals) at points spaced 0.3 m apart and only measured values are used throughout the text, unless otherwise stated. This eliminates the need to account for any extraneous effects in terms of estimation of the amplitude of the long wave envelope.

2.4.4 Correlation of Bar Characteristics and Infragravity Waves

This part of the study was basically an extension of that conducted by Dally (1987b) in which the incident primary wave spectra were biharmonic. However, portions of the method of analysis differ. The two pronounced and discrete primary peaks in the spectrum of the drive signal result in an infragravity (IG) wave corresponding to the difference frequency of the primary waves. Reflection of the infragravity component from the wavemaker, an artificiality due to the wave tank, modifies its amplitude (depending on the phase of the reflected wave).

The rationale for the present analysis was that infragravity waves can be efficiently reflected and form a standing wave system, whence the position of the bar may be correlated to the nodes/antinodes of the wave envelope. The investigations of Suhayda (1974), Short (1975), Bowen (1980), Katoh (1984) and Sallenger, Holman and Birkemeier (1985) tend to support such hypotheses. With the objective of investigating these hypotheses, four experiments were conducted in this part of the investigation in which the frequency of the monochromatic IG wave was varied to assess its impact on bar formation, while the carrier frequency was maintained at 0.5 Hz. The carrier frequency is defined as the average of the primary frequencies. The maximum wave height at the toe of the beach ($x = 18$ m) was 0.16 m in all cases.

Table 2.6: Characteristics of experiments with biharmonic waves

Case	Primary Frequency (Hz)		Difference Frequency (Hz)	Nodal Position (m)	Antinodal Position (m)	Bar Position (m)
	f_1	f_2				
1	0.53	0.47	0.06	14.3	15.3	14.8
2	0.54	0.46	0.08	13.5	15.0	14.9
3	0.55	0.45	0.10	12.5	15.0	14.8
4	0.57	0.45	0.12	11.6	13.1	14.5

The test conditions are documented in Table 2.6.

Spectral characteristics

The signal from the wave gages, after calibration, was transformed into the frequency domain with a Fast Fourier Transform (no windowing was used). The resultant signal was interpreted in terms of energy density as a function of frequency. An example set of measurements for Case 1 is presented to display evolution along the initially planar beach. Figure 2.26 documents the incident measured total and long waves and associated energy spectra. This data set was measured at the toe of the beach at 18 m. Most of the energy is contained in the two primary frequencies ($f_1 = 0.53$ and $f_2 = 0.47$ Hz). Lower energy levels are discernible at frequencies f_- , $f_1 + f_-$ and $2f_2$, where

$$f_- = f_1 - f_2. \quad (2.28)$$

It is also seen that the stilling well acts to damp the amplitude of the IG wave in the tank. Figure 2.27 is for $x = 15.5$ m which is seaward of the surf zone. It is seen that $E(f_1)$ has sharply diminished and energies at f_+ , f_- , $f_+ + f_-$, $f_+ - f_-$ are visible, where

$$f_+ = f_1 + f_2, \quad (2.29)$$

while that at the IG frequency is almost unchanged. Thus, it is seen that the higher primary frequency (f_1) component decays even in the shoaling region. Figure 2.28 is for $x = 15$ m which is just inside the surf zone while Figure 2.29 is for $x = 14$ m (well inside the surf zone) and energy at $f = f_2$ is still dominant. Some energy is now apparent at $f = 2f_-$ (Figure 2.29). The landwardmost measurement point was at x

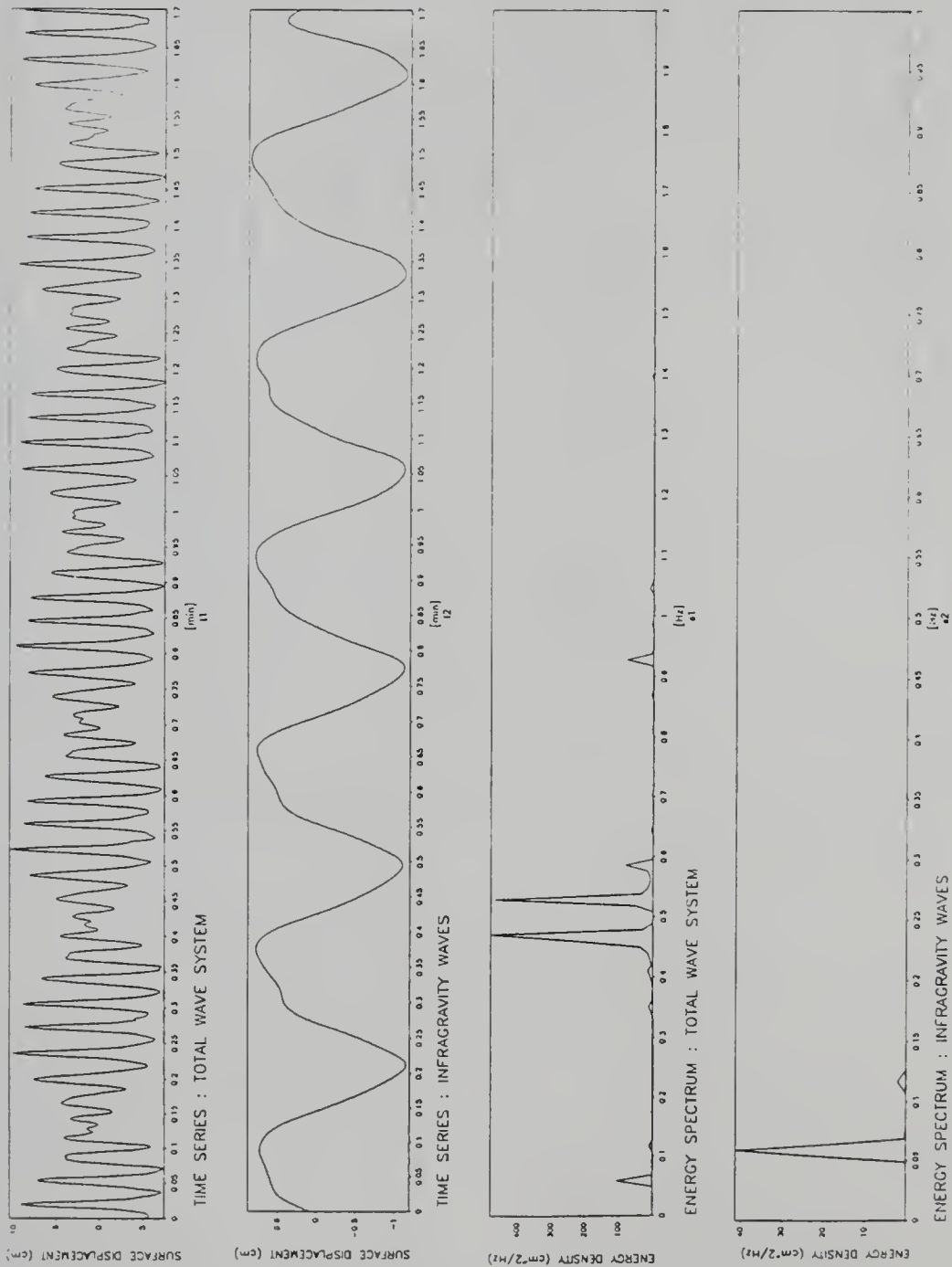


Figure 2.26: Case 1. $x = 18\text{m}$ (toe of beach). (a) Measured total wave system (b) Measured long wave (c) Energy spectrum of the total wave system (d) Energy spectrum of long waves.

= 11 m, and the data for the same are presented in Figure 2.30 where it is seen that the magnitudes of wave energies are relatively small and the majority of wave energy is at frequency $f = f_-$.

Two general features were observed in the four experiments. The first, not totally surprising, feature is the dominance of IG energy only in the region close to the waterline; the other was the rapid decay of the higher primary frequency component ($E(f_1)$) in the sloping portion of the beach (Cases 1-3) and in the horizontal portion of the tank (Case 4).

Bed profile evolution

Figure 2.31 documents the evolution of the bed profile for Case 1. The presented profiles were measured after successive one-hour intervals (except one profile at 0.5 hour). The longshore bar formed quickly within the first half-hour with $x_c=14.2$ m and the height of the bar was 0.08 m. The position of the crest of the bar was quite well established by 1.5 hours. The crest of the bar had moved slightly offshore to $x_c=14.8$ m in the final profile and the height of the bar was about 0.11 m. As mentioned above, IG energy was dominant in the region flanked by $\sim x = 8.5$ m and $x = 12$ m. This region exhibited onshore transport and a substantial, triangular berm was deposited above the still water level. Figure 2.32 presents the measured sediment transport rates at different times for Case 1. The rates were computed by spatially integrating the sediment conservation equation

$$\frac{dq}{dx} = \frac{dh}{dt} \quad (2.30)$$

where q is the sediment transport rate, x is the cross-shore direction, h is the local depth and t is time. It is seen that changes in the bed profile were greatest in the beginning of an experiment (as evidenced by the transport curve for the time interval 0-0.5 hours in the figure). Substantial transport occurred at the position of the longshore bar. Transport was minimal during the last hour (3.5-4.5 hours) of the experiment. The overall sediment transport rate, between 00 and 4.5 hours, is also shown in the figure.

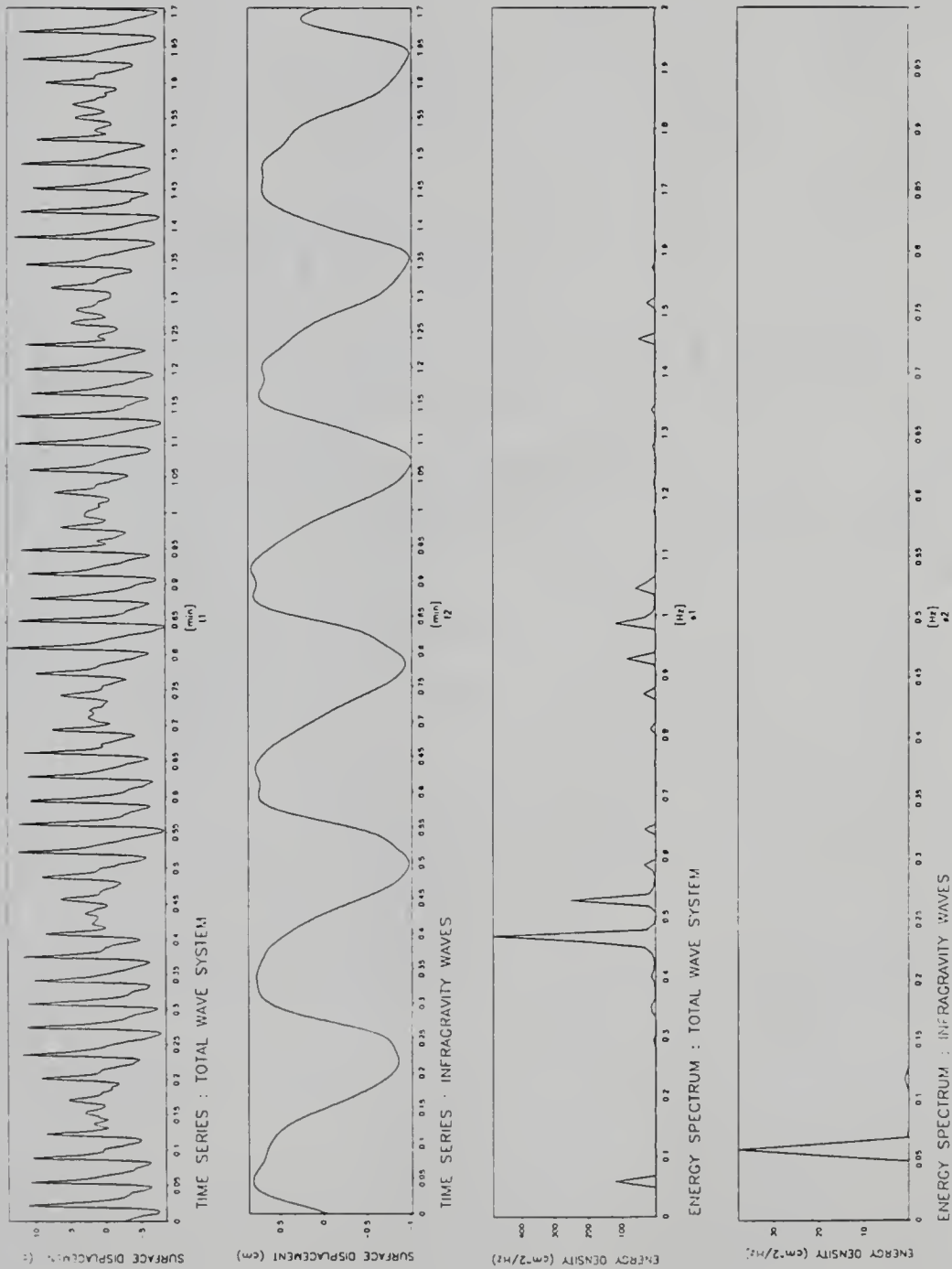


Figure 2.27: Case 1. $x = 15.5$ m (just seaward of the surf zone). (a) Measured total wave system (b) Measured long wave (c) Energy spectrum of the total wave system (d) Energy spectrum of long waves.

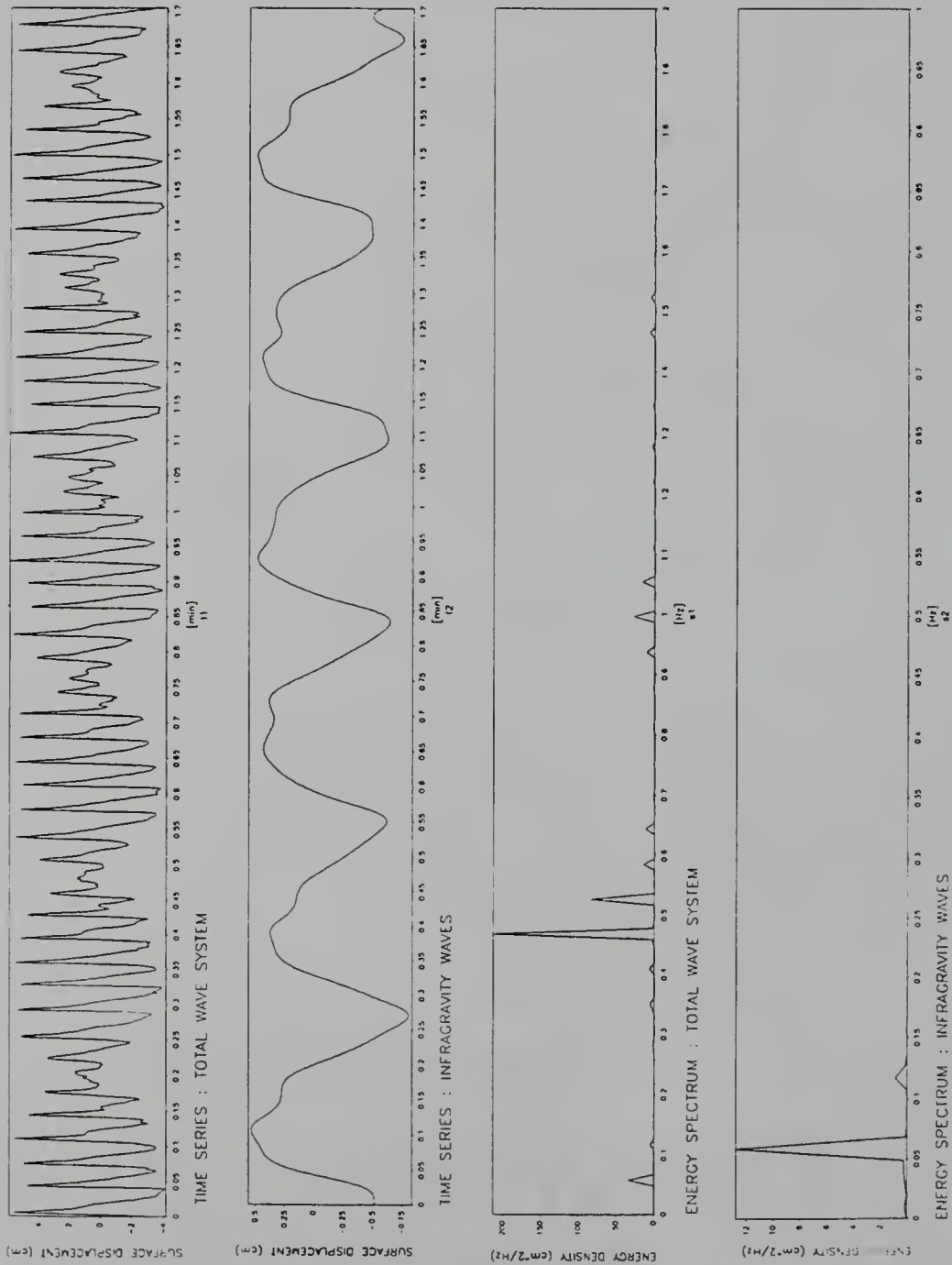


Figure 2.28: Case 1. $x \approx 15$ m. (just inside the surf zone) (a) Measured total wave system (b) Measured long wave (c) Energy spectrum of the total wave system (d) Energy spectrum of long waves.

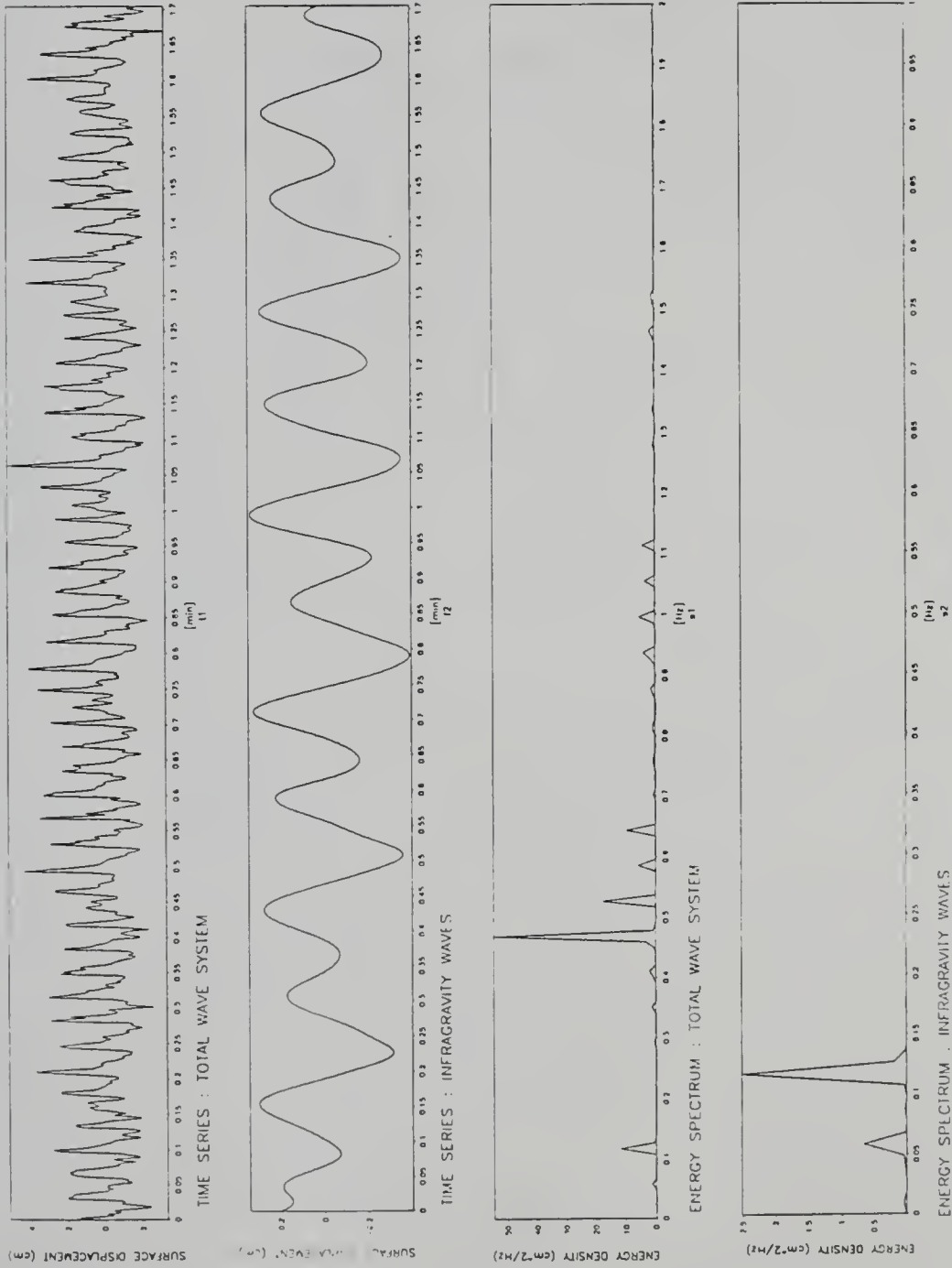


Figure 2.29: Case 1. $x = 11$ m (well inside the surf zone). (a) Measured total wave system (b) Measured long wave (c) Energy spectrum of the total wave system (d) Energy spectrum of long waves.

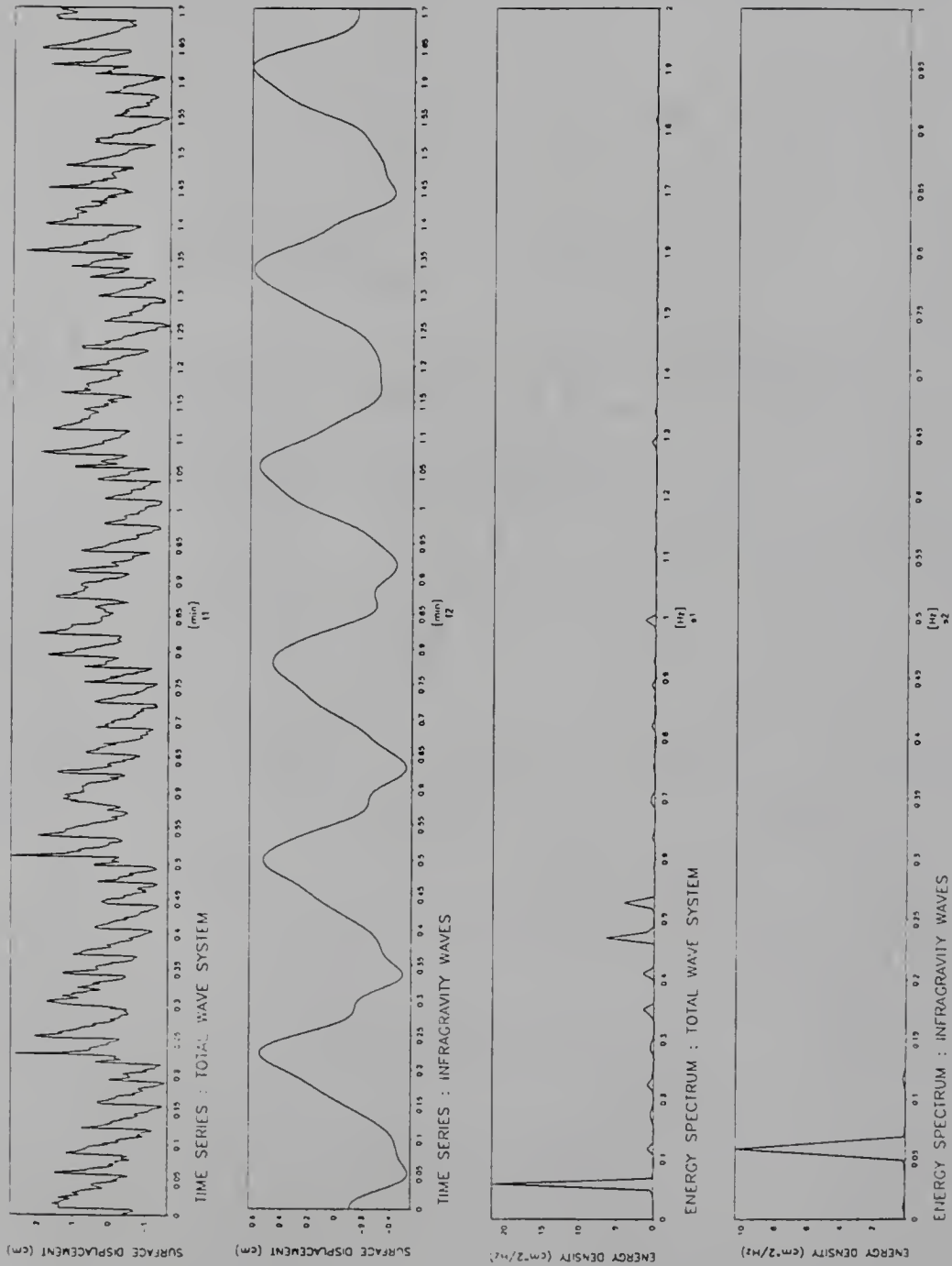


Figure 2.30: Case 1. $x = 11.6$ m (nearshore). (a) Measured total wave system (b) Measured long wave (c) Energy spectrum of the total wave system (d) Energy spectrum of long waves.

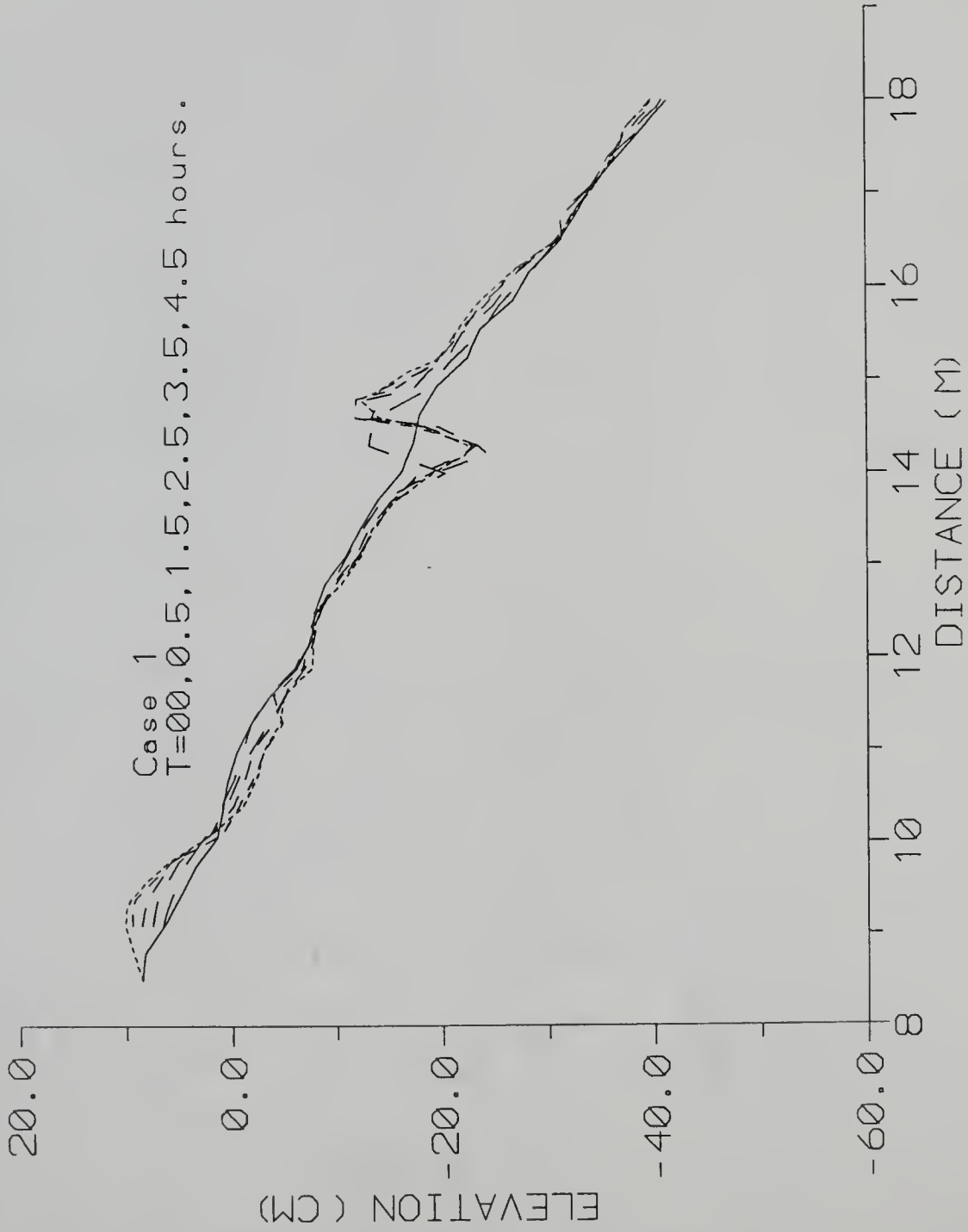


Figure 2.31: Case 1 Evolution of the bed profile 0-4.5 hours.

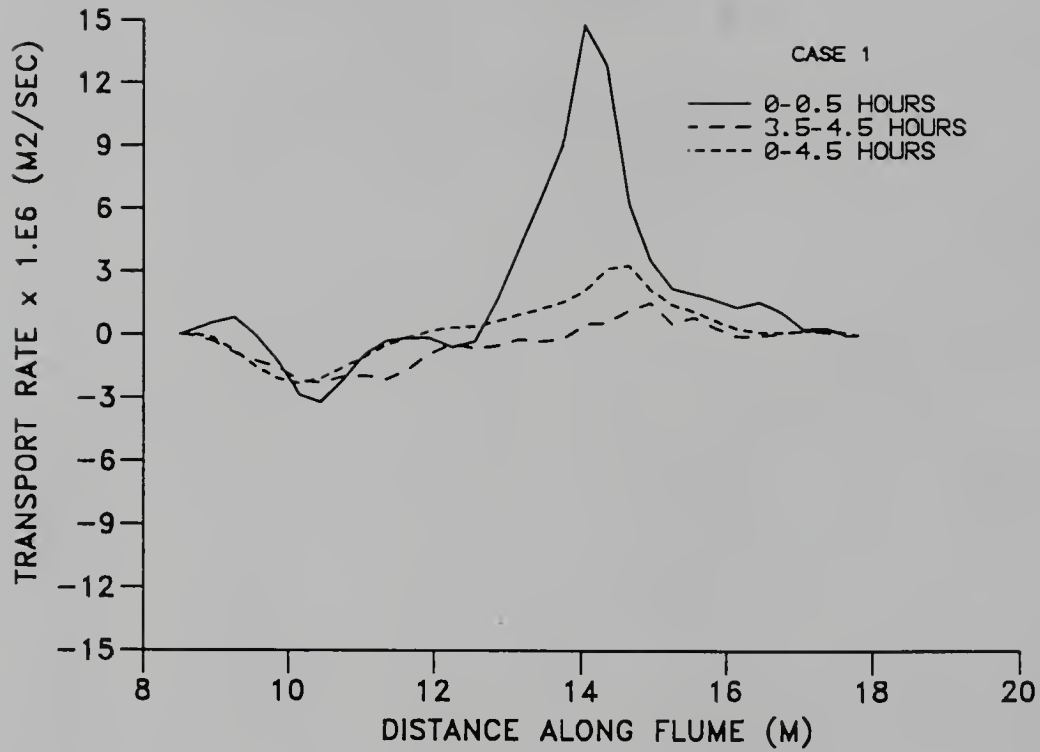


Figure 2.32: Case 1: Sediment transport rates at different times for Case 1.

Documentation of IG wave

The positions of the long-wave nodes and antinodes were fixed by the long wave period and bottom profile. In addition to measuring and documenting the long-wave structure via the stilling well arrangement, they were also evaluated by considering a numerical solution of the free long wave equation. The linearized long wave equations (continuity and momentum) can be cross- differentiated resulting in

$$\frac{\partial^2 \eta}{\partial t^2} = g \frac{\partial}{\partial x} \left(h \frac{\partial \eta}{\partial x} \right) \quad (2.31)$$

where η is the free surface displacement, h is the water depth and g is the acceleration due to gravity.

Assuming a harmonic form

$$\eta(x, t) = \hat{\eta}(x) e^{-i\sigma t} \quad (2.32)$$

where σ is the wave angular frequency, we have

$$\sigma^2 \eta + g \frac{\partial}{\partial x} \left(h \frac{\partial \eta}{\partial x} \right) = 0 \quad (2.33)$$

where the circumflexes have been dropped. For the special case of a planar beach with

$$h = mx \quad (2.34)$$

where m is the beach slope, we get

$$\frac{\partial^2 \eta}{\partial x^2} + \frac{1}{x} \frac{\partial \eta}{\partial x} + \frac{1}{x} \frac{\sigma^2}{gm} \eta = 0 \quad (2.35)$$

which is a Bessel equation with solution

$$\eta \sim J_0(\sqrt{\kappa x}) \quad (2.36)$$

where J_0 is the zeroth order Bessel function of the first kind, and

$$\kappa = \frac{4\sigma^2}{gm}. \quad (2.37)$$

Recourse must be taken to numerical methods to solve the equation for cases with non planar bathymetry.

The long wave equation (2.33) was non-dimensionalized with

$$\begin{aligned}\eta' &= \frac{\eta}{\eta_0} \\ h' &= \frac{h}{h_0} \\ x' &= \frac{x}{L}\end{aligned}\tag{2.38}$$

where η_0 is the shoreline amplitude, h_0 is the depth at the toe of the beach and L is the distance of the toe of the beach from the shoreline, and the primes indicate non-dimensional quantities. Dropping the primes, we get

$$\eta + \gamma \left[h \frac{\partial^2 \eta}{\partial x^2} + \frac{\partial h}{\partial x} \frac{\partial \eta}{\partial x} \right] = 0 \tag{2.39}$$

where

$$\gamma = \frac{gh_0}{L^2 \sigma^2} \tag{2.40}$$

with the boundary conditions

$$\begin{aligned}\eta &= 1 \quad (\text{at } x=0), \\ h &= 0 \quad (\text{at } x=0).\end{aligned}\tag{2.41}$$

Equation (2.39) was represented in finite-difference form and numerically evaluated for the wave envelope. In this form, we have (with $i=1$ at $x=0$)

$$\eta_1 = 1 \qquad h_1 = 0 \tag{2.42}$$

whence

$$\eta_2 = 1 - \frac{(\Delta x)^2}{h_2 \gamma} \tag{2.43}$$

Also,

$$\eta_{i-1} \left[\frac{\gamma h_i}{(\Delta x)^2} \right] + \eta_i \left[1 - \frac{\gamma(h_i + h_{i+1})}{(\Delta x)^2} \right] + \eta_{i+1} \left[\frac{\gamma h_{i+1}}{(\Delta x)^2} \right] = 0 \tag{2.44}$$

The solution was tested and compared favorably with the analytical solution for planar beaches, Equation (2.36). Figure 2.33 presents an example of the numerical and analytical solutions for the wave conditions of Case 3 on a planar beach of 1:19 slope.

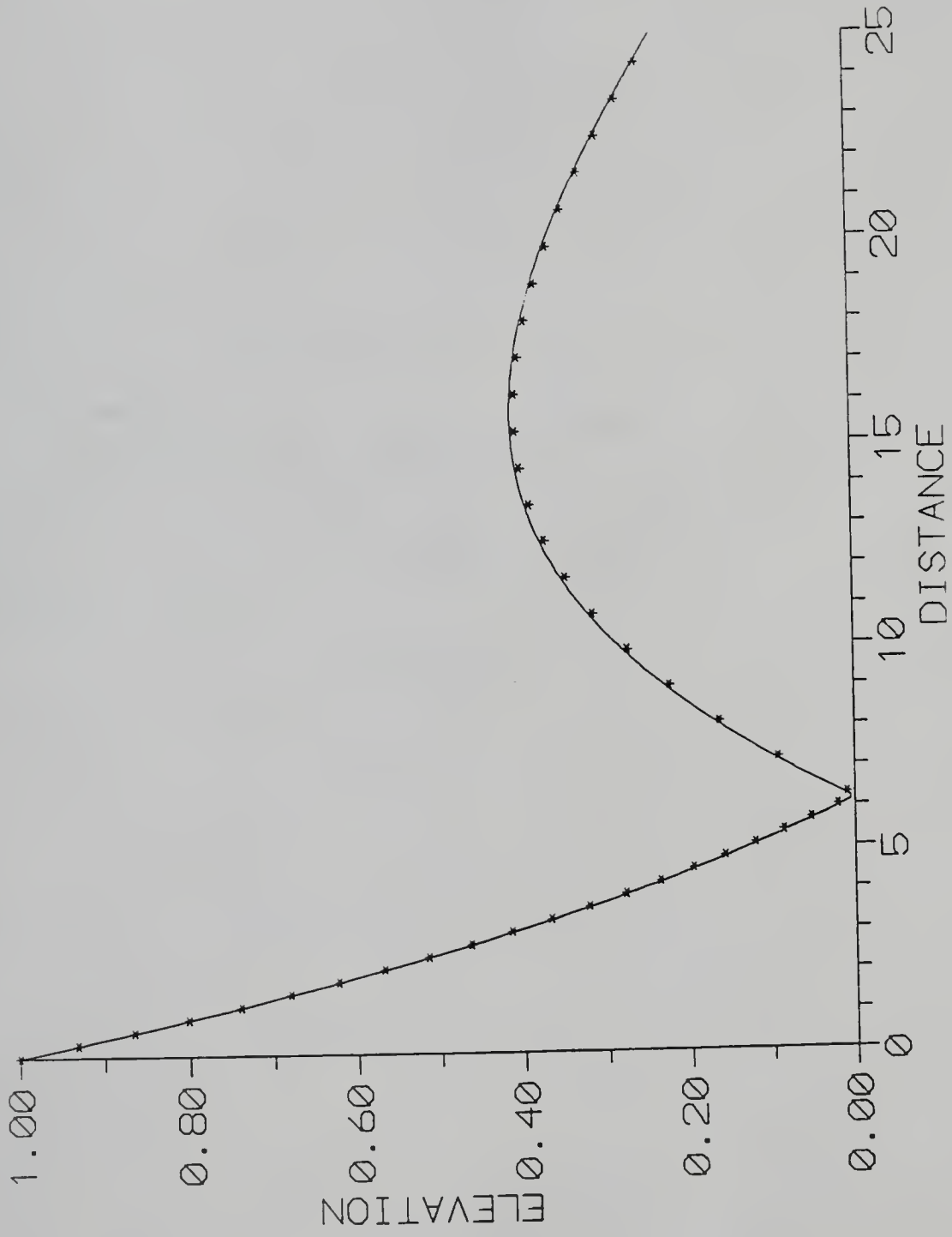


Figure 2.33: Numerical (line) and analytical (symbols) solutions for a long wave with a frequency of 0.10 Hz on a planar (1:19) beach.

Results

Figures 2.34, 2.35, 2.36 and 2.37 document the measured and predicted long wave envelopes for the four cases, together with the initial and final (after 4.5 hours) bed profiles. A least-squares procedure was used to scale the measured to the predicted amplitudes. As the IG wave frequency was increased (from Case 1 to Case 4), the first node was shifted closer to the shoreline. The antinode at the shoreline was generally not very well predicted as measurements were not possible immediately around the MSL position; however, there seems to be reasonable agreement in the prediction of the next node and anti-node in all cases. It is noted that measurements close to the shoreline were hindered by the fact that the shallow water depths made it difficult to keep the pressure-sensing end of the stilling well system under water at all times. This sometimes resulted in the intake of air bubbles in the tubing of the stilling well system and possible concomitant error. It is interesting to note that the results of a numerical model developed by Kirby et al. (1981) for trapped long waves over an arbitrary profile exhibited the feature of trapping antinodes over multiple bar systems. For the present experiments, it was noted that the bar did not trap the antinode of the IG wave in position.

Figure 2.38 shows the change in bar position with change in the measured position of the nearest node and antinode of the IG wave envelope. Changes are plotted relative to the next lower IG wave frequency. If the hypotheses involving bar formation at nodal or antinodal positions is valid, the change in bar position should coincide with change in nodal/antinodal position. This is the line of equivalence in the figure. The nearly unchanging position of the bar does not support the hypothesis that bar formation is due to the position of the IG wave envelope. The position of the exterior edge of the surf zone was the same for all cases as the maximum wave height was the same in all the experiments. This leads to the conclusion that the break-point hypothesis is more relevant. It is also relevant to note that the scales of the standing wave features are much broader than those of the bar.

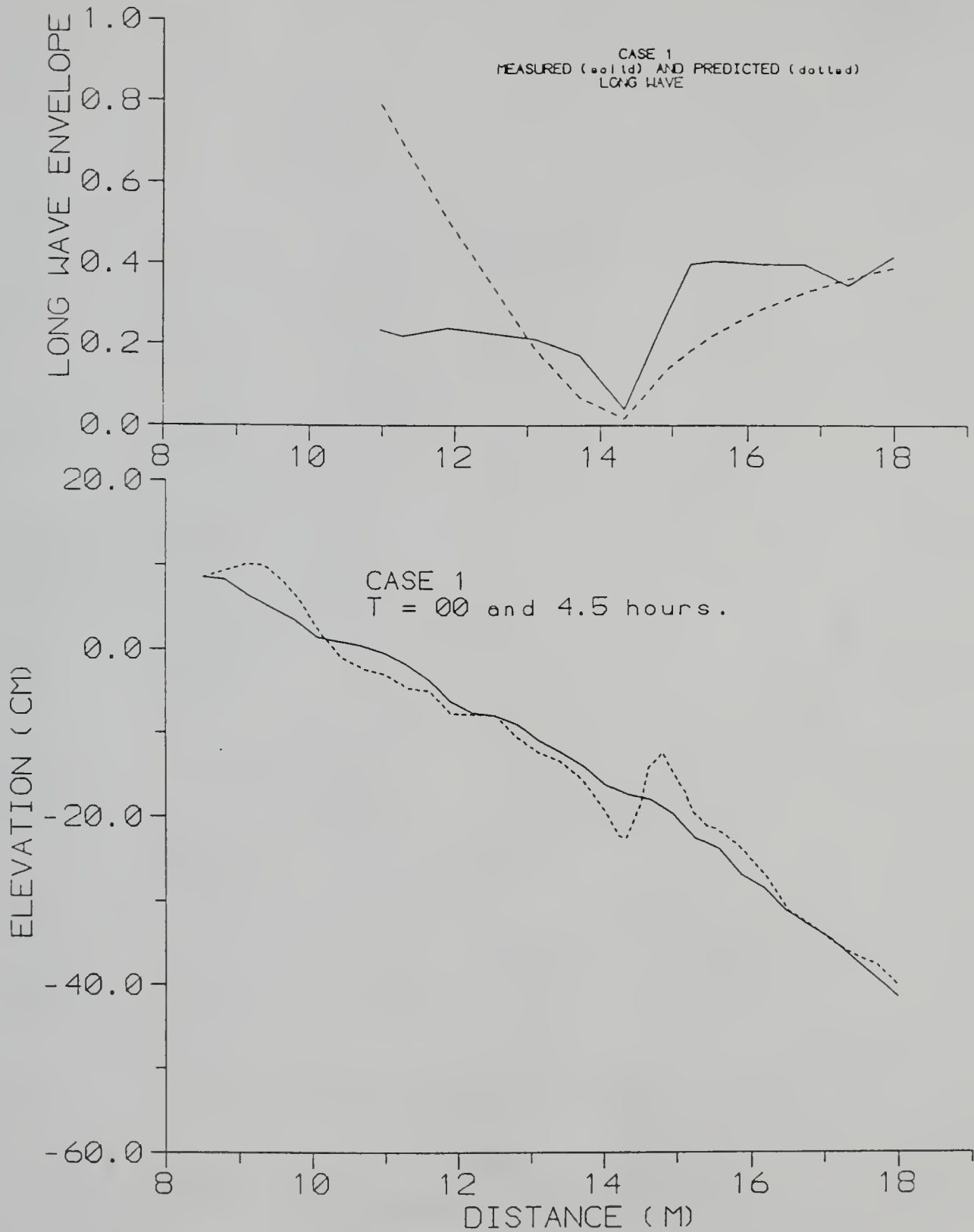


Figure 2.34: Case 1 (a) Measured and predicted IG wave envelope, (b) Initial and Final (4.5 hours) bed profiles.

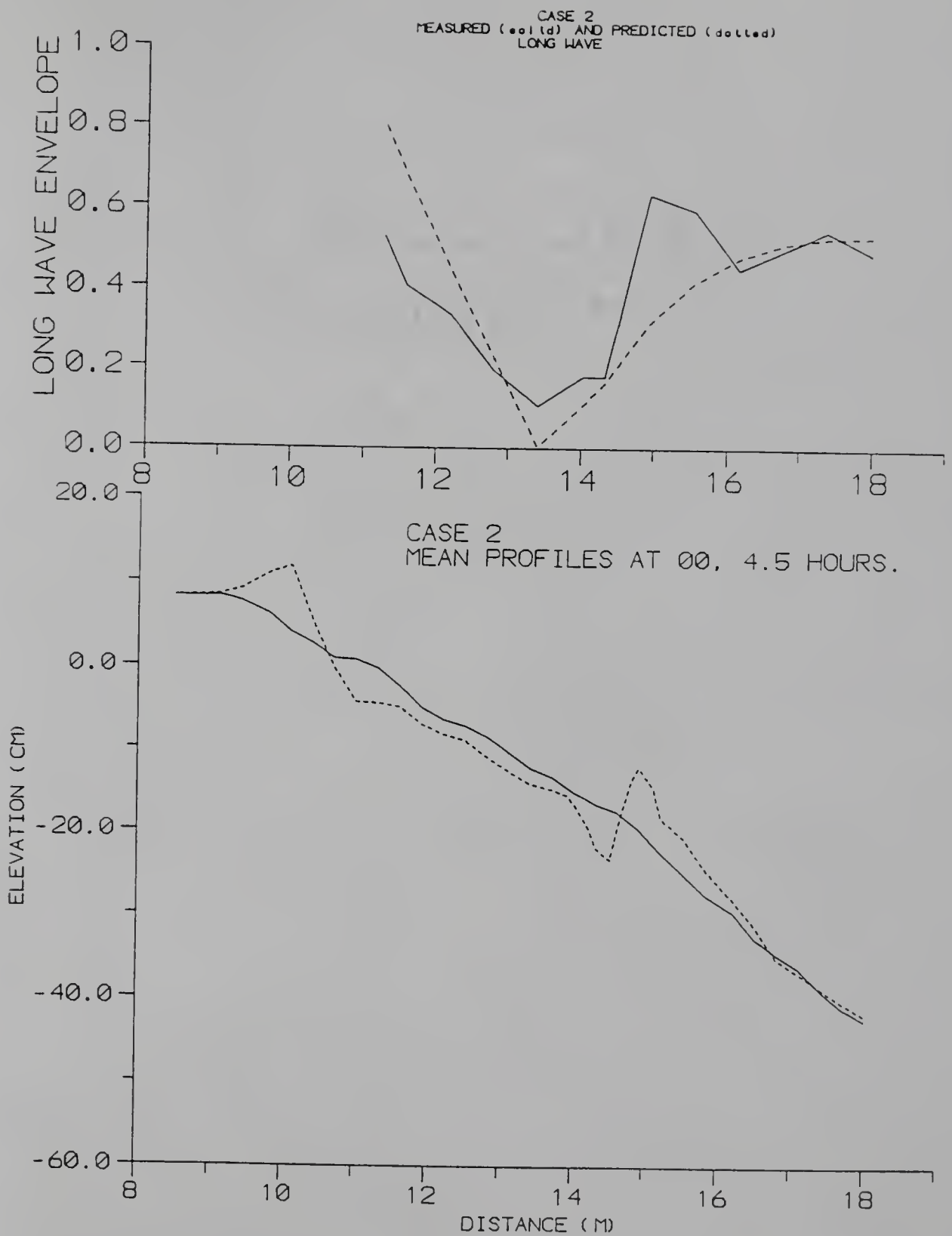


Figure 2.35: Case 2 (a) Measured and predicted IG wave envelope, (b) Initial and Final (4.5 hours) bed profiles.

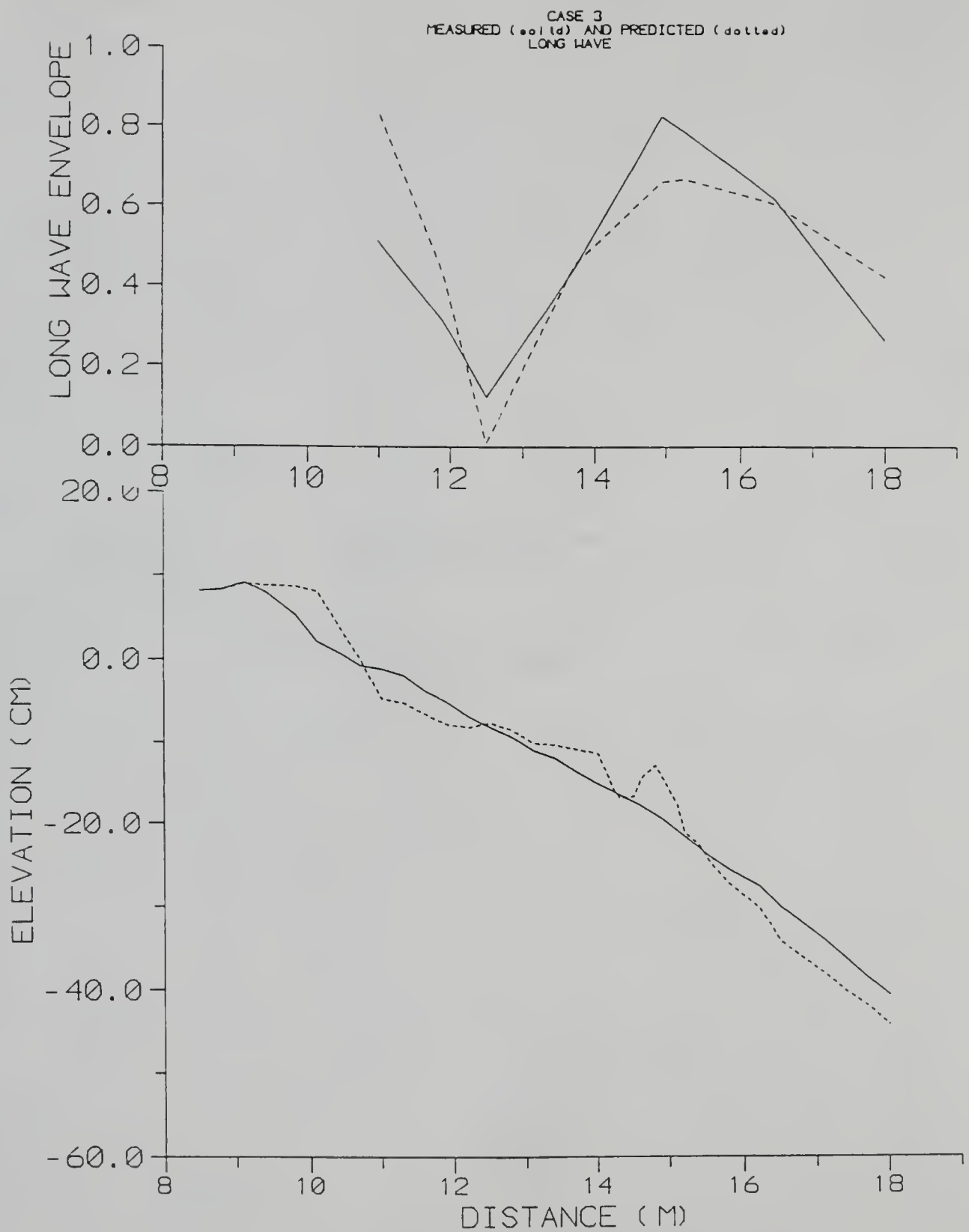


Figure 2.36: Case 3 (a) Measured and predicted IG wave envelope, (b) Initial and Final (4.5 hours) bed profiles.

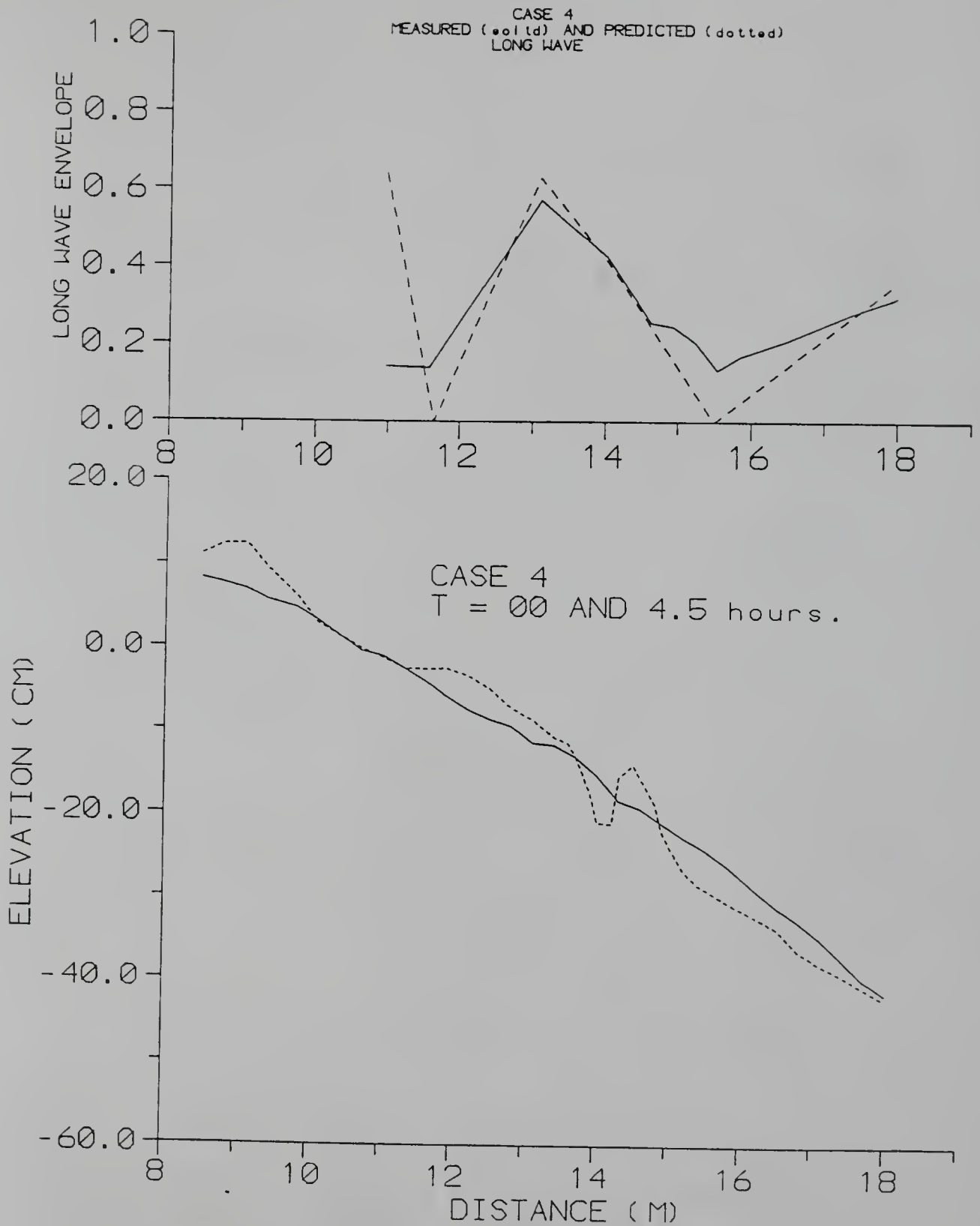


Figure 2.37: Case 4 (a) Measured and predicted IG wave envelope, (b) Initial and Final (4.5 hours) bed profiles.

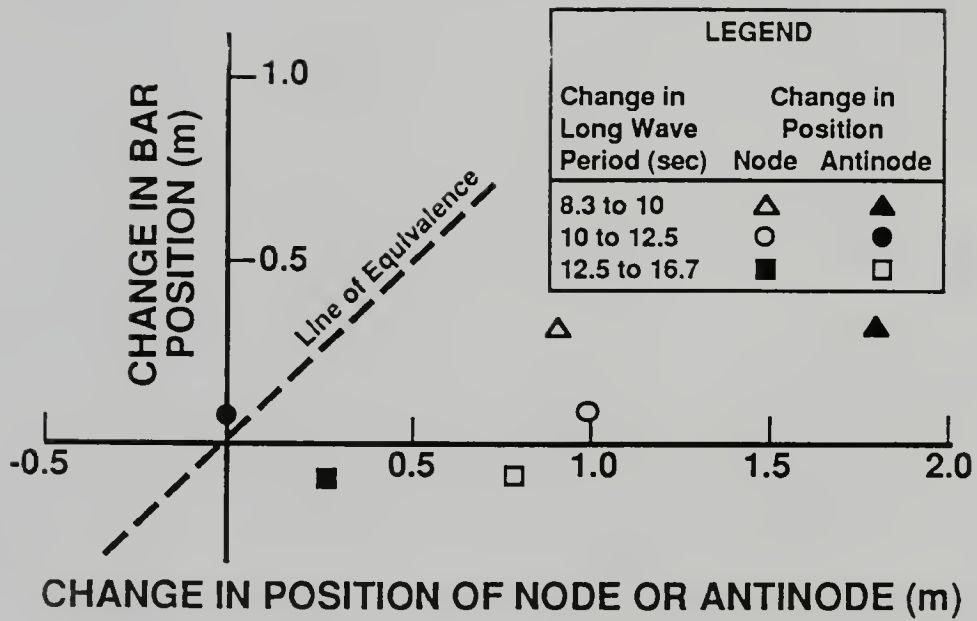


Figure 2.38: Change in bar position with changes in position of nodes and antinodes.

Table 2.7: Characteristics of experiments with non biharmonic waves.

Case	Initial Profile	Spectral Characteristic	Mean Frequency (Hz)	Bar Position (m)	Max. Offshore Wave Height (m)
5	Planar	Multifrequency	0.5	15.0	0.16
6	Barred	Multifrequency	0.5	15.0	0.16
7	Planar	Continuous	0.5	14.3	0.13
8	Planar	Monochromatic	0.5	13.9	0.13
9	Planar	Monochromatic	0.5	14.8	0.15

2.4.5 Effects of Wave Spectra and Height Distributions

This section consisted of five experiments, Cases 5 through 9. The test conditions are listed in Table 2.7. Effects of discrete multifrequency (Case 5,6), irregular (Case 7, continuous spectrum) and monochromatic (Cases 8,9) waves were investigated.

Figure 2.39 shows the time and frequency domain characteristics of the total and long waves for Case 5 at the toe of the beach. The dominant primary waves were in the band 0.45-0.55 Hz with modal frequency $f = 0.5$ Hz. There was almost no energy in the interaction frequencies corresponding to infragravity scales (i.e., less than 0.1 Hz here). Figure 2.40 shows the measured waves and computed energy spectra close to the waterline where IG (frequencies less than 0.1 Hz) energies are dominant. It is noted that the long wave was no longer monochromatic. Case 6 had very similar wave characteristics and the only difference from Case 5 was that the initial bed profile was barred. Case 7 had waves in a narrow, continuous spectrum with a peak at 0.5 Hz. The various spectral characteristics produce different wave height distribution functions. Cases 8 and 9 had regular, 0.5 Hz, monochromatic waves. The initial and final bed profiles with associated wave height probability distribution (WHPD) functions for the five Cases are shown in Figures 2.41 through 2.45.

Cases 5 and 6 with multifrequency spectral characteristics had extremely groupy incident waves (referring to Figures 2.39 and 2.41, small waves, less than ~ 0.06 m wave height, occur most of the time, while there are other, fewer times with much larger waves of up to 0.16 m wave height). In spite of differing spectra, the final position of the longshore bar in Cases 5 and 6 was approximately the same as that

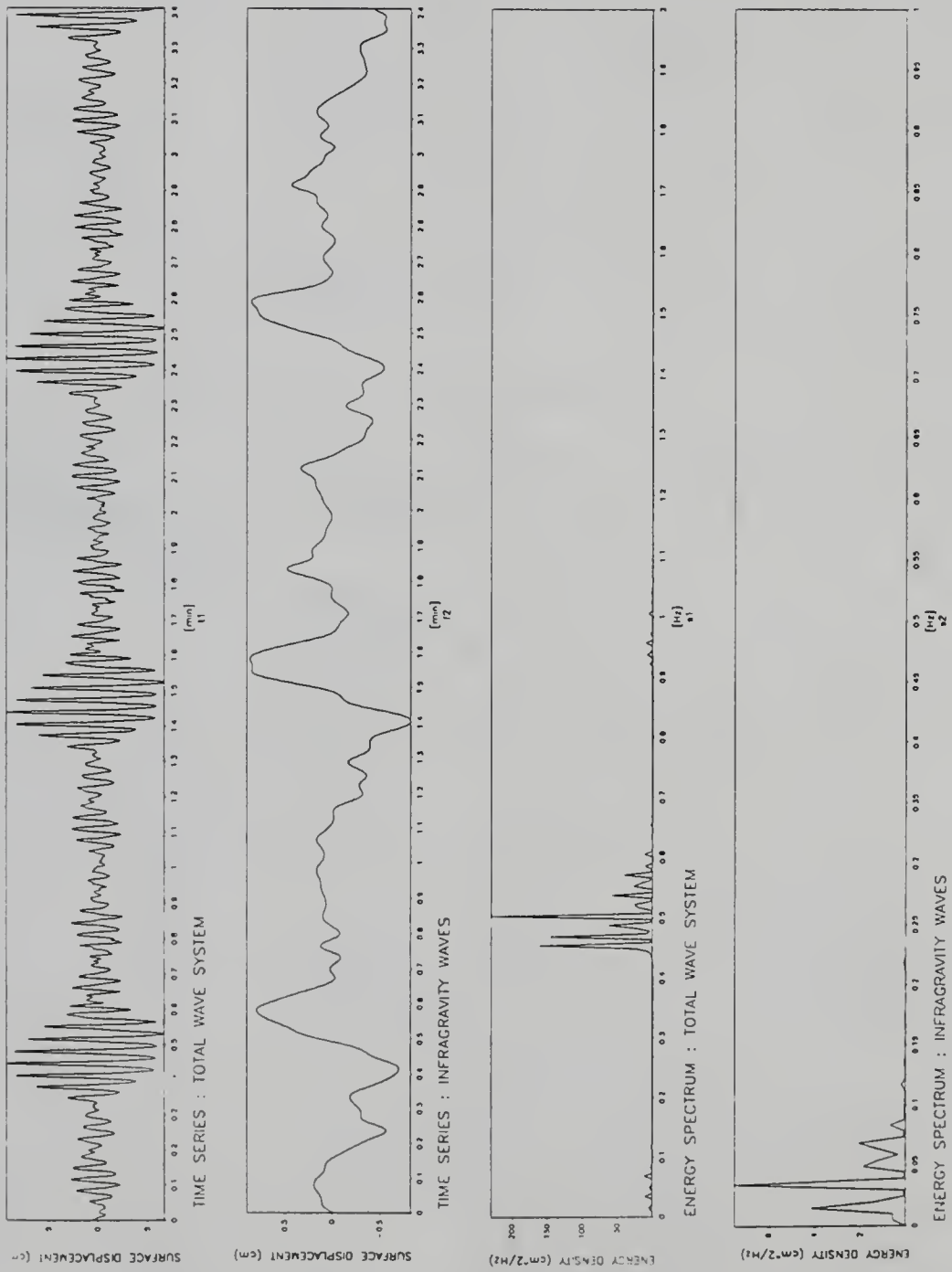


Figure 2.39: Case 5, Multifrequency waves. Total and long waves and associated energy spectra at $x = 18$ m (toe of beach).

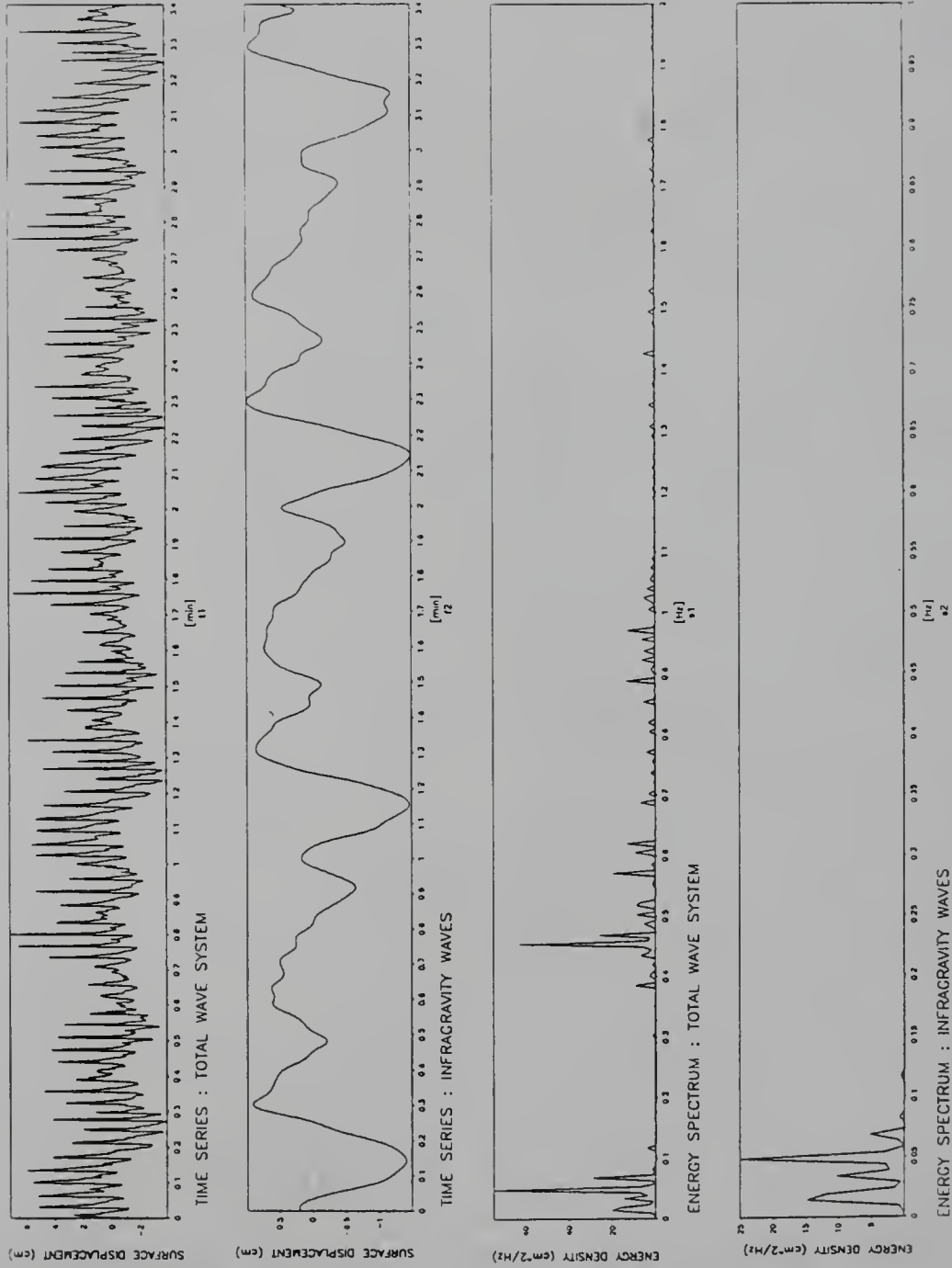


Figure 2.40: Case 5, Multifrequency waves. Total and long waves and associated energy spectra at $x = 12$ m (nearshore).

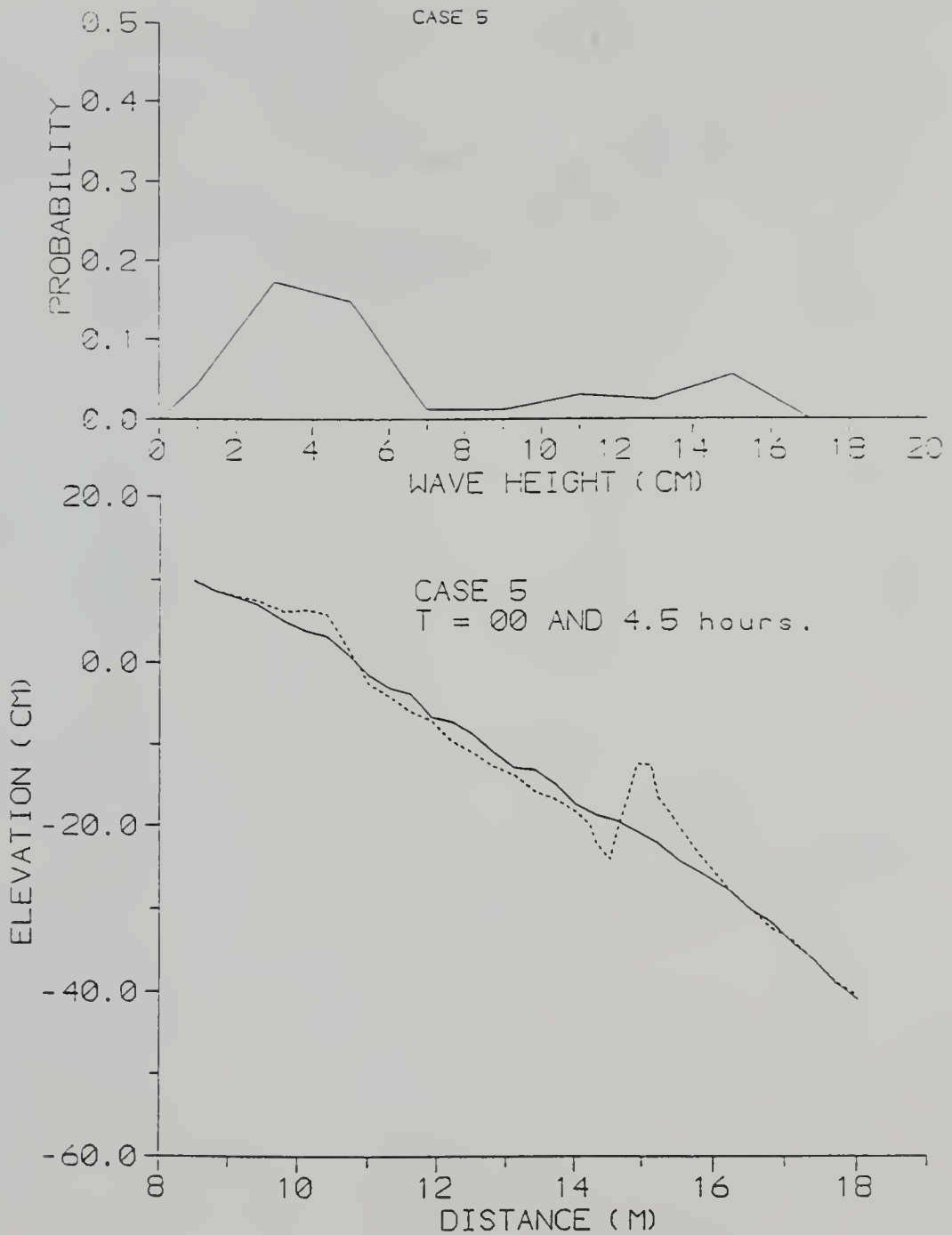


Figure 2.41: Case 5 WHPD, Initial and Final bed profiles.

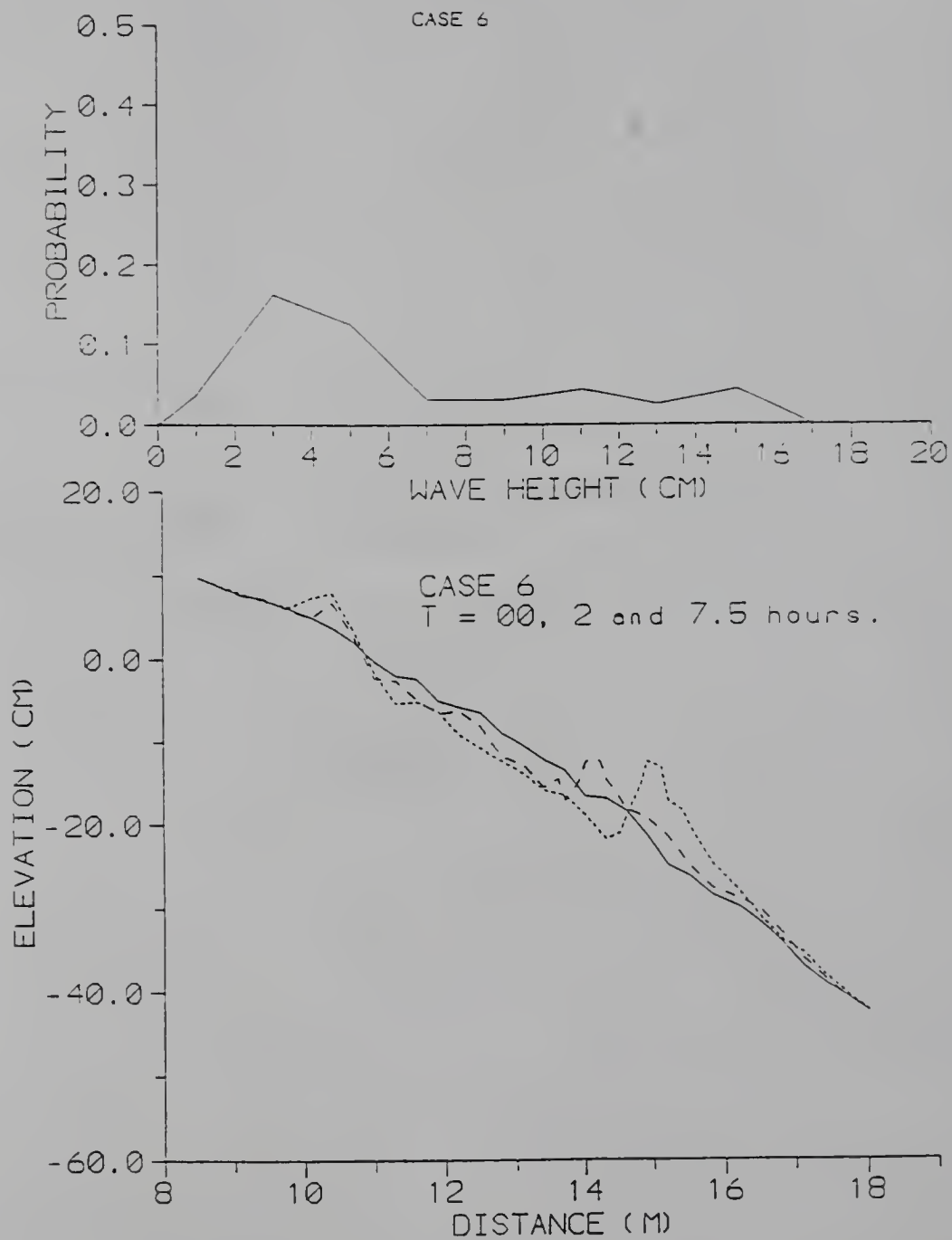


Figure 2.42: Case 6 WHPD, Initial and Final bed profiles.

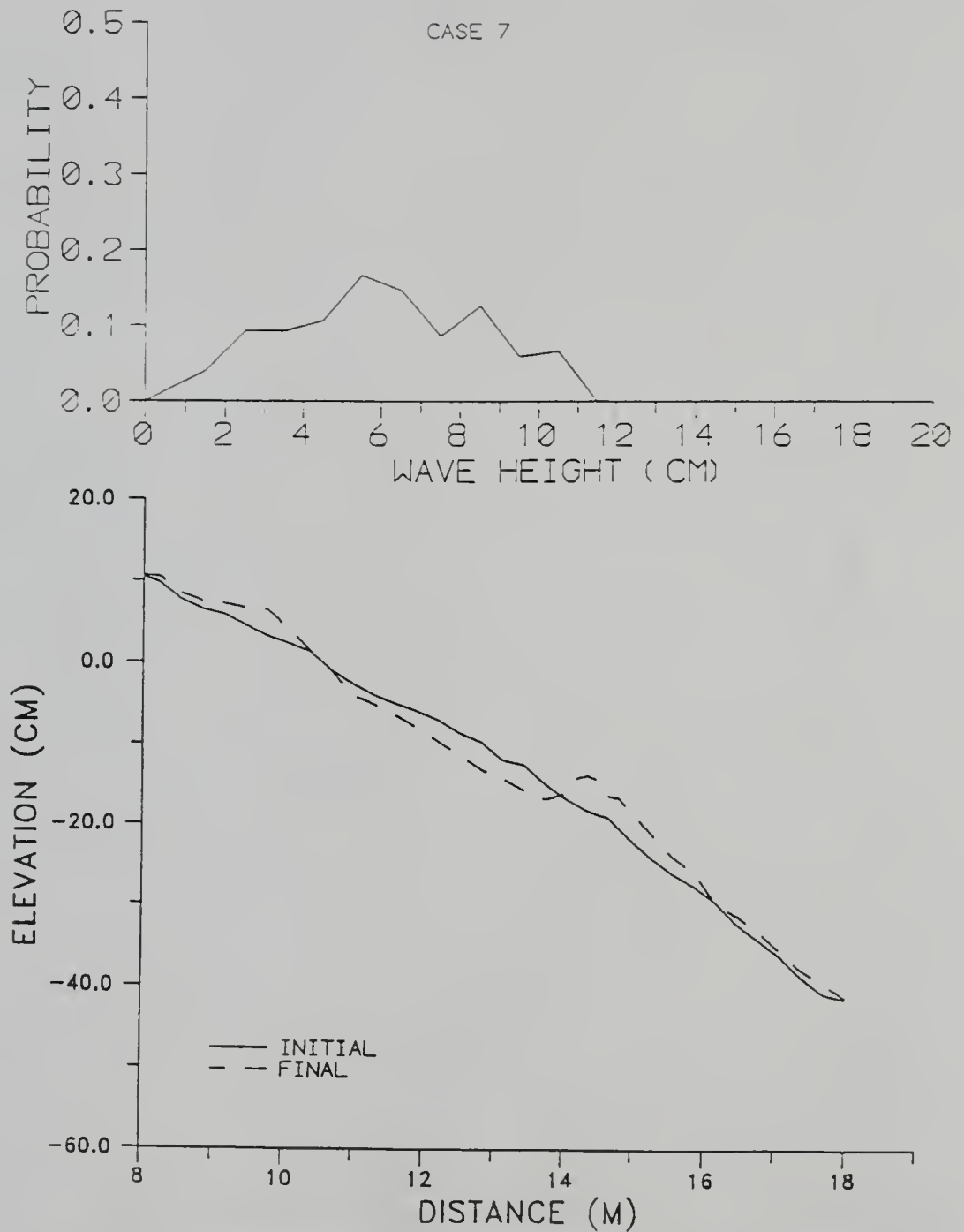


Figure 2.43: Case 7 WHPD, Initial and Final bed profiles.

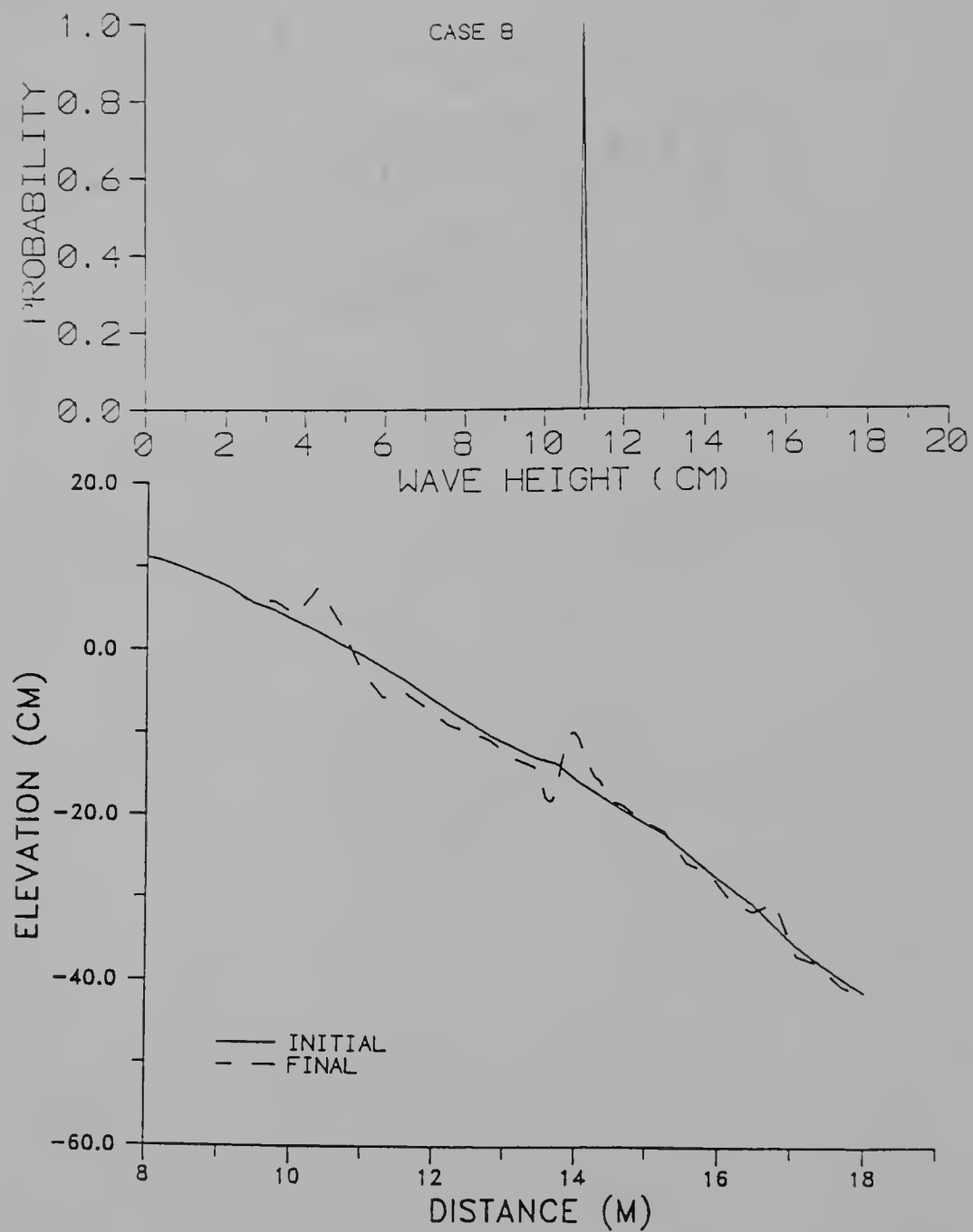


Figure 2.44: Case 8 WHPD, Initial and Final bed profiles.

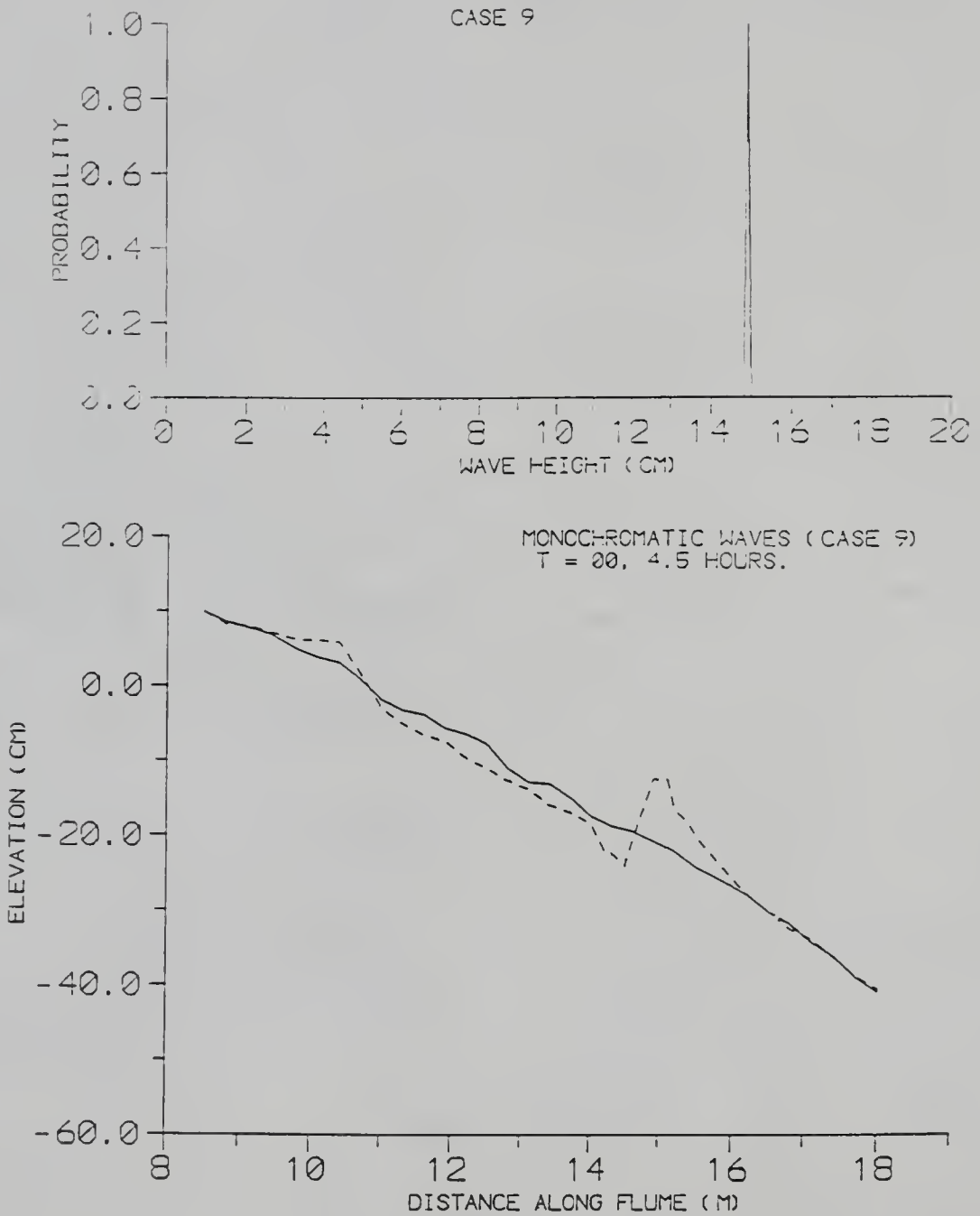


Figure 2.45: Case 9 WHPD, Initial and Final bed profiles.

for Cases 1 through 4 and Case 9. It is noted that the maximum wave height is the same for Cases 1 through 6 and Case 9. Almost no change was noted in the position, relief or size of the bar as compared to the bichromatic cases. It is interesting to note the results of Case 6. The initial profile was the result of 2 hours of wave action by 0.12 m high monochromatic waves on a planar beach. A longshore bar developed with $x_c = 14.1$ m. The experiment was then reset and multifrequency waves were run for another 5.5 hours with a maximum wave height of 0.16 m at the toe of the beach. This resulted in seaward movement of the location of the exterior edge of the surf zone and a concurrent seaward shift in the location of the bar with $x_c = 15.0$ m.

However, the bar in Case 7 with a continuous, narrow spectrum was considerably more subtle whereas that in Cases 8 and 9 with monochromatic waves again exhibited strong relief. The bar was visually verified to be at the stationary break-point in Cases 8 and 9. The effect of the WHPD function seems to be more important. The WHPD for Cases 1 through 4 are presented in Figures 2.46 and 2.47. It is seen that the WHPD functions for Cases 1-6,8,9 (with prominent bars) have primary or secondary peaks near the respective maximum wave heights whereas the peak is at nearly one-half the maximum wave height in Case 7. Obviously, the peak is at the maximum wave height for the monochromatic waves in Cases 8 and 9. The maximum wave height of the wave train defines the exterior edge of the surf zone and again reinforces the break-point hypothesis for bar formation.

2.4.6 Discussion of Results

The monitoring of the physical model of a barrier island (Section 2.3, Experiments E1-E9) under a variety of imposed wave forcings (monochromatic and narrow-banded spectrums) and overtopping conditions indicated that the position of the bar was always proximate to and correlated with the break-point. This is in concord with Dally (1987) who examined surf beat vis-à-vis undertow in the laboratory and concluded that undertow is the causative mechanism for bar generation. The conclusions of Dolan and Dean (1985) were similar for longshore bars in the Upper Chesapeake Bay. These findings are reinforced by the present series of experiments. In light of

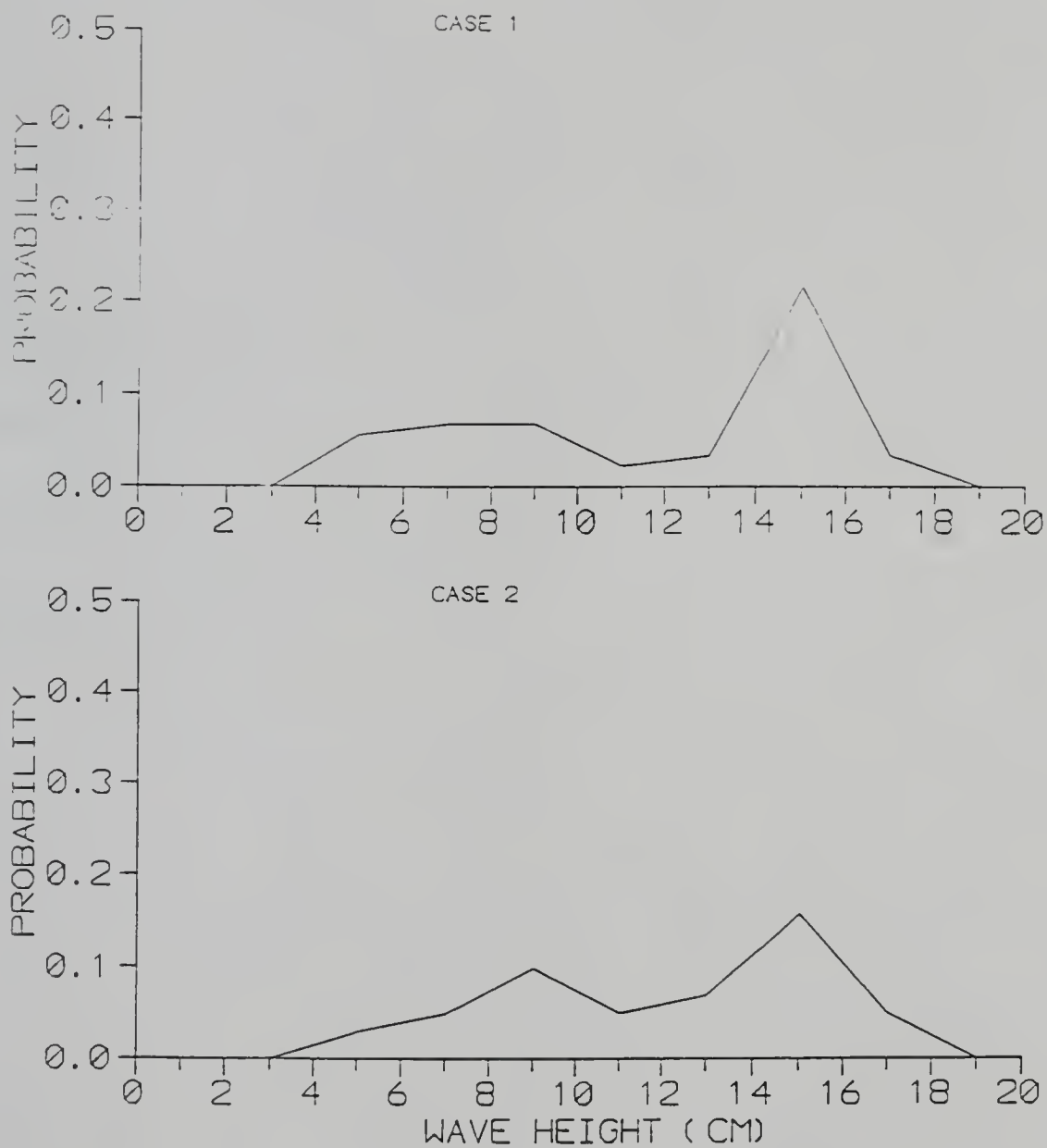


Figure 2.46: Wave Height Probability Distribution Function for Cases 1 and 2.

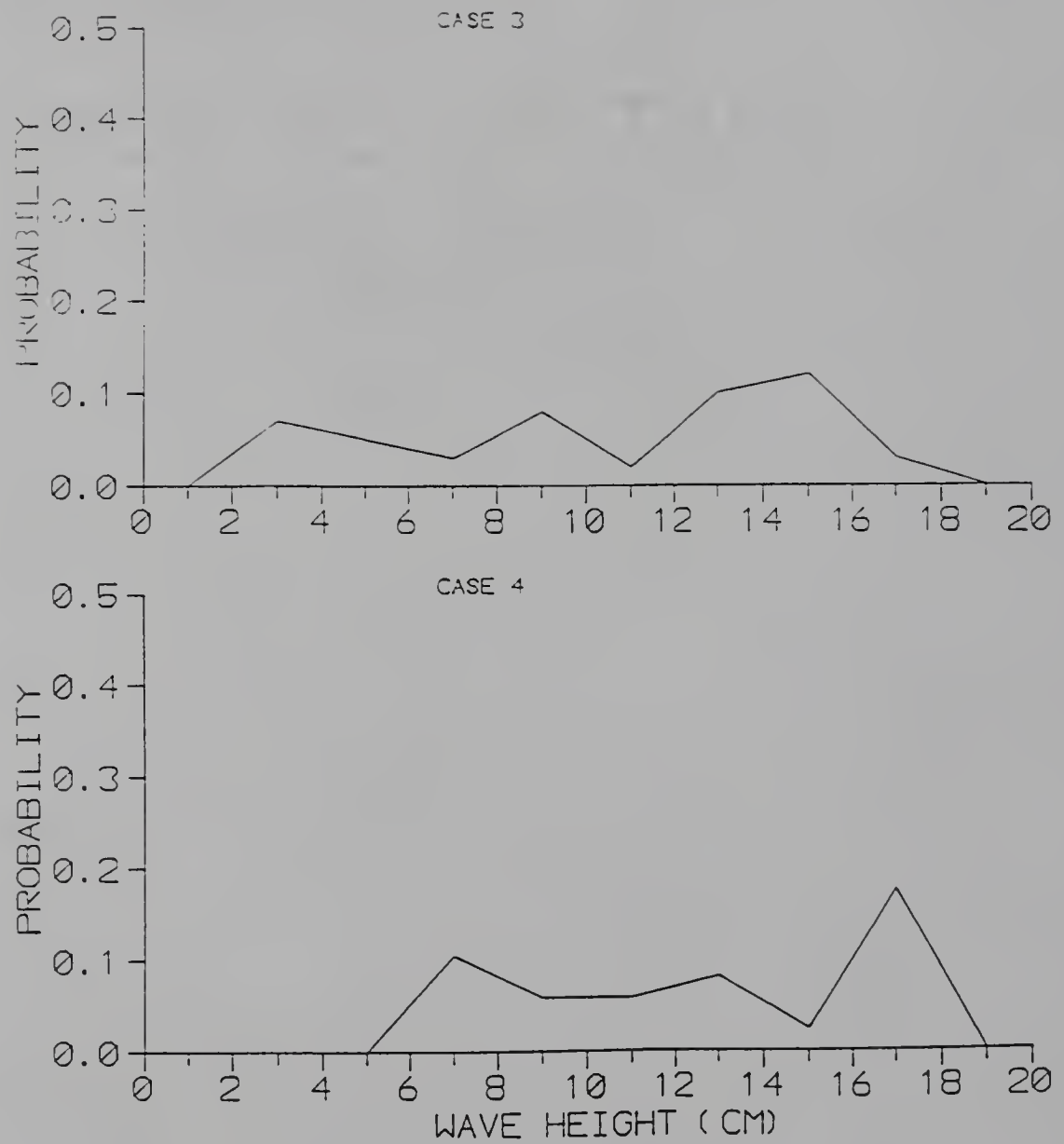


Figure 2.47: Wave Height Probability Distribution Function for Cases 3 and 4.

present and past findings, it appears that the break- point (undertow) hypothesis is the dominant causative mechanism for longshore bar generation, at least for the cases investigated here in the laboratory.

With monochromatic waves, a longshore bar developed in an initially planar profile, with the crest of the bar at the break-point. The bar had a steep shoreward face. Primary biharmonic and multifrequency spectra with accompanying IG components caused the beach to behave similarly, with the position of the bar at the exterior edge of the surf zone. Turbulence due to wave breaking appears to be the dominant stirring mechanism and cross shore flows in the surf zone are responsible for the strong sediment transport gradients necessary for bar formation. It is thus very important to correctly model cross-shore flows inside the surf zone such that bar formation is the natural effect of a coupled sediment transport model. This aspect is considered in the following chapters.

Various spectral characteristics with concomitant varying infragravity wave structures did not significantly affect the longshore bar. The longshore bar experienced little change with changes in the positions of the nodes and antinodes of the long wave envelope. Kriebel et al. (1986) suggested that the fall velocity parameter, $H_0/w_s T$ (where H_0 is the deep-water wave height, w_s is the sediment fall velocity and T is the time period), should be greater than about 3 for bar formation. The fall velocity parameter was about 3 for the present set. For marginally favorable conditions for bar formation, the shape of the WHPD function is important. The presence of primary or secondary peaks of the WHPD function near the maximum wave height is essential. Bars form at the exterior edge of the surf zone and tend to be self- maintaining by trapping waves to break on the bar. The mechanism(s) for bar formation can be conceptually considered in terms of a transport influence function with origin fixed at the time-varying breakpoint. There is seaward transport landward of the breakpoint and onshore transport seaward of the breakpoint. When wave breaking occurs over a wide range of positions, the mechanisms promoting bar generation are not positionally stable for a long enough time for the bed profile to reach dynamic equilibrium. Thus, in cases with *intense* breaking occurring over a wide breaking zone,

bar generating transport mechanisms are attenuated as compared to when breaking occurs over a narrow zone. It is strongest for a stationary breakpoint (monochromatic case). In order to reach dynamic equilibrium, there must be a negative feedback to the influence function.

The nearshore (close to the waterline) exhibited dominance of energy at IG frequencies. In all cases, a triangular berm was deposited centered about the still water line (SWL).

It appears that three regions can be identified in terms of the forcing functions and sediment transport:

- Offshore (wave shoaling) region : The first region is that from the toe of the beach to the crest of the bar which may experience onshore or offshore transport.
- Surf zone : Wave breaking results in offshore transport and return-flow (undertow) modeling is essential here. Turbulence acts as an effective stirring agent for sediment.
- Swash zone : Most of the energy is at IG frequencies and sediment transport is onshore.

These mechanisms need to be accounted for in the cross-shore sediment transport model to be developed. The next issue to be addressed is the quantification of hydrodynamics causing suspended sediment transport as they shape the prominent features of the beach.

CHAPTER 3 CROSS-SHORE TRANSPORT HYDRODYNAMICS

3.1 Background

As mentioned before, in Chapter 1, the ultimate objective was the development of a numerical cross-shore sediment transport model. Cross-shore sediment transport models in use in Europe include LITCROSS (Danish Hydraulic Institute, Denmark), UNIBEST (Delft Hydraulics, Netherlands), NPM (Hydraulic Research Wallingford Ltd., U.K.), WATAN 3 (University of Liverpool, U.K.), SEDITEL (Laboratoire National d'Hydraulique, France) and REPLA (Sogreah, France). The state-of-art in cross-shore modeling of beach systems (including the offshore) in U.S.A. with practical and commercial viability/applicability is well represented by the numerical model SBEACH (developed by Larson and Kraus 1989). This model has been developed into a user-friendly menu-driven beach profile modeling software and is in current use by the Corps of Engineers for predicting beach response to storms events. Sediment transport in the surf zone is modeled from the input wave conditions given the local water depths. This transport is modeled after the ideas of Dean (1977), Moore (1982) and Kriebel (1982) and additionally allows for the effects of local slope. The concept is that the sediment transport rate is proportional to the excess of the actual energy dissipation per unit volume from the "equilibrium or stable" energy dissipation per unit volume. The local stable energy dissipation is of course a function of the local water depth. The formulation is simple and inherently stable as the asymptotic form of the beach profile is specified (the "equilibrium" beach). But, the question is: can we specify the stable form exactly? The concept of an equilibrium beach including its limitations was further elaborated in the section on longshore bar mechanisms. Results of extensive testing of the equilibrium beach hypothesis by Dean over a number of years have been mostly positive (1991 has an excellent overview

of equilibrium beach concepts), though some investigators (e.g., Pilkey et al. 1992) dissent about the applicability of this concept. The sediment transport in the model SBEACH in zones other than the surf zone are specified totally empirically and will not be discussed further. The model predicts erosion or deposition depending upon an empirical specification. Anyway, the dissipation term is modeled as due to the measured or computed gradient in the wave energy flux, and so the driving force for such a model is the wave field specification. A drawback of applying standard equilibrium specifications is that the predicted bed profile is monotonic (though this is not the case with SBEACH). Now, reflecting back to Sections 2.3 and 2.4, the present laboratory experiments conducted to investigate beach response under overtopping conditions with shore-normal waves revealed the almost ubiquitous presence of a longshore bar. With the need to represent the longshore bar and the depositional characteristics over the crest of the barrier island in cases of overtopping, and because of the intent of developing a physics-based transport model, the closed-loop approach of an equilibrium profile-type model was discounted and the open-loop approach was adopted. Finally, although the predictions of a formulation including equilibrium beach concepts is generally good on macroscales, it is felt that with the aid of recent measurements and analyses of surf zone dynamics, a more physics-based cross-shore transport model is possible. It is added that the pitfalls of such an approach lie in the extensive modeling required of, hopefully, independent processes or effects causing superposable sediment transport.

In the following, the simplest wave theory, that for linear waves carried to second-order (in the relevant small parameter, e.g., wave steepness), is used wherever possible. The advantages of such an approach are that the integral quantities like energy flux, momentum flux, etc. are well represented in terms of the first order solutions which in turn are easily specified; and for quantities such as the momentum flux excess from the hydrostatic or “radiation stress”, the effect of turbulent contributions can be simply superposed. The modeling of surf zone processes strictly requires the abandonment of a wave theory based on a potential-flow approach. Hydrodynamics in the surf zone must consider the effects of rotation and turbulence, linear and angular

momentum fluxes resulting from wave breaking, and to the author's knowledge, there does not exist a theory which can handle this complication rigorously. For example, as discussed in Dally and Dean (1986), all other methods require the use of measurements (of velocities, for example) with substantial calibration (in the form of flexibility offered by the "calibration factors") and end up with results not much better than those obtained by using linear wave theory. Application of the theory in shallow water leads to expressions for the local sediment transport which are specified in terms of the local wave height. It is emphasized that the modeling of surf zone hydrodynamics and associated sediment transport is a combination of science and a modicum of art. This is not a reflection of the status of the oceanographic/coastal engineering scientific community but, rather, it is an indication of the complexity of the actual problem because of the number of variables and uncertainties involved. Thus, the best approach seems to be to keep the mathematics and physics as fundamental as possible, while taking into account many of the recent phenomenological observations wherever required. The analytical portion of the model requires that a sinusoidal disturbance be considered, which does affect the generality at second order, though by Fourier's theorem, any arbitrary disturbance can be represented as the sum of sinusoids which to first order propagate independently.

Recapitulating, the investigation of longshore bar formation mechanisms (Chapter 2) supported the hypothesis that longshore bar formation, at least for the cases investigated here, was primarily due to wave breaking. Thus, the aspects of sediment transport resulting in this convergence of transport near the breakpoint need to be clarified first.

3.2 Convergence of Sediment Transport

As demonstrated by Trowbridge and Young (1989), Longuet-Higgins' (1953) pioneering method of solution for the mass transport in the bottom boundary layer can be extended to simply compute the mean bottom shear stress. With shallow water approximations, assuming weak non-linearity and a quadratic drag law for the instantaneous shear stress in the boundary layer, the mean bottom shear stress τ_b can

be expressed as a function of moments of the bottom velocity vector or the surface elevation, i.e., of a form

$$\tau_b \sim \Pi(U_1^2|U_1|) \quad (3.1)$$

$$\sim \Theta(\eta_1^2|\eta_1|) \quad (3.2)$$

where the subscripts indicate the order of the variable in terms of powers of the small parameter a/h , where a and h are the characteristic (local) wave amplitude and water depth respectively and U_1 , the free stream velocity outside the boundary layer, has been specified in terms of the free surface elevation. Assuming simple forms of the surface elevation as in, for example, normally distributed Gaussian waves, the relation becomes

$$\tau_b \sim \mathcal{G}(<\eta_1^2>^{3/2}) \quad (3.3)$$

where $<>$ indicates ensemble-type averaging and the expression is in terms of the free surface. Assuming conservation of wave energy flux given by

$$F = \overline{\eta^2} \sqrt{gh} \quad (3.4)$$

the mean bottom shear stress can then be expressed as a simple function of the energy flux. In the general case, the shear stress and transport can be expressed as simple functions of the bottom velocity which can be prescribed in terms of measured or computed surface elevations. In any case, the shear stress and the bedload transport are necessarily only in the direction of wave propagation (onshore). Now, in the shoaling or non-breaking region, a similar treatment of the streaming velocity in the bottom boundary layer results in onshore directed sediment transport. The approximations involved in these formulations may limit their applicability to before breaking conditions where non-linearity is not appreciable. Furthermore, the first formulation requires shallow water approximations. Bagnold's (1963) energetics-based sediment transport formulation also leads to onshore transport. Noting the fact that natural beaches have a concave upwards shape, it can be concluded that these models offer attractive mechanisms for modeling onshore sediment transport which is always present in nature, as the subaqueous beach profile would otherwise be flat or convex!

Of course, gravity is a pervasive force contributing to offshore transport. The other causes of offshore transport are slightly more subtle. The first analytical analysis of cross-shore currents in the surf zone was by Dally (1980). There have been various extensions to the same idea; this idea is discussed in greater quantitative detail later, as this mechanism forms a core part of the present suspended transport model. The mechanism(s) responsible for offshore transport in the surf zone can be briefly described as follows. Wave breaking results in a transfer of linear and angular momentum to the water column and an offshore directed mean flow develops close to the bottom. The augmented mass flux near the wave crest due to wave breaking together with the integral form of the linear momentum equations indicate a strong mean return flow (commonly termed undertow for brevity) in the lower regions, i.e., below the level of the wave trough of the water column, within the surf zone. This return flow can cause substantial offshore transport of suspended sediment at/near the breakpoint and in the surf zone. This results in conditions favorable for the formation of a longshore bar. It is stressed that the imbalance (in the vertical) between the local radiation stress gradient and the pressure gradient (which is invariant over depth) is the driving force for these cross-shore currents which are of second or higher order. These cross-shore currents can be interpreted as a vertical circulation pattern because the flow is not constant over the vertical. Furthermore, as the gradient of the radiation stress is not constant in the cross-shore direction, the undertow is a function of the position in the surf zone.

In the following, we discuss the pertinent factors in breaking waves which affect the cross-shore sediment transport.

3.3 A Note on Breaking Waves

Broadly speaking, incident waves cause motion (in the fluid) of different regimes due to breaking and non-breaking waves, which correspond to the dissipative and non-dissipative states respectively. Only the dissipative state is discussed here. Some theoretical criteria for the breaking of periodic waves on an uniform slope have been derived as limiting conditions for solutions of non-breaking standing waves; these

differ in the definition of the limiting condition and its evaluation in terms of the bottom slope α and the deepwater wave steepness $k_0 a_0$ with k_0 and a_0 being the deepwater wavenumber and amplitude respectively. The pioneering theoretical work was that of Carrier and Greenspan (1958) with extensions by Keller (1963) and Munk and Wimbush (1969). Wave breaking on a beach can occur in a continuous gradation of regimes. The type of breaker and degree of reflection is generally predicted based on two ordering parameters ϵ and χ_0 (Galvin 1968, Battjes 1974, Guza and Bowen 1976, Battjes 1988), where

$$\epsilon = \frac{\sqrt{2}\pi\omega^2 a_0}{g\alpha^{5/2}} \quad (3.5)$$

$$= \sqrt{2\pi} k_0 a_0 \alpha^{-5/2} \quad (3.6)$$

$$\chi_0 = 2\omega^2 a_0 \alpha^{-2} \quad (3.7)$$

and ω is the wave frequency.

Breakers are usually characterized as spilling, plunging or collapsing (Galvin 1968). Collapsing breakers occur at the shoreline and a surf zone does not exist, so these are not included in the current discussion. Plunging and spilling breakers differ only in their description of the initial breaking process. Plunging breakers are characterized by the steepening and overturning of the wave crest while the shape is quite symmetric in the case of spilling breakers with smaller instabilities developing on the crest; whitecapping or aeration in spilling breakers is first evident near the top of the wave and then spreads downwards across the front face. Both types of breakers may be modeled as turbulent bores further inside the surf zone with the preservation of wave shape and self-similarity hypotheses. These bores collapse as they reach the shoreline and the thin layer of water rushing up and then back the shoreface is termed runup or swash.

3.4 Characteristics of Breaker Evolution

An early qualitative model of turbulence associated with a spilling breaker by Peregrine and Svendsen (1978) suggests a combination of a mixing layer and a wake. In a coordinate system moving with the breaking wave front, the flow in a narrow “wedge” region near the front of the wave is similar to that in a mixing layer and

there exists wake flow in the dominant region seaward of the breaking region, where turbulence spreads and decays. In effect, the fully developed region may be modeled similar to a wake. Only lately have there been major advances in the documentation of internal flow characteristics of breaking waves with accurate and high-resolution velocity measurements in the surf zone generally using laser Doppler velocity meters (LDV) and hot-film anemometers (including Stive 1980, Nadaoka and Kondoh 1982, Sakai, Inada and Sandanbata 1982, Sakai, Sandanbata and Uchida 1984, Hattori and Aono 1985, Mizuguchi 1986, Okayasu, Shibayama and Mimura 1986, Stive 1988 and Nadaoka, Hino and Koyano 1989). These measurements have significantly contributed to our understanding of surf zone processes. The pertinent features of some of these measurements and analyses are discussed below. In particular, some of Nadaoka's (1986) findings, who conducted extensive laboratory experiments in a closed end flume with a 1:20 slope wooden beach to measure velocities and the structure of turbulence in the surf zone, are elaborated.

In plunging breakers, wave overturning eventually causes the front of the wave to close down on the water surface and trap a cavity of air. The cavity eventually collapses and a region of high vortical motion with air bubbles develops. The formation of a large scale vortex implies a loss of energy to the wave motion but not to the total large scale kinetic energy. The impingement of the front or "jet" causes another splash-up of a wedge of water. Several of such cycles are possible for each breaker (including Miller 1976, Nadaoka 1986 and Jansen 1986). Each of these splash ups then produces a large-scale two-dimensional vortex rotating in the same direction, at least for the initial jets, with concomitant high shear rates between the vortices resulting in strong dissipation of wave energy. The scales of these impulsively generated coherent or organized vortex-like structures decay shoreward into the surf zone with the wave height. At any instance, the point remains that the initial, superficial appearance of chaos and whitecapping in the transition does not reflect in any loss of energy or momentum attributable to large-scale organized motions.

Thus, considering normally incident waves breaking well away from the shoreline and with a continuously decreasing depth, two regions of breaker evolution are

distinguished. The first region, commonly termed the transition region, actually has two zones: the first a narrow zone of essentially irrotational motion (wave steepening, overturning and first jet formation) during instability. The following is the zone with sharp wave height decay and the first stages of turbulence develop. Most of the initial turbulent energy in this zone is carried by large-scale coherent vortex-like structures. This process of overturning and formation of large-scale vortex motions takes place in a relatively short distance, a few wave heights, before evolving into a well developed quasi-steady breaking wave mode. Velocity measurements (e.g., Nadaoka 1986) from this following region, the inner surf zone, show that this is similar to an “established bore” region with typical turbulent (small) scales and the mean motion is quasi-steady. The normal turbulent Reynolds stress is small compared to the momentum flux due to wave motion in the inner surf zone.

The presence of the transition zone is also evident when considering the fact that, in the region of initial breaking, in many cases a strong decay of wave height is noticed which is not immediately accompanied by a positive gradient of the mean water level (or setup). Thus, wave energy dissipates with a shorter time scale than that of the transfer of convective wave momentum flux to the water column or that of the total kinetic energy of ordered large-scale motion (also, Battjes 1988).

The mean momentum balance can be written as

$$\rho g(h + \bar{\eta}) \frac{d\bar{\eta}}{dx} + \frac{dS_{xx}}{dx} + \bar{\tau}_b = 0 \quad (3.8)$$

where S_{xx} is the total stress excess from the hydrostatic, the radiation stress. The radiation stress calculated using wave (orbital) contributions only provides the right balance to explain observations in the inner surf zone (Bowen et al. 1968). However, the setup gradient is zero in the transition zone indicating redistribution of the radiation stress. If the transition zone is modeled as

$$S_{xx} \neq f(x) \quad (3.9)$$

then, to second order in wave height,

$$S_{xx} = \rho \int_h^0 (\overline{u^2} - \overline{w^2}) dz + \frac{1}{2} \rho g (\overline{\eta - \bar{\eta}})^2 \quad (3.10)$$

$$= S'_{xx} + S''_{xx} = \text{constant} \quad (3.11)$$

across the transition zone, where S'_{xx} is the radiation stress associated with the turbulence and S''_{xx} is the radiation stress associated with the orbital motion. The contribution of the turbulent correlations of the velocity fluctuations to the radiation stress in the momentum balance cannot be neglected in the transition zone and its gradient must be of opposite sign as compared to the source term of the balance which is a function of the gradient of the wave energy. In terms of analytical or numerical modeling, some of the advective transport terms of the turbulent kinetic energy (tke) equation cannot be neglected. As the production of tke in this region is sudden and severe, the dissipation mechanisms cannot keep pace with it, and there should be advection of tke. It is noted that the alternative approach of Thieke (1992). He assumes the momentum balance across the transition region (where the slope of the mean water surface is zero) as a balance between the wave and mean flow contributions to the radiation stress while neglecting the turbulent contribution. The transition region is then modeled as

$$S''_{xx} + S_{xx,m} = \text{constant} \quad (3.12)$$

where the (depth-integrated) momentum or radiation stress, S_{xx} , has contributions from the wave (S''_{xx}) and mean flows ($S_{xx,m}$) only. This parameterization yields estimates for the wave height at the end of the transition zone. He further estimated the partitioning of net momentum flux amongst the wave, mean flow and turbulent fluctuation contributions. Data from Nadaoka and Kondoh (1982) and Nadaoka (1986) were used for parameterization of the turbulent component, and he concluded that the significant feature of the momentum balance in the surf zone is the contribution from orbital wave motion (as predicted by Fourier wave theory).

It is remarked that separation of the wave component from the turbulent component in data analysis of, say, velocity-time series is not straight-forward because the wave motion itself is oscillatory. An ensemble-type averaging with sampling at a fixed phase is the best available option. The drawback is that the wave period in the surf zone is not exactly constant because the nonlinearities causing small irregulari-

ties in the propagation speed of individual breakers tend to accumulate. Furthermore, Nadaoka and Kondoh (1982) filter away energies below 10 Hz when estimating the turbulent intensities whereby the low frequency part of the tke, which are the large-scale eddies (as recorded by Hattori and Aono 1985), was evidently neglected. Accordingly, the values of turbulent intensities using Nadaoka and Kondoh (1982) may not be truly representative.

The evolution of the eddies produced by breaking has implications for sediment transport modeling. Usage of undertow models considering the gradient of the wave radiation stress run into trouble at the break point because of the unrealistic effect of the sharp gradient of wave radiation stress on the numerical model. The transfer of at least some of the wave momentum flux to these large-scale eddies may have a smearing or cushioning effect on the water column. Now, in general terms, the most efficient eddies (in terms of extraction of energy from the mean flow) are those vortices whose axes are roughly aligned with that of the mean strain rate (Tennekes and Lumley 1972). Surf zone measurements by Nadaoka (1986) show that the eddies are two-dimensional and stationary with a horizontal axis parallel to the wave crest. With time, the lower edge of these eddies develop oblique protuberances downward into the water column, the eddies become three-dimensional and the axes of the eddies align in the direction of the mean strain rate of the phase averaged velocity field around and behind the wave crest. This mean strain rate is in a plane perpendicular to the wave crest and tilted at an angle of $\sim 45^\circ$ or less to the horizontal which is the direction of stretch of these oblique eddies. When the high speed upper fluid moves down due to the evolution of the eddy structure into oblique eddies, it thus experiences a velocity surplus and contributes to the generation of Reynolds stresses at the interface of the upper and lower regions. Tracers injected into the region affected by these oblique eddies moved down and almost reached the bottom suggesting a mechanism for sediment entrainment.

Of more direct relevance to undertow or cross-shore current modeling is the comparison of mass flux in the inner surf zone to predictions of linear and the Dean stream function theories. As is obvious to even the casual observer, there is augmented mass

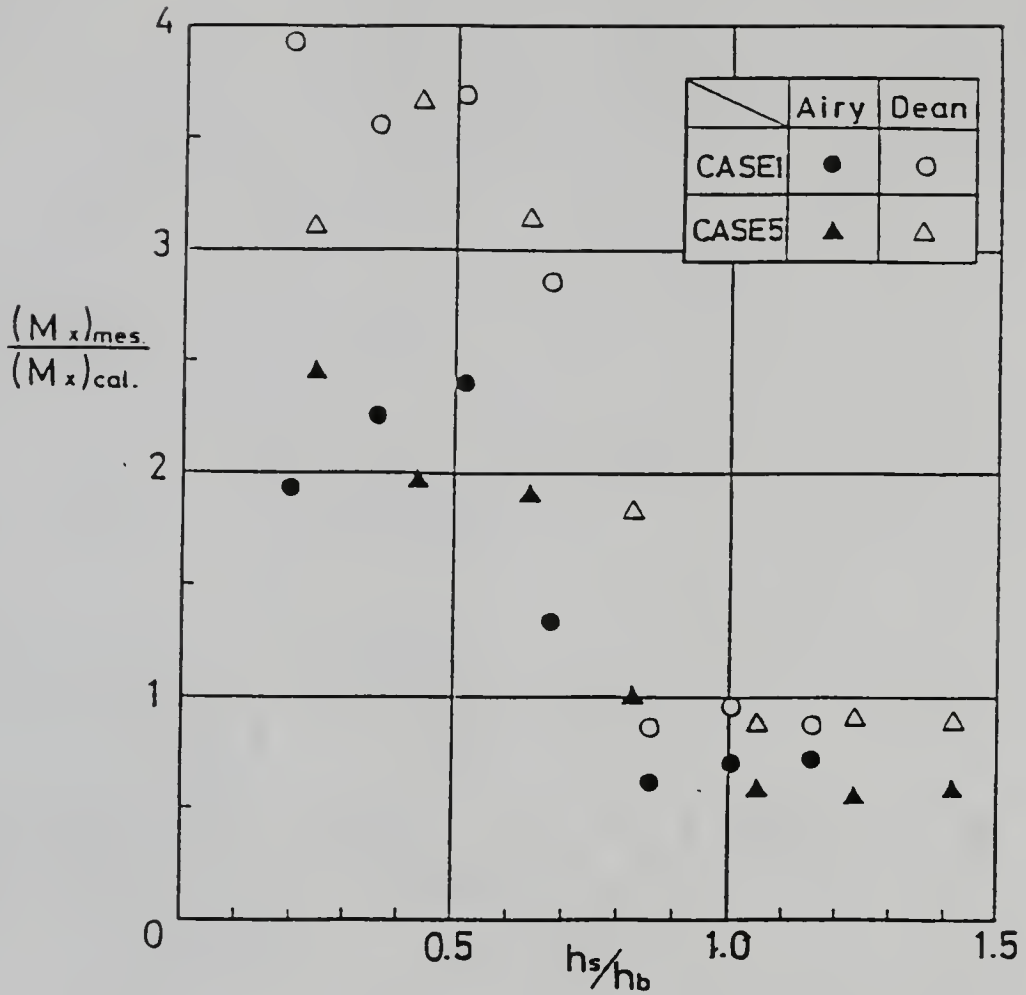


Figure 3.1: Comparison of mass flux predictions and measurements (from Nadaoka 1986).

flux in the region above that of the wave trough. Simple application of continuity shows that a relatively strong return flow in the region below (for non- overtopping cases) the trough level is required to balance the total mass flux. Now, the Dean stream function wave theory is considered the most reliable for estimating orbital velocities in the surf zone if the wave profile is known. Comparison of the mass flux measurements of Nadaoka (1986) with predictions using linear wave theory and the Dean symmetric stream function theory are shown in Figure 3.1. The predictions of Dean's theory are in close agreement with measurements outside the surf zone, however, the mass flux is obviously well underpredicted inside the surf zone. It is at first surprising to note that linear wave theory is slightly better. It appears more logical on considering that linear wave theory overpredicted mass flux outside the surf zone.

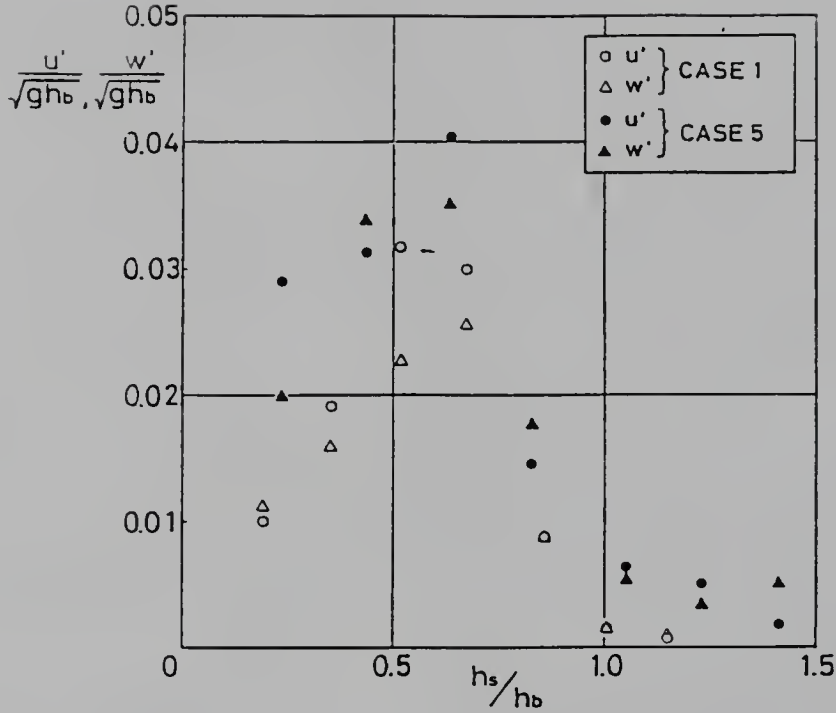
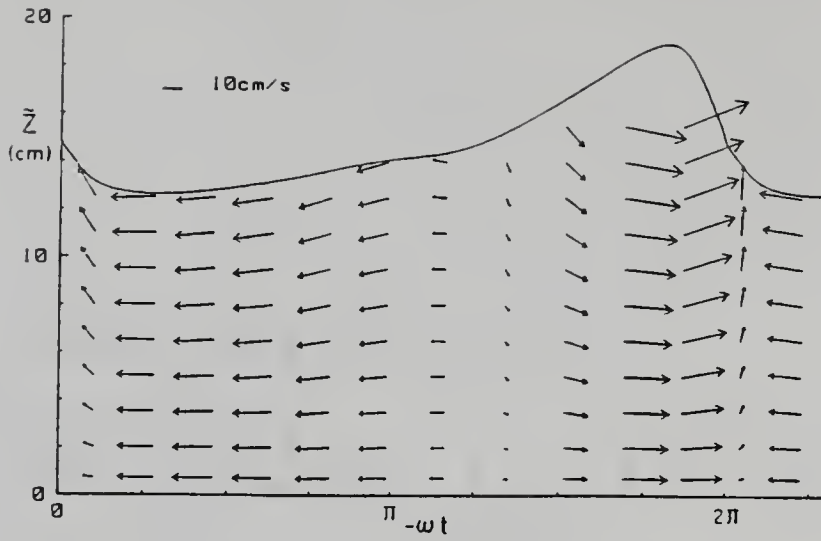


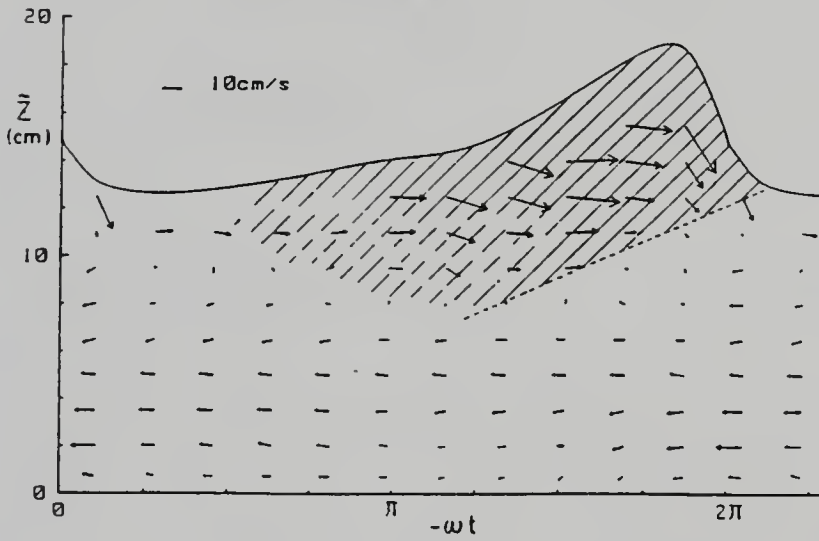
Figure 3.2: Turbulent intensities immediately below the trough level (from Nadaoka 1986).

Now, the magnitudes of measured turbulent intensities (u' and w') immediately below the trough level show a similar behavior (see Figure 3.2) with a substantial increase of turbulent intensity from the breakpoint into the surf zone. The values are constant landward of $h/h_b \sim 0.7$. These measurements indicate that the region $h/h_b \sim 1 - 0.7$ can be considered a transition zone where the wave motion has become unstable but the transition to turbulence is not complete, and the rest being a region with almost fully developed turbulent flow where self-similarity can be applied.

The separation of the velocity field into rotational and irrotational components in Nadaoka (1986) shows that, for broken waves in the 'established bore' region in a horizontal portion of the bottom, there is a large rotational contribution (see Figure 3.3) to shoreward flow beneath the wave crest which is comparable in magnitude



Separated irrotational velocity component, $\langle u_p \rangle$.



Separated rotational velocity component, $\langle u_e \rangle$.

Figure 3.3: Irrotational and rotational velocity components in a breaking wave (from Nadaoka 1986).

to the irrotational contribution. There is also some shoreward flow below the level of the wave trough implying that the large-scale eddies advect and diffuse into otherwise irrotational fluid. Video imaging revealed the existence of large-scale eddies containing substantial air bubbles in the hatched area of Figure 3.3. The contribution of the rotational velocity component to (or the effect of vorticity on) the ensemble average value of the Reynolds stress $-\overline{uw}$ shows the same behavior of substantial contribution in the region above the wave trough. This suggests that large-scale eddies act in a manner to considerably increase the flux of mass and momentum into the surf zone. The development of Svendsens' (1984) "surface roller" parameterization has a similar basis.

If the quasi-steady breaking waves in the inner surf zone are considered similar to turbulent bores, the continuous shearing results in wave energy decay directly. As the bore height decreases, the decrease in the water depth is generally sufficient to maintain the bore Froude number at the high levels necessary to sustain the turbulence. The turbulent Reynolds stress is much smaller than that due to the wave momentum in this region, and thus a decrease in wave energy and momentum is accompanied by a water level slope. As mentioned earlier (Peregrine and Svendsen 1978), the motion in the turbulent bore can be modeled as a wake (also Battjes and Sakai 1981, Duncan 1981, Sakai et al. 1982).

A practical case of study was by Svendsen (1987) who studied the variations of turbulent kinetic energy (tke) within the surf zone using the measurements of Nadaoka and Kondoh (1982), Stive and Wind (1982) and Hattori and Aono (1985). The turbulent kinetic energy

$$k = \frac{1}{2}(\overline{u'^2} + \overline{v'^2} + \overline{w'^2}) \quad (3.13)$$

where k is the turbulent kinetic energy, u' , v' , w' are the turbulent fluctuations in the x,y and vertical (z) directions, respectively. A characteristic value of velocity which provides the scaling for the time-mean value k is required for comparison of data. Since turbulence is initiated at the toe of the wave front which is propagating with

the wave celerity c ,

$$\sqrt{k} \propto c = \sqrt{gh} \quad (3.14)$$

where h is the water depth. Examination of $\sqrt{k/gh}$ as a function of the non dimensional elevation η/h at different positions along the surf zone indicate only a modest variation over depth. This indicates that large-scale vortices cause internal mixing which includes convective dispersion of turbulence over almost the full depth, in accordance with Peregrine and Svendsen (1978) who noted that turbulence under a breaker is spread by convection rather than by diffusion. In plunging breakers, the level of turbulence shortly after breaking is lower than that farther onshore - it is surmised that this is in the transition zone discussed earlier. The vertical profiles of turbulent intensity attain maximum values around $h/h_b \sim 0.7 - 0.8$ and then slowly decrease shoreward. The cases with spilling breakers exhibit maximum non-dimensional tke at points closest to the breakpoint.

In terms of the general turbulent energy budget for monochromatic waves incident normally and breaking well away from the shoreline, the effect of the sharp change and decay of the wave momentum flux due to breaking is significant for large-scale (small wavenumber) eddies in the transition zone close to the breakerline and diminishes rapidly landward. Here, it is mentioned that the data of Hattori and Aono (1985) for the spectra of the turbulent fluctuations reveal the importance of large scale vortices of frequencies less than ten times the incident wave frequency. It seems that in the transition zone, the sharp wave height decay which is not accompanied by a concomitant change in the sign of the slope of the mean water line is manifested into the transfer of energy to large scale (or low frequency) vortices. This is consistent with the theory that the energy of turbulence extracted from the mean flow enters the turbulence at integral or macroscales.

Now, in most general terms, the rate of change of tke within a control volume is due to pressure-gradient work, transport of tke by the viscous stresses and the turbulent fluctuations, and two types of deformation work: production and dissipation. The transport terms can only redistribute energy within the control volume but not

change it; thus, in the case of analogy to steady, homogeneous, pure shear flow with mean velocity U , the tke equation for the fluctuating part of the flow is

$$\text{production } P \sim \text{dissipation } D \quad (3.15)$$

that is

$$-\overline{u'_i u'_j} S_{ij} \sim 2\nu \overline{s_{ij} s_{ij}} \quad (3.16)$$

where the LHS is the production term and the RHS is the viscous dissipation term. The mean strain rate is given by

$$S_{ij} = \frac{1}{2} \left(\frac{\partial U_i}{\partial x_j} + \frac{\partial U_j}{\partial x_i} \right) \quad (3.17)$$

and the turbulent strain rate is similarly

$$s_{ij} = \frac{1}{2} \left(\frac{\partial u'_i}{\partial x_j} + \frac{\partial u'_j}{\partial x_i} \right) \quad (3.18)$$

Of course, in wave breaking there is no source flow as such; the major production of tke occurs at the free surface (the production of turbulence at the bottom is comparatively negligible). We are not really concerned with the actual quantification of the source term in the tke budget as long as it is recognized. Anyway, if the turbulence is characterized by single length and velocity scales, we employ the scale relations $S_{ij} \sim u_c/l$ where u_c is the characteristic velocity scale and l is the typical turbulent integral (macro) scale, then

$$C_1 u_c l S_{ij} S_{ij} \sim 2\nu \overline{s_{ij} s_{ij}} \quad (3.19)$$

and as the local Reynolds number $u_c l/\nu$ is large, we have

$$\overline{s_{ij} s_{ij}} \gg S_{ij} S_{ij} \quad (3.20)$$

Thus, the turbulent strain rate is much larger than the mean strain rate and the eddies of dissipative scales have small convective time scales as compared to that of the source flow (of turbulence). Also, from the form of Equation (3.19), it is seen that the large scale eddies contribute most to the production of tke. The energy extracted from the flow enters the turbulence at integral, i.e., macro scales.

Also, if we consider the case of the wave propagating over a horizontal bottom immediately after the advent of breaking, it is seen that the wave height stabilizes after traveling a short distance as a breaking wave. In this short distance, the advective transport terms are necessary in the equation as the conditions of decreasing water depth are no longer present.

Of course, production and dissipation terms are not exactly in balance everywhere. As mentioned earlier, these large-scale eddies may have important effects on (1) the aspect of cushioning the instability effects on transport models involving, say, the sharp change in the radiation stress gradient at the break-point which occurs in nature, and (2) promoting scour of the trough of a longshore bar landward of the breakpoint by the eddies, as was experimentally observed in the present experiments.

While the preceding discussion considered primarily instantaneous quantities, evaluation of relevant contributors to mean cross-shore transport requires the direct application of integral quantities (e.g., gradients of the mean energy flux and momentum flux). One exception is in the specification of friction velocity necessary for the suspended transport computations. Inside the surf zone, it is obvious that turbulence is a major cause of sediment entrainment and revised surf zone parameterization is essential. Indeed, it is felt that the mean-flow hydrodynamics may be modeled in terms of the surface elevation neglecting detailed parameterizations of turbulence (except in the transition region), whereas the turbulence of wave breaking generally affects entrainment and stirring of sediment which is then transported by other processes. These facets are elaborated in the following, as required.

3.5 Cross-Shore Hydrodynamics Contributing to Suspended Transport

The local, instantaneous suspended sediment transport, \vec{q} , past any cross-section of the flow can be expressed as

$$\vec{q}(t) = \int_{-h}^0 \vec{u}(z, t) C(z, t) dz \quad (3.21)$$

where $\vec{u}(z, t)$ is the instantaneous sediment flow velocity and C the instantaneous concentration. These parameters can be split into mean (over the short-wave time

period) and fluctuating quantities:

$$\vec{u} = \vec{\bar{u}} + \vec{u'} \quad (3.22)$$

$$C = \bar{C} + C' \quad (3.23)$$

Sediment transport due to wave induced oscillatory velocities will be inculcated in terms of a mean flow (discussed later) and as a first approximation, the local mean sediment transport is

$$\vec{q} \simeq \int_{-h}^0 \vec{\bar{u}}(z) \bar{C}(z) dz \quad (3.24)$$

The requirement now is to satisfactorily model the vertical distribution of the mean (wave-induced) current and concentration such that computed profile changes due to sediment transport agree with observed changes.

If the sediment flow field is assumed to instantaneously follow the fluid flow field and if sediment is assumed to be instantaneously entrained to an elevation z_i during the passage of wave crests then, following the ideas of Dean (1973) and Dally (1980), the contributors of the flow field resulting in net (suspended) transport can be identified as

- the wave induced mean velocity (undertow or return flow)
- the first-order oscillatory component

Figure 3.4 displays the regions of heights D_f (Region 1) and $h-D_f$ (Region 2) where the above contributors are relevant. h is the total depth and

$$D_f = w_s T \quad (3.25)$$

where w_s is the sediment fall velocity, T the wave period and D_f is the distance the sediment can fall in a wave period. The mean flow acts to transport sediment everywhere in the water column (Regions 1 & 2) while the oscillatory motion results in a net transport only for sediments entrained into Region 1.

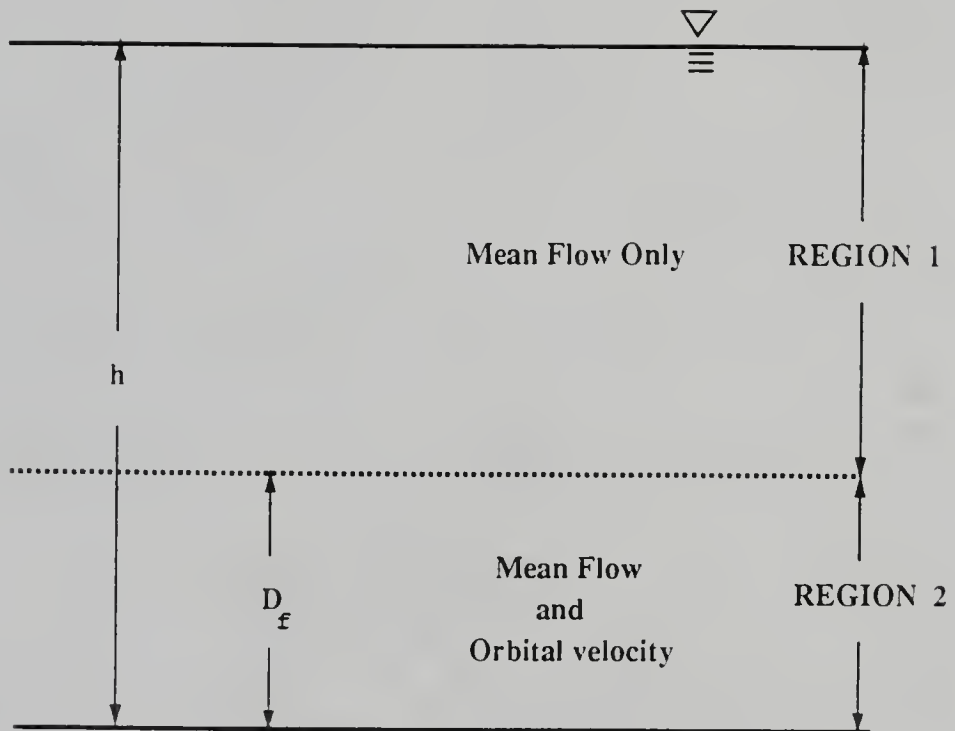


Figure 3.4: Suspended transport regions.

3.5.1 First-Order Contribution

If the sediment particle is entrained to an elevation z_i less than D_F during the passage of the wave crest, then the time taken for the particle to fall to the bottom is

$$t_F = \frac{h + z_i}{w_s} < T \quad (3.26)$$

where h is the local water depth. From linear wave theory, the horizontal distance, ζ_f (subscript f denotes first-order), traversed by a particle in falling to the bottom is

$$\begin{aligned} \zeta_f &= \int u \, dt \\ &= \frac{H}{2\sigma} \sqrt{\frac{g}{h}} \sin \sigma t_F \end{aligned} \quad (3.27)$$

Thus, an average traversing velocity can be defined as

$$\bar{u}_f = \frac{\zeta_f}{T} = \frac{H}{4\pi} \sqrt{\frac{g}{h}} \sin \sigma t_F \quad (3.28)$$

which is applicable for Region 1 only. This formulation runs parallel to the concept of “intermittent suspension” used by many investigators: essentially the arguments used in making the above formulation imply that sediment suspended in the region bounded $z = -h$ and $z = -h + D_f$ experiences a net shoreward or seaward motion as it experiences the fluid velocity for less than a full wave period.

3.5.2 Return Flow Model

Solutions to depth-integrated, time-mean continuity and momentum equations essentially lead to known depth-mean flow (which could be zero) and a balance between the radiation stress and steady mean setup. However, it is now well known that locally in the vertical, the mass and momentum fluxes are not in balance (e.g., Dally 1980 and Borekci 1982). This is the driving mechanism for the vertical circulation patterns termed undertow as the imbalance is matched by shear stresses induced by the mean velocity gradient and turbulence. The solution of integral quantities, for example, the momentum flux and energy density, can be obtained very simply from first-order solutions. As mentioned earlier, no generality is lost if the wave is considered a sinusoidal disturbance, as any disturbance can be described by a sum of such disturbances propagating independently of each other (e.g., Phillips 1977).

Adding the continuity equation to the vertical (z) momentum equation, we have

$$\frac{\partial w}{\partial t} + \frac{\partial uw}{\partial x} + \frac{\partial w^2}{\partial z} = -\frac{1}{\rho} \frac{\partial p}{\partial z} + \frac{1}{\rho} \frac{\partial \tau_{xz}}{\partial x} - g \quad (3.29)$$

Neglecting the shear stress terms, depth-integrating and time-averaging, we get

$$\bar{p}(z) = -\rho \overline{w^2}(z) + \rho g(\bar{\eta} - z) \quad (3.30)$$

which is the standard expression for the mean pressure, correct to second order, at elevations below the level of the wave trough.

The horizontal (x) momentum equation can similarly be written as

$$\frac{\partial u}{\partial t} + \frac{\partial u^2}{\partial x} + \frac{\partial uw}{\partial z} = -\frac{1}{\rho} \frac{\partial p}{\partial x} + \frac{1}{\rho} \frac{\partial \tau_{zx}}{\partial z} \quad (3.31)$$

With an eddy viscosity parameterization of the form

$$\tau_{zx} = \rho \nu_e \frac{\partial \bar{u}_s}{\partial z} \quad (3.32)$$

and depth-integrating (from z to the free surface η) and time-averaging Eq. (3.31), and using Eq. (3.30) we obtain

$$\nu_e \bar{u}_s(z) = \frac{\partial H^2}{\partial x} \frac{g}{8} \left(\frac{z^2}{2h} - \frac{z}{2} \right) + \frac{\partial \bar{\eta}}{\partial x} g \frac{z^2}{2} + C \quad (3.33)$$

where all quantities were evaluated using the first-order Stokes (linear) wave theory.

This is the general form of the mean velocity at any elevation due to momentum flux transfer where the effect of turbulence in terms of influencing mean flows below the trough region is considered minimal (also Stive and Wind 1986). There are two unknowns, as the slope of the mean water line, $\frac{\partial \bar{\eta}}{\partial x}$, is an unknown in addition to C . Thus, two boundary values are required for solution and a correct formulation is necessary for precise modeling. However, there is no clear consensus amongst researchers about the proper choice of boundary conditions as there actually are more constraints required to be satisfied (of continuity, at the bottom and at the wave trough level) than allowed. This aspect is now elaborated.

First boundary condition

One widely used condition is that the depth-integrated mass flux must satisfy continuity, i.e.,

$$\overline{\int_{-h}^{\eta} u(z) dz} = Q \quad (3.34)$$

where Q is the depth-integrated mean mass flux. Q is, of course, zero for a closed wave tank situation. In our tests with overtopping, water flowed over the back of the crest of the barrier island and was recirculated back whence the mass flux is not zero. A two-layer approach is used by dividing the flow at the level of the wave trough whereby the onshore mass transport above the trough is balanced by the return flow below. The regions before and after breaking need to be considered separately. The parameterizations required for the sediment transport are discussed below.

Outside the surf zone. In an Eulerian description, an extension of results of linear wave theory carried out to second-order yields a net mass flux in the direction of wave propagation, confined solely to the region above the wave trough, which can be shown to be (e.g., Phillips 1977)

$$M_f = \overline{\int_0^{\eta} u dz} = \frac{gH^2k}{8\sigma} \quad (3.35)$$

where k is the wave number, σ is the wave angular frequency and the datum is at the local mean water level. Thus, for cases with a return flow (no overtopping), we have

$$\int_{-h}^0 \bar{u}_s(z) dz = -M_f \quad (3.36)$$

while, for cases with overtopping

$$\int_{-h}^0 \bar{u}_s(z) dz = 0. \quad (3.37)$$

For the present case, this condition was applied at the toe of the beach (cross-section denoted by subscript 1). Thus, at any other cross-section (denoted by subscript 2) prior to the break-point, the discharge is given by

$$\int_{-h}^0 \bar{u}_s(z) dz = -(M_{f_2} - M_{f_1}). \quad (3.38)$$

Inside the surf zone. In addition to the above mentioned Eulerian mass transport for irrotational waves, measurements indicate a substantial contribution to mass flow,

after wave breaking, in the region above the trough level by a rotational component of velocity. As shown in Figure 3.1, the mass flux can be up to 3-4 times that attributable to wave motion (using the Dean stream function theory). Importantly, the ratio of the measured to calculated fluxes is approximately constant in the inner surf zone. This is parameterized as

$$M_{fa} = F_m M_f \quad (3.39)$$

where M_{fa} is now the actual mass flux and F_m is the proportionality factor. Svendsen (1984) parameterizes the augmented mass flux as contained in a “surface roller” riding along the bore front. His approximation results in an additional mass flux which can be simplified as of the form

$$M_{fa} = \left(1 + \frac{7kh}{2\pi}\right) M_f = M_f + M_r \quad (3.40)$$

where M_r is the additional mass flux due to the presence of the surface roller. Stive and Wind (1986) adopted another empirical approach with mass flux above the level of the wave trough given by

$$M_{fa} = 0.1 \sqrt{\frac{g}{h}} H(h - \eta_t). \quad (3.41)$$

where η_t is the elevation of the wave trough. In the present model, the following form is adopted. For cases with a return flow

$$\int_{-h}^0 \bar{u}_s(z) dz = -M_{fa} = -F_m M_f \quad (3.42)$$

whereas, for cases with overtopping, at a cross-section denoted by subscript 3,

$$\int_{-h}^0 \bar{u}_s(z) dz = -M_{fa} = -(F_m M_{f3} - M_{f1}) \quad (3.43)$$

These ideas are illustrated in Figures 3.5 and 3.6.

Second boundary condition

One method is basically to match velocities at the edge of the bottom boundary layer which has the no-slip condition at the bottom (Dally 1980, Borekci 1982 and Svendsen 1984):

$$\bar{u}_s(-h) = \bar{u}_B, \quad (3.44)$$

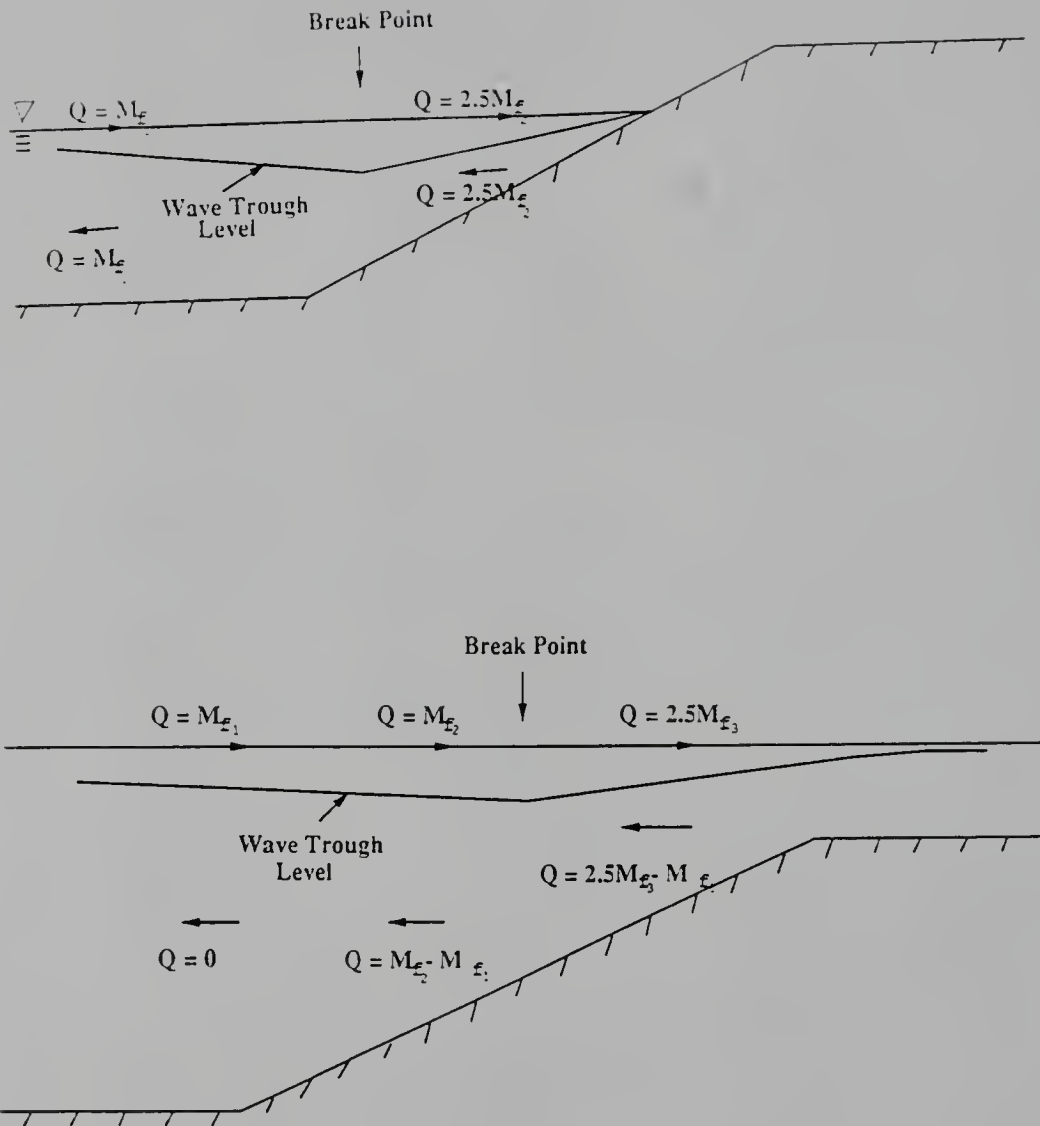


Figure 3.6: Mass flux distribution in cases with overtopping.

where \bar{u}_B is the velocity at the outer edge of the bottom boundary layer. Options available for modeling the bottom velocity include, for example, Longuet-Higgins' (1953) conduction solution for progressive waves over a locally horizontal bottom or Liang and Wang's (1973) solution for turbulent boundary layers. These lead to positive velocities for the undertow very close to the bottom which is contrary to general observations within the surf zone. Svendsen et al. (1988) modified this by allowing no-slip in a bottom boundary layer with a very small value of the eddy viscosity. A patching method was used to solve the momentum equations in two layers (the interior and the bottom boundary layer) whereby the velocity and shear stress at the edge of the oscillatory boundary layer are "patched" at the edge of the bottom boundary layer. However, the patching level is itself arbitrary. Stive and Wind (1986) specified the shear stress at trough level to compensate for the decay of radiation stress above it,

$$\begin{aligned} [\tau]_{z=-\eta_t} &= [\nu_e \frac{d\bar{u}_s}{dz}]_{z=-\eta_t} \\ &\propto \frac{\partial EC_g}{\partial x} \frac{1}{c} \end{aligned} \quad (3.45)$$

This specification of the shear stress at the trough level has sound physical meaning for breaking waves as the mean flow is primarily driven by the loss of momentum above the wave trough. In an Eulerian description, the wave momentum is entirely contained in the region above the wave trough. A decrease of mean momentum in this region due to wave breaking must be balanced by a viscous stress just under the level of the wave trough. Their undertow profiles indicate a non-zero bottom shear stress. Roelvink and Stive (1989) combined features of both Svendsen et al. (1988) and Stive and Wind (1986).

The present approach was as follows. The undertow measurements of Hansen and Svendsen (1984) inside the surf zone indicate at least a near-zero gradient near the bottom. The mean momentum balance for the bulk flow considering two-dimensional motion is reiterated as

$$\frac{dS_{xx}}{dx} + \rho g(h + \bar{\eta}) \frac{d\bar{\eta}}{dx} + \bar{\tau}_b = 0 \quad (3.46)$$

with

$$S_{xx} = \int_h^0 \rho(\overline{u^2} - \overline{w^2})dz + \frac{1}{2}\rho g(\overline{\eta} - \bar{\eta})^2 \quad (3.47)$$

where S_{xx} is the excess momentum flux due to both wave motion and turbulent fluctuations and $\bar{\tau}_b$ is the mean bottom shear stress. Measurements of Stive and Wind (1982) indicate only a modest contribution to the radiation stress by the turbulent velocity fluctuations. From the measurements of Stive and Wind (1982), it is possible to assess the individual contributions of the first and second terms of Equation (3.46) and these are presented in Figure 3.7. Except for the region near the breakpoint, the calculations from measurements show that the two terms are essentially in balance and thus the bottom shear stress is negligibly small. Velocity measurements around the breakpoint are uncertain because extrapolation procedures used in their computations are strictly not valid in the region of rapid change. Their measured flows near the bottom show only a mild change which would be reflected in modest changes in the bottom shear stress. The variance of the water surface, the second term in Equation (3.46), was computed using bottom pressure measurements and tends to be underestimated for peaky, non-linear waves. Thus, it is concluded that within the limits and uncertainties imposed by measurement techniques, the bottom shear stress is negligibly small. The discrepancies in the transition zone also follow from the arguments presented in Section 3.4. The detailed model of Svendsen et al. (1988), which considers the interaction of the mean flow with that in the bottom boundary layer, when calibrated against undertow measurements of Hansen and Svendsen (1984) support the same conclusion that the bottom shear stress is negligibly small as the value of eddy viscosity inside the bottom boundary layer is assumed to be three orders of magnitude smaller than the value outside the boundary layer. Sensitivity analyses of Svendsen et al. (1988) show that undertow computations were markedly independent of the level of patching and that the standard boundary layer approach of asymptotic matching gives similar results. The conclusions of Svendsen and Hansen (1988) reinforce the argument for using zero bottom shear stress for undertow computations in breaking waves.

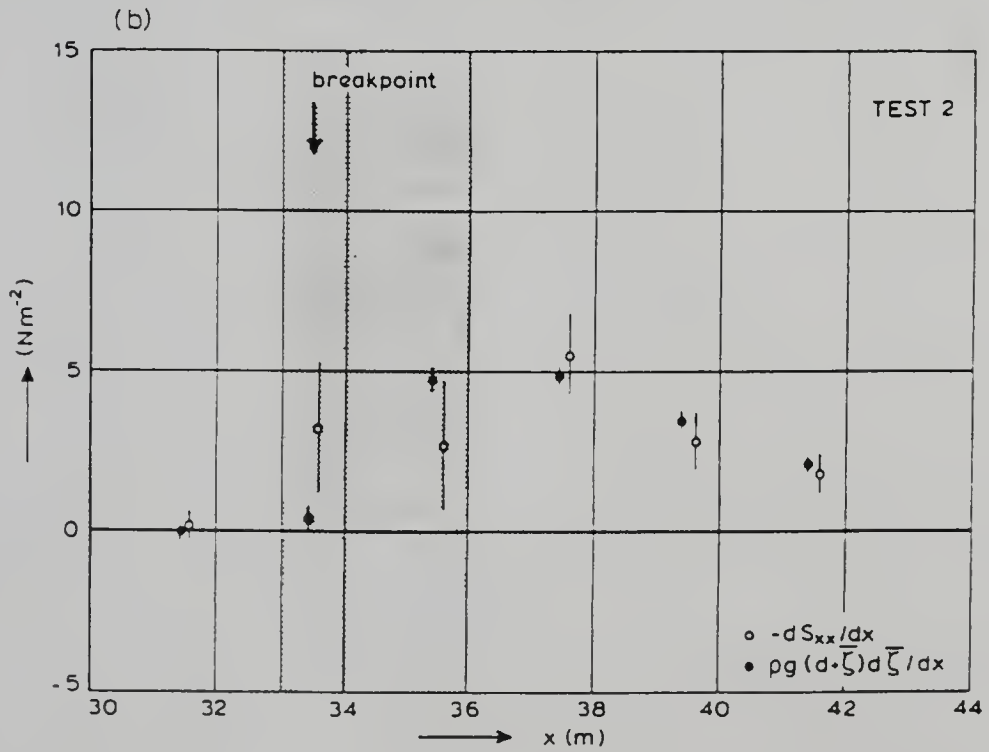
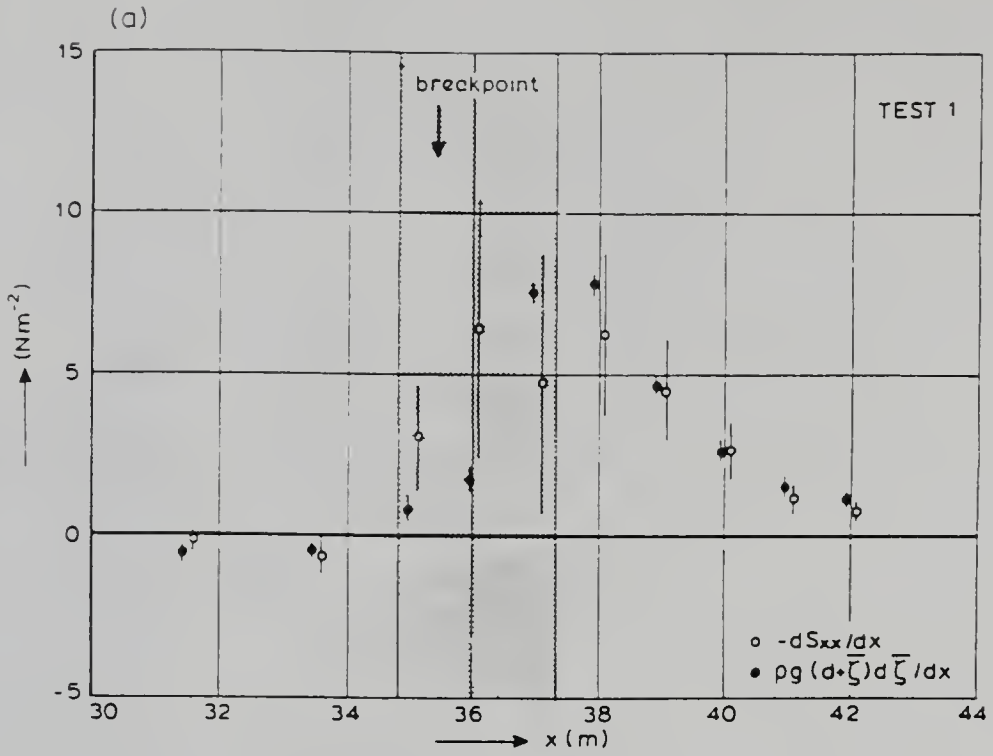


Figure 3.7: Measurements of radiation stress and the mean water line (from Stive and Wind 1982).

In accordance with the preceding discussion, the regions before and after breaking were considered separately.

Outside the surf zone. The mass transport (“streaming”) velocity at the edge of the boundary layer first given by Longuet-Higgins (1953) was used outside the surf zone, which yields

$$\bar{u}_B = \frac{5}{16} \frac{H^2 \sigma k}{\sinh^2 kh} \quad (3.48)$$

Inside the surf zone. The zero bottom shear stress condition was specified, i.e.,

$$\frac{\partial \bar{u}_s}{\partial z} = 0 \quad (3.49)$$

This condition should not be considered as implying that the bottom shear stress is actually zero, rather, this is a statement about the gradient of the mean velocity at the exterior edge of a relatively thin boundary layer. The tacit assumptions are that undertow is driven entirely by the momentum transfer at the surface and that the production of turbulence at the surface is dominant compared to that at the bottom.

Cross-shore velocity profile

Outside the surf zone. Incorporating the boundary conditions, the general form of second-order mean velocity at any elevation due to momentum flux transfer is

$$\begin{aligned} \bar{u}_s(z) = & \frac{gh}{8\nu_e} \frac{\partial H^2}{\partial x} \left[-\frac{3}{8} \left(\frac{z}{h} \right)^2 - \frac{1}{2} \left(\frac{z}{h} \right) - \frac{1}{8} \right] + \\ & \bar{u}_B \left[\frac{3}{2} \left(\frac{z}{h} \right)^2 - \frac{1}{2} \right] + \frac{3M_f}{2h} \left[\left(\frac{z}{h} \right)^2 - 1 \right] \end{aligned} \quad (3.50)$$

applicable for sediment entrained beyond Region 1 (Figure 3.4).

For Region 1: Defining

$$\zeta_s(t) = \int_0^{t_F} \bar{u}(t) dt \quad (3.51)$$

with instantaneous fall time

$$t = \frac{z_i - z}{w_s} \quad (3.52)$$

a change of variables results in

$$\begin{aligned} \bar{u}_{s,l}(z_i) &= \frac{\zeta_s(z_i)}{T} \\ &= \frac{1}{w_s T} \int_{-h}^{z_i} \bar{u}_s(z) dz \end{aligned} \quad (3.53)$$

whereby

$$\begin{aligned}\bar{u}_{s,l}(z_i) = & \frac{1}{w_s T} \left\{ \frac{gh}{8\nu_e} \frac{\partial H^2}{\partial x} \left[-\frac{1}{8} \left(\frac{z^3}{h^2} \right) - \frac{1}{4} \left(\frac{z^2}{h} \right) - \frac{z}{8} \right] \right\} \\ & + \bar{u}_B \left[\frac{1}{2} \left(\frac{z^3}{h^2} \right) - \frac{z}{2} \right] + \frac{3M_f}{2h} \left[\left(\frac{z^3}{3h^2} \right) - z \right] \Big\}_{-h}^{z_i}\end{aligned}\quad (3.54)$$

Inside the surf zone. With the appropriate boundary conditions, we get

$$\bar{u}_s(z) = -\frac{gh}{16\nu_e} \frac{\partial H^2}{\partial x} \left[\frac{1}{2} \left(\frac{z}{h} \right)^2 + \frac{z}{h} + \frac{1}{3} \right] - \frac{M_{fa}}{h} \quad (3.55)$$

for entrainment elevations beyond Region 1.

For Region 1:

$$\begin{aligned}\bar{u}_{s,l}(z_i) = & \frac{1}{w_s T} \left\{ -\frac{gh}{16\epsilon} \frac{\partial H^2}{\partial x} \left[\frac{1}{6} \left(\frac{z^3}{h^2} \right) + \frac{1}{2} \left(\frac{z^2}{h} \right) + \frac{z}{3} \right] \right. \\ & \left. - \frac{M_{fa} z}{h} \right\}_{-h}^{z_i}\end{aligned}\quad (3.56)$$

With the mean currents specified everywhere, the next step is the specification of the concentration profile such that suspended sediment transport can be computed. The concentration profile must consider the additional effects of turbulence-induced stirring in the surf zone.

CHAPTER 4 CONCENTRATION MODEL

The two-dimensional mass transport equation for suspensions equating the net flux of sediment into a volume element with the rate of accumulation is written as

$$\frac{\partial}{\partial t}(C) + \frac{\partial}{\partial x}(Cu) + \frac{\partial}{\partial z}(Cw) - \frac{\partial}{\partial z}(Cw_s) = 0 \quad (4.1)$$

where C is the concentration of sediment, w_s is the sediment settling velocity, u , w are velocities in the horizontal x and the vertical z directions. With turbulent averaging, through Fickian closure and neglecting advective transport, we have

$$\frac{\partial C}{\partial t} - \frac{\partial}{\partial z}(w_s C + K_z \frac{\partial C}{\partial z}) = 0 \quad (4.2)$$

where K_z is the vertical mass diffusivity. Assuming steady state, i.e., ignoring the effects of the sediment on the flow field and buoyancy effects, or slowly varying time scales for purposes of our model,

$$K_z \simeq \nu_e \quad (4.3)$$

$$C(z, t) = C(z) \quad (4.4)$$

where ν_e is the kinematic eddy viscosity. Assuming uniform turbulence distribution, we have

$$C = C_a \exp\left[-\frac{w_s(z - z_a)}{\nu_e}\right] \quad (4.5)$$

where C_a is the reference sediment concentration at elevation z_a . The reference concentration can be evaluated using criteria given by Nielsen (1986). If the temporal variation in the C at a fixed point over a wave period is assumed to be relatively small, a time-independent eddy viscosity model may be used for undertow computations (Svendsen 1987). Following Rouse (1949) and Dally (1980), a depth-integrated form of

$$\nu_e = -0.4u_*z\left(1 + \frac{z}{h}\right), \quad (4.6)$$

where u_* is the friction velocity, is used whence

$$C(z) = C_a \exp\left[\frac{-15w_s(z - z_a)}{u_*h}\right] \quad (4.7)$$

As bottom shear stress in any direction will entrain sediment, for these purposes the bottom shear stress can be considered to be

$$\bar{\tau}_B = \rho \frac{f}{2} \overline{u_B^2} \quad (4.8)$$

$$= \rho u_{*B}^2 \quad (4.9)$$

where f is an aptly defined friction factor, with the bottom velocity being defined, for example, by linear theory as

$$u_B = \frac{H}{2} \sqrt{\frac{g}{h}} \cos(kx - \sigma t) \quad (4.10)$$

whereby

$$u_{*B} = \sqrt{\frac{fH^2g}{16h}}. \quad (4.11)$$

It is noted that lack of complete Reynolds number similitude can result in a different friction factor in the prototype as compared to that in the model (discussed later).

The above definition is sufficient for non-breaking wave conditions. As mentioned in Chapter 3, turbulence generated at the free surface due to wave breaking is responsible for stirring up sediment and causing additional entrainment. The next step is the delineation of friction velocity which includes the effect of wave-breaking induced turbulence.

Wave breaking transforms ordered wave energy into disordered turbulence. Vertical diffusion effects can be eliminated by considering a control volume corresponding to the penetration depth of turbulence. In this case, the turbulent kinetic energy (tke) equation can be written as

$$\mathcal{P} - \mathcal{D} = \rho \frac{\partial}{\partial x} \int_{\text{depth}} \langle kc_{adv} \rangle dz \quad (4.12)$$

where \mathcal{P} is the production and \mathcal{D} is the dissipation of tke k , and c_{adv} is an advection velocity for tke, with

$$k = \frac{1}{2}(\overline{u'^2} + \overline{v'^2} + \overline{w'^2}) \quad (4.13)$$

Wave breaking is the source of the whence the production term is

$$\mathcal{P} = -\frac{\partial EC_g}{\partial x} \quad (4.14)$$

From the form of Equation (4.12), some of this tke is dissipated and the rest is advected away. The dissipation term is quantified as (e.g., Tennekes and Lumley 1972)

$$\mathcal{D} = \rho \int_{\text{depth}} c_d < \frac{k^{3/2}}{l_v} > dz \quad (4.15)$$

where the integration is necessary because of the control volume. c_d is a dissipation coefficient and l_v is the vortex length scale. These are estimated as

$$c_d \simeq 0.08 \text{ (Launder and Spalding 1972)} \quad (4.16)$$

$$l_v \simeq 0.07h \text{ (Deigaard et al. 1986)} \quad (4.17)$$

Also, turbulence is initiated at the toe of the breaking wave front, whence

$$c_{adv} = c \quad (4.18)$$

We now turn to experimental data for estimation of the required variables. Svendsen's (1987) analysis of the data of various investigators reveals some interesting details.

1. Measurements, Figure 4.1 (from Svendsen 1987), show that the ratio of the near the surface to near the bottom is in the range $\sim 1-3$ (in the figure, ζ is the distance from the bottom). The decrease in tke with depth, away from the source of turbulence at the surface, is relatively small. The local tke can then be assumed to be almost the same as the depth-mean tke for purposes of the present model:

$$k \sim \frac{1}{h} \int_{-h}^0 k(z) dz \quad (4.19)$$

This result seems to indicate the presence of strong large-scale mixing caused by large-scale vortices whose presence has been well-documented by Nadaoka (1986). Thus, the turbulent penetration depth is assumed to be the entire water depth.

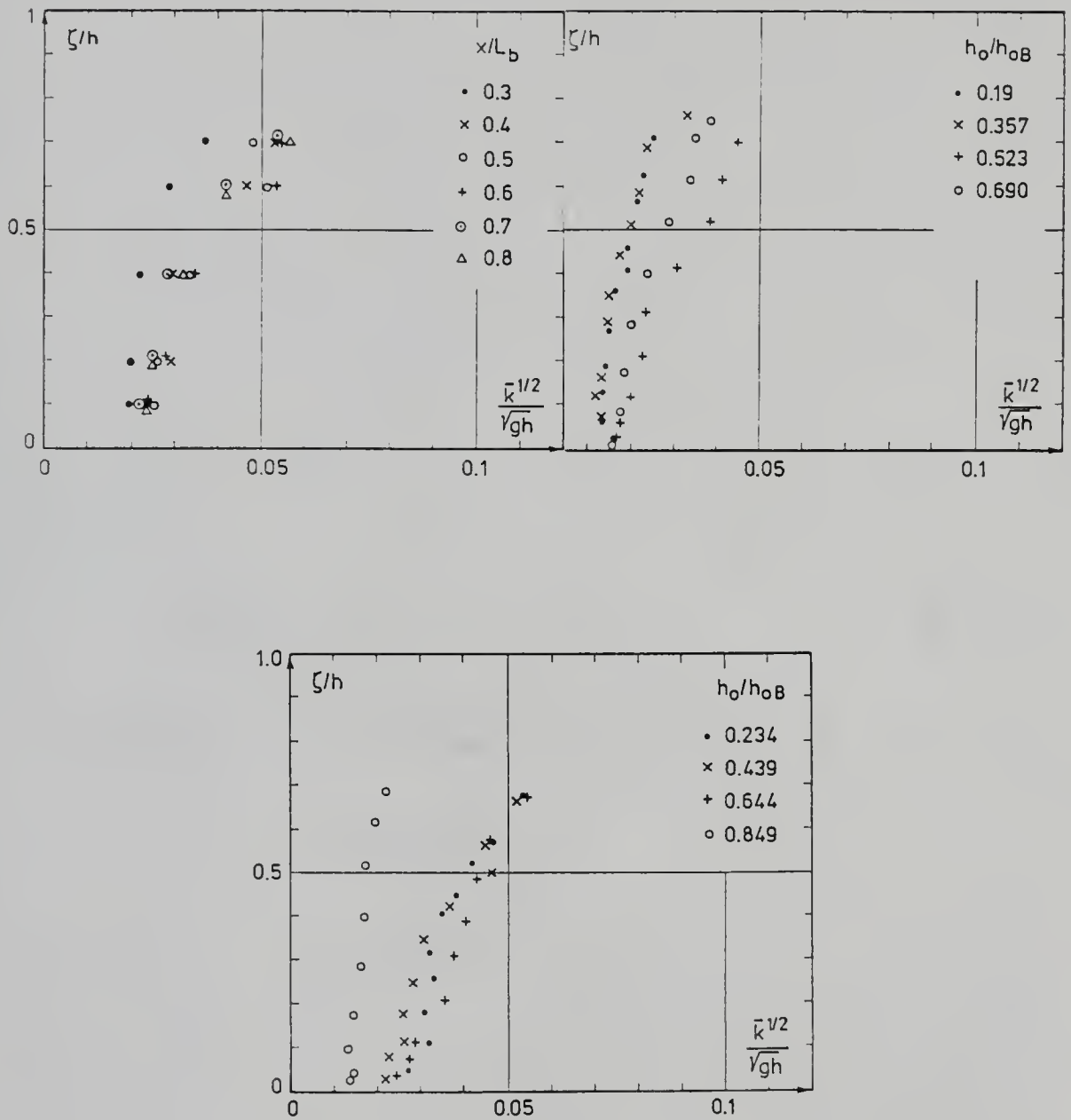


Figure 4.1: Measured levels of tke (from Svendsen 1987).

2. The temporal variation of tke is weak (Svendsen 1987)

$$\frac{1}{T} \int_0^T k(z, t) dt = \bar{k}(z) \simeq k(z, t) \quad (4.20)$$

With these considerations, we have

$$\int_{\text{depth}} < kc_{adv} > dz = \beta_f \bar{k} ch \quad (4.21)$$

and

$$\mathcal{D} \simeq \rho \beta_d \bar{k}^{3/2} \quad (4.22)$$

with the coefficients β_f and β_d expected to be of order 1.

The dissipation of tke, \mathcal{D} , can be evaluated by solving Equation (4.12) and using the above estimations. An example of predictions of this one-dimensional tke energy equation is presented in Figure 4.2. The production, dissipation and flux of tke for the initial conditions of Experiment E1 are shown in the figure. We now relate the effect of turbulence on the sediment concentration by assuming that the dissipation of turbulence directly affects the sediment transport by changing the friction velocity, $u_{*,BT}$. We define

$$\mathcal{D} = \tau_{B,T} U \quad (4.23)$$

with

$$U = \frac{H}{2} \sqrt{\frac{g}{h}} \quad (4.24)$$

as the maximum first-order velocity, then

$$u_{*,BT} = \left[\frac{2h}{\rho H \sqrt{gh}} \mathcal{D} \right]^{1/2} \quad (4.25)$$

Finally,

$$u_* = u_{*,B} \text{ outside the surf zone} \quad (4.26)$$

$$= u_{*,B} + u_{*,BT} \text{ inside the surf zone} \quad (4.27)$$

Thus, the concentration profile is fully realized.

With the formulation of representations for mean cross-shore currents and the concentration profile complete, the next step is to formulate the equations for the cross-shore sediment transport model. Model formulation, including mechanisms for bedload transport, and verification are discussed next.

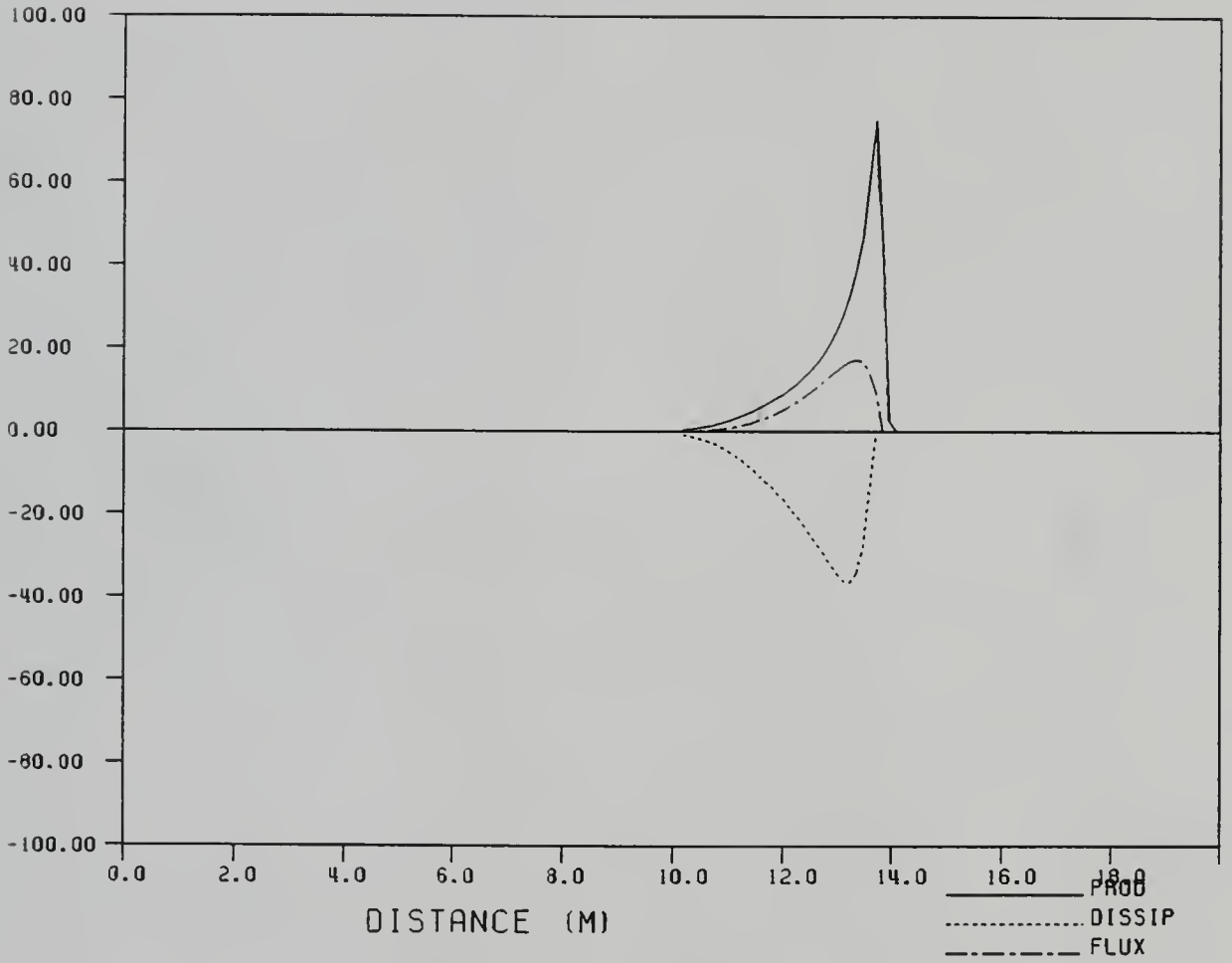


Figure 4.2: Predictions of production, dissipation and flux of tke, Experiment E1.

CHAPTER 5 CROSS-SHORE SEDIMENT TRANSPORT MODEL

In the following, simple expressions are developed for the cross-shore sediment transport rate. The primary focus of the present model is on transport in the surf zone where suspended transport dominates, prominent erosion occurred and longshore bars developed at the seaward edge (Overwash experiments, Chapter 2). The model also includes onshore transport in terms of sheet flow or bedload transport inculcating simple bottom boundary layer approximations such that cases with overtopping exhibit accretion over the crest of the barrier island.

5.1 Suspended Sediment Transport

The present cross-shore suspended sediment transport model incorporates rationale developed in the preceding text. Only two-dimensional motion is considered here. Sediment is assumed to be entrained to an elevation z_i during the passage of the crest of the waveform. The entrained sediment then follows the cross-shore flow dynamics. The definition of the symbols in the following text is consistent with the definitions of Chapters 3 and 4.

5.1.1 Contribution due to Intermittent Suspension

Sediment experiences onshore or offshore transport due to the oscillatory first-order velocity depending on the height of entrainment (Section 3.5.1). Then the first order contribution to the sediment transport is

$$\begin{aligned}
 Q_f &= \int_{-h}^{-h+D_f} \bar{u}_f(z_i) C(z_i) dz_i \\
 &= \frac{H}{4\pi} \sqrt{\frac{g}{h}} C_a \left\{ \exp[-F(z - z_a)] \right. \\
 &\quad \left. \left[\frac{-F \sin \frac{\sigma(h+z)}{w_s} - \frac{\sigma}{w_s} \cos \frac{\sigma(h+z)}{w_s}}{F^2 + \frac{\sigma^2}{w_s^2}} \right] \right\}_{-h}^{-h+D_f} \quad (5.1)
 \end{aligned}$$

where

$$F = 15 \frac{w_s}{u_* h} \quad (5.2)$$

5.1.2 Contribution due to Mean Cross-Shore Currents

As the cross-shore velocity profiles inside the surf zone were different from those outside the surf zone (Section 3.5.2), the contributions of the mean cross-shore currents or undertow to suspended sediment transport inside the surf zone are different from those outside the surf zone.

Outside the surf zone

The contribution of the undertow to transport in the lower layer (Region 1, Figure 3.4) is

$$\begin{aligned} Q_{s1,o} &= \int_{-h}^{-h+D_f} \bar{u}_{s,l}(z) C(z) dz \\ &= \frac{C_a}{w_s T} \exp[-F(z - z_a)] \left\{ \left[\frac{I}{8h^2 F} - \frac{M_{fa}}{2h^3 F} - \frac{\bar{u}_B}{2h^2 F} \right] z^3 \right. \\ &\quad + \left[\frac{I}{F} \left(\frac{3}{8h^2 F} + \frac{1}{4h} \right) - \frac{3M_{fa}}{2h^3 F^2} - \frac{3\bar{u}_B}{2h^2 F^2} \right] z^2 \\ &\quad + \left[I \left(\frac{3}{4h^2 F^2} + \frac{1}{2hF} + \frac{1}{8} \right) - \frac{3M_{fa}}{h^3 F^2} + \frac{3M_{fa}}{2h} - \frac{3\bar{u}_B}{h^2 F^2} + \frac{\bar{u}_B}{2} \right] \frac{Fz + 1}{F^2} \\ &\quad \left. + \frac{M_{fa}}{F} \right\} \Big|_{-h}^{-h+D_f} \end{aligned} \quad (5.3)$$

where

$$I = \frac{1}{\nu_e} \frac{\partial H^2}{\partial x} \frac{gh}{8} \quad (5.4)$$

The contribution of the undertow to transport in Region 2 is

$$\begin{aligned} Q_{s2,o} &= \int_{-h+D_f}^0 \bar{u}_s(z) C(z) dz \\ &= C_a \exp(-F(z - z_a)) \left[\left(\frac{3I}{8h^2 F} - \frac{3M_{fa}}{2h^3 F} - \frac{3\bar{u}_B}{2h^2 F} \right) z^2 \right. \\ &\quad + \left(\frac{3I}{4h^2 F^3} + \frac{I}{2hF^2} - \frac{3M_{fa}}{h^3 F^3} - \frac{3\bar{u}_B}{h^2 F^3} \right) (Fz + 1) \\ &\quad \left. + \frac{I}{8F} + \frac{3M_{fa}}{2hF} + \frac{\bar{u}_B}{2F} \right] \Big|_{-h+D_f}^0 \end{aligned} \quad (5.5)$$

The total contribution due to the mean cross-shore currents outside the surf zone can then be written as

$$Q_{s,o} = Q_{s1,o} + Q_{s2,o} \quad (5.6)$$

Inside the surf zone

The transport due to the undertow in Region 1 is given by

$$\begin{aligned}
 Q_{s1,i} &= \int_{-h}^{-h+D_f} \bar{u}_{s,i}(z) C(z) dz \\
 &= \frac{C_a}{w_s T} \exp[-F(z - z_a)] \\
 &\quad \left\{ \frac{\partial H^2}{\partial x} \frac{g}{96h\nu_e} \left[\frac{z^3}{F} + \frac{3z^2}{F^2} + \frac{6z}{F^3} + \frac{6}{F^4} \right] \right. \\
 &\quad + \frac{\partial H^2}{\partial x} \frac{g}{32\nu_e} \left[\frac{z^2}{F} + \frac{2z}{F^2} + \frac{2}{F^3} \right] \\
 &\quad \left. + \frac{\partial H^2}{\partial x} \frac{gh}{48\nu_e} \left[\frac{z}{F} + \frac{1}{F^2} \right] + \frac{M_{fa}}{h} \left[\frac{z}{F} + \frac{1}{F^2} \right] + \frac{M_{fa}}{F} \right\}_{-h}^{-h+D_f} \quad (5.7)
 \end{aligned}$$

Similarly, the transport due to the undertow in Region 2 is

$$\begin{aligned}
 Q_{s2,i} &= \int_{-h+D_f}^0 \bar{u}_s(z) C(z) dz \\
 &= C_a \exp[-F(z - z_a)] \\
 &\quad \left\{ \frac{\partial H^2}{\partial x} \frac{g}{32\nu_e h} \left(\frac{z^2}{F} + \frac{2z}{F^2} + \frac{2}{F^3} \right) \right. \\
 &\quad + \frac{\partial H^2}{\partial x} \frac{g}{16\nu_e} \left(\frac{z}{F} + \frac{1}{F^2} \right) \\
 &\quad \left. + \frac{\partial H^2}{\partial x} \frac{gh}{48\nu_e} \left(\frac{1}{F} \right) + \frac{M_{fa}}{hF} \right\}_{-h+D_f}^0 \quad (5.8)
 \end{aligned}$$

The total contribution due to the mean cross-shore currents inside the surf zone can then be written as

$$Q_{s,i} = Q_{s1,i} + Q_{s2,i} \quad (5.9)$$

Finally, the total suspended sediment transport can be written as

$$Q_s = Q_{s,f} + Q_{s,o} \quad (5.10)$$

outside the surf zone, and as

$$Q_s = Q_{s,f} + Q_{s,i} \quad (5.11)$$

inside the surf zone.

5.2 Bedload Transport

5.2.1 Transport due to Effects of the Bottom Boundary Layer

The following is a slight extension of the ideas presented by Trowbridge and Young (1989). Sediment transport is the result of energy dissipation in the bottom boundary layer.

An empirical, dimensionally consistent form for the instantaneous bedload sediment transport, $q_{b,1}(t)$, can be written as

$$\frac{q(t)}{w_s d} = K \frac{\tau_b(t)}{\rho g d(s-1)} \quad (5.12)$$

where w_s is the fall velocity of the sediment of diameter d , K is a dimensionless constant, $\tau_b(t)$ is the instantaneous bottom shear stress, ρ is the density of the fluid, g is the acceleration due to gravity and s is the specific gravity of the sediment. The time-mean value of sediment transport is then in terms of the time-mean bottom shear stress which can be specified by considering bottom boundary layer approximations.

Considering two-dimensional motion, the equations of continuity and x-momentum within the boundary layer can be written as

$$\frac{\partial u}{\partial x} + \frac{\partial w}{\partial z} = 0 \quad (5.13)$$

and

$$\frac{Du}{Dt} = -\frac{1}{\rho} \frac{\partial p}{\partial x} + \nu \frac{\partial^2 u}{\partial z^2} \quad (5.14)$$

where

$$\frac{D}{Dt} = \frac{\partial}{\partial t} + u \frac{\partial}{\partial x} + w \frac{\partial}{\partial z} \quad (5.15)$$

is the substantial derivative operator, u, w are the velocity components in the x, z directions, p is the pressure and the onshore direction is considered positive. A boundary layer approximation for the z-momentum equation is (e.g., Hunt and Johns 1963)

$$g + \frac{1}{\rho} \frac{\partial p}{\partial z} = O(\delta) \quad (5.16)$$

where δ is the boundary layer thickness. Thus, the pressure change across the boundary layer is $O(\delta^2)$ at most, whence the streamwise external flow given by

$$u(x, t) = U(x, t) \quad (5.17)$$

imposes the pressure gradient

$$-\frac{1}{\rho} \frac{\partial p}{\partial x} = \frac{DU}{Dt} \quad (5.18)$$

The flow in the boundary layer is imposed by the external flow $U(x, t)$ which occurs in the interior of the fluid. Thus, using Equations (5.13) and (5.18) the x-momentum equation within the boundary layer can be finally written as

$$\frac{\partial u}{\partial t} + \frac{\partial u^2}{\partial x} + \frac{\partial uw}{\partial z} = \frac{\partial U}{\partial t} + U \frac{\partial U}{\partial x} + \frac{1}{\rho} \frac{\partial \tau}{\partial z} \quad (5.19)$$

where τ is the shear stress in the boundary layer.

The boundary conditions at the outer edge of the boundary layer are

$$u, \tau \rightarrow U, 0 \text{ as } z \rightarrow \infty \quad (5.20)$$

As bedload is considered, the normal no-slip condition is not applied, however

$$w = 0 \text{ at } z = 0 \quad (5.21)$$

where $z = 0$ at the outer edge of the moving bedload layer which is considered to be much thinner than the bottom boundary layer.

A standard perturbation approach is applied where u, w, U, τ are expanded in a power series, e.g.,

$$u = u_1 + u_2 + \dots \quad (5.22)$$

in a small parameter ϵ which is of the order of the ratio of the wave amplitude (a) to water depth (h). Solutions are by the method of successive approximations to each order. Taking the mean of the first-order x-momentum equation and applying the boundary condition (Equation 5.20), we have

$$\bar{\tau}_{b,1} = 0 \quad (5.23)$$

where the overbar indicates time-averaging. Thus, the mean bottom shear stress vanishes to first-order. The second-order expansion of Equation (5.19) becomes

$$\frac{\partial u_2}{\partial t} + \frac{\partial u_1^2}{\partial x} + \frac{\partial u_1 w_1}{\partial z} = \frac{\partial U_2}{\partial t} + U_1 \frac{\partial U_1}{\partial x} + \frac{1}{\rho} \frac{\partial \tau_2}{\partial z} \quad (5.24)$$

Taking the mean of Equation (5.24), integrating in the z -direction from $z = 0$ to $z = \delta$ and applying the boundary conditions,

$$\frac{\overline{\tau_{b,2}}}{\rho} = \delta U_1 \frac{\partial U_1}{\partial x} - \frac{\partial}{\partial x} \int_0^\delta \overline{u_1^2} dz - \overline{U_1 w_1}_{z=\delta} \quad (5.25)$$

Substituting for w_1 using Equation (5.13),

$$\frac{\overline{\tau_{b,2}}}{\rho} = \frac{\partial}{\partial x} \int_0^\infty \overline{(U_1^2 - u_1^2)} dz - \overline{U_1 \frac{\partial}{\partial x} \int_0^\infty (U_1 - u_1) dz} \quad (5.26)$$

where the upper limits are set to infinity as the integrands vanish outside the boundary layer.

If changes in mean flow properties are considered to occur over longer distances as compared to the typical wavelength, then, following Trowbridge and Young (1989), Equation (5.26) may be approximated as

$$\overline{\tau_{b,2}} \simeq -\tau_{b,1} \overline{\frac{\partial}{\partial x} \int U_1 dt} \quad (5.27)$$

If a progressive wave form is assumed, we have

$$\frac{\partial U_1}{\partial x} = -\frac{1}{c} \frac{\partial U_1}{\partial t} \quad (5.28)$$

where c is the celerity of the wave, whence Equation (5.28) becomes

$$\overline{\tau_{b,2}} \simeq \frac{1}{c} \overline{\tau_{b,1} U_1} \quad (5.29)$$

where (e.g., Kajiura 1968) $\overline{\tau_{b,1} U_1}$ is the mean rate of energy dissipation in the boundary layer. As the mean rate of energy dissipation is positive, the second-order bottom shear stress is always onshore. Assuming a quadratic friction law for the first-order bottom shear stress of the form

$$\tau_{b,1} = \rho \frac{f}{2} U_1 |U_1| \quad (5.30)$$

Equation (5.29) becomes

$$\overline{\tau_{b,2}} = \rho \frac{f}{2} \frac{1}{c} \overline{U_1^2 |U_1|} \quad (5.31)$$

Combining Equations (5.12) and (5.31), we have

$$Q_{b,1} = \bar{q} \simeq (Kf) \frac{w_s}{2cg(s-1)} \overline{U_1^2 |U_1|} \quad (5.32)$$

From linear wave theory, the first-order near-bottom velocity is given by

$$U_1 = \frac{gHk}{2\sigma \cosh kh} \cos(kx - \sigma t) \quad (5.33)$$

whence Equation (5.32) can be written as

$$Q_{b,1} \simeq (Kf) \frac{w_s}{6\pi(s-1)} \frac{H^3 k^2}{\sinh kh \sinh 2kh} \quad (5.34)$$

with a recommended value (Trowbridge and Young 1989) of $Kf = 0.50 \pm 0.14$.

5.2.2 Transport due to Wave Asymmetry

A sediment transport model in terms of moments of the total velocity vector is useful in order to accommodate the effects of wave asymmetry. In the following, the bedload transport model developed by Bailard and Inman (1981), an extension of earlier works by Bagnold (1963, 1966), is adopted. An energetics approach is followed together with the assumption that the granular bed moves as a sheet under the action of vigorous fluid flow. The instantaneous sediment transport rate, $q(t)$, is considered proportional to the instantaneous rate of energy dissipation, ϵ_w and the constant of proportionality is then a function of time. The instantaneous energy dissipation is assumed to be given by

$$\epsilon_w = \tau_b u \quad (5.35)$$

where the bottom shear stress, τ_b , and the near-bottom velocity, u , are instantaneous quantities. Assuming a quadratic friction law of the form

$$\tau_b = \rho \frac{f}{2} u |u| \quad (5.36)$$

where ρ is the density of fluid and f is the wave friction factor, it is then possible to show that the expression for the mean bedload transport is

$$Q_{b,2} = \frac{\rho f \epsilon_b}{2 \tan \phi} [\overline{u^3} - \frac{\tan \beta}{\tan \phi} \overline{|u|^3}] \quad (5.37)$$

where ϕ is the angle of internal friction of sediment and $\tan \beta$ is the local bed slope. ϵ_b is the bedload efficiency, i.e., the fraction of the energy dissipation rate spent in transporting the bedload and contains the relation between the fluid and granular

velocities. An auxiliary advantage of such an approach is that sediment transport equation in its final form includes the “downshaking” effect of gravity (the modulating $\tan \beta$ term), which is absent in the previous formulation (Equation 5.34). In this form, the equation is completely general and is not restricted to wave motion alone. The velocity terms are difficult to evaluate exactly and approximations need to be made.

The simplest way is to consider the velocity to be of the form

$$u = U_1 + U_2 \quad (5.38)$$

where U_1 is the first-order orbital velocity and U_2 is a perturbation. Assuming that the magnitude of the perturbation is small compared to the magnitude of U_1 , a general equation

$$u^n |u| = U_1^n |U_1| + (n+1)U_2 U_1^{n-1} |U_1| + \frac{n(n+1)}{2} U_2^2 U_1^{n-2} |U_1| + \dots \quad (5.39)$$

developed by Bowen (1980) can then be applied. We now consider the effects of wave-induced motion and include the effects of the Stokes’ second harmonic.

Thus, we define

$$U_1 = \hat{u}_1 \cos(kx - \sigma t) \quad (5.40)$$

$$U_2 = \hat{u}_2 \cos 2(kx - \sigma t) \quad (5.41)$$

where

$$\hat{u}_1 = \frac{Hgk}{2\sigma \cosh kh} \quad (5.42)$$

$$\hat{u}_2 = \frac{3H^2 \sigma k}{16 \sinh^4 kh} \quad (5.43)$$

whereby

$$\begin{aligned} \overline{u^3} &= \overline{U_1^3} + 3\overline{U_1^2 U_2} + 3\overline{U_1 U_2^2} + \overline{U_2^3} \\ &= \frac{3}{4} \hat{u}_1^2 \hat{u}_2 \end{aligned} \quad (5.44)$$

and

$$\begin{aligned} \overline{|u|^3} &= \overline{U_1^2 |U_1|} + 3\overline{U_1 U_2 |U_1|} + 3\overline{U_2^2 |U_1|} + O(U_2^4) \\ &\simeq \frac{4\hat{u}_1^3}{3\pi} + \frac{14\hat{u}_1 \hat{u}_2^2}{5\pi} \end{aligned} \quad (5.45)$$

The transport can then be easily computed using Equations (5.37), (5.44) and (5.45).

An alternative is to consider the mean sediment transport to be simply proportional to the mean bottom shear stress, i.e.,

$$Q_{b,3} \propto \bar{\tau}_b \quad (5.46)$$

and again assuming a quadratic friction law of the form

$$\tau_b = \rho \frac{f}{2} u |u| \quad (5.47)$$

where τ_b is the bottom shear stress, ρ is the density of fluid, f is the wave friction factor and u is the bottom velocity, we have

$$Q_{b,3} = K_a \rho \frac{f}{2} \overline{u |u|} \quad (5.48)$$

where K_a is an empirical constant. As the objective is to represent the effects of wave asymmetry, the velocity u may again be represented as

$$u = U_1 + U_2. \quad (5.49)$$

Thus, we have

$$u |u| = U_1 |U_1| + 2U_2 |U_1| + U_2^2 \frac{|U_1|}{U_1} + \dots \quad (5.50)$$

and Equation (5.48) can be written as

$$Q_{b,3} \simeq K_a \rho \frac{f}{2} \frac{4}{3\pi} u_1 u_2. \quad (5.51)$$

Houston and Dean (1990) simplified the velocity moment term in Equation (5.48) by using Dean's (1965) stream function wave theory as

$$\overline{u |u|} = \frac{0.09 L_0}{h} \frac{H^2}{T^2} \quad (5.52)$$

where L_0 is the deep water wavelength. They obtained a value for the calibration constant, which, with the present definitions becomes

$$K_a = 2.1 \times 10^{-5} \text{m}^4/(\text{Ns}). \quad (5.53)$$

Table 5.1: Parameters required in the numerical model.

Parameter	Value
Fall velocity, w_s	0.035 m/sec
Reference conc., C_a	10^{-3}
$z - z_a$	z
Eddy viscosity, ν_e	$0.1 \text{ m}^2/\text{s}$
Kf	0.5
Bedload efficiency, ϵ_b	0.10
Friction factor, f	0.005
K_a	$2.1 \times 10^{-5} \text{ m}^4/(\text{Ns})$

5.3 Parameterization of Constants

In the present experiments, the sediment was medium sand with a mean diameter of 0.2 mm which has a fall velocity, w_s , of approximately 0.035 m/sec. For purposes of the numerical model, the effective bed level was assumed to be the top of the grains, i.e., $z - z_a \sim z$. The reference concentration was set at 10^{-3} following empirical criteria developed by Nielsen (1986: Figure 2). The eddy viscosity, ν_e , was set to a representative value of $0.1 \text{ m}^2/\text{s}$ (Dally and Dean 1984). The value of Kf in Equation (5.34) was set to 0.5 (Trowbridge and Young 1989). The constants in Equation (5.37) were also set to the recommended values: ϵ_b , the bedload efficiency factor, was set to 0.10 and f , the friction factor was set to 0.005 (Bailard 1982). The values of the various parameters required in the numerical solution of the transport equations are summarized in Table (5.1).

5.4 Model Verification

The total sediment transport past any cross-section of the flow can be written as

$$Q = Q_s + Q_b \quad (5.54)$$

where Q_s and Q_b are the sediment transports due to suspended load and bedload respectively. Q_s was evaluated using Equation (5.10) outside the surf zone and using Equation (5.11) inside the surf zone, while Q_b was evaluated as the sums of Equations (5.32) and (5.37).

The sediment continuity equation

$$\frac{dh}{dt} = \frac{dQ}{dx} \quad (5.55)$$

can then solved to give profile adjustment.

The transport and continuity equations were represented in standard finite difference form and programmed in FORTRAN on a VAX 8352 mini-computer. For verification, the above sediment transport model was tested against data obtained in the nine overwash experiments. These data present an opportunity for rigorously examining the performance of the computational model because of the variety of test conditions. Experiments E1 through E4 were conducted with different water levels, while the wave characteristics were monochromatic (2 second) and of approximately the same wave height throughout. Experiment E5 simulated the effects of a storm hydrograph with equal rising and falling rates. Experiments E6 through E9 were conducted with the same conditions as Experiments E1 through E4 respectively except that the wave spectra were narrow-banded and with a range of 1.9 to 2.1 seconds. The maximum wave heights in Experiments E6-E9 were the same as the wave heights in Experiments E1-E4 respectively (see Section 2.3 for details).

The simplified bedload equations derived earlier included the Stokes' second harmonic as a perturbation for assessing the velocity moments. It is recognized that the Stokes' expansion carried out to second-order is applicable in deep water only while the waves in the present overwash tests were in intermediate to shallow water. The criterion of no secondary crest at the trough level yields

$$ka \leq \frac{\sinh^3 kh}{\cosh kh(2 + \cosh kh)} \quad (5.56)$$

(e.g., Dean and Dalrymple 1984) for a second-order expansion, whence the equations for the velocity moments developed above have restricted applicability. Usage of higher order (Stokes') expansions is extremely tedious. Thus, an alternative and more accurate method to evaluate the velocity moments was used by applying the numerical stream function wave theory, first developed by Dean (1965) and later extended by Dalrymple (1974).

Briefly, the two-dimensional boundary value problem of wave motion over a rigid, horizontal bottom is solved using the stream function (rather than the traditional velocity potential) approach. The problem is rendered steady by using co-ordinates moving with the wave. A form for the stream function is chosen such that the governing Laplace equation, the bottom boundary condition and the kinematic free surface boundary condition are exactly satisfied. The parameters of the stream function representation are estimated by applying the non-linear method of least squares to minimize the errors in the non-linear free surface conditions, and obtaining convergence of the solution to the prescribed wave height and zero net free surface displacement. Once the parameters of the stream function representation are obtained, the bottom velocities and moments can then be easily computed. In addition, the discharge past a cross-section was also evaluated using the stream function approach.

The equations for suspended sediment transport due to undertow have terms which are functions of the gradient of the wave momentum, i.e., $\frac{\partial H^2}{\partial x}$. As there is a sharp discontinuity in this gradient at the break-point, this causes unrealistic filling of the cell seaward of the break-point. Also, the superposition of various components of sediment transport cause additional “kinks” in the sediment transport. To overcome these difficulties, following Dally and Dean (1984), an empirical transport smoothing or weighting function of the following form was adopted

$$w(x) = \frac{1}{1 + (\frac{x}{\beta_i})^2} N \quad (5.57)$$

where N is the factor for normalization given by

$$N = \frac{2}{\pi(\beta_- + \beta_+)}. \quad (5.58)$$

$i = -/+$ where $-$ and $+$ denote the negative and positive directions about the reference cell being considered. The factors β_- and β_+ skew the transport if they are unequal and were specified in terms of the local wave height. The weighting function satisfies the conservation requirement:

$$\int_{-\infty}^{\infty} w(x) dx = 1 \quad (5.59)$$

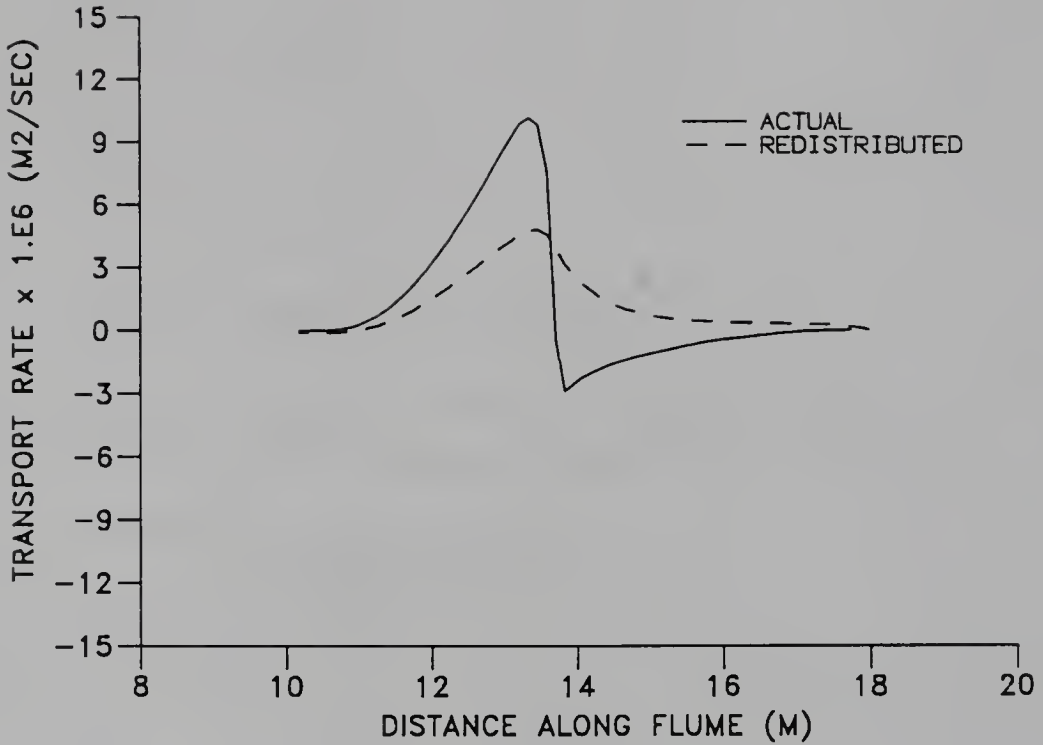


Figure 5.1: Experiment E1: Actual suspended sediment transport and redistributed suspended sediment transport due to the weighting function.

and skews the transport in the direction of transport at each cell. The redistributed transport is then computed at each cell as

$$Q_r = \int_{-\infty}^{\infty} w(x) Q_a(x) dx \quad (5.60)$$

where Q_r is the redistributed transport and Q_a is the actual transport. Figure 5.1 presents an example of the capability of the weighting function, as applied to initial conditions of Experiment E1. Transport is onshore till breaking, there is a sudden change in the gradient at the break-point, and offshore transport exists landward of the break-point. The weighting function skews the transport in the direction of net transport and shifts the point of maximum change slightly landward.

The incident wave height was specified at the toe of the beach. The initial bed profile was divided into equally-spaced grids, though this is not a necessity. The wave field, and concomitant set-up, across the profile was estimated using Dally's

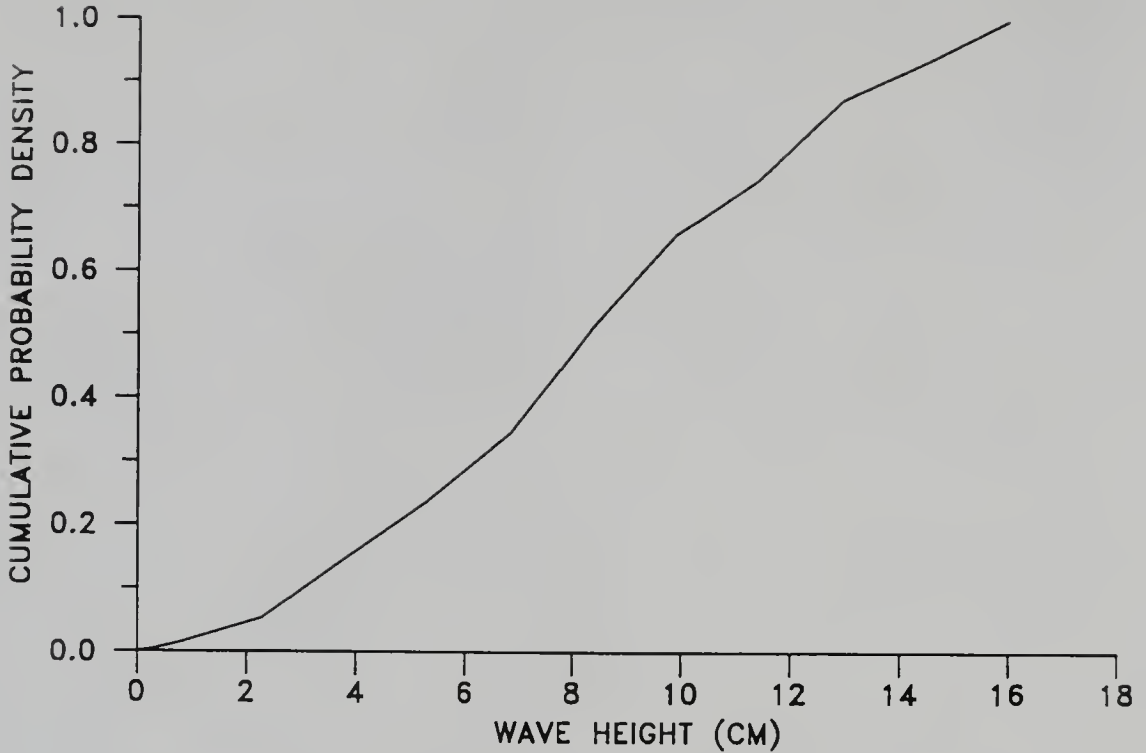


Figure 5.2: An example cumulative probability function for random waves at the toe of the beach ($x=18$ m): Experiment E8.

(1980) breaking wave model, which is documented in Appendix A. Next, the various transport constituents were evaluated at each cell location of the grid. The sediment continuity equation was then applied to obtain changes in depth due to the transports and the new depths were calculated. This procedure was repeated for each time step.

A simple formulation was applied for estimating the wave field in cases with random waves. A cumulative probability distribution function (pdf) was developed from the measured wave heights at the toe of the beach (an example for Experiment E8 is presented in Figure 5.2). A random number generator, an IMSL subroutine GGUBFS which employs deviates from uniform distributions, was used to generate a sequence of random numbers between 0 and 1. These numbers were assumed to correspond to the cumulative pdf of the waves. The corresponding wave height at the toe of the beach was thus estimated for the current time step. The procedures for computing the wave field, transports and changes in depths were the same as for cases with monochromatic waves. In the next time step, a new wave height at the toe

of the beach was estimated from the next random number generated in the sequence and the whole procedure was repeated. Thus, a random series of monochromatic waves was allowed to act on and shape the beach.

The predictions of the numerical model are next compared with the profiles actually measured in the wave tank. Table (5.2) summarizes some of the primary aspects of the experiments. All dimensions are in model units.

Experiment E1

Experiment E1 was conducted with water level at the mean sea level (MSL) and monochromatic waves were allowed to impinge upon the initially planar beach. There was no overtopping of the crest of the barrier island in this case. Incident waves were 0.16 m high at the toe of the beach and had a time period of 2 seconds.

Figure 5.3 displays the measured initial and final (after 4.5 hours) profiles and also the prediction of the numerical model for the profile after 4.5 hours of wave action. The model predicts offshore erosion, a prominent longshore bar with its crest at the break-point, aggravated erosion inside the surf zone and deposition around the mean water level (MWL) shoreline. The actual measurements indicated slight offshore erosion, a prominent longshore bar, prominent surf zone erosion and deposition landward of the MWL shoreline. The model predicts more offshore erosion than actually occurred. It is interesting to note that even though swash mechanisms have not been included in the present numerical model, the bedload sediment transport mechanisms do predict the deposition of a berm at the shoreline. Swash mechanisms appear to increase the “reach” of the affected area where deposition occurs and cause some additional erosion seaward of the MWL shoreline. The position of the predicted bar is slightly offshore (~ 0.4 m) than actually observed, however, the height of the bar is well predicted. The model cannot replicate the local “scouring” action of plunging breakers which was observed in the experiments and the resultant prominent trough landward of the crest of the bar; the model tends to spread the erosion: the predicted net volume of eroded sediment in the surf zone is very close to that measured. The overall characteristics of model predictions are quite encouraging.

The predictions of the model without the inclusion of bedload mechanisms is

Table 5.2: Test conditions of Experiments E1-E9 (model units).

Expt. No.	Water Level		Wave Characteristics		
	Duration (hrs)	Level (m)	Type	Max. Height (m)	Period (sec)
1	0-4.5	MSL	Regular	0.13	2.0
2	0-4.5	0.12	Regular	0.16	2.0
3	0-4.5	0.19	Regular	0.16	2.0
4	0-4.5	0.22	Regular	0.16	2.0
5	0-1.5	MSL	Regular	0.16	2.0
	1.5-2.0	0.01			
	2.0-2.5	0.055			
	2.5-3.0	0.13			
	3.0-3.5	0.19			
	3.5-4.0	0.215			
	4.0-4.5	0.19			
	4.5-5.0	0.13			
	5.0-5.5	0.055			
	5.5-6.0	0.01			
6	0-5.5	MSL	Random	0.16	1.9
7	0-4.5	0.12	Random	0.16	2.0
8	0-4.5	0.19	Random	0.16	2.0
9	0-4.5	0.22	Random	0.16	2.0

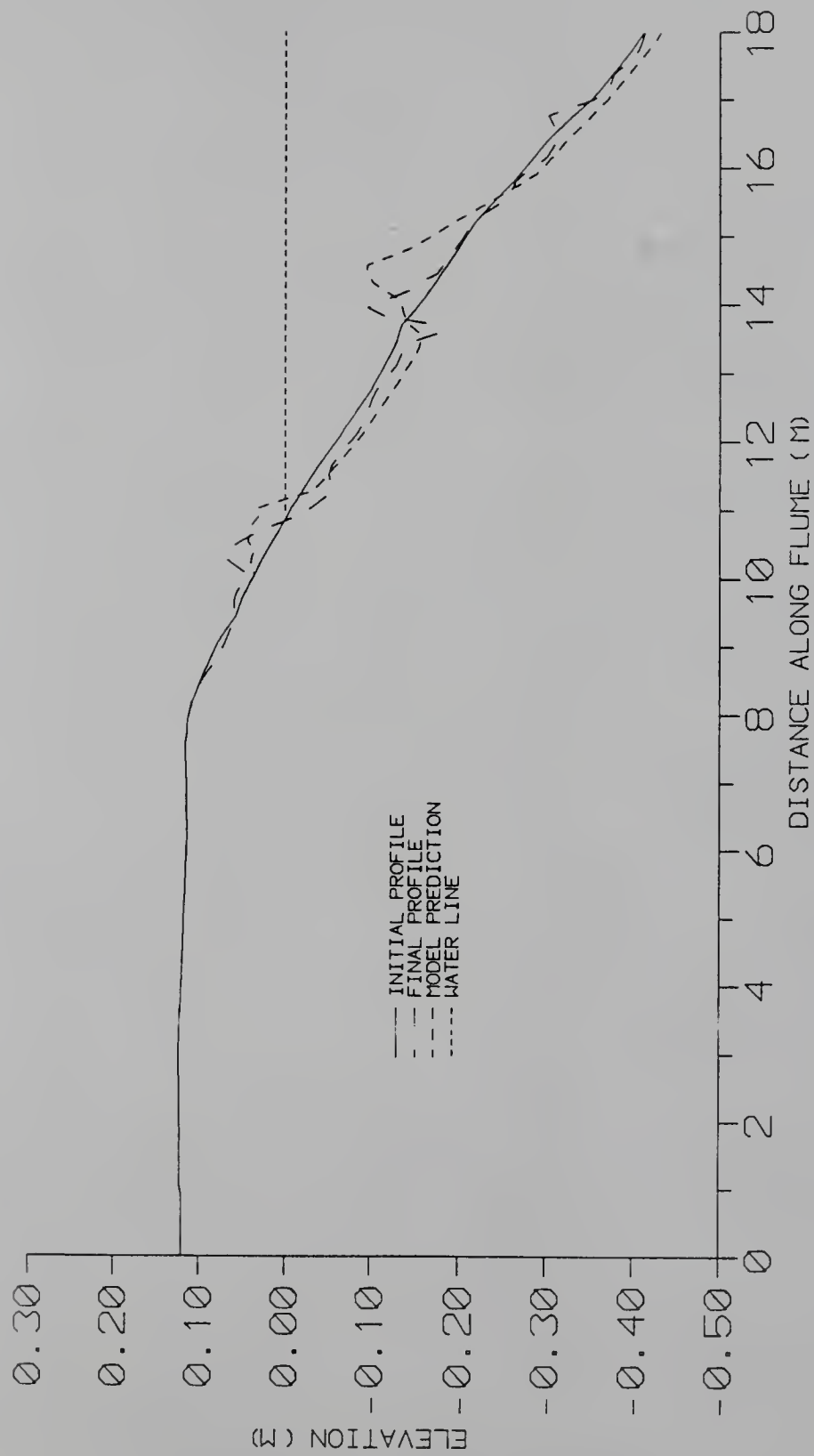


Figure 5.3: Experiment E1: initial profile and model prediction compared with the measured final profile.

presented in Figure 5.4. The slight erosion measured offshore cannot be represented now. The model predicts larger volumes of erosion in the surf zone as compared to that actually observed, and there is no deposition seaward of the MWL shoreline. It appears that inclusion of bedload transport is important to model the sediment transport processes as it improves the erosional and depositional characteristics of the predictions. An estimate for the error can be written as

$$\epsilon_{c,a} = \frac{1}{N} \sum \left| \frac{z_{p,a} - z_m}{z_m} \right| \quad (5.61)$$

where $\epsilon_{c,a}$ is the cumulative error in the model prediction using all transport mechanisms, N is the number of points being considered, $z_{p,a}$ is the predicted elevation using all mechanisms in the model and z_m is the measured (actual) elevation. Similarly,

$$\epsilon_{c,s} = \frac{1}{N} \sum \left| \frac{z_{p,s} - z_m}{z_m} \right| \quad (5.62)$$

is the cumulative error in the model prediction using suspended sediment transport only where $z_{p,s}$ is the predicted elevation using only suspended load mechanisms in the model. The values of cumulative error are $\epsilon_{c,a} = 0.13$ and $\epsilon_{c,s} = 0.11$. By this method of analysis, the absence of bedload mechanisms is not detrimental to the “goodness” of model predictions.

To investigate the stability of the model, the time of wave action in the model was increased to 14 hours. The results are presented in Figure 5.5. The longshore bar has moved offshore and started to grow unreasonably large. Substantial erosion is evident in the surf zone. The presence of both onshore and offshore transport mechanisms lends some stability, however, the absence of any explicit stabilizing mechanisms, in terms of specification of an asymptotic form, causes the model to slowly grow unstable with time.

Experiment E2

Experiment E2 was conducted with the water level 0.12 m above the MSL; thus, the MWL was approximately coincident with the elevation of the crest of the barrier island. The incident monochromatic waves were of 2 seconds period and the wave height was 0.16 m at the toe of the beach.

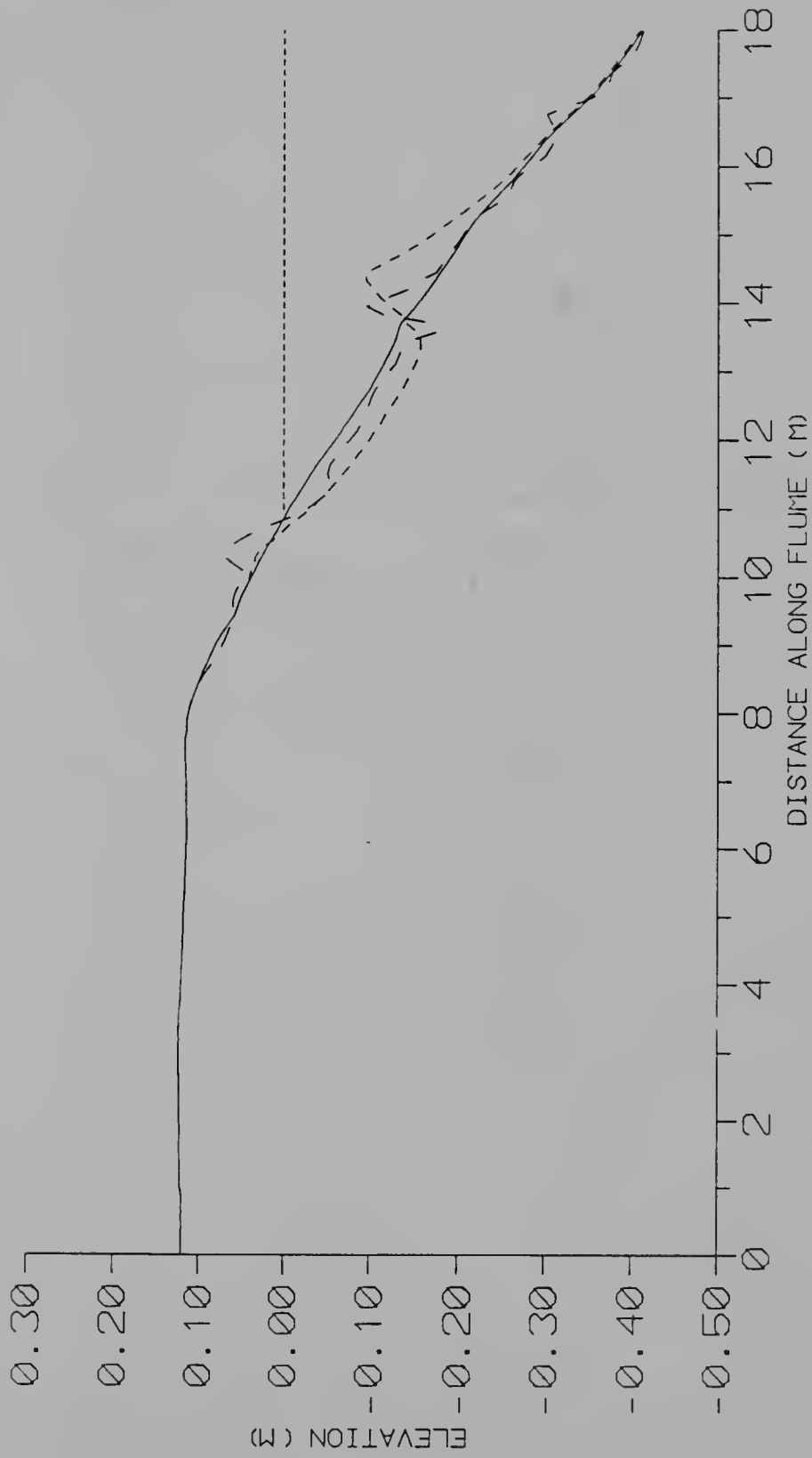


Figure 5.4: Experiment E1: initial profile and model prediction (without bedload) compared with the measured final profile.

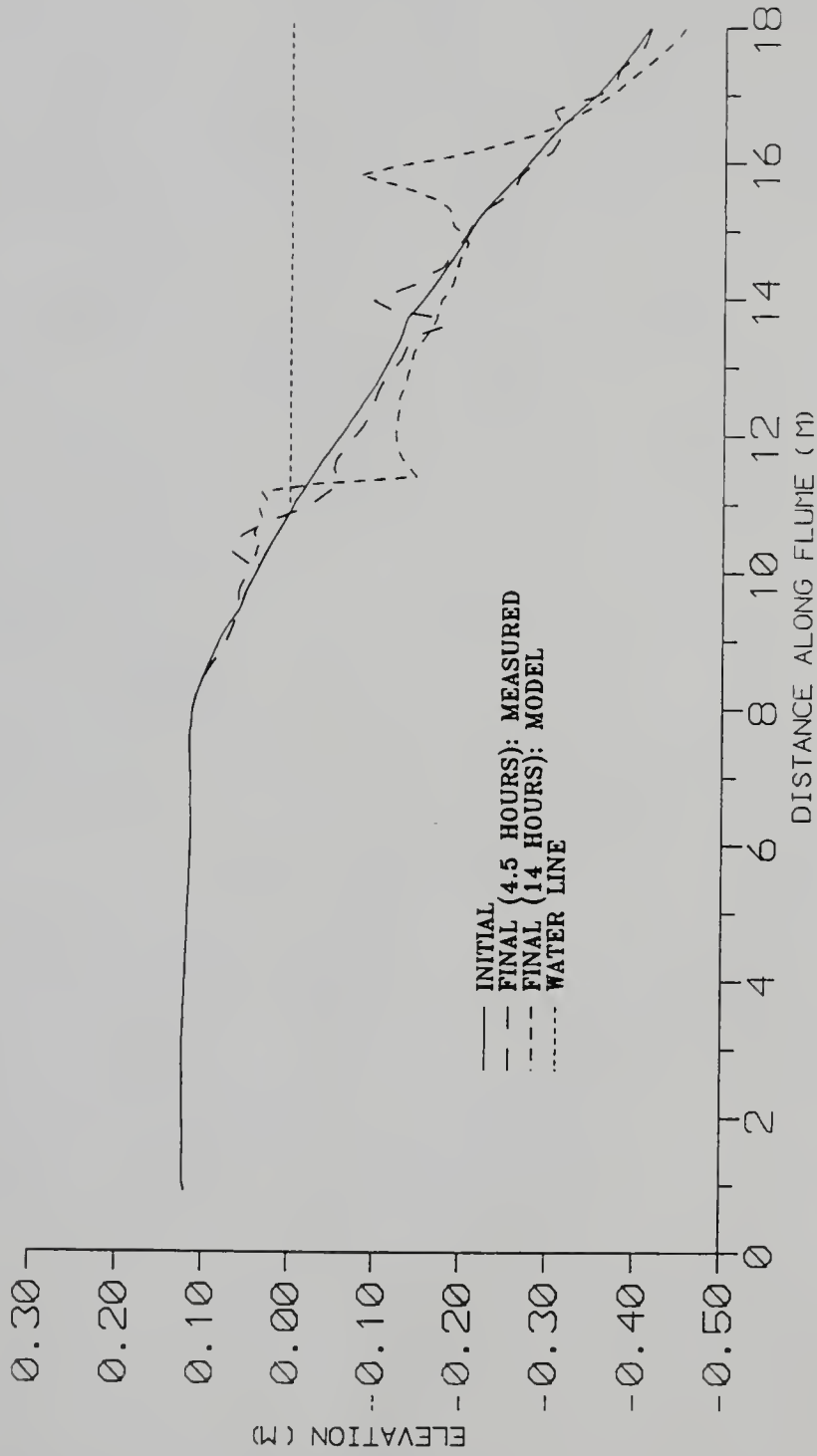


Figure 5.5: Experiment E1: initial profile and model prediction after 14 hours of wave action compared to the measured final profile (after 4.5 hours).

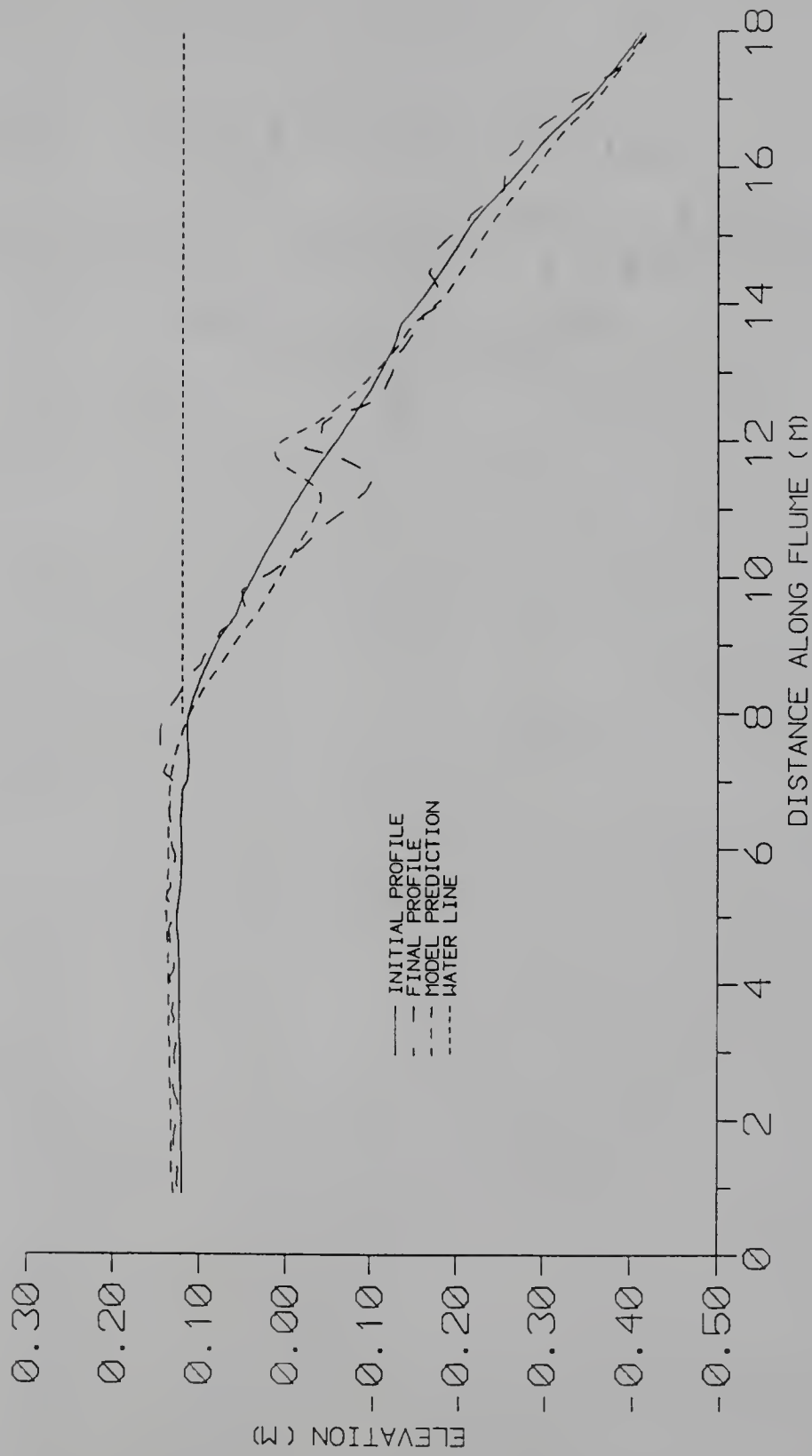


Figure 5.6: Experiment E2: initial profile and model prediction compared with the measured final profile.

Figure 5.6 displays the measured initial and final profiles and also the prediction of the numerical model for the profile after 4.5 hours of wave action. The model predicts slight offshore erosion, a prominent break-point bar, aggravated surf-zone erosion till the slope break of the barrier island and slight deposition over the crest of the barrier island. Measurements indicated slight offshore deposition followed by slight erosion just seaward of the crest of the bar, a prominent longshore bar, aggravated erosion landward of the crest of the bar and deposition over the crest of the barrier island. The model succeeds in predicting the position of the bar, however, the bar is higher as compared to measurements. Again, the model distributes erosion landward of the bar as compared to the severe erosion noticed immediately landward of the bar crest (due to the “scouring” action of plunging breakers). The aspect of washover deposition over the crest of the barrier island is fairly well reproduced.

Experiment E3

Monochromatic waves of 2 seconds period and 0.16 m height (at the toe of the beach) were allowed to impinge upon the barrier island for 4.5 hours. The water level was raised to 0.19 m over the MSL resulting in a nominal inundation of 0.07 m over the crest of the barrier island.

Figure 5.7 presents the measured initial and final profiles and also the prediction of the numerical model for the profile after 4.5 hours of wave action. The model predicts offshore erosion with the amount of erosion increasing landward from the toe of the beach. This feature was also observed in the measured profile. The extensive erosion observed immediately seaward of the crest of the bar is not reproduced in the model result. The position of the prominent longshore bar is well predicted, however, the crest of the longshore bar is higher as compared to that measured. Overall erosion within the surf zone is well represented. The model correctly simulated the deposition pattern over the crest of the barrier island: decreasing levels of deposition landward of the crest of the barrier island. The amount of sand deposited over the crest of the barrier island (0–7.6 m) was $0.044 \text{ m}^3/\text{m}$ as compared to a measured overwashed amount of $0.013 \text{ m}^3/\text{m}$.

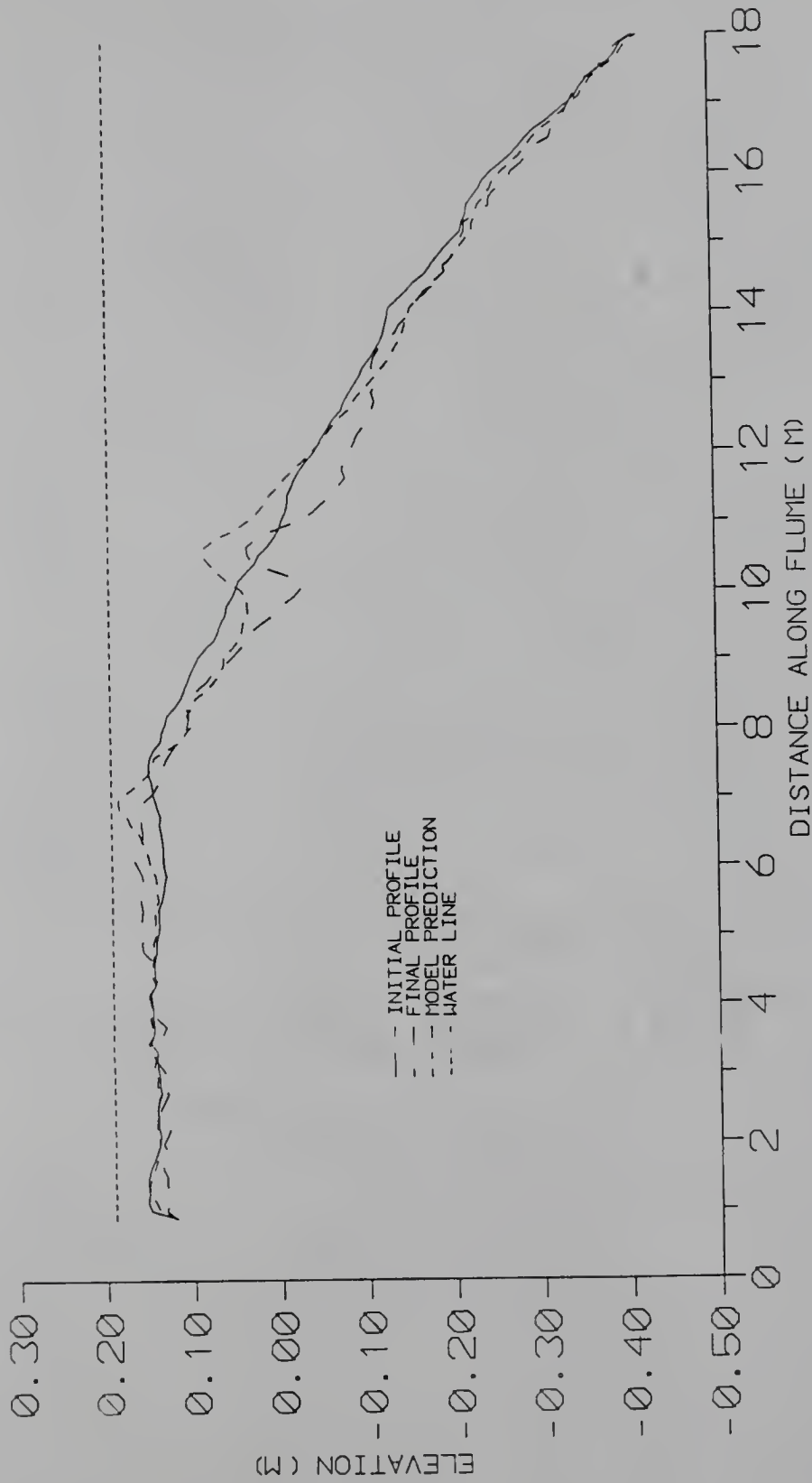


Figure 5.7: Experiment E3: initial profile and model prediction compared with the measured final profile.

Experiment E4

Monochromatic waves of 2 seconds period and 0.16 m height (at the toe of the beach) were allowed to impinge upon the barrier island for 4.5 hours. The water level was raised to 0.22 m over the MSL resulting in a nominal inundation of 0.10 m over the crest of the barrier island.

Figure 5.8 presents the measured initial and final profiles and also the prediction of the numerical model for the profile after 4.5 hours of wave action. The model predicts offshore erosion with the amount of erosion increasing landward from the toe of the beach up to the bar. The measured profile does exhibit some offshore erosion followed by aggravated erosion on either side of the crest of the longshore bar. The model distributes the erosion. The model results cannot reproduce the extensive erosion immediately seaward of the crest of the bar. The position of the predicted bar is slightly seaward and the level is higher than that observed. Erosional characteristics landward of the crest of the bar and the depositional characteristics over the crest of the barrier island are well simulated. Again, the model exhibits the correct trend of decreasing deposition landward of the slope-break of the barrier island. Another positive aspect of the model is that the longshore bar appears more subdued as compared to previous cases and this is apparent in the measured profile as well. The amount of sand deposited over the crest of the barrier island (0–7.6 m) was $0.037 \text{ m}^3/\text{m}$ as compared to a measured overwashed amount of $0.047 \text{ m}^3/\text{m}$.

Figure 5.9 is an example of the model prediction without bedload mechanisms. It presents the measured initial and final profiles and also the prediction of the numerical model for the profile after 4.5 hours of wave action. The measured prominent erosion over the sloping portion of the beach cannot be reproduced. The depositional characteristics over the crest of the barrier island cannot be represented either. The model only predicts offshore transport and the pronounced changes observed in the measured profile are not reproduced. In fact, the model definitely fails to predict most of the principal morphological features apparent in the measured profiles. The model predictions are apparently improved by including all mechanisms. However, $\epsilon_{c,a} = 0.577$ and $\epsilon_{c,s} = 0.596$, and by this method of estimation, the absence of bedload does

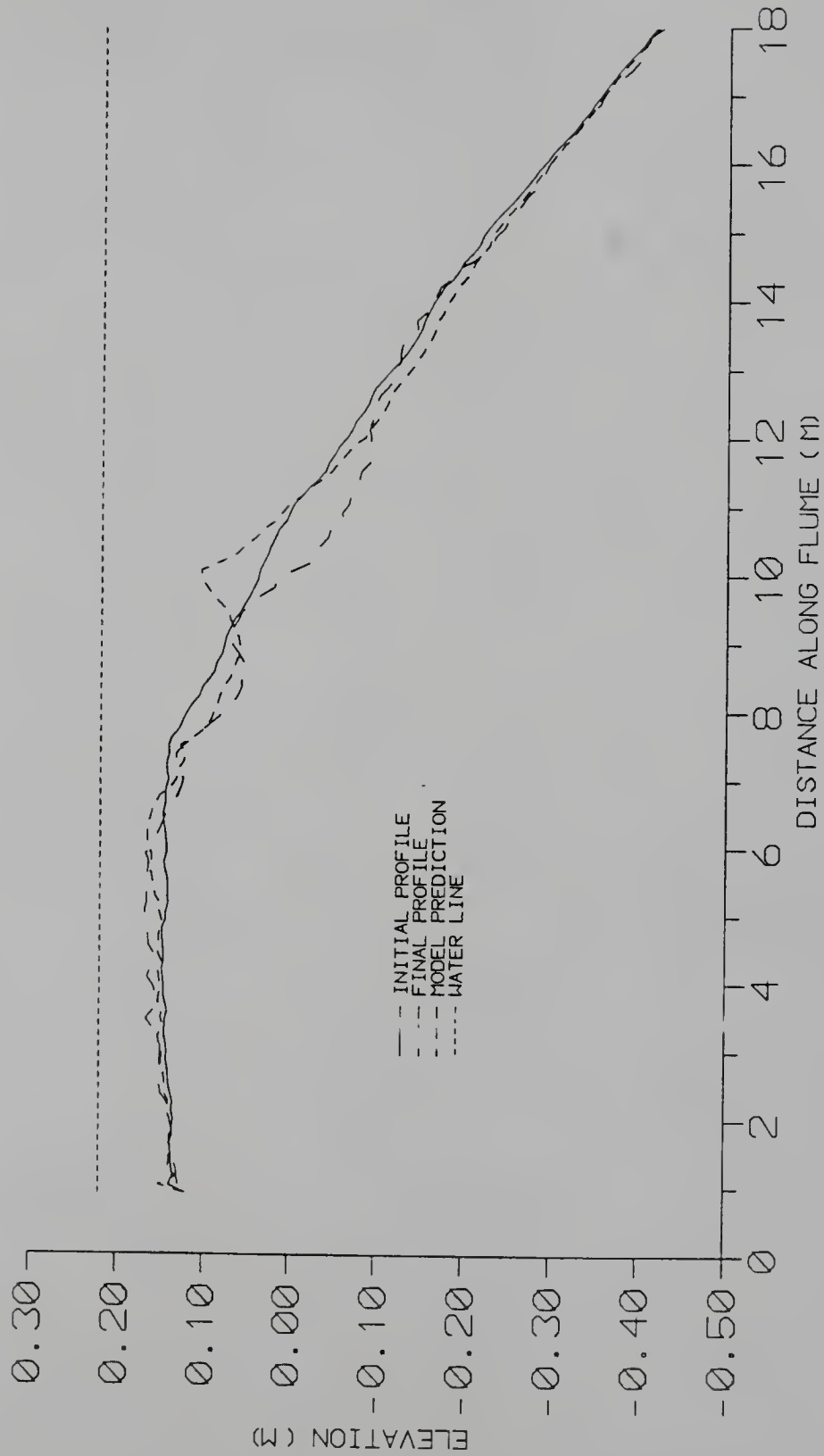


Figure 5.8: Experiment E4: initial profile and model prediction compared with the measured final profile.

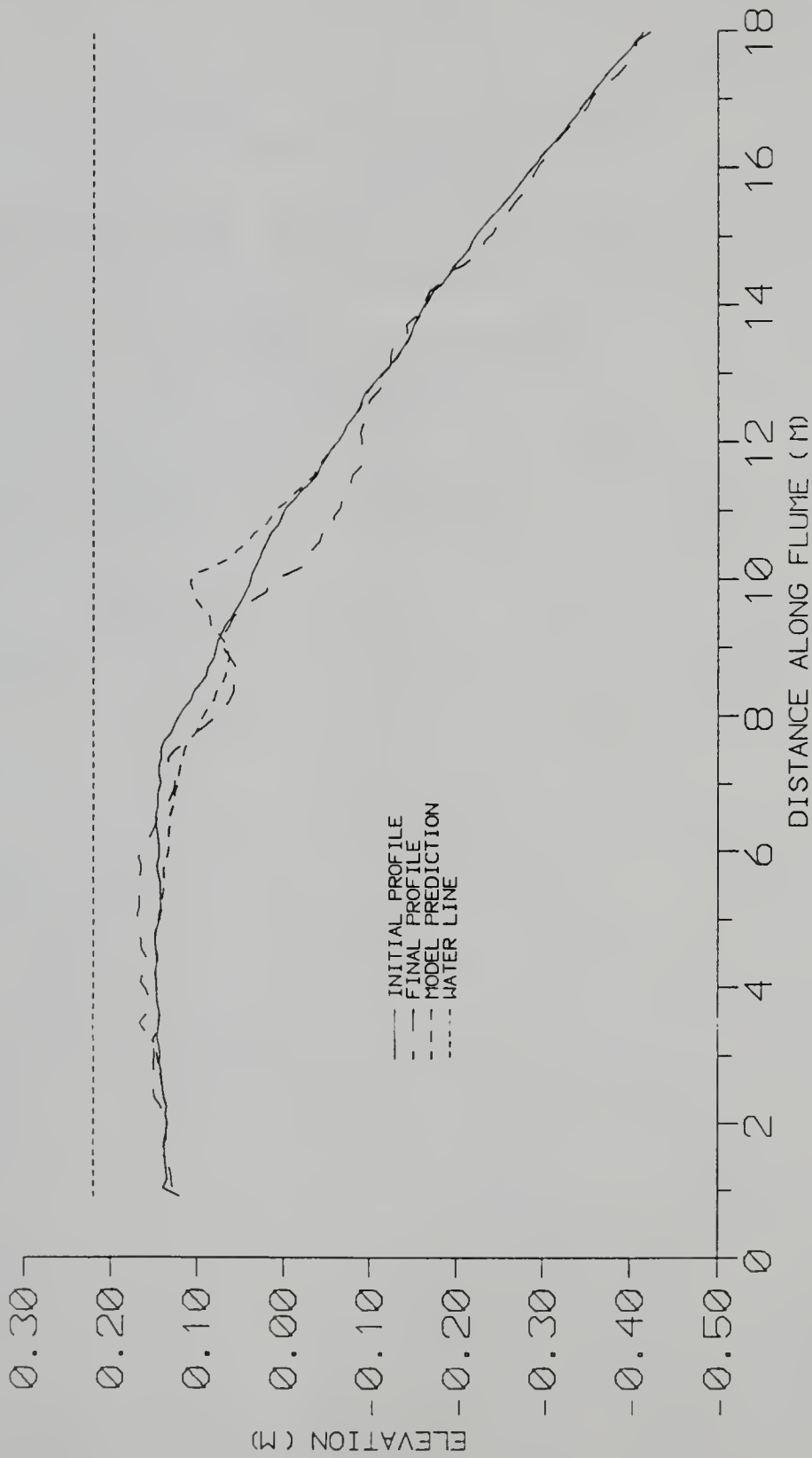


Figure 5.9: Experiment E4: initial profile and model prediction (no bedload) compared with the measured final profile.

not appreciably diminish the “goodness” of model predictions. A better method needs to be developed to quantify the “goodness of fit” in a more representative manner.

Experiment E5

Experiment E5 was conducted to simulate the effects of a rising and falling storm tide of 4.5 hours duration. Waves were first allowed to mold the beach to near-equilibrium by acting on the beach for 1.5 hours prior to the advent of the storm tide.

Figure 5.10 presents the measured initial and final profiles and also the predicted profile after the storm. Some offshore accretion is evident in the measured profile while the predicted profile exhibits erosion. The position of the bar is reasonably well predicted. Surf zone erosion is evident in both the measured and model profiles. A small accretionary feature, due to swash mechanisms during conditions of no overtopping, is evident close to the MSL waterline in both the measured and predicted profiles. The depositional characteristics over the crest of the barrier island are fairly well reproduced. The amount of sand deposited over the crest of the barrier island (0–7.6 m) was $0.032 \text{ m}^3/\text{m}$ as compared to a measured overwashed amount of $0.076 \text{ m}^3/\text{m}$.

Figure 5.11 presents the measured and predicted profiles just before the recession of the storm tide (after 4 hours). The predicted profile exhibits a subtle bar while the measured profile does not have a bar. Changes landward of the bar are fairly well reproduced. However, the model results show less accretion over the barrier island than measured.

Experiment E6

Experiment E6 was conducted with conditions the same as in Experiment E1 except that the wave characteristics were changed to random (instead of monochromatic). The maximum wave height at the toe of the beach was 0.16 m and the spectrum was narrow-banded with a mean period of 2 seconds. The water level was at MSL (no surge, no overtopping condition).

Figure 5.12 presents the measured initial and final profiles and also the prediction of the numerical model for the profile after 4.5 hours of wave action. The model

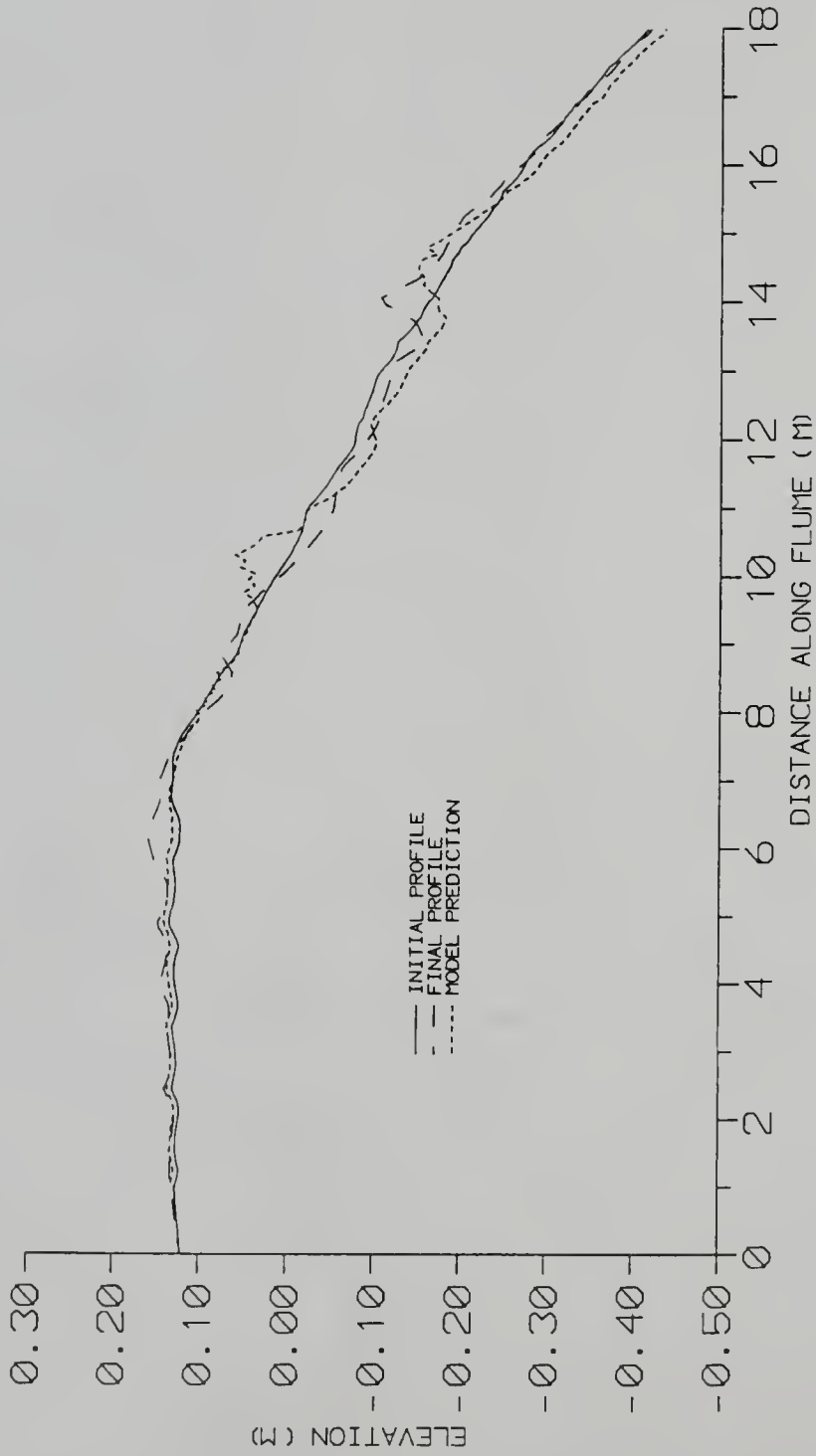


Figure 5.10: Experiment E5: initial profile and model prediction (no bedload) compared with the measured final profile.

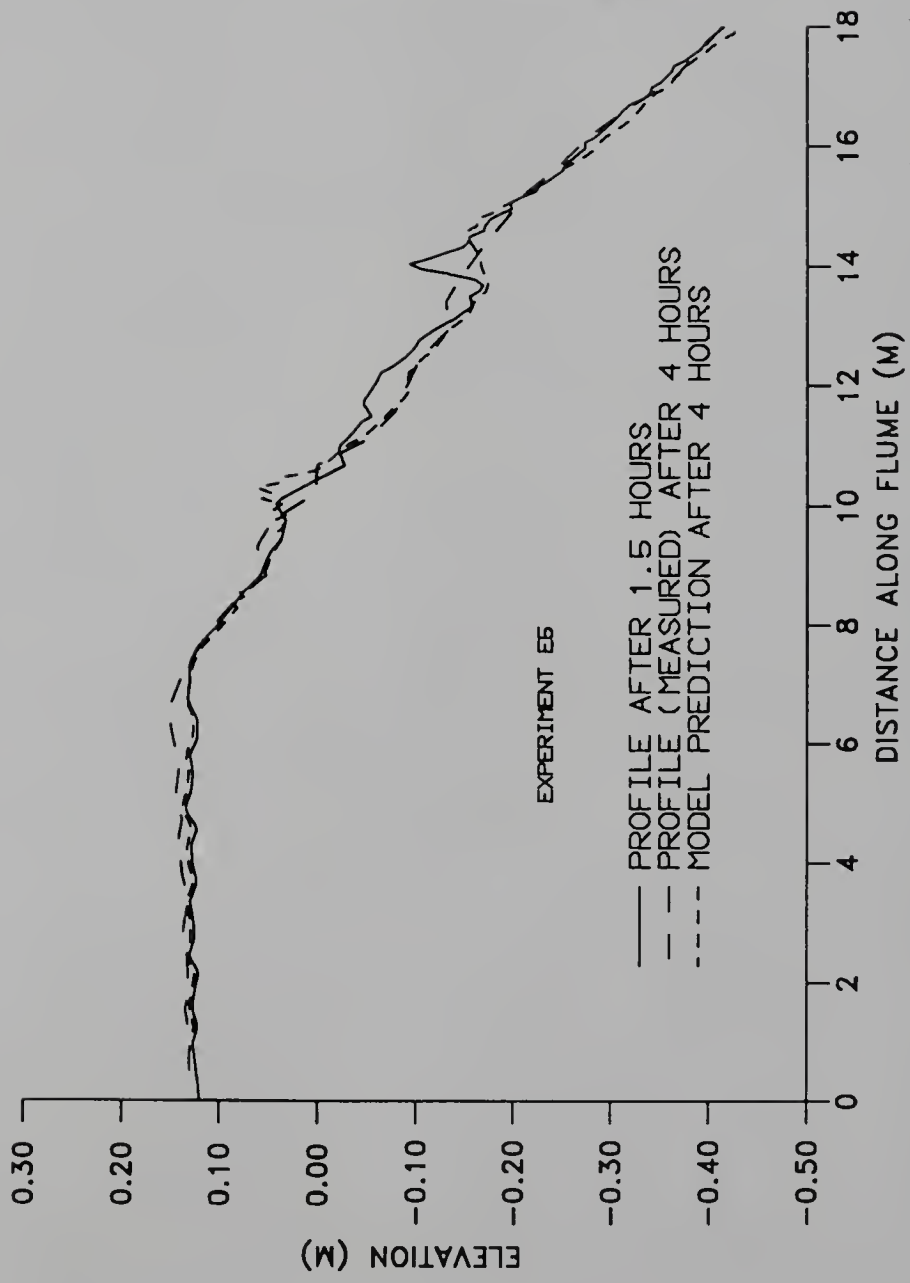


Figure 5.11: Experiment E5: measured profile before the advent of the storm (1.5 hours) and the model prediction after 4 hours (peak storm tide) compared with the measured profile after 4 hours.

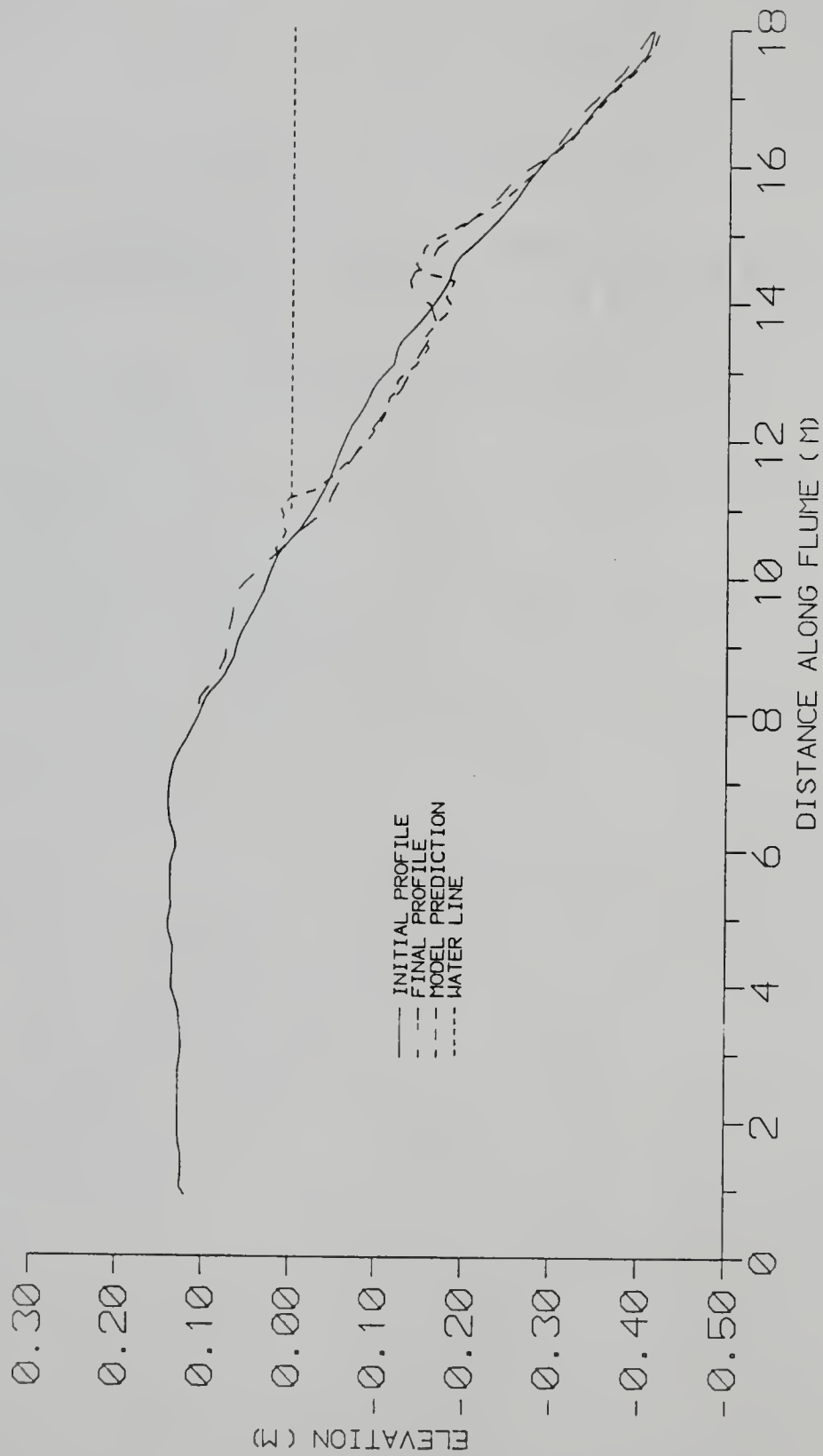


Figure 5.12: Experiment E6: initial profile and model prediction compared with the measured final profile.

predicts almost no change seaward of the longshore bar while the measured profile indicated small amounts of deposition. The size and shape of the bar is well simulated while the crest of the bar is slightly seaward of the actual position. It is worthwhile to note that the longshore bar is correctly simulated to be much subdued as compared to the final profile in the corresponding monochromatic case, Experiment E1. The erosion pattern in the surf zone landward of the bar is well reproduced. Bedload mechanisms in conjunction with wave set-up deposited a small berm near the shoreline. The absence of swash mechanisms in the model causes berm deposition slightly seaward as compared to that actually observed.

Figure 5.13 presents the measured initial and final profiles and also the prediction of the numerical model without bedload mechanisms for the profile after 4.5 hours of wave action. The profile seaward of the bar is well reproduced. The position of the longshore bar is shifted slightly seaward as compared to the prediction of the model with bedload. Surf zone erosion is modeled quite well. However, the deposition of the berm is now absent. It appears that inclusion of all mechanisms gives better results. However, $\epsilon_{c,a} = 0.17$ and $\epsilon_{c,s} = 0.007$ and by this method of analysis, the prediction is apparently better without bedload mechanisms.

Experiment E7

Experiment E7 was conducted with conditions the same as in Experiment E2 except that the wave characteristics were changed to random (instead of monochromatic). The maximum wave height at the toe of the beach was 0.16 m and the wave spectrum was narrow-banded with a mean period of 2 seconds. The water level was 0.12 m above MSL which was almost level with the crest of the barrier island. The advent of wave action resulted in slight overtopping of the barrier island due to swash.

Figure 5.14 presents the measured initial and final profiles and also the prediction of the numerical model for the profile after 4.5 hours of wave action. The model correctly predicts deposition seaward of the longshore bar, however, the amount of predicted accretion is less than actually observed. The longshore bar is correctly reproduced to be of less relief as compared to the corresponding case with monochromatic waves, Experiment E2. The extent and amount of surf zone erosion is well

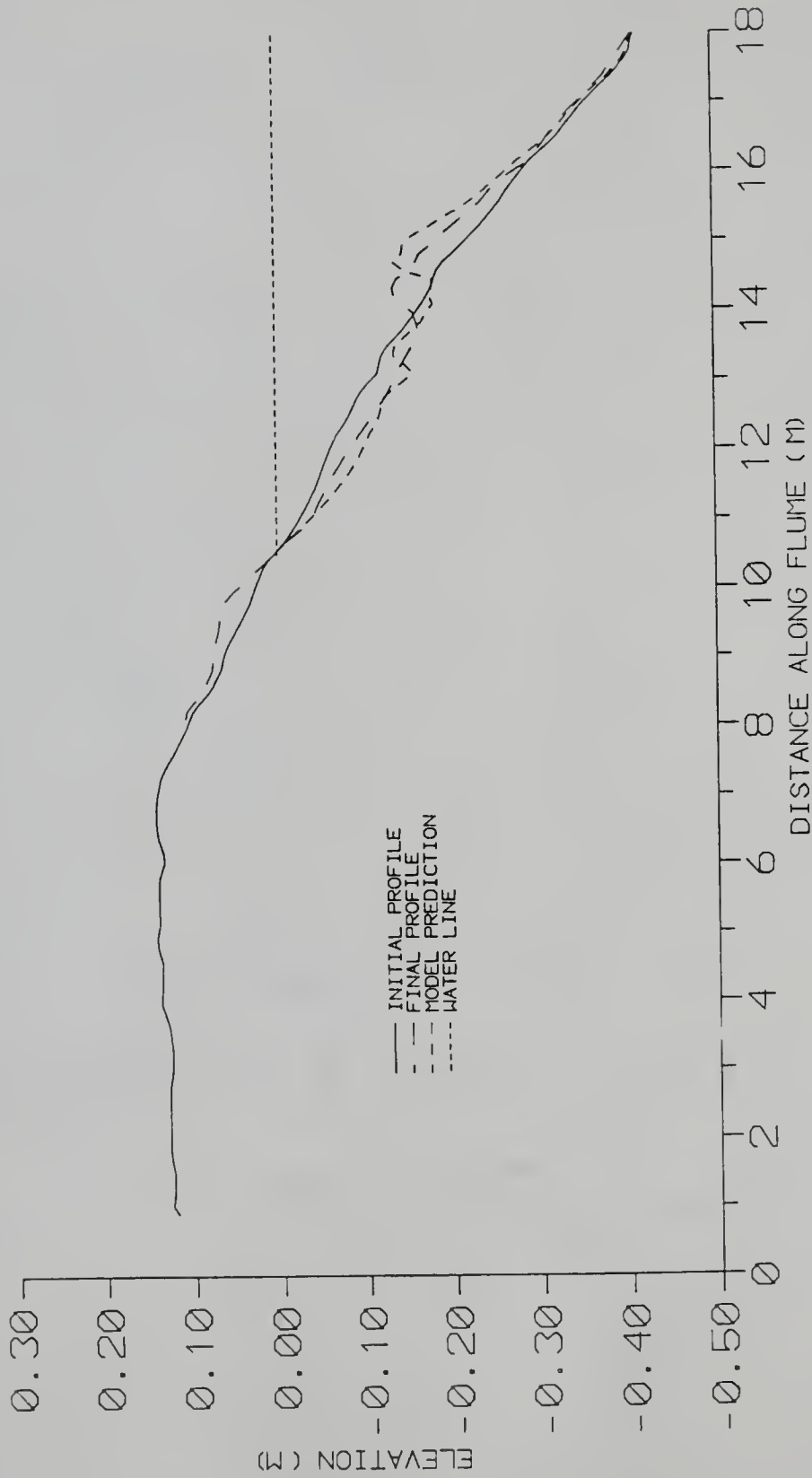


Figure 5.13: Experiment E6: initial profile and model prediction (no bedload) compared with the measured final profile.

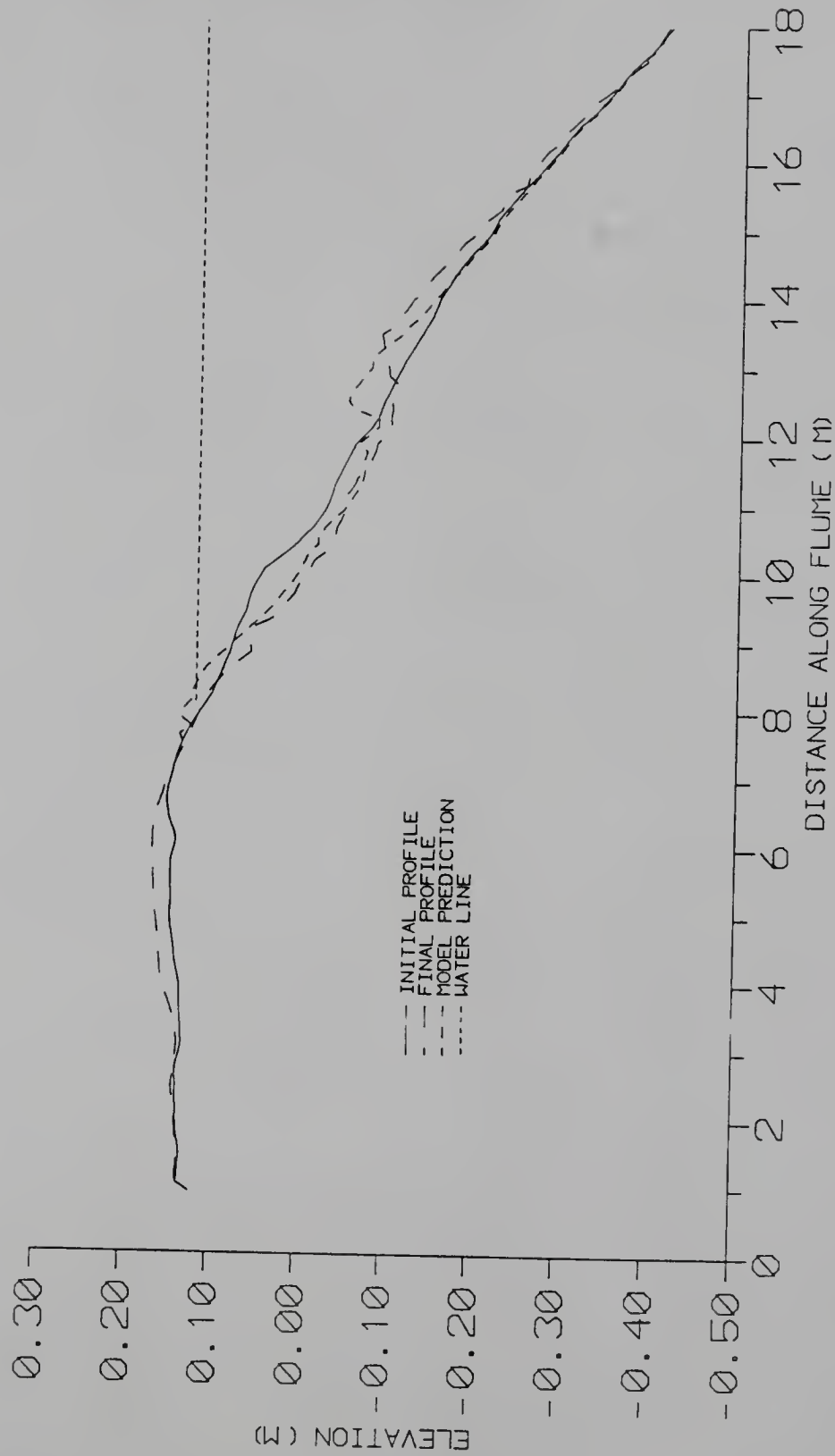


Figure 5.14: Experiment E7: initial profile and model prediction compared with the measured final profile.

predicted. Again, the absence of swash mechanisms in the model causes the deposition of a berm around the slope break of the barrier island, while the observed profile had slight deposition landward of the slope-break.

Experiment E8

Experiment E8 was conducted with conditions the same as in Experiment E3 except that the wave characteristics were changed to random (instead of monochromatic). The maximum wave height at the toe of the beach was 0.16 m and the wave spectrum was narrow-banded with a mean period of 2 seconds. The water level was 0.19 m above MSL which resulted in a 0.07 m nominal overtopping depth over the crest of the barrier island.

Figure 5.15 presents the measured initial and final profiles and also the prediction of the numerical model for the profile after 4.5 hours of wave action. The model does not reproduce the offshore deposition which was evident in the measured profile. The advent of overtopping with random waves produced a profile without a longshore bar, and this facet of absence of a longshore bar is correctly reproduced. The model does not predict the volume of surf zone erosion correctly, however, the extent of erosion is well represented. The deposition characteristics over the crest of the barrier island are correctly represented with the amount of deposition slowly decreasing landward from the crest of the barrier island. The amount of sand deposited over the crest of the barrier island (0–7.6 m) was $0.072 \text{ m}^3/\text{m}$ as compared to a measured overwashed amount of $0.067 \text{ m}^3/\text{m}$.

Experiment E9

Experiment E9 was conducted with conditions the same as in Experiment E4 except that the wave characteristics were changed to random (instead of monochromatic). The maximum wave height at the toe of the beach was 0.16 m and the wave spectrum was narrow-banded with a mean period of 2 seconds. The water level was 0.22 m above MSL which resulted in a 0.10 m nominal overtopping depth over the crest of the barrier island.

Figure 5.16 presents the measured initial and final profiles and also the prediction of the numerical model for the profile after 4.5 hours of wave action. The model

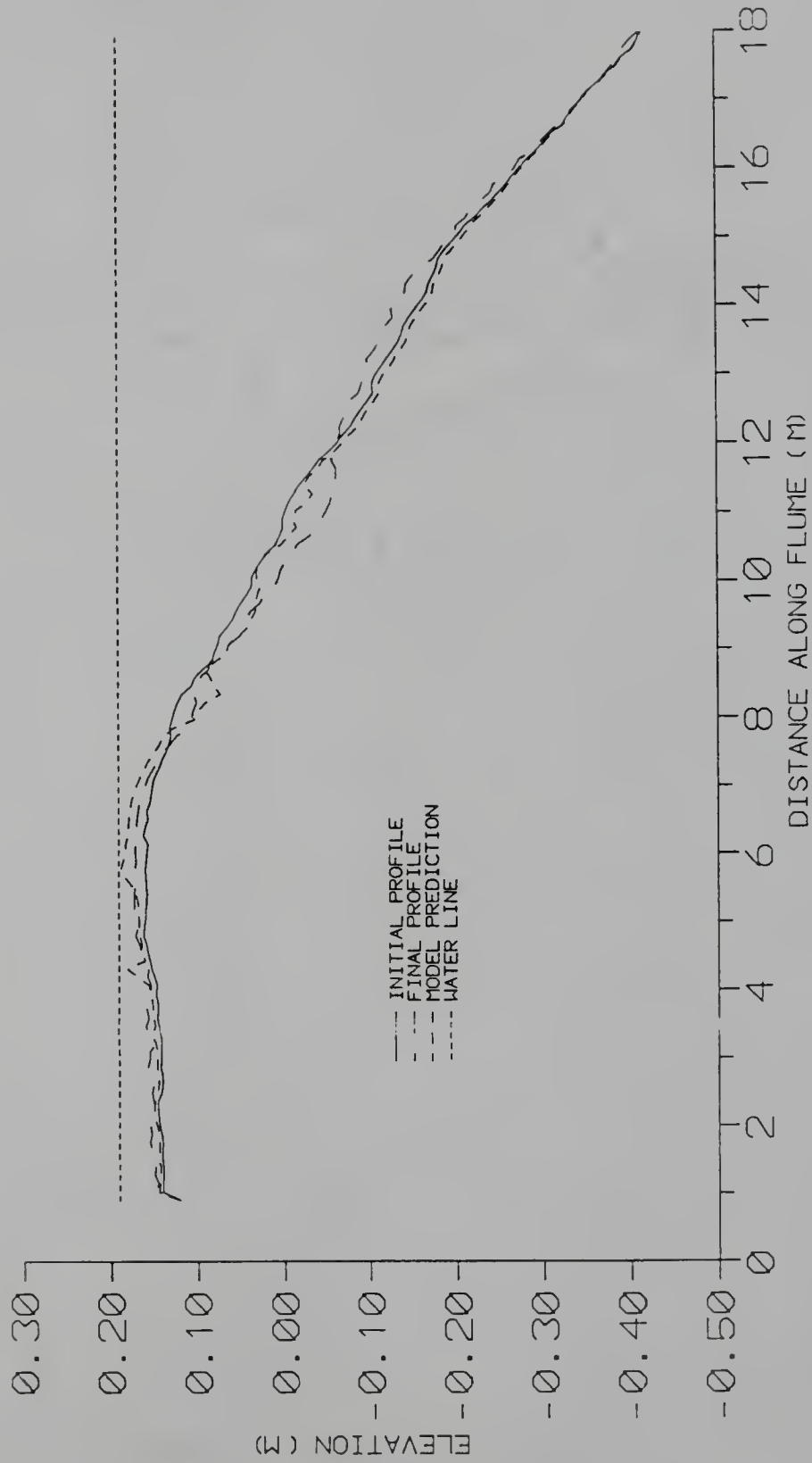


Figure 5.15: Experiment E8: initial profile and model prediction compared with the measured final profile.

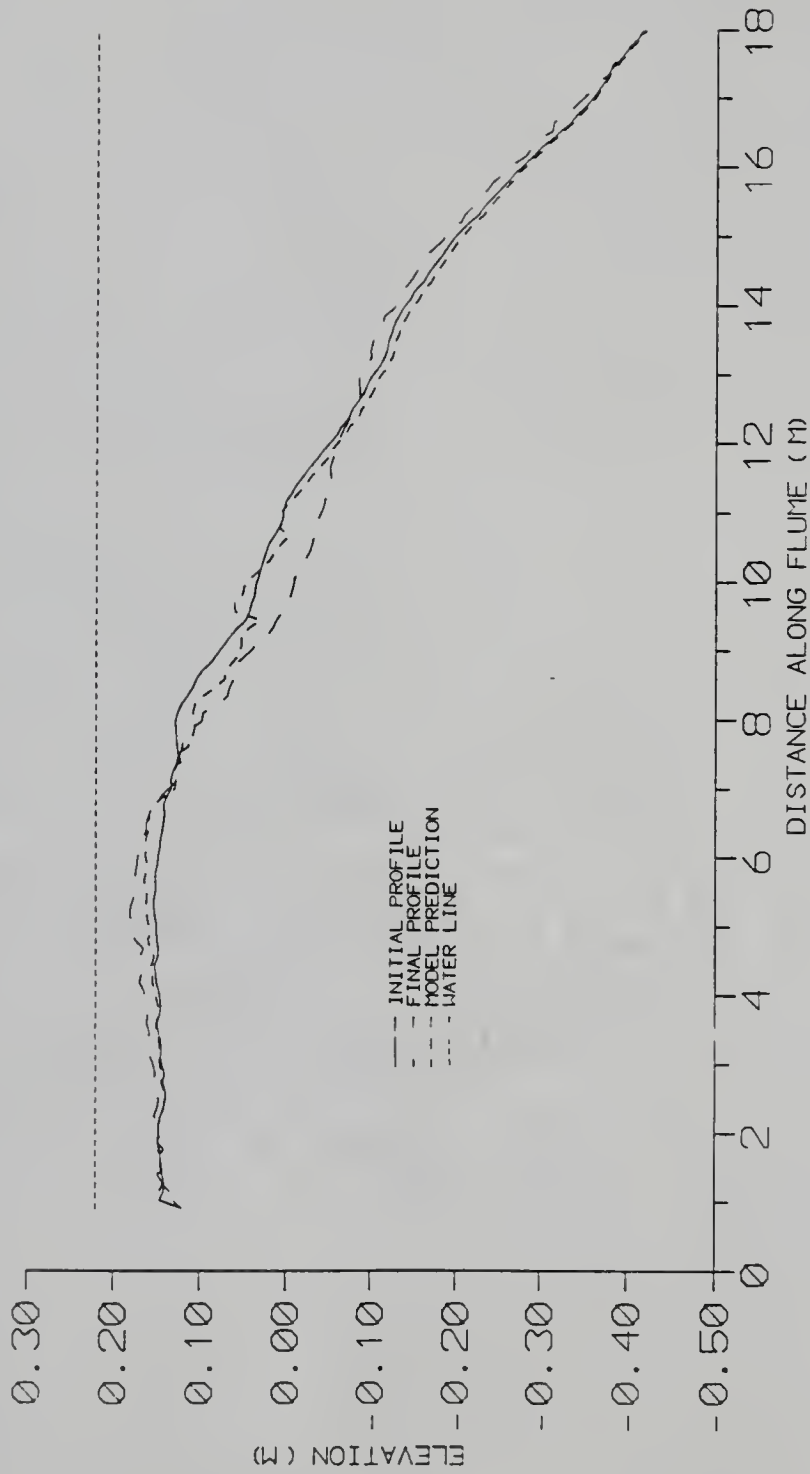


Figure 5.16: Experiment E9: initial profile and model prediction compared with the measured final profile.

incorrectly predicts offshore erosion while the measured profile indicates offshore deposition. The model predicts some erosion in the surf zone which is less than that actually observed. The model prediction improves close to the slope-break and over the crest of the barrier island. The model correctly reproduces the decreasing amounts of deposition landward of the slope-break. There is no longshore bar in the measured profile and the model profile does not exhibit one either. The amount of sand deposited over the crest of the barrier island (0–7.6 m) was $0.031 \text{ m}^3/\text{m}$ as compared to a measured overwashed amount of $0.083 \text{ m}^3/\text{m}$.

5.5 Assessment of Model Limitations

The present sediment transport model has not been established as a rigorously accurate simulation of the various transport components. A brief discussion of model limitations is as follows. A wave Reynolds number at the bottom can be defined as

$$Re_b = \frac{u_b A_b}{\nu} \quad (5.63)$$

where u_b is the bottom orbital velocity from potential flow theory and A_b is the maximum water particle excursion at the bottom (from inviscid theory) just outside the bottom boundary layer. ν is the kinematic viscosity. Assuming shallow water conditions,

$$u_b = \frac{H}{2} \sqrt{\frac{g}{d}} \quad (5.64)$$

$$A_b = \frac{HT}{4\pi} \sqrt{\frac{g}{d}} \quad (5.65)$$

Typical model values for Experiment E1 at the toe of the beach are: $H = 0.16 \text{ m}$, $T = 2 \text{ seconds}$ and $d = 0.46 \text{ m}$. Thus,

$$Re_b \sim 4 \times 10^4 \quad (5.66)$$

which is in the laminar range (Fredsoe and Deigaard 1992). With the present scaling, the Reynolds number in the prototype will be 64 times that in the model; thus,

$$Re_{b,p} \sim 2.6 \times 10^6 \quad (5.67)$$

(where the subscript p denotes prototype) which is in the turbulent range (Fredsoe and Deigaard 1992). The lack of complete Reynolds number similarity creates problems in achieving reasonably comprehensive dynamic similitude and caution must be exercised in interpreting test results in terms of the prototype.

The bottom shear stress affects the reference concentration C_a and bedload transport. The sediment transport equations were developed assuming a constant friction factor in the descriptions of bottom shear stress. Now, considering the Stanton diagram for friction factors under waves (Kamphuis 1975), it is seen that the friction factor is a function of Reynolds number and the ratio A_b/k_e where k_e is the bed roughness. The friction factor is independent of Reynolds number only in the rough turbulent range. The ratio, A_b/k_e where k_e is the bed roughness, is about 200 for model conditions (assuming $k_e \sim 2d_{90}$ where d_{90} is the sand size for which 90% of sand is finer). If the sediment size distribution in the prototype is assumed to be similar to that in the model, A_b/k_e is about 1300 for prototype conditions whence the model conditions are in the transition range while the prototype conditions are in the rough turbulent range. For the mentioned conditions, the friction factor is slightly higher in the model and as compared to that in the prototype (a factor of about 1.5). In spite of the above limitations, it is reiterated (also Section 2.1) that the experience of previous researchers regarding coastal modeling strongly suggests that achieving fall velocity parameter similarity produces model results which are most consistent with prototype results. The friction factor was increased by a factor of ten to examine its influence on model results; the model prediction for Experiment E1 with this augmented friction factor is presented in Figure 5.17. On comparison with the results presented in Figure 5.3, it is seen that the only changes are as follows: the crest of the bar moves slightly seaward and erosion in the surf zone is greater. Overall, it can be concluded that a small change in the friction factor will not significantly change model predictions.

An example of model capability with only bedload mechanisms is presented in Figure 5.18, which can be compared with the model predictions with all mechanisms, Figure 5.3, and the model predictions without bedload mechanisms, Figure 5.4, pre-

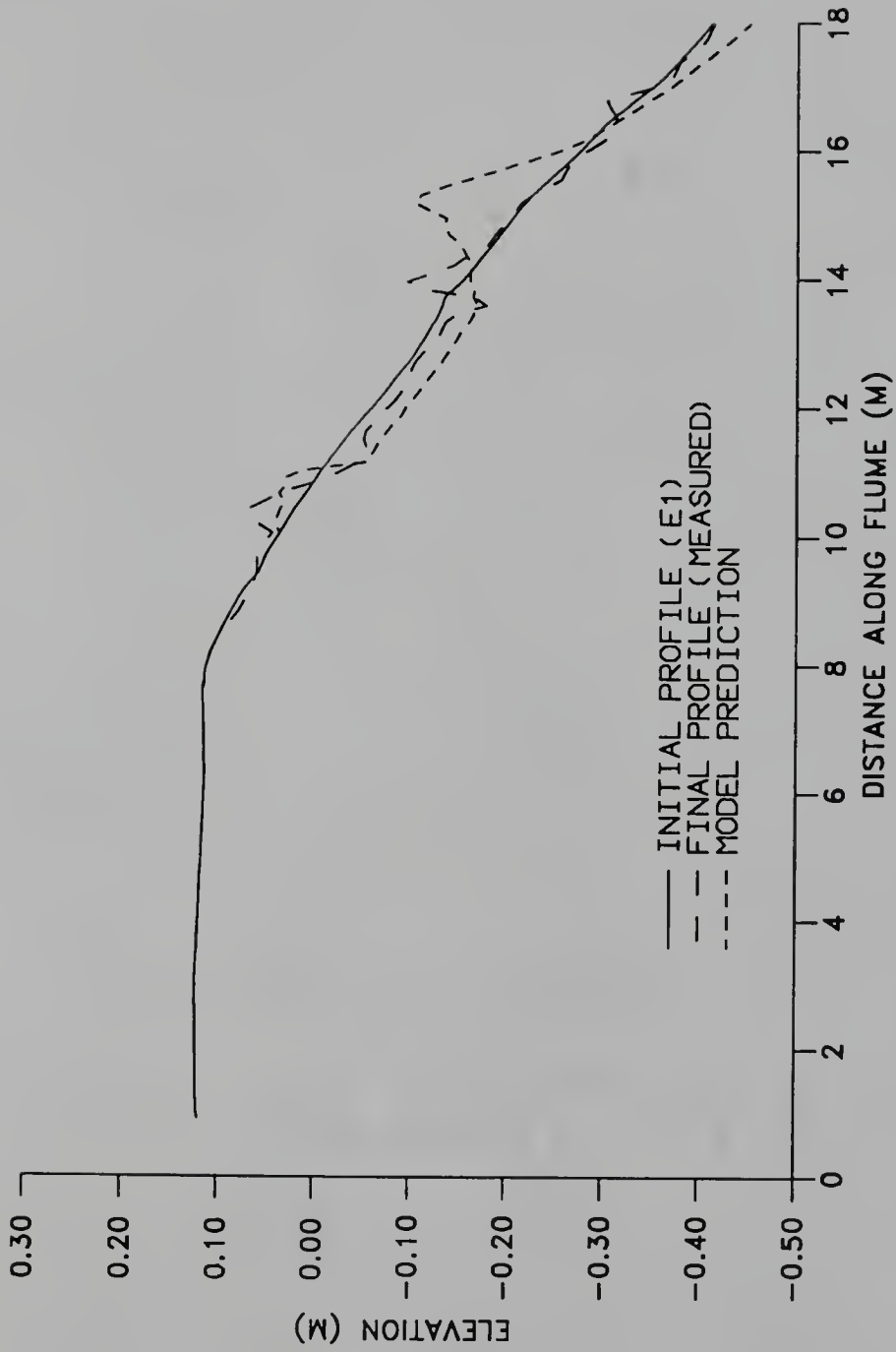


Figure 5.17: Model prediction for Experiment E1 with the friction factor increased by a factor of 10.

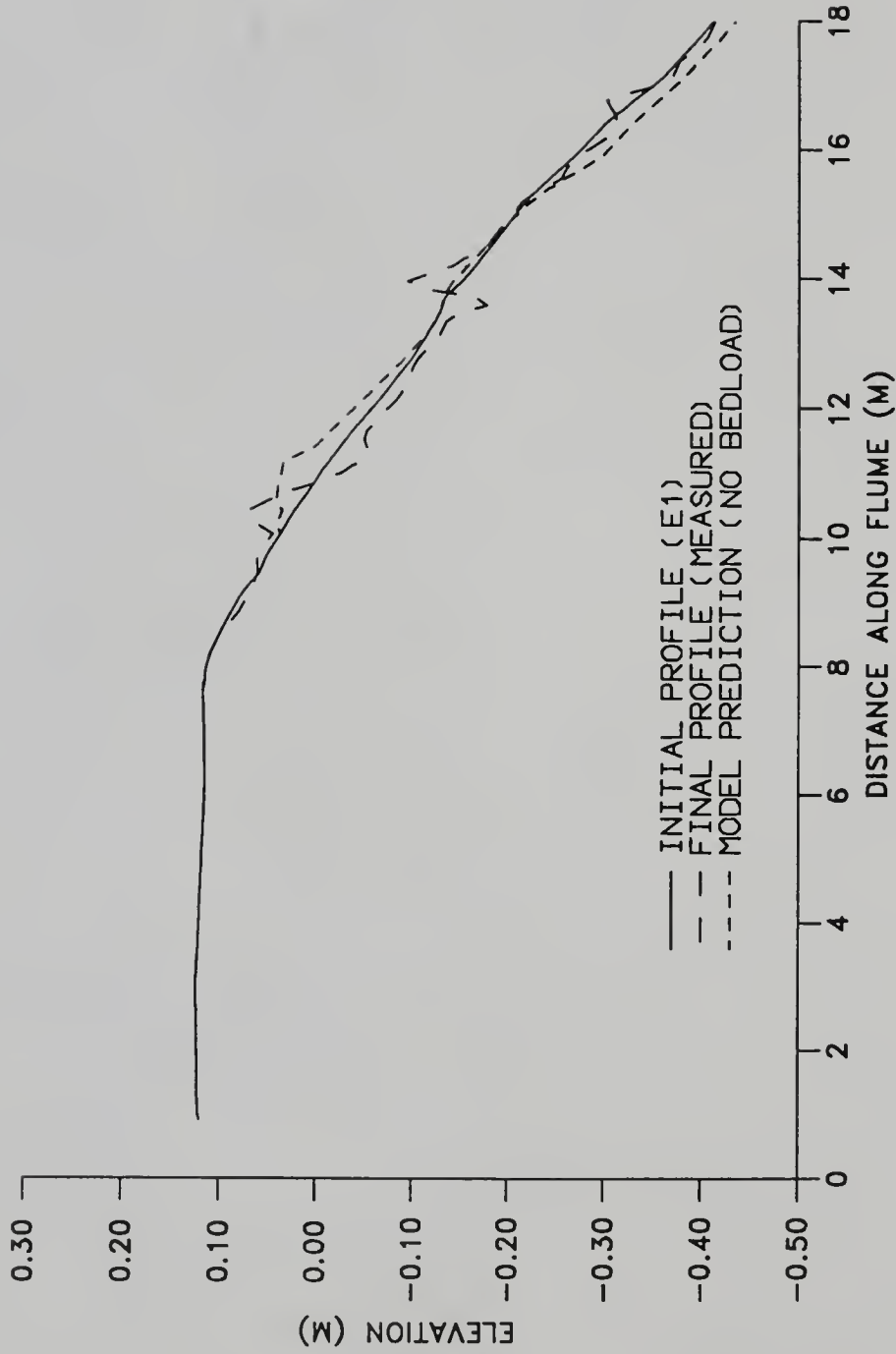


Figure 5.18: Experiment E1, measured profiles and model prediction with bedload mechanisms only.

sented earlier. The sediment eroded seaward of the break-point is deposited in the surf zone in the present case and the depositional characteristics are totally incorrect. The method presented earlier to quantify the “goodness” of fit of predicted profiles with and without the inclusion of bedload mechanisms was not truly conclusive. Now, the numerical cross-shore sediment transport model assumed sheet flow conditions to calculate bedload transport. This requires the presence of fairly vigorous fluid flow with a turbulent bottom boundary layer. The test conditions do not strictly satisfy these requirements. However, the effect of bedload on overall transport is not very significant as transport mechanics are primarily driven by undertow; thus, the present representation of bedload should not result in appreciable inaccuracies.

A final aspect to be addressed concerns the reproducibility of the measured profile evolution if the experimental conditions are repeated. The experimental conditions for the first 1.5 hours of Experiment E5 were the same as those of Experiment E1. The measured local change in the elevation at each cross-shore location with the measured profiles For Experiments E1 and E5 are presented in Figure 5.19. It is seen that the changes are identical.

The model cannot predict profile equilibrium when exposed to constant forcings for a long time. As was presented in Figure 5.5, the model slowly grows unstable with continuous erosion in the surf zone and growth of the longshore bar. This is attributed to the absence of any specification of an asymptotic form and to the author’s knowledge, there does not exist any “open-loop” model which can handle this complication.

5.6 Discussion of Results

The preceding sections documented the formulation and testing of the cross-shore sediment transport model. Both suspended and bedload transport mechanisms were included in the model formulation. Mean cross-shore currents due to the transfer of wave momentum and the phenomenon of intermittent suspension contribute to suspended sediment transport. Augmented mass flux in the surf zone results in substantial surf zone erosion. The suspended sediment transport equations are different

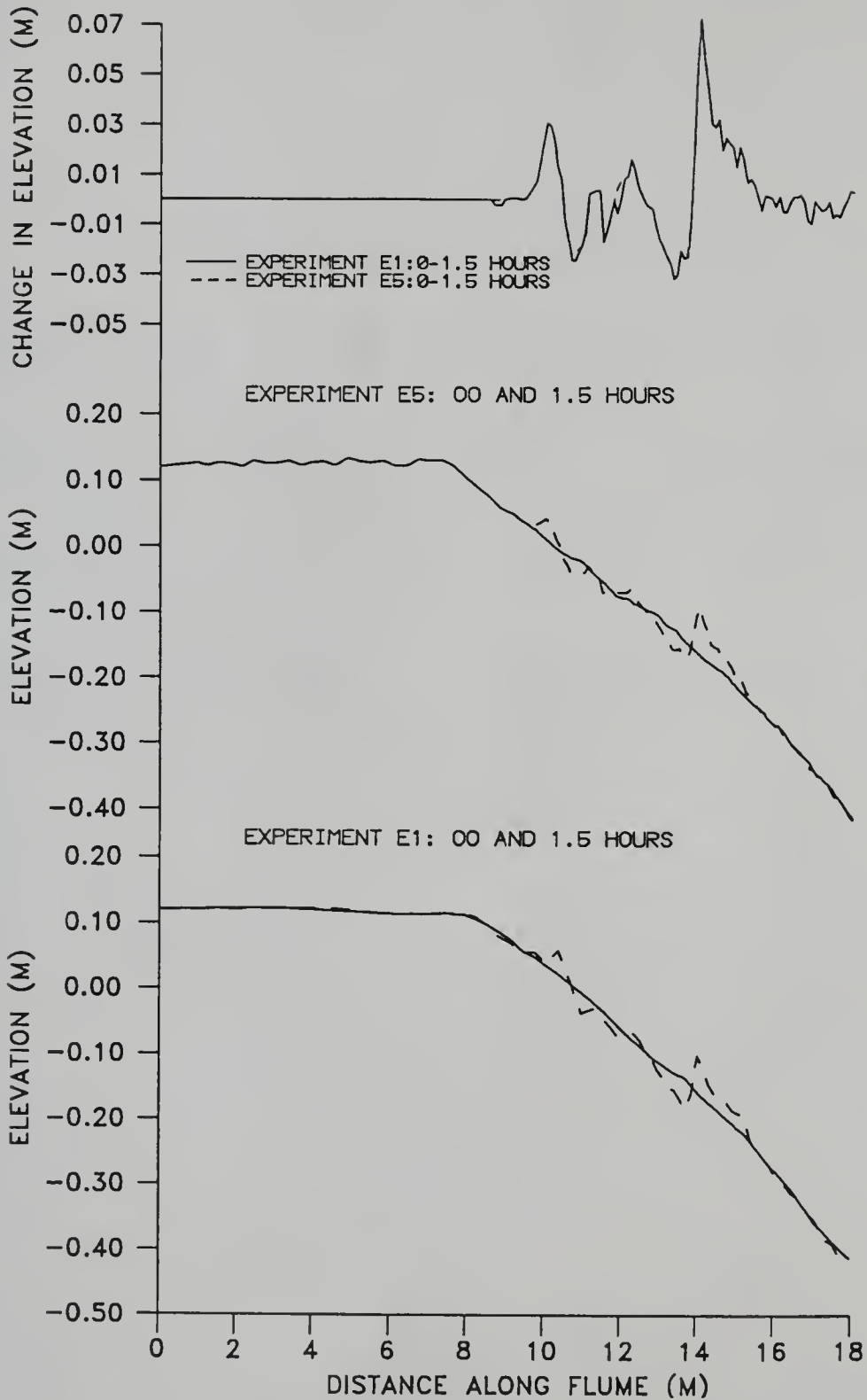


Figure 5.19: (a) Measured local changes in elevation after 1.5 hours, and measured profiles for Experiments (b) E5 and (c) E1.

inside and outside the surf zone, because the boundary conditions for the cross-shore currents are different (Chapter 3) and the friction velocity formulation in the representation of the concentration profile includes the effects of turbulence within the surf zone. Mean cross-shore currents cause offshore transport in the surf zone. The bedload formulations inculcated two aspects: (a) effects of dissipation in the bottom boundary layer and (b) wave asymmetry about the horizontal plane, and caused on-shore transport. Simple equations for bedload transport were derived for Stokes' second-order waves using theories developed by Trowbridge and Young (1989) and Bailard and Inman (1981). As these equations were limited in their applicability to deep-water, their applicability was extended by using the stream function theory to compute the required moments of the velocity vector.

The model was tested by comparing the predictions with measurements from the overwash experiments documented earlier (Section 2.3). These experiments provided nine different conditions for testing, including the aspects of various degrees of overtopping and wave types (monochromatic and random). The calibration factors in the bedload formulations were set to the standard values suggested by Trowbridge and Young (1989) and Bailard (1981). No extra calibration factors were introduced. An overall smoothing function was applied to remove "kinks" or discontinuities in the net transport caused by (a) the discontinuity in the gradient of wave momentum at the break-point, and (b) the addition of independent transport components.

The results of model testing with monochromatic waves and steady water level (Experiments E1-E4) are discussed first. In this series of tests, the wave characteristics were reasonably constant while the water level was raised from test to test.

For all tests, the model predicted the formation of a longshore bar with its crest close to the position of the break-point. This aspect of the model predictions was consistent with observations and measurements. As the water level increased from test to test, the longshore bar formed further landward as the waves broke closer to the slope-break. The model predicted a higher crest elevation of the longshore bar than measured in the cases with overtopping (Experiments E2-E4). The model correctly reproduced the feature of decreasing bar relief with higher overtopping levels.

The results of the model indicated erosion in the offshore portions of the beach profile, with the degree of erosion being greater for shallower water depths. This facet of the model capability was verified by measurements for Experiments E1, E3 and E4 while Experiment E2 exhibited slight offshore deposition in the measured profile. The model could not reproduce the extensive erosion immediately seaward of the longshore bar for cases with moderate and severe overtopping (Experiments E3, E4).

Though the model cannot reproduce the “scouring” action of plunging breakers in excavating a prominent trough landward of the bar crest, the documented erosion in the surf zone was well reproduced by the model for Experiments E1, E3 and E4. However, for Experiment E2, the model results indicate excessive erosion when compared to measurements. Experiment E2 is unique in the respect that the choice of the value of mass flux below the level of the wave trough in the undertow equations is not very clear as, with the advent of wave action, minimal overtopping develops due to swash and wave setup. This condition is intermediate between the two extremes of no overtopping and complete overtopping.

For the case without overtopping, Experiment E1, the model exhibits the deposition of a substantial berm at the still water level (SWL) while the corresponding berm in the measured profile was slightly landward. The absence of swash mechanisms in the model formulation causes this discrepancy. The depositional characteristics over the crest of the barrier island are well represented by the model for all cases. The trend of decreasing deposition landward of the slope-break is evident in both measurements and predictions.

The case of simulation of a storm tide with rising and falling water levels, Experiment E5, is considered next. The model predicts erosion seaward of the longshore bar which was not evident in the measurements. The size and position of the longshore bar was well represented but the crest of the bar was lower in the model result than observed. Surf zone erosion and depositional characteristics over the crest of the barrier island were fairly well simulated by the model.

The effects of wave action by random waves was investigated in Experiments E6-E9 whose test conditions were otherwise similar to Experiments E1-E4 respectively.

The model was tested by generating a random series of monochromatic waves by using a random number generator in conjunction with the computed probability density function of measured waves at the toe of the beach. The results of the transport model for these cases are discussed next.

In the case without overtopping, Experiment E6, the model correctly reproduced a longshore bar at the exterior edge of the surf zone which was of lesser relief as compared to the corresponding case with monochromatic waves. The model predicted negligible change seaward of the bar while the measured profile exhibited slight deposition. Surf zone erosion and berm deposition around the MWL was well reproduced. Experiment E7 had minimal overtopping due to swash and wave setup. The model results correctly exhibited a subdued bar, but with its crest landward of that actually observed. The shape and size of the bar were fairly well reproduced. The model also reproduced the feature of negligible change in the offshore. Surf zone erosion was again well predicted. The absence of swash mechanisms in the model precluded any deposition over the crest of the barrier island while the measured profile showed slight deposition. The cases with overtopping, Experiments E8 and E9, displayed offshore deposition while the model predicted negligible change. Also, measurements exhibited more erosion in the surf zone than predicted by the transport model. The prediction characteristics improved in the landward portions of the surf zone and over the crest of the barrier island.

For the present set of experimental conditions, the cross-shore transport model was successful in reproducing the principal morphological features of longshore bar formation and surf zone erosion. Washover deposition over the crest of the barrier island in cases with overtopping was well predicted and showed the correct trend of decreasing deposition landward of the slope-break. The position of the longshore bar was fairly well predicted in all the cases where bar formation was evident. The model correctly predicted the longshore bar to be of greater relief in cases with monochromatic waves as compared to cases with random waves. Cases with random waves and overtopping conditions were correctly simulated to be devoid of longshore bars. The model consistently predicts erosion offshore of the crest of the longshore bar, which

was not always evident in the measured profiles. Surf zone erosion was well reproduced as were the depositional characteristics over the crest of the barrier island in cases with overtopping. The absence of swash mechanisms in the sediment transport model causes berm deposition slightly seaward as compared to measured profiles in cases without overtopping. Although the model correctly predicts less changes in cases with random waves and overtopping as compared to cases with monochromatic cases and overtopping, the degree of change in cases with random waves was less than actually observed.

It is again noted that Dally (1980), who considered the effects of intermittent suspension and undertow, was the first to attempt a physics-based approach in sediment transport modeling and was the first to quantify undertow. However, his choice of boundary conditions for the undertow equations are moot in view of recent experimental evidence. Also, he did not account for wave asymmetry, effects of the bottom boundary layer (bedload transport) and random waves in his transport model. Finally, it is emphasized that the present numerical model is an attempt to formulate a relatively "complete" physics-based sediment transport model which only requires the initial conditions and not any local velocity or profile information as the response unfolds. Recognizing the inherent difficulties in combining several models for various processes each with their own degrees of uncertainty, modeling of processes has been kept as simple as possible. The model provides a reasonable framework for future research and comparison of various effects, acting independently or in concert.

CHAPTER 6 SUMMARY, CONCLUSIONS AND RECOMMENDATIONS

6.1 Summary

With the aim of simulating the effects of storms on barrier islands and characterizing their response to overtopping conditions, nine experiments were conducted at the Coastal Engineering Laboratory of the University of Florida. Considering a geometric scale of 1:16, the barrier island was simulated by a 122 m (prototype units) wide horizontal crest and an initially planar (1:19) beach. The effects of various storm levels and accompanying overtopping conditions were investigated. Experiments were conducted with both regular (monochromatic) and irregular (random) waves while the remaining wave characteristics were kept reasonably constant. As a prominent longshore bar was noticed in most experiments, another series of experiments was conducted to specifically investigate the causes of longshore bar formation. Bichromatic and multifrequency primary waves were generated in the wave facility such that long waves or “surf beat” were produced at the interaction (difference) frequencies. Different combinations of the primary wave frequencies resulted in different long wave characteristics. Finally, an “open-loop” cross-shore transport model including suspended and bedload sediment transport mechanisms was developed and the model’s predictive capacity was tested against data from the overwash experiments. The model accounted for the following: (a) transfer of linear wave momentum, (b) intermittent suspension, (c) energy dissipation in the bottom boundary layer, (d) wave asymmetry and (e) turbulence due to wave breaking (f) augmented mass flux in the surf zone. Including these mechanisms allowed the development of both onshore and offshore transport components. The model had the additional capacity to predict longshore bars.

6.2 Conclusions

The main conclusions of the experimental investigation of overwash were as follows. Overtopping water levels in cases with monochromatic waves resulted in sand overwash, significant erosion of the sloping beach and some difference in the relief of the longshore bar. The major differences in experiments with irregular waves were in the characteristics of the longshore bar, which was either subtle or absent, and in the degree of profile change, which was less as compared to cases with regular waves.

1. Monochromatic waves with no overtopping, Experiment E1, caused a prominent longshore bar, and a fairly substantial berm was established immediately landward of the waterline.
2. Monochromatic waves with marginal overtopping, Experiment E2, resulted in a prominent longshore bar, but the sediment which had formed the berm in the first case (Experiment E1) was now deposited over the crest of the barrier island.
3. Monochromatic waves with substantial overtopping, Experiments E3 and E4, caused transport of sediment over the crest of the barrier island resulting in a substantial loss of sediment to the beach system. The longshore bar was subtle in the case with the larger overtopping depth, Experiment E4.
4. There was substantial surf zone erosion in the above four tests. The position of the longshore bar was always proximate to the break-point and moved landward from test to test as the water level was raised.
5. In the case with monochromatic waves and a rising and falling water level associated with a storm, Experiment E5, the longshore bar formed and persisted during times of slowly changing water level, while it was subdued to non-existent during times of rapidly changing water level because the bar formation processes could not keep pace.

6. Experiments with random waves displayed similar characteristics over the crest of the barrier island and in the surf zone landward of the breaking region.
7. The berm was more subtle in the case with random waves and no overtopping, Experiment E6, as compared to the corresponding case (Experiment E1) with monochromatic waves.
8. The degree and characteristics of bar formation was different in cases with random waves as compared to cases with monochromatic waves. As mentioned above, the longshore bar was less prominent as compared to the corresponding case with monochromatic waves when no overtopping occurred. In cases with overtopping, bar formation was subtle with the water level coincident with the barrier island crest and the profile was devoid of the presence of a bar in cases with substantial overtopping.

The main conclusions of the investigation of bar formation mechanisms were as follows:

1. Various spectral characteristics of primary waves accompanied by forced infra-gravity components of different spectral characteristics caused almost no change in the characteristics of the longshore bar.
2. In all cases, the bar formed at the exterior edge of the surf zone.
3. The cases investigated had conditions marginally favorable for bar formation (fall velocity parameter about 3). For these conditions, the shape of the wave height probability distribution (WHPD) function is important. The cases with primary or secondary peaks close to the maxima of the WHPD exhibited prominent bars while the presence of primary peaks towards the center of the WHPD resulted in subtle bars.
4. For the cases investigated here, undertow is clearly the causative mechanism for bar formation.

Insight gained by the above experiments provided a foundation for the development of a cross-shore sediment transport model including offshore and onshore transport mechanisms. The results of testing the model against data from the overwash experiments revealed the following:

1. The model is successful in reproducing the main features observed in the experiments including (a) prominent erosion in the surf zone, (b) berm deposition in cases without overtopping, and (c) washover deposition in cases with overtopping. The berm deposited in cases without overtopping is slightly seaward relative to measurements. This is interpreted as due to the absence of swash modeling. Bedload modeling is essential to reproduce berm or washover deposition. An attempt to quantify the “goodness of fit” of predicted profiles with and without bedload mechanisms could not truly establish the necessity of including bedload mechanisms in the model. However, as mentioned before, the prediction of overwashed sand necessitates the presence of bedload mechanisms in the model. With the inclusion of bedload mechanisms, the depositional characteristics over the crest of the barrier island exhibit the correct trend of decreasing deposition landward of the slope-break.
2. The model is successful in predicting longshore bar formation, location, size and relief. The model correctly predicts prominent bar formation for the overwash cases with monochromatic waves and the degree of relief of the bar reduces for the case with substantial overtopping. A longshore bar of less relief is predicted for the case of no and marginal overtopping with random waves while the cases with substantial overtopping exhibit no longshore bars.
3. The success of the model in reproducing all aspects of morphological change, except those caused by swash of course, landward of the exterior (seaward) edge of the surf zone indicates that the modeling of surf zone hydrodynamics is fairly accurate.

4. The model predicts some or no erosion in the offshore portions of the profile while some of the measured profiles indicated deposition.
5. Changes in the predicted profile using random waves are lesser than measured.
6. Lack of complete Reynolds number similarity implies that caution must be exercised when applying model results to prototype conditions.
7. The model does not have long-term stability.

6.3 Recommendations for Further Work

1. Swash mechanisms need to be accounted for in the model.
2. The radiation stress contribution above the level of the wave trough can be considered to act as a shear stress at the mean water level. The effects of the shear stress on each cell should not be considered in isolation, rather, an appropriate hydrodynamic coupling to neighboring cells should be incorporated. The aspect of transfer of angular momentum by breaking waves needs to be considered in future modeling of surf-zone hydrodynamics. The large-scale eddies present immediately after breaking, especially obvious in plunging breakers, should have a “cushioning” impact on the water column and tend to smooth out the effects of the discontinuity in the gradient of linear momentum. This should reduce the need for the empirical transport spreading function of the present model.
3. An improved representation needs to be developed for sediment transport seaward of the break-point. The present model predicts none to some offshore erosion in the experiments considered here, while some experiments exhibited offshore deposition.
4. A better formulation needs to be inculcated in the model for modeling the evolution of random waves.
5. Bedload due to surf zone waves can be better represented by considering velocity moments of a horizontally asymmetric (“saw-tooth”) wave form.

6. An effective feedback mechanism should be developed in the model such that long-term stability can be attained.

APPENDIX A BREAKING WAVE MODEL

Considering steady state, one-dimensional propagation and no interaction with the mean flow, the wave energy balance becomes

$$\frac{dF}{dx} + D = 0 \quad (\text{A.1})$$

where F is the wave energy flux per unit width and D is the rate of energy dissipation per unit area. Further,

$$F = Ec_g \quad (\text{A.2})$$

where E is the energy density and c_g is the wave group velocity, which in shallow water is given by

$$c_g = \sqrt{gd} \quad (\text{A.3})$$

where g is the acceleration due to gravity and d is the local depth (including set-up, $\bar{\eta}$), i.e.

$$d = h + \bar{\eta}. \quad (\text{A.4})$$

Wave energy dissipation is assumed to be proportional to the amount by which the local energy flux exceeds the ‘stable’ energy flux (Dally 1980). Thus, Equation (A.1) becomes

$$\frac{d}{dx}(Ec_g) = 0 \quad (\text{A.5})$$

before breaking and

$$\frac{d}{dx}(Ec_g) = -\frac{K}{d}[(Ec_g) - (Ec_g)_s] \quad (\text{A.6})$$

after breaking, where K is an empirical constant. The stable wave height, H_s , is modeled as

$$H_s = \kappa h \quad (\text{A.7})$$

where κ is a constant. The equation for set-up (following Longuet-Higgins and Stewart 1963) can be written as

$$\frac{d\bar{\eta}}{dx} = -\frac{3}{16} \frac{1}{h + \bar{\eta}} \frac{dH^2}{dx} \quad (\text{A.8})$$

Equations (A.6) and (A.8) can now be iteratively solved with a finite difference scheme. The recommended values (Dally 1980) of the empirical constants are

$$K \sim 0.17 \quad (\text{A.9})$$

$$\kappa = 0.4. \quad (\text{A.10})$$

BIBLIOGRAPHY

- Bagnold, R.A. 1963 Mechanics of marine sedimentation *The Sea* ed. M.N. Hill, John Wiley & Sons, New York, 3, 507-528.
- Bagnold, R.A. 1966 An approach to the sediment transport problem from general physics *U.S. Geol. Surv. Prof. Pap.* 422(1), 137p.
- Bailard, J.A. 1981 An energetics total load sediment transport model for a plane sloping beach *J. Geophys. Res.* 86(C11), 10938-10954.
- Bailard, J.A. 1982 Modeling on-offshore transport in the surfzone *Proc. 18th Conf. Coastal Eng.* ASCE, Cape Town, South Africa, 1419-1438.
- Bailard, J.A. and D.L. Inman 1981 An energetics bedload model for a plane sloping beach: local transport *J. Geophys. Res.* 86(C3), 2035-2043.
- Battjes, J.A. 1974 Surf similarity *Proc. 14th Conf. Coastal Eng.* ASCE, Copenhagen, Denmark, 466-480.
- Battjes, J.A. 1988 Surf zone dynamics *J. Fluid Mech.* 20, 257-293.
- Battjes, J.A. and T. Sakai 1981 Velocity field in a steady breaker *J. Fluid Mech.* 111, 421-437.
- Battjes, J.A. and M.J.F. Stive 1985 Calibration and verification of a dissipation model for random breaking waves *J. Geophys. Res.* 90, 9159-9167.
- Boczar-Karakiewicz, B. and R.G.D. Davidson-Arnott 1987 Nearshore bar formation by nonlinear wave processes – a comparison of model results and field data *Mar. Geol.* 77, 287-304.
- Borekci, O.S. 1982 Distribution of wave-induced momentum fluxes over depth and application within the surf zone *Dissertation* Dept. of Civil Eng., University of Delaware, Newark, DE.
- Bowen, A.J. 1980 Simple models of nearshore sedimentation: Beach profiles and longshore bars *Coastline of Canada* S.B. McCann ed., 1-11, Geological Survey of Canada, Ottawa.
- Bowen, A.J. and D.L. Inman 1971 Edge waves and crescentic bars *J. Geophys. Res.* 76, 8662-8671.
- Bowen, A.J., D.L. Inman and V.P. Simmons 1968 Wave “set-down” and set-up *J. Geophys. Res.* 73(8), 2569-2577.

- Bruun, P. 1954 Coast erosion and development of beach profiles *Tech. Memorandum* 44, BEB, CERC, US Army Engineer WES, Vicksburg, MS.
- Carrier, G.F. and H.P. Greenspan 1958 Water waves of finite amplitude on a sloping beach *J. Fluid Mech.* 4, 97-107.
- Carter, T.G., P.L.F. Liu and C.C. Mei 1973 Mass transport by waves and offshore sand bed forms *J. Waterw. Harbors Coastal Eng. Div.* ASCE, 99, 165-183.
- Coastal Engineering Research Center 1979 Coastal Hydraulic Models, U.S. Army Corps of Engineers *Special Report* 5, Chapter V.
- Dally, W.R. 1980 A numerical model for beach profile evolution *M.S. Thesis* Dept. of Civil Eng., University of Delaware, Newark, DE.
- Dally, W.R. 1987a Wave transformation in the surf zone *Dissertation* Dept. of Coastal and Ocean. Eng., University of Florida, Gainesville, FL.
- Dally, W.R. 1987b Longshore bar formation—surf beat or undertow? *Coastal Sediments* ASCE, New Orleans, LA, 71-86.
- Dally, W.R. and R.G. Dean 1984 Suspended sediment transport and beach profile evolution *J. Waterw. Port Coastal Ocean Eng. Div.* ASCE 110(1), 15-33.
- Dally, W.R., R.G. Dean and R.A. Dalrymple 1985 Wave height variation across beaches of arbitrary profile *J. Geophys. Res.* 90(C6), 11917-11927.
- Dally, W.R. and R.G. Dean 1986a Transformation of random breaking waves on surf beat *Proc. 20th Conf. Coastal Eng.* ASCE, Taipei, Taiwan, 109-123.
- Dally, W.R. and R.G. Dean 1986b Mass flux and undertow in a surf zone, by I.A. Svendsen— Discussion *Coastal Eng.* 10, 289-307.
- Dalrymple, R.A. 1974 A finite amplitude wave on a linear shear current *J. Geophys. Res.* 79(30), 4498-4504.
- Dalrymple, R.A. 1992 Prediction of storm/normal beach profiles *J. Waterw. Port Coastal Ocean Eng. Div.* ASCE, 118(1), 193-200.
- Dalrymple, R.A. and W.W. Thompson 1976 Study of equilibrium beach profile *Proc. 15th Conf. Coastal Eng.* ASCE, Honolulu, HI, 1277-1296.
- Davis, R.A., R.B. Burke and J.W. Brame 1979 Origin and development of barrier island on west central peninsula of Florida. AAPG-SEPM Annual Convention, Abstract, 74-75.
- Dean, R.G. 1965 Stream function representation of nonlinear ocean waves *J. Geophys. Res.* 70(18), 4561-4572.
- Dean, R.G. 1973 Heuristic models of sand transport in the surf zone *Proc. Conf. Eng. Dyn. Surf Zone* Inst. of Engineers, Sydney, Australia, 208-214.

- Dean, R.G. 1977 Equilibrium beach profiles: U.S. Atlantic and Gulf Coasts *Ocean Eng. Rep.* 12, Dept. of Civil Eng., University of Delaware, Newark, DE.
- Dean, R.G. 1991 Equilibrium beach profiles: characteristics and applications *J. Coastal Res.* 7(1), 53-84.
- Dean, R.G. and R.A. Dalrymple 1991 *Water Wave Mechanics for Engineers and Scientists* World Scientific Press, Singapore.
- Deigaard, R., J. Fredsoe and I. Broker Hedegaard 1986 Suspended sediment in the surf zone *J. Waterw. Port Coastal Ocean. Eng. Div.* ASCE, 112, 115-127.
- Dolan, R. 1972 Barrier dune system along the Outer Banks of North Carolina: a reappraisal *Science* 176, 286-288.
- Dolan, R. and P. Godfrey 1973 Effects of Hurricane Ginger on the barrier islands of North Carolina *Geol. Soc. Amer. Bull.* 84, 1329-1334.
- Dolan, T.J. 1983 Wave mechanisms for the generation of multiple longshore bars with emphasis on the Chesapeake Bay *M.C.E. Thesis* Dept. of Civil Eng., University of Delaware, Newark, DE.
- Dolan, T.J. and R.G. Dean 1985 Multiple longshore bars in the Upper Chesapeake Bay *J. Estuarine, Coastal and Shelf Science* 21, 727-743.
- Duncan, J.H. 1981 An experimental investigation of breaking waves produced by a towed hydrofoil *Proc. R. Soc. London Ser. A* 377, 331-348.
- Dyhr-Nielsen, M. and T. Sorensen 1970 Sand transport phenomena on coasts with bars *Proc. 12th Conf. Coastal Eng.* ASCE, Washington, D.C., 855-866.
- Evans, O.F. 1940 The low and ball of the eastern shore of Lake Michigan *J. Geol.* 48(5), 476-511.
- Fisher, J.J. 1968 Barrier island formation: discussion. *Geol. Soc. Amer. Bull.* 79, 1421-1426.
- Flick, R.E. and R.T. Guza 1980 Paddle generated waves in laboratory channels *J. Waterw. Port Coastal Ocean Eng. Div.* ASCE, 106, 79-97.
- Fredsoe, J. and R. Deigaard 1992 *Mechanics of Coastal Sediment Transport* World Scientific Press, Singapore.
- Galvin, C.J. 1968 Breaker type classification on three laboratory beaches *J. Geophys. Res.* 73, 3651-3659.
- Godfrey P.J. 1970 Oceanic overwash and its ecological implications on the Outer Banks of North Carolina, Office of Natural Science Studies, National Park Service, Washington, D.C., 37p.
- Godfrey, P.J. 1976 Comparative ecology of East Coast barrier islands: hydrology, soils, vegetation, in barrier islands and beaches. The Conservation Foundation, Washington, D.C., 5-34.

- Godfrey, P.J. 1978 Management guidelines for parks on barrier beaches *Parks* 2, 5-10.
- Godfrey, P.J. and M.M. Godfrey 1976 Barrier island ecology of Cape Lookout National Seashore and vicinity, North Carolina *National Park Service Scientific Monograph Series* 9.
- Graaff, J. van de 1977 Dune erosion during a storm surge. *Coastal Eng.* 1(2), 99-133.
- Guza, R.T. and A.J. Bowen 1976 Resonant interactions for waves breaking on a beach *Proc. 15th Conf. Coastal Eng.*, ASCE, Honolulu, HI, 560-579.
- Guza, R.T. and D.L. Inman 1975 Edge waves and beach cusps *J. Geophys. Res.* 80, 2997-3012.
- Hansen, J.B. and I.A. Svendsen 1974 Laboratory generation of waves of constant form *Proc. 14th Conf. Coastal Eng. Div.* ASCE, Copenhagen, Denmark, 321-339.
- Hansen, J.B. and I.A. Svendsen 1984 A theoretical and experimental study of undertow *Proc. 19th Conf. Coastal Eng.* ASCE, Houston, TX, 2246-2262.
- Hartnack, W. 1924 Uber sandriff *Jahrbuch der Geografischen Gesellschaft zu Greifswald* Band XL/XLII, 47-70.
- Hattori, M. and T. Aono 1985 Experimental study on turbulent structures under spilling breakers *The Ocean Surface* ed. Y. Toba, H. Mitsuyasu, 419-424, Dordrecht:Reidel.
- Hayes M.O. 1967 Hurricanes as geological agents: case studies of Hurricane Carla 1961, and Cindy 1963 *Report of Investigations* 61, Bureau of Economic Geology, University of Texas, Austin.
- Holman, R.A. and A.J. Bowen 1982 Bars, bumps and holes : models for the generation of complex beach topography *J. Geophys. Res.* 87, 457-468.
- Houston, S.H. and R.G. Dean 1990 Method for prediction of bar formation and migration *Proc. 22nd Conf. Coastal Eng.* ASCE, Delft, Netherlands, 2145-2158.
- Howd, P.A. and W.A. Birkemeier 1987a Beach and nearshore survey data: 1981-1984 CERC Field Research Facility *Tech. Report* CERC 87-9, US Army Engineer WES, Vicksburg, MS.
- Howd, P.A. and W.A. Birkemeier 1987b Storm-induced morphology changes during DUCK85 *Coastal Sediments '87* ASCE, New Orleans, LA, 834-847.
- Hunt, J.N. and B. Johns 1963 Currents induced by tides and gravity waves *Tellus* XV(4), 343-351.
- Inman, D.L. and R.A. Bagnold 1963 Littoral Processes *The Sea* ed. M.N. Hill, John Wiley & Sons, New York, 3, 529-553.

- Jansen, P.C.M. 1986 Laboratory observations of the kinematics in the aerated region of breaking waves *Coastal Eng.* 9, 453-477.
- Johnson, D.W. 1919 *Shore Processes and Shoreline Development* John Wiley & Sons, New York, NY.
- Kajima, R., T. Shimizu, K. Maruyama, H. Hasegawa, and T. Sakakiyama 1982 Experiments of beach profile change with a large wave flume *Proc. 18th Conf. Coastal Eng.* ASCE, Cape Town, South Africa, 1385-1404.
- Kajiura, K. 1968 A model of the bottom boundary layer in water waves *Bull. Earthquake Res. Inst.* 46, 75-123.
- Kamphuis, J.W. 1975 Friction factor under oscillatory waves *J. Waterw. Harbors Coastal Eng. Div.* ASCE, 101, 135-144.
- Katoh, K. 1984 Multiple longshore bars formed by long period standing waves *Tech. Report* Port & Harbor Research Institute, Japan Ministry of Transport, 23(3).
- Keller, J.B. 1963 Tsunamis—water waves produced by earthquakes *Int. Union Geod. Geophys. Monogr.* 24 Tsunami Hydrodyn. Conf., Honolulu, 154-166.
- Kemp, P.H. 1960 The relationship between wave action and beach profile characteristics *Proc. 7th Conf. Coastal Eng.* ASCE, The Hague, Netherlands, 262-277.
- Kemp, P.H. and D.T. Plinston 1968 Beaches produced by waves of low phase difference *J. Hydr. Div.* ASCE, 94, 1183-1195.
- Keulegan, G.H. 1945 Depths of offshore bars *Engineering Notes* 8, BEB, CERC, US Army Engineer WES, Vicksburg, MS, 18p.
- King C.A.M. 1972 *Beaches and Coasts* 2nd ed., St. Martins Press, New York, NY.
- Kirby, J.M., R.A. Dalrymple and P.L.F. Liu 1981 Modification of edge waves by barred-beach topography *Coastal Eng.* 5, 35-49.
- Kohler, R.R. and C.J. Galvin 1973 Berm-bar criterion *Tech. Report* CERC Laboratory Report, Vicksburg, MS, 70 p.
- Kraus, N.C. and M. Larson 1988 Beach profile change measured in the tank for large waves, 1956-1957 and 1962 *Tech. Report* CERC 88-6, US Army Coastal Eng. Res. Ctr., Vicksburg, MS.
- Kriebel, D.L. 1982 Beach and dune response to hurricanes *M.S. Thesis* University of Delaware, Newark, DE.
- Kriebel, D.L. and R.G. Dean 1985 Numerical simulation of time-dependent beach and dune erosion *Coastal Engineering* 9(3), 221-246.
- Kriebel D., W.R. Dally and R.G. Dean 1986 Beach response following severe erosional events *Tech. Report* UFL/COEL-86/016 Dept. of Coastal and Ocean. Eng., University of Florida, FL.

- Kriebel, D., W.R. Dally and R.G. Dean 1987 Undistorted Froude model for surf zone sediment transport *Proc. 20th Conf. Coast. Eng.* ASCE, Taipei, Taiwan, 1393-1406.
- Larson, M. and N.C. Kraus 1989 SBEACH: Numerical model for simulating storm-induced beach profile change *Tech. Report CERC 89-9*, US Army Coastal Eng. Res. Ctr., Vicksburg, MS.
- Lau, J. and B. Travis 1973 Slowly varying Stokes waves and submarine longshore bars *J. Geophys. Res.* 78, 4489-4497.
- Launder, B.E. and D.B. Spalding 1972 *Mathematical Models of Turbulence* Academic, San Diego, CA, 169pp.
- Leatherman, S.P. 1976 Barrier island dynamics: overwash processes and aeolian transport *Proc. 15th Conf. Coastal Eng.* ASCE, Honolulu, Hawaii, 1958-1974.
- Leatherman, S.P. 1977 Overwash hydraulics and sediment transport *Coastal Sediments '77*, ASCE, Charleston, SC, 135-148.
- Leatherman, S.P. 1979a *Barrier Island Handbook* National Park Service, Cooperative Research Unit, The Environmental Institute, University of Massachusetts at Amherst.
- Leatherman S.P., 1979b Beach and dune interaction during storm conditions *Q. J. Eng. Geol.* 12, 281-290.
- Lehmann, F.W.P. 1884 Das Kustengebiet Hinterpommerns *Zeitschrift der Gesellschaft für Erdkunde zu Berlin* Band XIX.
- Liang, S.S. and H. Wang 1973 Sediment transport in water waves *Tech. Report 26*, College of Marine Studies, University of Delaware, Newark, DE.
- Lippman, T.C. and R.A. Holman 1990 The spatial and temporal variability of sand bar morphology *J. Geophys. Res.* 95(C7), 11575-11590.
- Lobeck, A.K. 1939 *Geomorphology—An Introduction to the Study of Landscapes* McGraw-Hill Book Company, New York, NY, 349 pp.
- Longuet-Higgins, M.S. 1953 Mass transport in water waves *Philos. Trans. R. Soc. London Ser. A* 245, 535-581.
- Madsen, O. 1971 On the generation of long waves *J. Geophys. Res.* 76(36), 8672-8683
- Mei, C.C. 1985 Resonant reflection of surface water waves by periodic sandbars *J. Fluid Mech.* 152, 315-335.
- Meyer R.E., (Ed.) 1972 *Waves on Beaches and Resulting Sediment Transport* Academic Press, New York.

- Miller, R.L. 1976 Role of vortices in surf zone prediction: sedimentation and wave forces *Beach and Nearshore Sedimentation, Soc. Econ. Paleontol. Mineral. Spec. Publ.* 24, ed. R.A. Davis, R.L. Ethington, 92-114.
- Mizuguchi, M. 1986 Experimental study on kinematics and dynamics of wave breaking *Proc. 20th Conf. Coastal Eng.* ASCE, Taipei, Taiwan, 589-603.
- Moore, B.D. 1982 Beach profile evolution in response to changes in water level and wave height *M.S. Thesis* Dept. of Civil Eng., University of Delaware, Newark, DE.
- Munk, W.H. 1949 Surf beats *EOS Trans. AGU*, 30, 849-854.
- Munk, W. and M. Wimbush 1969 A rule of thumb for wave breaking over sloping beaches *Oceanology* 6, 56-59.
- Nadaoka, K. 1986 A fundamental study on shoaling and velocity field structure of water waves in the nearshore zone *Tech. Report* Dept. of Civil Eng., Tokyo Inst. of Tech., Japan.
- Nadaoka, K., Hino, M. and M. Koyano 1989 Turbulent flow field structure of breaking waves in the surf zone *J. Fluid Mech.* 204, 359-387.
- Nadaoka, K. and T. Kondoh 1982 Laboratory measurements of velocity field structure in the surf zone by LDV *Coastal Eng. Japan* 25, 125-146.
- Nielsen, P. Suspended sediment concentrations under waves *Coastal Eng.* 10, 23-31.
- Noda, E.K. 1972 Equilibrium beach profile scale-model relationship *J. Waterw. Harbors Coastal Eng. Div.* ASCE, 98, 511-528.
- Okayasu, A., T. Shibayama and N. Mimura 1986 Velocity field under plunging waves *Proc. 20th Conf. Coastal Eng.* ASCE, Taipeh, Taiwan, 660-674.
- Otensen Hansen, N.E., S.E. Sand, H. Lundgren, T. Sorensen, and H. Gravesen 1980 Correct reproduction of group-induced long waves *Proc. 17th Conf. Coastal Eng.* ASCE, Sydney, Australia, 784-800.
- Otto, T. 1911 Der darss und zingst *Jahrbuch der Geografischen Gesellschaft zu Greifswald* Band XIII, 393-403.
- Parchure T.M., R.G. Dean and R. Srinivas 1991 Laboratory study of overwash on barrier islands *Tech. Report* Dept. of Coastal and Ocean. Eng., University of Florida, Gainesville, FL.
- Peregrine, D.H. and I.A. Svendsen 1978 Spilling breakers, bores and hydraulic jumps *Proc. 16th Conf. Coastal Eng.* ASCE, Hamburg, West Germany, 540-550.
- Phillips, O.M. 1977 *The Dynamics of the Upper Ocean* Cambridge University Press, New York, 336 pp.

- Pilkey, O.H., R.S. Young, S.R. Riggs, A.W.S. Smith, H. Wu and W.D. Pilkey 1993 The concept of shoreface profile of equilibrium: a critical review *J. Coastal Res.* 9(1), 255-278.
- Pirrello, M.A. 1992 The role of wave and current forcing in the process of barrier island overwash *M.S. Thesis* 92/018, Dept. of Coastal and Ocean. Eng., University of Florida, Gainesville, FL, 118 pp.
- Price, W.A. 1947 Environment and formation of the chenier plain *Quaternaria* 2, 35-86.
- Roelvink, J.A. and M.J.F. Stive 1989 Bar-generating cross-shore flow mechanisms on a beach *J. Geophys. Res.* 94(C4), 4785-4800.
- Rouse, H. 1949 Engineering hydraulics *Proc. 4th Hydr. Conf.* Iowa Institute of Hydraulic Research, June 12-15, John Wiley and Sons, Inc., New York.
- Sakai, T., Y. Inada and I. Sandanbata 1982 Turbulence generated by wave breaking on beach *Proc. 18th Conf. Coastal Eng.* ASCE, Cape Town, South Africa, 3-21.
- Sakai, T., I. Sandanbata and M. Uchida 1984 Reynolds stress in surfzone *Proc. 19th Conf. Coastal Eng.* ASCE, Houston, TX, 42-53.
- Sallenger, A.H., R.A. Holman and W.A. Birkemeier 1985 Storm-induced response of a nearshore-bar system *Mar. Geol.* 64, 237-257.
- Sallenger, A.H. and P.A. Howd 1989 Nearshore bars and the break-point hypothesis *Coastal Eng.* 12, 301-313.
- Saville, T. 1957 Scale effects in two-dimensional beach studies *Trans. 7th Gen. Meet.* International Association of Hydraulic Research, 1, A3-1-A3-10.
- Schaffer, H.A. and I.A. Svendsen 1988 Surf beat generation on a mild slope beach *Proc. 21st Conf. Coastal Eng.* ASCE, Costa del Sol, Malaga, Spain, 1058-1072.
- Scott, T. 1954 Sand movement by waves *Tech. Memorandum* 48, BEB, CERC, US Army Engineer WES, Vicksburg, MS.
- Short, A.D. 1975 Multiple offshore bars and standing waves *J. Geophys. Res.* 80, 3838-3840.
- Srinivas, R., R.G. Dean and T.M. Parchure 1992 Barrier island erosion and overwash study, volume 1 *Tech. Report* Dept. of Coastal and Ocean. Eng., University of Florida, Gainesville, FL.
- Stauble, D.K. 1989 *Barrier Islands: Progress and Management* Series ed. O.T. Magoon, ASCE, New York, NY, 324pp.
- Stive, M.J.F. 1980 Velocity and pressure field of spilling breakers *Proc. 17th Conf. Coastal Eng.* ASCE, Sydney, Australia, 547-566.
- Stive, M.J.F. 1986 A model for cross-shore sediment transport *Proc. 20th Conf. Coastal Eng.* ASCE, Taipeh, Taiwan, 1550-1564.

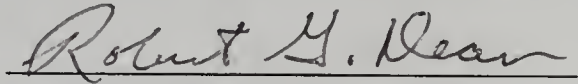
- Stive, M.J.F. and J.A. Battjes 1984 A model for offshore sediment transport *Proc. 19th Conf. Coastal Eng.* ASCE, Houston, TX, 1420-1436.
- Stive, M.J.F. and H.G. Wind 1982 A study of radiation stress and set-up in the nearshore region *Coastal Eng.* 6, 1-25.
- Stive, M.J.F. and H.G. Wind 1986 Cross shore mean flow in the surf zone *Coastal Eng.* 10, 325-340.
- Suhayda, J.N. 1975 Standing waves on beaches *J. Geophys. Res.* 79, 3065-3071.
- Sunamura, T. and K. Horikawa 1974 Two dimensional beach transformation due to waves *Proc. 14th Conf. Coastal Eng.* ASCE, Copenhagen Denmark, 920-938.
- Svendsen, I.A. 1984a Wave heights and set-up in a surf zone *Coastal Eng.* 8, 303-329.
- Svendsen, I.A. 1984b Mass flux and undertow in a surf zone *Coastal Eng.* 8, 347-365.
- Svendsen, I.A. 1987 Analysis of surf zone turbulence *J. Geophys. Res.* 92(C5), 5115-5124.
- Svendsen, I.A. and J.B. Hansen 1988 Cross-shore currents in surf zone modeling *Coastal Eng.* 12, 23-42.
- Svendsen, I.A., H. Schaffer and J.B. Hansen 1988 The interaction between the undertow and the boundary layer flow on a beach *J. Geophys. Res.* 92, 11845-11856.
- Swart, D.H. 1976 Predictive equations regarding coastal transports *Proc. 15th Conf. Coastal Eng.* ASCE, Honolulu, HI, 1113-1132.
- Swift, D.J.P. 1975 Barrier island genesis: evidence from the central Atlantic Shelf, Eastern U.S.A *Sedimentary Geology* 14, 1-43.
- Symonds, G., D.A. Huntley and A.J. Bowen 1982 Two dimensional surf beat: long wave generation by a time-varying breakpoint *J. Geophys. Res.* 87(C1), 492-498.
- Tennekes, H. and J.L. Lumley 1972 *A First Course in Turbulence* MIT Press, Cambridge, MA, 300 pp.
- Thieke, R.J. 1992 Wave, turbulent and mean momentum fluxes across the breaking wave transition region in the surf zone *Proc. 23^d Conf. Coastal Eng.* ASCE, Venice, Italy, 698-711.
- Trowbridge, J. and D. Young 1989 Sand transport by unbroken water waves under sheet flow conditions *J. Geophys. Res.* 94(C8), 10971-10991.
- Tucker, M.J. 1956 Surf beats: sea waves of 1 to 5 minutes' period *Proc. R. Soc. London Ser. A* 202, 565-573.
- Vanoni, V.A. 1975 *Sedimentation Engineering* ASCE, New York.

- Vellinga, P. 1978a Movable bed model tests on dune erosion, Delft Hydraulics Laboratory, Publication No. 205.
- Vellinga, P. 1978b Movable bed model tests on dune erosion *Proc. 16th Conf. Coastal Eng.* ASCE, Hamburg, Germany, 2020-2039.
- Vellinga, P. 1982 Beach and dune erosion during storm surges Delft Hydraulics Laboratory, Publication No. 276.
- Waters, C.H. 1939 Equilibrium slopes of sea beaches *M.S. Thesis* University of California, Berkeley, CA.
- Williams, P.J. 1978 Laboratory development of a predictive relationship for washover volume on barrier island coastlines *M.E. Thesis* University of Delaware, Newark, Delaware.
- Wright, L.D. and A.D. Short 1984 Morphodynamic variability of surf zones and beaches: a synthesis *Mar. Geol.* 56, 93-118.

BIOGRAPHICAL SKETCH

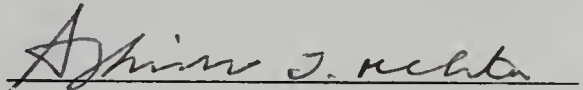
Rajesh Srinivas was born in Hassan, India, on June 27, 1964. He earned his Bachelor of Engineering degree in mechanical engineering from Birla Institute of Technology, Mesra, India, in 1986. He worked for a year as a graduate engineer trainee with Tata Iron and Steel Company in Bihar, India, before the lure of graduate study landed him at the University of Florida, Gainesville, where he has been working as a graduate assistant while earning his Master of Science and Doctor of Philosophy degrees in coastal and oceanographic engineering.

I certify that I have read this study and that in my opinion it conforms to acceptable standards of scholarly presentation and is fully adequate, in scope and quality, as a dissertation for the degree of Doctor of Philosophy.



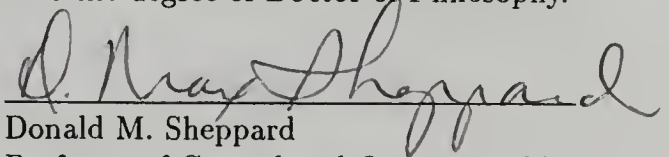
Robert G. Dean, Chairman
Graduate Research Professor of
Coastal and Oceanographic Engineering

I certify that I have read this study and that in my opinion it conforms to acceptable standards of scholarly presentation and is fully adequate, in scope and quality, as a dissertation for the degree of Doctor of Philosophy.




Ashish J. Mehta
Professor of Coastal and Oceanographic
Engineering

I certify that I have read this study and that in my opinion it conforms to acceptable standards of scholarly presentation and is fully adequate, in scope and quality, as a dissertation for the degree of Doctor of Philosophy.




Donald M. Sheppard
Professor of Coastal and Oceanographic
Engineering

I certify that I have read this study and that in my opinion it conforms to acceptable standards of scholarly presentation and is fully adequate, in scope and quality, as a dissertation for the degree of Doctor of Philosophy.

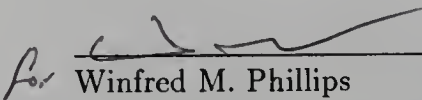

Bent A. Christensen
Professor of Civil
Engineering

I certify that I have read this study and that in my opinion it conforms to acceptable standards of scholarly presentation and is fully adequate, in scope and quality, as a dissertation for the degree of Doctor of Philosophy.


Robert J. Thicke
Assistant Professor of Coastal
and Oceanographic Engineering

This dissertation was submitted to the Graduate Faculty of the College of Engineering and to the Graduate School and was accepted as partial fulfillment of the requirements for the degree of Doctor of Philosophy.

December 1993


Winfred M. Phillips
Dean, College of Engineering

Dean, Graduate School

